THE ELECTROCHEMICAL REACTIONS OF PYRIDOXINE (VITAMIN B_6) AND SOME PHENOLIC COMPOUNDS IN APROTIC ORGANIC SOLVENTS

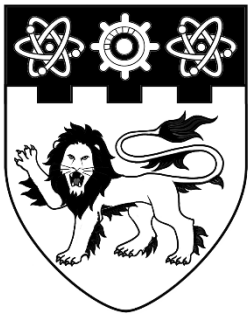

NANYANG TECHNOLOGICAL UNIVERSITY

THE ELECTROCHEMICAL REACTIONS OF PYRIDOXINE (VITAMIN B_6) AND SOME PHENOLIC COMPOUNDS IN APROTIC ORGANIC SOLVENTS

JAZREEN HUI QI LEE

SCHOOL OF PHYSICAL AND MATHEMATICAL SCIENCES

NANYANG TECHNOLOGICAL UNIVERSITY

2016

JAZREEN H. Q. LEE

2016

This page has been intentionally left blank

THE ELECTROCHEMICAL REACTIONS OF PYRIDOXINE (VITAMIN B_6) AND SOME PHENOLIC COMPOUNDS IN APROTIC ORGANIC SOLVENTS

JAZREEN HUI QI LEE

School of Physical and Mathematical Sciences

A thesis submitted to the Nanyang Technological University

in partial fulfilment of the requirement for the degree of

Doctor of Philosophy

2016

This page has been intentionally left blank

Acknowledgments

Firstly, I would like to thank Nanyang Technological University (NTU) for awarding me with a Research Scholarship and for their financial support to attend an overseas conference.

My utmost gratitude also extends to my supervisor, Prof. Richard D. Webster, for his continuous support and guidance throughout my graduate studies and during the preparation of this thesis. My PhD was definitely also made an extremely enriching experience because of the countless opportunities provided by Prof. Webster to explore and learn many new and interesting concepts within the field of electrochemistry.

I would like to acknowledge my previous mentor, Prof. M. Senthilkumar, for bringing so much fun and laughter during my undergraduate days, and for giving his invaluable advice and encouragement to pursue a PhD.

My sincere appreciation is also conveyed to Dr. S. A. Pullarkat and Prof. D. Vidovic for imparting to me essential laboratory skills when I was an undergraduate student, and at the same time introducing me to the world of scientific research which also piqued my interest in it.

Many thanks to my fellow lab mates, Bahareh, Dejan, Diane, Gabriel, Gwen, Kwok Kiong, Maja, Malcolm, Novi, Raymond, Sherman, Serena, Sherli, Shu Jun, Yanni, Ya Yun, Ying Shang, and Xiuhui, for all the intriguing discussion and their help in one way or another. In addition, I am also grateful to Boon Kee, Yu Rong and Weiqi for all their invaluable hard work put into the projects. Special thanks to Kek Foo for his continuous help.

I also wish to thank the CBC administration and laboratory staff (Ai Hua, Celine, Charlene, Dr. Li Yongxin, Dr. Rakesh, Eeling, Janice Low, Lynette, Wen Wei, Yan Lin and Yean Chin) for their assistance and technical support during my stay in NTU.

Last but not least, my sincere gratitude goes out to my family for believing in me, and giving their constant support and understanding.

Contents

This page has been intentionally left blank

Abstract

Phenols are invaluable structural units found in a wide range of natural and artificial compounds, and have been used for numerous applications that are necessary for our daily lives. As a result, this has led to many remarkable papers on the voltammetric studies of this class of compounds.

In this thesis, the detailed redox chemistry of four phenolic and phenolic-type compounds, sesamol (Chapter 2), vanillin (Chapter 3), diethylstilbestrol (DES) (Chapter 4) and pyridoxine (PN) (Chapter 5) were investigated in acetonitrile (CH_3CN) solutions. As the four aforementioned compounds are food and/or food-related molecules, examination on the electrochemical pathways of these chemicals can provide information such as the number of electrons involved and the identities of the associated intermediates that may be useful in obtaining insights into the metabolic pathways partaken by these four molecules in the biological system and possibly relate to some of their proposed biological functions such as antioxidant properties. In addition, an aprotic organic solvent (CH_3CN) was used in this work since a search of literature reveals that majority of the electrochemical accounts of these compounds are documented in protic and/or aqueous media, with reports focusing on the aprotic system remaining less well-developed.

By means of a combination of various electrochemical techniques such as cyclic voltammetry (CV) and controlled potential electrolysis (CPE), and consistent with the behavior of a typical phenol, the compounds were generally found to undergo an electrochemical oxidation reaction, with some also exhibiting reduction phenomena. Using the electrochemical responses gathered, identities of the intermediates and products involved together with their mechanistic pathways were proposed.

In addition, it is worthwhile to highlight that phenols (e.g. the essential micronutrient vitamin E, α-tocopherol) have been demonstrated to be highly sensitive to the presence of trace amounts of moisture, such as by actively participating in hydrogen bonding interactions. As such, the effect of low levels of water on the electrochemical behavior of the aforementioned compounds were also examined. In particular, the voltammetric profiles of sesamol and vanillin were found to be affected by the presence of moisture, whereby their respective oxidation peak potentials were generally found to shift towards more negative potentials as the water content was increased.

This page has been intentionally left blank

Abbreviations and Symbols

BPA	Bisphenol A
Bu_4NPF_6	Tetrabutylammonium hexafluorophosphate
Bu_4NOH	Tetrabutylammonium hydroxide
C step	Chemical step
CH_3CN	Acetonitrile
CPE	Controlled potential electrolysis
CV	Cyclic voltammetry
DES	Diethylstilbestrol
DMF	*N*,*N*-dimethylformamide
DMSO	Dimethyl sulfoxide
E^o	Formal potential
E_p^{ox}	Oxidative peak potential
E_p^{red}	Reductive peak potential
E_{pp}	Peak to peak potential separation
E step	Electrochemical step
EPR	Electron paramagnetic resonance
Fc/Fc^+	Ferrocene/Ferrocenium redox couple
GC	Glassy carbon
h	Hour (time)
HPF_6	Hexafluorophosphoric acid
i_p^{ox}	Oxidative peak current
i_p^{red}	Reductive peak current
k_b	Backward rate constant

K_{eq}	Equilibrium constant
k_f	Forward rate constant
k_s	Heterogeneous electron transfer rate constant
M	Molar (concentration)
min	Minute (time)
mM	Millimolar (concentration)
mV	Millivolts
$NOSbF_6$	Nitrosonium hexafluoroantimonate
NMR	Nuclear magnetic resonance
PN	Pyridoxine
s	Second (time)
V	Volts
^oC	Degree centigrade
α	Transfer coefficient

List of Publications

1. Chapter 2

Lee, J.H.Q.; Tay, B.K.; Ganguly, R.; Webster, R.D., The Electrochemical Oxidation of Sesamol in Acetonitrile Containing Variable Amounts of Water. *Electrochim. Acta* **2015**, 184, 392–402.

2. Chapter 3

Lee, J.H.Q.; Lauw S.J.L.; Webster, R.D., The Electrochemical Study of Vanillin in Acetonitrile. *Electrochim. Acta* **2016**, 211, 533–544.

3. Chapter 4

Lee, J.H.Q.; Koh, Y.R.; Webster, R.D., The Electrochemical Oxidation of Diethylstilbestrol (DES) in Acetonitrile. *Manuscript in preparation.*

4. Chapter 5

Lee, J.H.Q.; Yue, Y.; Ganguly, R.; Webster, R.D., Electrochemical Study of Pyridoxine (Vitamin B_6) in Acetonitrile. *ChemElectroChem* **2015**, 2, 412–420.

5. Chapter 6

Lee, J.H.Q.; Lauw S.J.L.; Webster, R.D., The Electrochemical Reduction of Carbon Dioxide (CO_2) to Methanol in The Presence of Pyridoxine (Vitamin B_6). *Electrochem. Commun.* **2016**, 64, 69–73.

This page has been intentionally left blank

Chapter 1

Phenolic Compounds

This page has been intentionally left blank

1.1. Introduction to Phenols

1.1.1. Background

Phenols are common structural groups found in a plethora of natural and synthetic molecules, with selected examples illustrated in Scheme 1.1, which include plant-derived chemicals such as sesamol, vanillin, vitamin E (tocopherols and tocotrienols), hydroxycinnamic acids, and man-made complexes like bisphenol A (BPA) and diethylstilbestrol (DES). Due to their wide occurrence in a myriad of compounds, phenols and their derivatives are typically used as building blocks in organic synthesis, as well as in commercial materials that are employed in various areas including the food, plastics (phenolic resins), and pharmaceutical industries. Not surprisingly, this class of compounds are readily found in a diverse array of consumer and household products such as beverages, antiseptic agents, electrical devices, insecticides, dyes, surfactants, lubricants, substrates for medical drugs such as aspirin, and others.

1.1.2. Origin of phenols

As a component present in coal tar, phenol was first partially isolated by Runge et al. in 1834, and was successfully crystallized in 1841 by a French chemist Auguste Laurent, who also initiated the name phène for benzene and described phenol as the hydrate of phène. The term phènol only arose later in 1843 when phenol was formed by the heating of salicylic acid with lime in 1843. Since then, the development of phenol and discovery of its many other analogues became actively pursued [1].

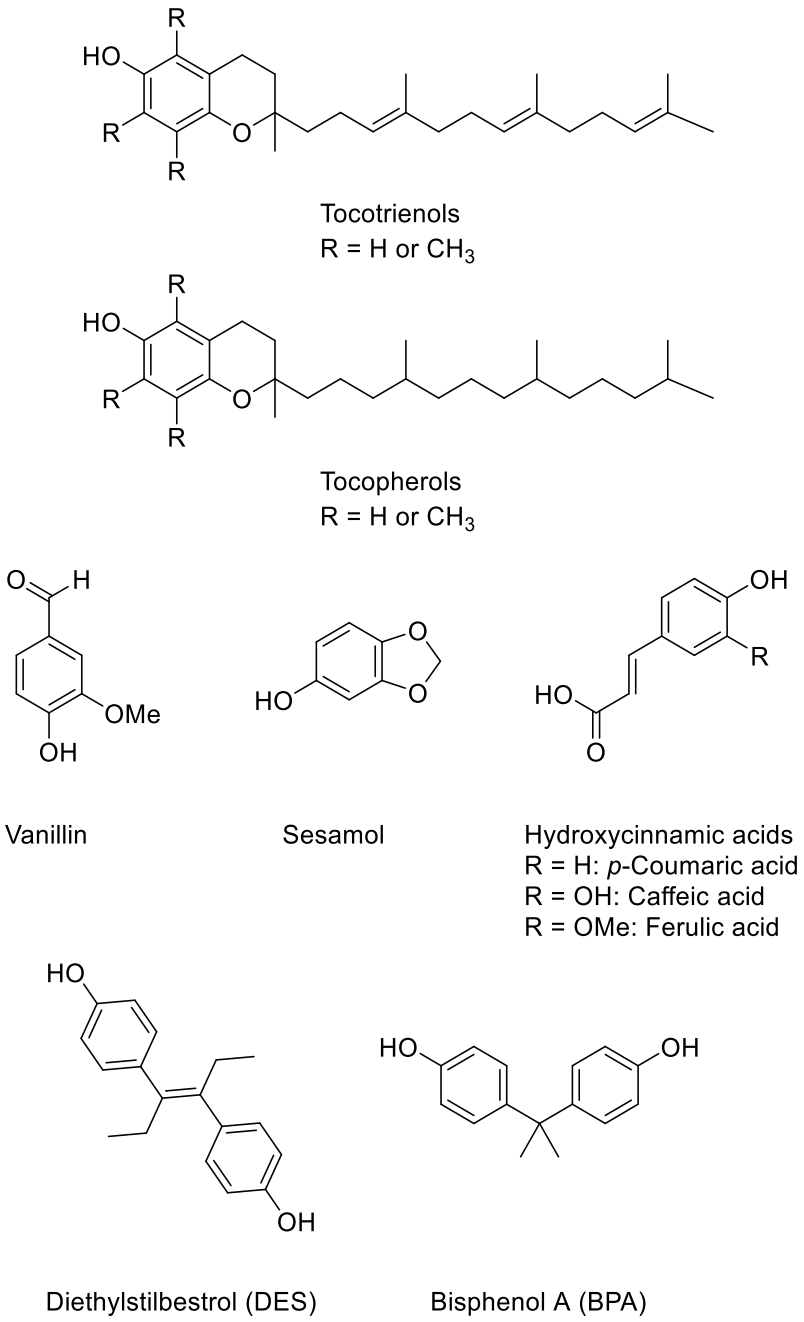

Scheme 1.1. Selected examples of phenolic compounds.

1.1.3. Functions and applications of phenols

Similarly bearing the hydroxybenzene moiety, it is intriguing to observe dual properties in phenolic compounds, with some (e.g. sesamol [2-4], vanillin [5-7]) functioning as antioxidants that aid in reducing oxidative degradation caused by free radical species, while others (e.g. BPA, DES) are being regarded as endocrine disruptive chemicals which interfere with

endogenous hormone levels, and are consequently associated with various pathologies like hepatoxicity, carcinogenicity, cardiovascular diseases, and genital malformations [8-11]. Owing to its labile hydrogen, the desirable antioxidant characteristics of phenolic compounds are mostly attributable to the reaction of its readily abstractable hydrogen atom with free radicals that suppress lipid peroxidation in biological and food systems, with vitamin E as an illustrative example [12-14]. By taking advantage of this beneficial property, phenol-containing compounds are often used as food additives and in dietary supplements.

1.1.4. Electrochemical oxidation of phenols

In view of the biological importance and versatile applications of phenols (and their derivatives), it is not unexpected that the electrochemical study of their anodic transformations are extensively reported. As depicted in Scheme 1.2, in aprotic organic media, phenols can undergo oxidation via an ECE sequence, where E and C denote an electrochemical and chemical step respectively, to form a reactive diamagnetic cation [15-17].

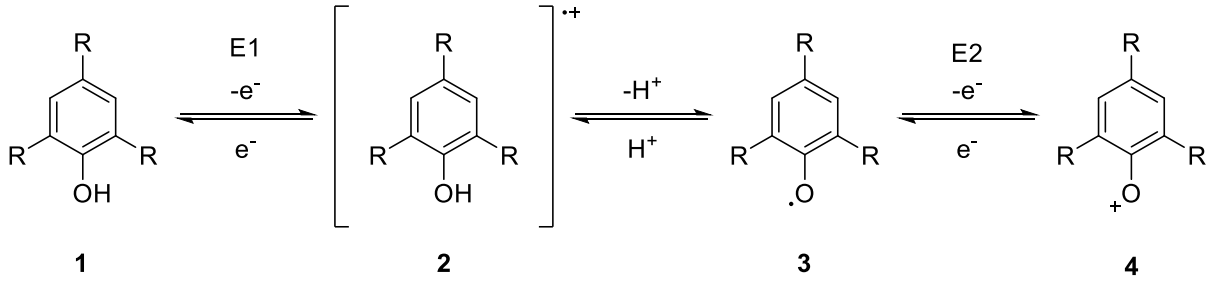

Scheme 1.2. Proposed ECE mechanism for the electrochemical oxidation of phenol. For simplicity, only one resonance structure is displayed.

Typically, the extraction of an electron from a compound (oxidation) would tend to weaken a chemical bond within the molecule, thereby making the species more acidic than its parent. Hence, the cationic radical product **2** formed after the initial one-electron oxidation of phenol will readily deprotonate to deliver a neutral phenoxyl radical (compound **3**). Following which,

as the second oxidation potential (E2) occurs at a lower oxidation potential than the first electron transfer step (E1) (E1 > E2), the phenoxyl radical will immediately undergo a second electrochemical process, affording the cationic phenoxonium ion (compound **4**). Notably, because the phenoxyl radical is easier to oxidize than its associated phenol (E1 > E2), a single two-electron voltammetric wave is observed instead of two sequential one-electron oxidation steps [18-21].

However, it is possible that instead of the second oxidation step occurring at the electrode-solution interface (heterogeneous process), the same product can also be formed by the homogenous reaction of compounds **2** and **3** via disproportionation (DISP) mechanism, and as such it is sometimes very difficult to distinguish between the two different pathways [15-17].

Nevertheless, the diamagnetic phenoxonium ion (compound **4**) generated is usually highly reactive, with few instances of very stable and long-lived cation, of which an example is the oxidized form of α-tocopherol (a fully methylated tocopherol) which was disclosed to exhibit long lifetimes in very dry acetonitrile [18, 20, 22-24]. Being highly electrophilic, the phenoxonium cation can readily react with nucleophiles that are present in the electrolyte or solvent such as water. Also, the cation can engage in other follow-up homogenous processes like coupling reactions or dealkylation, depending on the nature of the functionality on its 2-, 4-, 6-positions [15-17, 25].

1.1.5. Effect of water on the electrochemical behavior of phenols

Trace water is an ubiquitous impurity present in all organic solvents and understanding its effect on the electrochemistry of redox active compounds is important because it can sometimes cause significant changes to their voltammetric behavior due to several possible interactions with the substrate such as hydrolysis (which is often chemically irreversible) and hydrogen bonding (which is chemically reversible) [26-33]. This is all the more so given the low concentrations of analyte used in typical electrochemical measurements, thus making low levels of moisture present in the sample solution critically important.

While it is essential to reduce such inferences in voltammetric measurements, it is often challenging to completely exclude water in a typical electrochemical experiment unless it is performed in a strictly controlled environment such as inside a glovebox [34]. Moreover, other possible sources of water can arise from the chemicals/reagents used such as the solvents and supporting electrolyte. Other possible contributors include limitations imposed by the multiple ports in the electrochemical cells, the use of a reference electrode comprising of its own internal filling solution and the regular requirement of removing and polishing of the working electrode after every measurement [29, 34, 35].

Phenols have been well-documented to participate in hydrogen bonding [36]. For instance, it has been shown that the rate of reaction between phenols with reactive free radicals is affected by the kinetics of hydrogen bonding between the former and the surrounding solvent molecules, which can consequently alter their antioxidant properties [37-40]. One approach to gaining insights on the hydrogen bonding of phenols is to control the amount of water present in organic solvents, which requires the use of Karl Fisher coulometric titrations to accurately measure the water content.

The effect of water on the voltammetric behavior of phenols has been previously described by Webster and co-workers [30, 32]. In these accounts, it was found that the oxidation potentials of phenolic compounds generally shifted to less positive potentials with increasing water content. This phenomenon was reasoned to be due to weak hydrogen bonds that were formed between the hydroxyl functional group of the phenolic substrates with water. Owing to this interaction, the phenolic oxygen-hydrogen bond is surmised to be weaken, which then confers the phenols some phenolate anions characteristics; including the ability to oxidize much more easily than its corresponding (non-hydrogen bonded) phenols. This premise was supported by computational work that showed longer oxygen-hydrogen bond length (and thus weaker bond strength) for phenols with higher degree of hydrogen bonding [32].

1.1.6. Scope of thesis

In this thesis, detailed examinations on the redox chemistry of four electroactive phenolic and phenolic-type compounds, sesamol, vanillin, diethylstilbestrol and pyridoxine (Scheme 1.1), were performed. Additionally, the influence of water on the electrochemistry of these compounds are disclosed.

The abovementioned chemicals were selected with the purpose of covering structurally-varied types of molecules, namely food (sesamol and vanillin), vitamin (pyridoxine) and contaminant (diethylstilbestrol), of which the first two groups originate from natural or food sources while the latter is an artificial complex. As these compounds are consumed by humans, the obtained knowledge may serve in unravelling information on their roles, and in vivo transformations inside the biological systems.

1.2. Introduction to Sesamol

1.2.1. Background

Although sesame is considered as one of the oldest crops in the world, its exact origin remains uncertain, and it is often believed to have originated from Africa, since the flowering plant family Pedaliaceae that sesame belongs to, is comprised of many other genera that are derived from Africa [41]. Notwithstanding, there are also indications on the record of sesame as an oil crop harvested in Babylon and Assyria nearly 4000 years ago [42].

Today, with an annual production of approximately 3 million tons, sesame is cultivated in many regions such as Asia, Africa, Central and South America, with Asia constituting as one of the major manufacturers that contributes up to 50% of the world's sesame production. The high demand for sesame can be ascribed to its many beneficial effects such as anti-inflammatory [4, 43-45], anti-microbial [46, 47], anti-mutagenicity [2-4] properties, and in particular, its superior resistance to oxidative degradation as compared to other dietary oils [48-50] (e.g. groundnuts and sunflower oil) which also renders it useful in the treatment of oxidative stress associated health problems [48, 51-53]. Hence, it is not surprising that sesame is employed widely for various industrial applications like food, chemical, cosmetic, and medical uses which include numerous consumer goods such as perfumes, soap, confectionary, mouthwash, insecticide, among others [54, 55].

Comprising of a large proportion (50-60%) of oil, the sesame seeds can either be sold directly in its seed form or processed into oil and meal, where the latter is a protein rich compound remaining after oil extraction, and is frequently used as animal feed [56]. The sesame fruits are typically made up of pubescent and oblong-shaped capsules which contains numerous sesame

seeds that are ovate, small and can exist in varying colors such as white, brown, and black, with the assorted seed colors reported to have different free fatty acid contents [57].

1.2.2. Functions and applications of sesamol

One of the constituents contributing to the desirable characteristics of sesame is sesamol (3,4-methylenedioxyphenol, Scheme 1.3) [58-62], a fat soluble aglycon lignan that is typically found in roasted sesame seed oil [63-65]. Bearing a phenolic functionality, sesamol is able to function as a free radical quencher by transferring its labile hydrogen atom to reactive radical species [60, 66-68]. This enables sesame to be less susceptible to free radical induced oxidation reactions in food systems, which increases the foods' shelf life and stability and also curtails rancidity and the possible formation of deleterious food by-products [69]. Additionally, other therapeutic benefits of sesamol include hepatoprotection [70, 71], neuroprotection [72, 73], anticarcinogenicity [74, 75], anti-inflammatory [76, 77] and anti-mutagenicity [78].

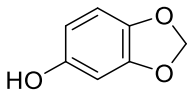

Scheme 1.3. Chemical structure of sesamol.

1.2.3. Studies on sesamol

Significant interest has been received on the antioxidant ability of sesamol as demonstrated by the extensive research into the evaluation of its efficiency in scavenging free radicals such as DPPH radicals [60, 68, 79]. In the context of these ongoing efforts, besides pursuing the radical quenching capability of sesamol, one less well-explored approach is the examination on the toxicity of its oxidative products generated [80-82]. In order to mimic oxidative products that can possibly be produced in food and relevant systems, in these reported studies, sesamol was subjected to an iron-catalyzed oxidation reaction where several products were isolated and

identified, of which selected examples are displayed in Scheme 1.4 [80]. Unfortunately, these products were found to exhibit adverse effects when tested for their cytotoxicity on rat thymocytes. Furthermore, as compared to other well-recognized antioxidant phytophenols, which include caffeic acid, catechin, and rosmarinic acid, the oxidative products generated from sesamol demonstrated a markedly higher cytotoxicity activity [81].

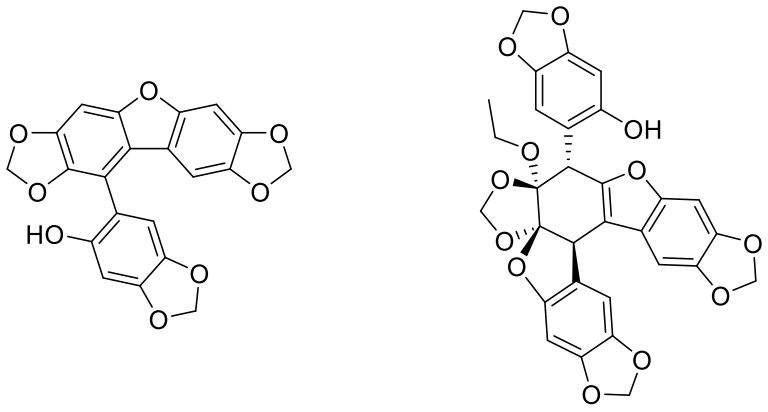

5 **6**

Scheme 1.4. Selected examples of oxidative products of sesamol. (**5**) Sesamol trimer (**6**) Sesamol tetramer (adapted from ref. [80]).

In light of the abovementioned information, voltammetry can be offered as an alternative technique which enables the generation of the oxidative product as well as be used for the analysis of the intermediates involved in the oxidation transformation. Moreover, electrosynthetic methods such as preparative scale electrolysis also allows the separation and isolation of the final oxidation product(s).

1.2.4. Electrochemical studies of sesamol

Due to its diverse biological importance, studies that have focused on the detection of sesamol from sesame oil have been extensively reported [83-86]. In comparison, however, in depth electrochemical mechanistic reports on sesamol remain sparse [87, 88], and has been limited to two literature works which were both directed towards aqueous and/or protic media. Some similarities were disclosed in both accounts, in which a ring-opened structure was postulated to be generated upon the electrochemical oxidation of sesamol via similar mechanistic pathways [87, 88], albeit slight differences in the identities of the oxidation intermediates and final product.

In an earlier work by Shiragami et al., it was delineated that a chemically irreversible oxidation peak was observed on the forward scan of the cyclic voltammogram of sesamol in a 1 M sulfuric acid solution, in conjunction with a separate reduction peak seen on the return scan which upon continuous cycling resulted in the observation of its corresponding anodic peak. After further exploration of the analyte, the initial oxidation peak was posited to involve a two-electron ($-2e^-$) oxidation, affording a hydroxyhydroquinone, which can subsequently undergo reduction to generate a benzene-1,2,4-triol. The new anodic peak observed on the second scan was then reasoned to be the oxidation of the triply hydroxylated product back to the hydroxyhydroquinone (Scheme 1.5) [87]. This mechanistic premise was substantiated by the close agreement of the obtained voltammogram of sesamol with that of a model compound, hydroxyhydroquinone, conducted under similar conditions. In addition, the cleavage and demethylenation of the methylene-dioxy functional group was suggested to plausibly occur due to the large supply of hydroxonium ions provided by the strongly acidic media.

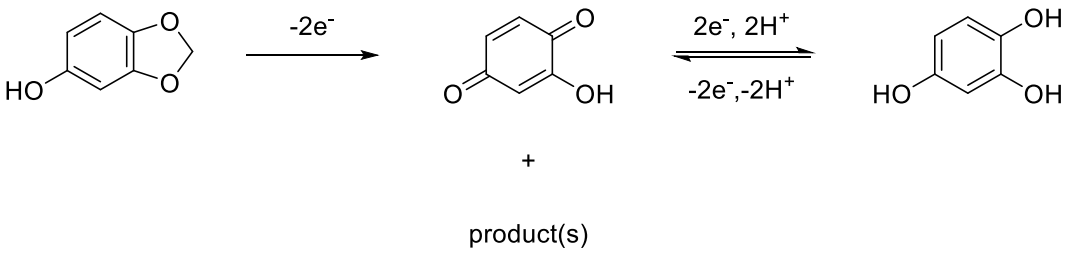

Scheme 1.5. Proposed electrochemical oxidation of sesamol in 1M sulfuric acid solution (adapted from ref. [87]).

On the contrary, in a more recent study conducted using a glassy carbon electrode in an aqueous system, sesamol was observed to give two oxidation peaks on the forward sweep (instead of one oxidation peak, as described in the initial study discussed above) and when the scan direction was reversed, a cathodic peak was recorded, together with its corresponding anodic peak which could be seen on the second cycle. However, the second anodic peak seen on the forward scan appeared at a potential too close in proximity to the end of the solvent's potential window, thereby making its analysis difficult. As such, only the first oxidation process was investigated [88].

In this case, sesamol was suggested to undergo a two-electron/one-proton ($-2e^-/-H^+$) oxidation in the first oxidation process to form a cationic substituted 1,4-benzoquinone which subsequently undergoes hydrolysis to generate 2-(hydroxymethoxy)-1,4-benzoquinone (Scheme 1.6) [88]. This resultant substituted 1,4-benzoquinone was further reduced via a two-electron/two-proton ($2e^-/2H^+$) addition to form its corresponding substituted 1,4-hydroquinone, along with the observation of the anodic peak on the second cycle of the voltammogram assigned to the oxidation of the substituted 1,4-hydroquinone back to its 1,4-benzoquinone form.

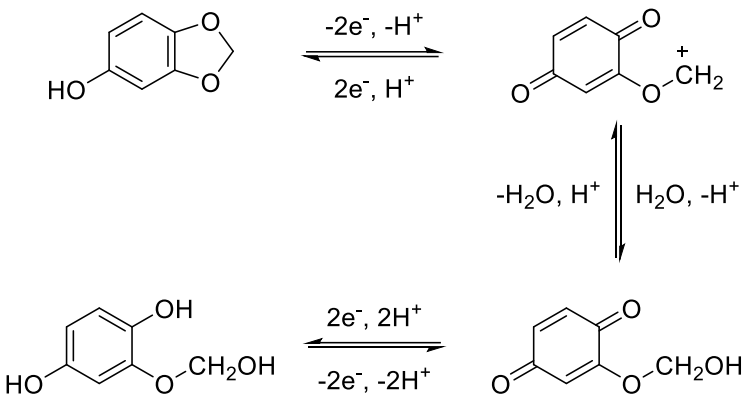

Scheme 1.6. Proposed electrochemical oxidation of sesamol in an aqueous solution (adapted from ref. [88]).

1.3. Introduction to Vanillin

1.3.1. Background

Vanilla is a prevalent flavoring agent that is used extensively in the food, fragrance and pharmaceutical industries. Found originally in Mexico, vanilla was initially used by the natives, the Aztecs, as flavoring for their drinks. Following the Spanish colonization of the Aztec empire (in 1520), vanilla was subsequently introduced to the European countries, and since then, vanilla has been widely cultivated in various parts of the world such as Madagascar, India, Indonesia, amongst others [89, 90].

Naturally, vanilla can be derived from the beans or pods (fruits) of the vanilla orchid which belongs to the family Orchidaceae. While the majority of orchids are grown for their ornamental flowers, vanilla is the only orchid genus comprising of species that can bear fruits for profitable use. Out of the 110 species present in the vanilla genus, three of the species *Vanilla planifolia*, *Vanilla tahitensis* and *Vanilla pompona* are commonly used for commercial production, and as compared to the others, the flowering plant *Vanilla planifolia* is more well-received due to its superior pods' quality, flavor and yield [89-91].

Among the numerous components present in the vanilla extract, vanillin (4-hydroxy-3-methoxybenzaldehyde, Scheme 1.7) makes up its chief constituent and is responsible for imparting vanilla its flavor [89, 92-94]. Hence, it is unsurprising that more than 12,000 tons of vanillin are manufactured annually [89]. However, the production of vanillin via the conventional cultivation methods are often labor-intensive, slow, costly, and with only ca. 1.5 to 2.5 % w/w of vanillin present in the vanilla beans. Therefore, owing to the limitations of traditional cultivation, less than 1% of the global production of vanillin originates from natural

means [89, 92], and to keep up with the high demand, synthetic methods such as the chemical [95-97] and biotechnological [98-100] approaches continue to be highly sought after.

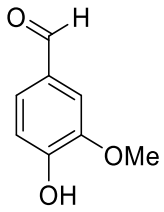

Scheme 1.7. Chemical structure of vanillin.

1.3.2. Functions and applications of vanillin

Besides playing a key role in contributing to the distinct aroma and flavor of vanilla, vanillin is also valued for having other beneficial properties such as antioxidant [6, 7, 101], anti-inflammatory [102, 103], antimicrobial [104-106] and corrosion inhibitory [107-109] effects. Exploiting these diverse range of useful qualities, vanillin is widely used in the food, chemicals and pharmaceutical industries for the manufacture of various consumer products such as confectioneries, beverages, candies, perfumery, air-fresheners, food preservatives, anti-bacterial, anti-foaming agents, herbicides, and as intermediate in the synthesis of drugs like L-dopa, methyl dopa and papaverine [90, 110].

1.3.3. Studies on vanillin

Following the vast utility of vanillin in numerous food products as a flavoring agent, increasing concerns has been gained regarding the stability of vanillin in food compounds, its interaction with other food components such as enzymes and proteins, and the corresponding effect on the flavor. For instance, vanillin was found to undergo an oxidative decomposition process to generate vanillic acid in fresh and pasteurized milk samples, likely attributable to the presence of the milk enzymes (Scheme 1.8) [111]. This oxidation product was similarly observed in a

separate enzymatic study of vanillin using guinea pig liver slices containing the metabolizing enzyme, aldehyde oxidase [112]. In addition, both accounts have demonstrated that such chemical degradation reactions resulted in the loss of vanillin, thereby resulting in a decrease in vanillin concentration.

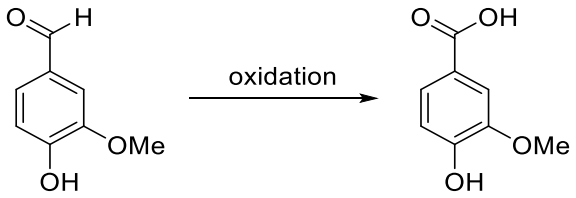

Vanillin Vanillic acid

Scheme 1.8. Proposed enzymatic oxidation of vanillin to vanillic acid (adapted from ref. [111]).

Another target of interest for food and flavor scientists is the interaction of vanillin with proteins as it can influence the perception of the flavor, lower its intensity and possibly distort the flavor profile of the food products. Vanillin has been documented to be able to bind with soy (plant milk) protein as well as proteins derived from animal products such as casein, whey, bovine serum album through various modes like hydrogen bonding, hydrophobic interaction and Schiff base formation, where the latter occurs via the condensation of the aldehyde functionality of vanillin with the amine groups of proteins (Scheme 1.9) [113-116]. Owing to these interactions, a reduction in the intensity of the vanilla flavor has been reported [117, 118], making knowledge gained from the understanding of food matrix useful in minimizing the potential loss of vanillin by disrupting the formation of such binding forces.

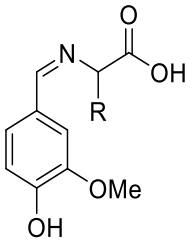

Scheme 1.9. Chemical structure of Schiff base vanillin.

Since vanillin has been established to undergo oxidation reactions in food products, voltammetry can be used as an accessible technique in examining this redox process in further detail. In addition, even though water is usually present as an ingredient in many food products, its interaction with vanillin has yet to be investigated, and as water has been shown to exhibit hydrogen bonding abilities, the information extracted from the study of vanillin with water might aid in supplementing existing knowledge of such interactions.

1.3.4. Electrochemical studies of vanillin

Besides seeking information regarding the complex matrices present in vanillin-flavored food systems, various analytical techniques (e.g. gas chromatography [119, 120], high performance liquid chromatography [121, 122], capillary electrophoresis [123, 124]) have also been actively used to assess the quality and content of vanillin in vanilla extracts, food products and batch samples during the manufacturing processes.

In particular, a diverse array of electrochemical works on devising sensors for vanillin detection have been disclosed over the years [125-129], with most of these accounts relying on the direct electrochemical oxidation of vanillin in protic solutions (Scheme 1.10) [125-128]. Generally, the cyclic voltammograms of vanillin showed an anodic peak on the forward scan of the CV which is associated with the loss of two-electron/one-proton ($-2e^-/-H^+$), and a separate cathodic wave on the return sweep (along with its corresponding oxidation peak seen on the subsequent

cycle) which was assigned to the reduction of the 1,2-benzoquinone unit (compound **9**) (and oxidation of its corresponding catechol-based product, compound **10**) that is formed after hydrolysis at the 2-methoxy group.

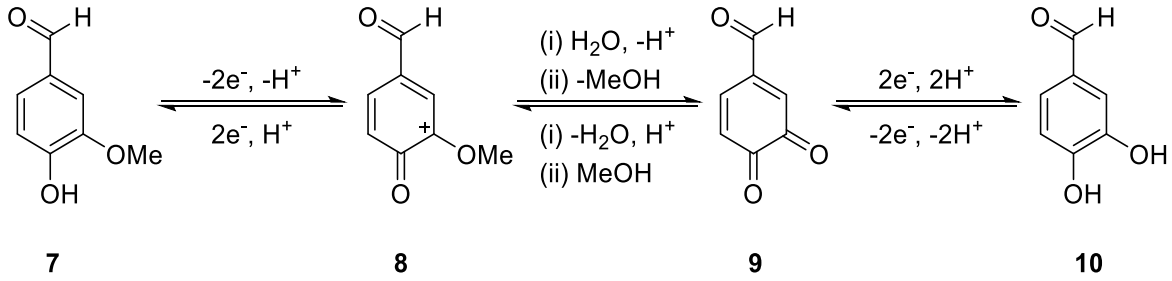

Scheme 1.10. Proposed electrochemical oxidation of vanillin (adapted from ref. [125-128]).

Similarly, this oxidative mechanism was proposed for other *ortho*-methoxy phenols which include eugenol, guaiacol and capsaicin, when investigated under aqueous conditions [126, 130].

In contrast, however, fewer reports have been focused on investigating the electrochemical reduction behavior of vanillin, where majority of the studies were conducted in protic systems (e.g. aqueous solution). In these articles, the formation of vanillyl alcohol (Scheme 1.11) was postulated [131, 132], along with the assessment of the effects of various parameters such as pH, temperature and electrode materials (e.g. copper, lead, zinc) on the cathodic process. On the other hand, results recorded in the less well-explored aprotic solvent revealed the presence of two reduction peaks in *N*,*N*-dimethylformamide (DMF), of which the latter electron transfer reaction was observed at a potential very close to that of the background cathodic processes. Further examination of the first reduction process suggests the possible involvement of a dimerization reaction following the initial one-electron reduction of vanillin [133, 134].

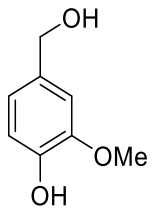

Scheme 1.11. Chemical structure of vanillyl alcohol.

1.4. Introduction to Diethylstilbestrol (DES)

1.4.1. Background

Once considered as a useful drug for the treatment of several gynecologic conditions, diethylstilbestrol (DES, Scheme 1.12), a synthetic estrogen, was extensively used due to its ability to elicit similar biological functions as natural estrogen hormones.

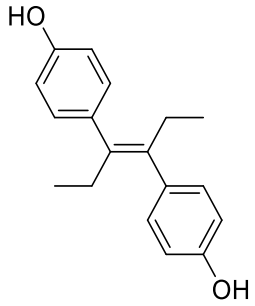

Scheme 1.12. Chemical structure of Diethylstilbestrol (DES).

Identified and synthesized in 1938, DES was first introduced as a drug, administered to prevent complications of women with high-risk pregnancy [135, 136]. Encouraged by the positive results provided by this initial study, further exploitation of this compound was extended into estrogen deficiency treatments for other pregnancy and miscarriages-related conditions. Therefore, from 1945 to 1971, DES was prescribed to an estimate of five million pregnant women in the United States for administration in various forms which include pills, vitamins, shots, and suppositories [137-141].

Throughout this period, the efficacy of DES was questioned but disregarded [8, 142], and it was only until 1971 that the first major adverse health effect of DES was revealed [143]. Included in this account were findings showing vaginal clear cell adenocarcinoma (CCAC) in female patients, whose ages ranged between 15 to 22, and have mothers whom had previously consumed DES. Furthermore, the gravity of this result was demonstrated by the fact that this

form of vaginal cancer was rarely seen in women younger than 50 years old before the introduction of DES. Subsequently, this was followed by many other reports of genital abnormalities found in children (both male and female) who are exposed to DES in utero [137-141]. As such, the use of DES for miscarriage prevention was banned by the Food and Drug Administration in 1971. Eventually, in 1997, the production of DES was ceased in the United States [137-141].

1.4.2. Studies on DES

Further exacerbation of the deleterious effects associated with DES were shown by its use as growth promoters in meat-producing animals in order to improve on the feed conversion efficiency [144-146]. Due to the wide usage of DES, this has also led to numerous studies conducted on the cumulative effects of DES on affected women and their offspring (exposed prenatally) [137, 138, 141, 147, 148], its mode of mechanism in the human bodies [140, 141, 149, 150], and the control and monitoring of its illegal usage in livestock [151-153] and their derived food products (e.g. milk) [154-158]. Hence, it is not surprising that research into various analytical methods (e.g. high performance liquid chromatography [155, 158], gas chromatography-mass spectrometry [152, 153, 159], chemiluminescence [160]) for the fast and accurate detection of DES in food products, patients' biological matrices (serum, blood, urine) has also been actively pursued in recent years.

1.4.3. Electrochemical studies of DES

While the sensitive determination of DES has led to the development of a number of impressive works [161-164], those that have focused on the electro-mechanistic study of its redox behavior have remained sparse [165-168]. In these accounts which were conducted in aqueous solutions, DES was established to undergo an electro-oxidation reaction, however with some uncertainty about the mechanistic pathways and intermediates involved.

Generally, DES was disclosed to oxidize through a two-electron/two-proton ($-2e^-/-2H^+$) process, giving rise to 4',4''-diethylstilbestrol (DES) quinone [165-168]. While the formation of 4',4''-diethylstilbestrol (DES) quinone during the oxidation of DES are agreed in these works, one particular report posited that the quinone species behaves as an intermediate (instead of being the final oxidation product) and can undergo further tautomerization and rearrangement of the molecule to afford a different eventual anodic product, Z,Z-dienestrol (Scheme 1.13) [165] .

Notably, the proposed mechanism outlined in Scheme 1.13 is similar to that of the oxidative metabolism pathway postulated during the in vivo transformation of DES, with the Z,Z-dienestrol product being identified as a metabolite found in hamster, rat and human urine [169-172].

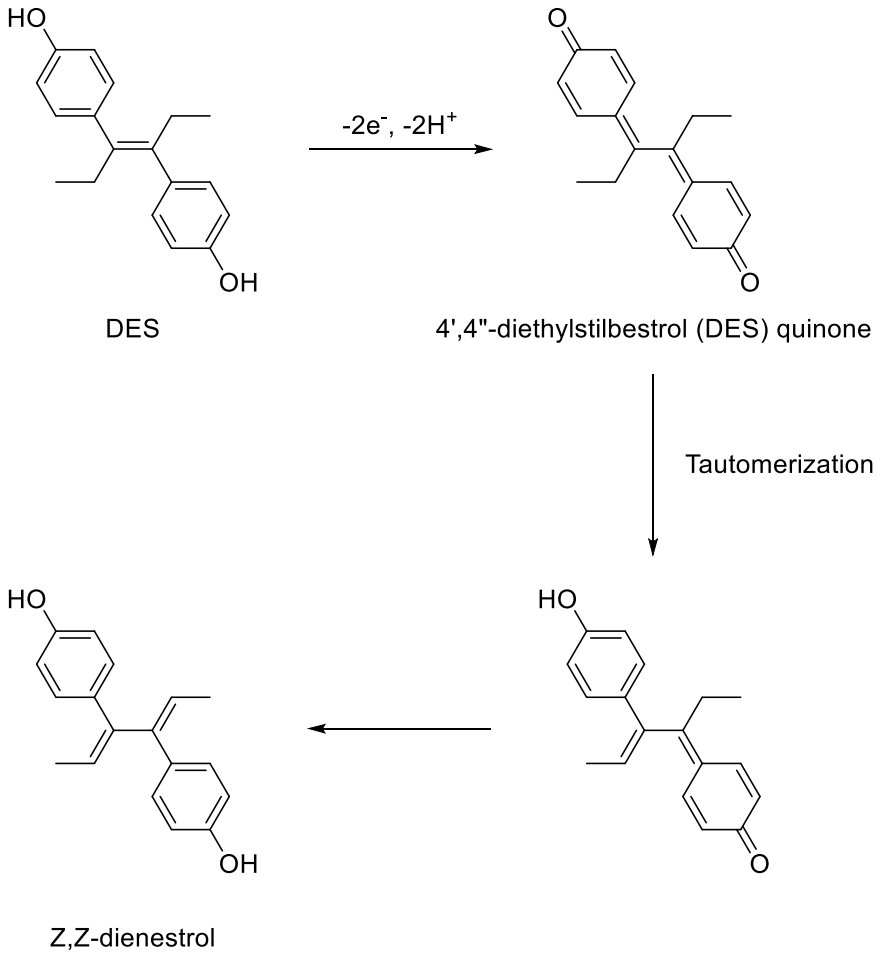

Scheme 1.13. Proposed oxidative mechanism of Diethylstilbestrol (DES) (adapted from ref. [165]).

1.4.4. Bisphenol A (BPA), a structurally-similar compound to DES

Bisphenol A (BPA, Scheme 1.14), a monomer that is extensively used in the production of plastics and epoxy resin, has likewise received increased attention due to its implication with numerous health problems [173-176]. Consequently, this has also led to the outlaw of BPA in consumer products like baby bottles in countries and territories such as the European Union, Canada and by the Food and Drug Administration agency in the USA.

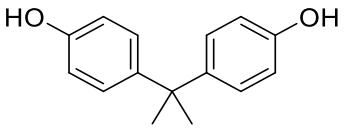

Scheme 1.14. Chemical structure of Bisphenol A (BPA).

Interested in uncovering information regarding the possible metabolic reactions that BPA can undergo, our group had previously delineated the electrochemical study of BPA in aprotic organic solvents and its associated redox transformations [177]. Besides being structurally similar compounds (both are bi-phenolic compounds linked by an alkyl bridge), BPA and DES are also well-established endocrine disruptors [9-11] that are known to interfere with normal hormonal activities. In a continuous effort to examine the redox properties of synthetic phenolic compounds that have raised concern regarding their potential toxicity, we envisaged an electrochemical study on the oxidation of DES, a chemical which is less well explored mechanistically.

Being a lipophilic molecule, with a log K_w value of 4.12 [178], DES is rationalized to reside in hydrophobic tissues in the biological system such as within the cavity of the ligand binding domain (LBD) of the estrogen receptor (ER) [140, 179]. Hence, it would be worthwhile to conduct the abovementioned electrochemical study of DES in aprotic solvent, an environment of low moisture content.

1.5. Introduction to Pyridoxine (PN)

1.5.1. Background

VB_6 is an essential micronutrient which plays a vital role in the sustenance of normal cellular functions, development and growth. Structurally, the VB_6 family is comprised of a 2-methyl-3-hydroxy-5-hydroxymethyl-pyridine skeleton, and consists of six analogous forms. The primary vitamers are pyridoxine (PN), pyridoxal (PL), pyridoxamine (PM), which vary from one another by the substituent on the C-4 position, with their respective phosphate derivatives making up the remaining three members; pyridoxine-5'-phosphate (PNP), pyridoxal-5'-phosphate (PLP), and pyridoxamine-5'-phosphate (PMP) (Scheme 1.15).

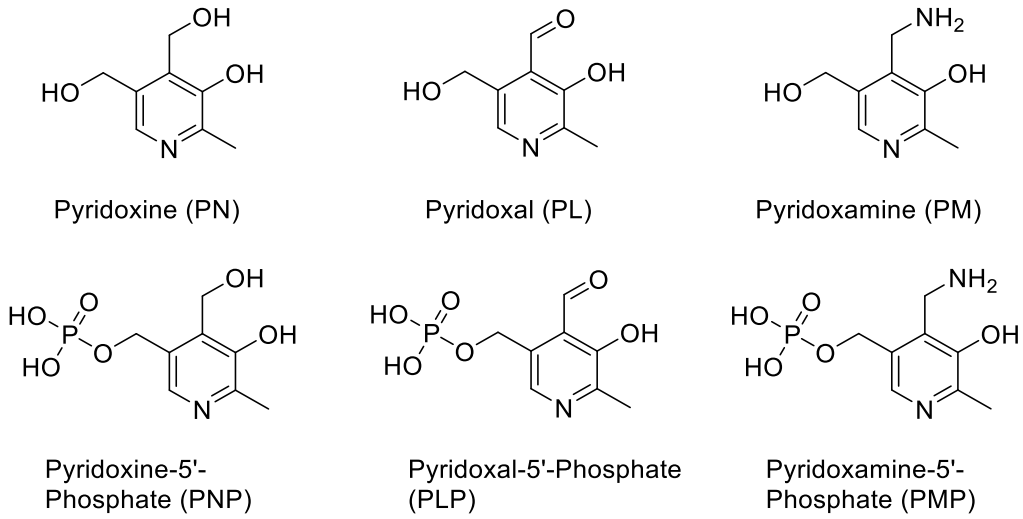

Scheme 1.15. Chemical structure of the different vitamers of vitamin B_6.

The importance of this class of vitamin is exemplified by its involvement in over 100 enzyme-catalyzed reactions in the human body, including amino acid metabolism [180], glycogen phosphorylation [181-183], modulation of steroid receptors [184], and transsulfuration processes [185-187]. Additionally, VB_6 has also been reported to exhibit antioxidant properties based on its ability to efficiently scavenge reactive oxygen species such as singlet oxygen [188-

191], superoxide [192-194], and hydroxyl radicals [195]. In particular, PN was found to be the most efficient singlet oxygen radical quencher, with quenching rates comparable to that of vitamins C and E [188].

1.5.2. Dietary sources and requirement of vitamin B_6

The recommended dietary allowance for VB_6 is approximately 1.3 to 1.7 mg/day for an average adult and ≤ 1.2 mg/day for a child, with the dosage varying according to age, gender, and level of physical activity. These requirements can be fulfilled by the intake of VB_6 from a wide variety of food of both plant and animal origin. In animal-derived food, which includes pork, chicken, beef, fish, and in particular organ meats, where VB_6 exits mainly as PLP, due to its large storage in the animals' muscle where the glycogen phosphorylation process takes place [196, 197]. On the other hand, PN and PNP are the major forms of VB_6 found in plant foods and examples include whole grains and whole wheat related food products, along with fruits and vegetables. Due to the numerous metabolic processes involving VB_6, deficiency in VB_6 can cause deleterious health problems such as depression, anaemia, or even permanent nerve damage while high doses can also cause adverse health effects like neurophysiological abnormalities [196, 197].

1.5.3. Origin of PN

PN was the first to be discovered amongst its counter-parts, and this revelation gave rise to the term vitamin B_6 in 1934 by György et al. during his study on the symptoms of pellagra in rats, a dermatitis condition proposed to be caused by vitamin deficiency [198]. For this reason, VB_6 is sometimes also used synonymously as PN. Thereafter, this impressive finding led to the isolation of pure crystalline PN (in 1938) [199] and its subsequent structural determination in 1939 [200].

1.5.4. Metabolism of PN

PN is often used in parenteral nutrition, vitamin supplements, and fortified foods as an alternative source of VB_6. Upon the consumption of PN, absorption of the vitamin will readily occur in the jejunum, and is later transported to the liver, where core VB_6 metabolic processes take place. In the liver, PN is readily phosphorylated to PNP by the enzyme pyridoxal kinase, and in the presence of zinc and adenosine triphosphate (ATP) which functions as a cofactor and phosphoryl donor respectively. After which, PNP is further transformed into PLP, which then serves as the fundamental basis for all co-enzymatic functions of VB_6 [201-204]. To ensure cellular homeostasis and a constant replenishment of VB_6, catabolism and elimination of VB_6 is necessary. During this process, PLP is converted into PL via dephosphorylation, which is in turn transformed into 4-pyridoxic acid (PA), the biologically inactive form of VB_6 and eventually excreted in the urine [205]. As depicted in Scheme 1.16, the overall in vivo transformation of PN involves some oxidation reactions, for instance during the conversion of the alcohol functionality of PNP into the aldehyde group in PLP, as well as the formation of PA (carboxylic acid) from PL (aldehyde). With this information in mind, voltammetric methods can serve as an alternative approach for more comprehensive understanding of these anodic reactions.

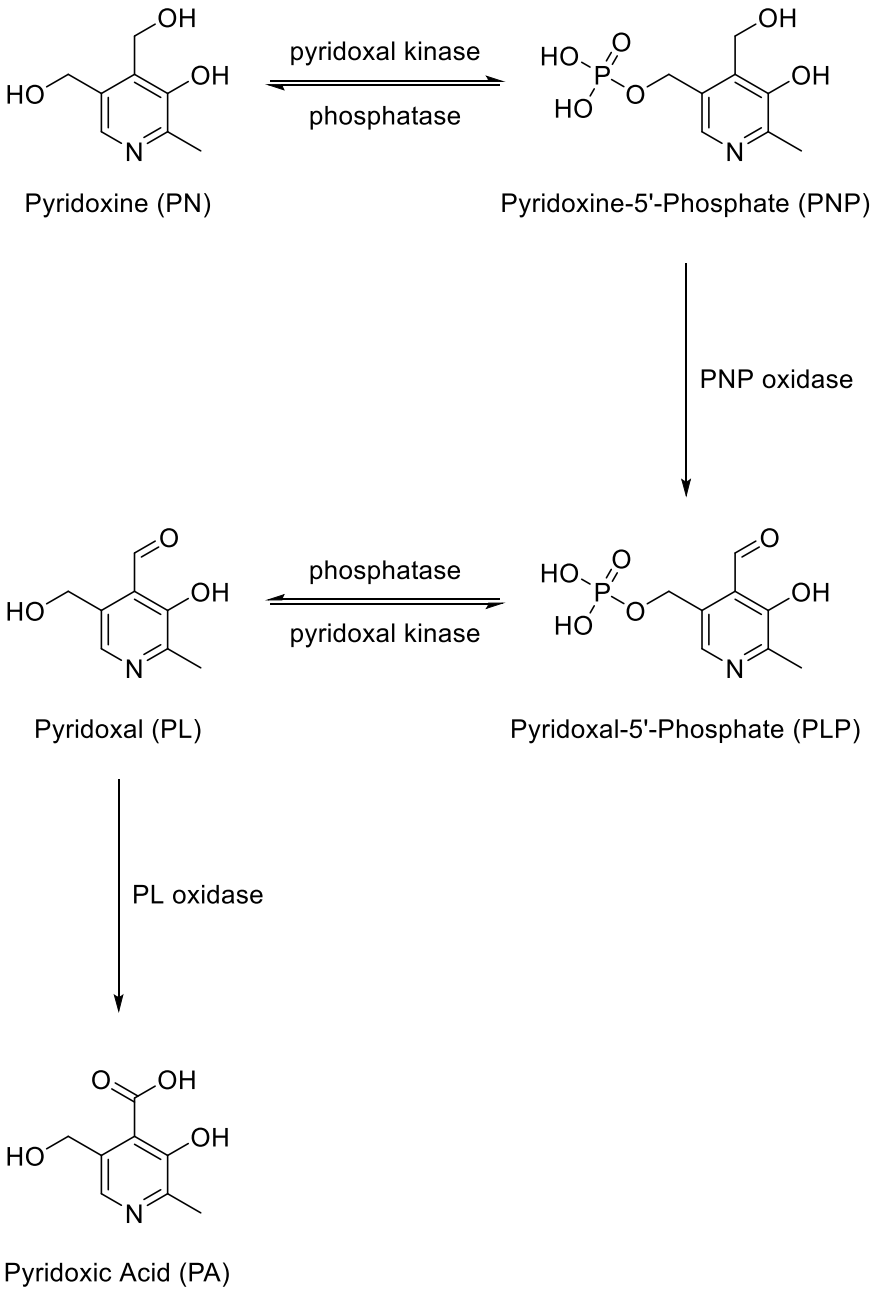

Scheme 1.16. Proposed in vivo chemical transformation of pyridoxine (PN) (adapted from ref. [205]).

1.5.5. Electrochemical studies of PN

It is well-established that PN is electro-oxidizable and the majority of electrochemical works on this compound have been directed towards its detection or quantification by employing various electrode materials, including carbon paste [206], glassy carbon [207-209], and gold [210, 211]. This has also extended to the use of chemically modified electrodes (CMEs) such as modified carbon paste [212-216], glassy carbon [217-219], carbon ceramic [220, 221], and aluminum [222] due to their ability to provide enhanced sensitivity, selectivity, and detection range. Furthermore, the use of other materials including screen-printed [223] and polyurethane-graphite [224] electrodes have also been studied. In contrast, however, studies involving platinum electrodes are relatively less well-explored [225], despite platinum classically being one of the most widely used materials for studies of anodic processes [35].

A survey of literature also reveals a lack of detailed information regarding the voltammetric behavior and redox mechanisms of PN, while the intermediate(s) and/or product(s) associated with this process also remain uncertain. For example, it was proposed that PN undergoes a two-electron/two-proton ($-2e^-/-2H^+$) oxidation reaction, giving PL as the oxidation product [221, 222, 226], whereas others have reported a four-electron/four-proton loss ($-4e^-/-4H^+$) of PN to afford PA [210, 211]. On the other hand, in some studies, it was proposed that PL and PN would result in the same eventual oxidation product. Therefore, it was postulated that with the involvement of water, PL, which is formed after the initial oxidation of PN can undergo further hydrolysis to form a lactone intermediate (hemiacetal form of pyridoxal) which subsequently oxidizes into PA (Scheme 1.17) [223, 227]. Moreover, characterization using spectroscopy techniques such as in situ Fourier transform infrared spectroscopy (FTIR) have corroborated the presence of this transient lactone species [211, 228]. As these reports were performed using aqueous systems, the differing results obtained were surmised to be attributable to the complex

acid-base and hydration equilibria affecting the distribution of the various species [223, 227, 229].

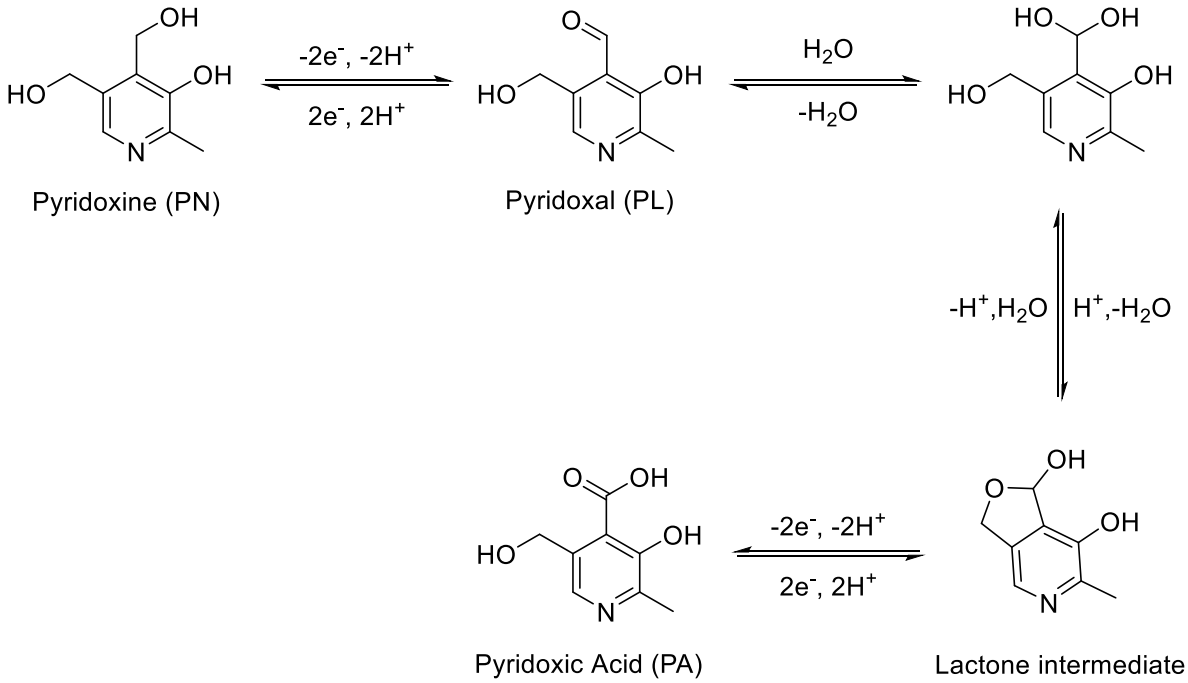

Scheme 1.17. Proposed oxidation of pyridoxine (PN) (adapted from ref. [223, 227]).

At variance with the abovementioned studies, however, PN was suggested in a separate account to undergo a one-electron oxidation to form radical ions which can undergo coupling with one another to yield a dimeric compound [214].

Therefore, it is evident that the oxidation of PN involves complex multiple step transformations bearing different possible mechanistic pathways. In addition, as these studies were performed in aqueous media, the anodic process was also found to be influenced by pH [223, 227, 229]. Hence, it is possible that PN would behave differently in an aprotic system, where it would be less likely to be affected by acidity and alkalinity of the solution. Furthermore, as many of the documented electrochemical studies examined PN in the form of a hydrochloride salt, plausibly because it is the common form that PN exists in vitamin supplements and fortified food, it

would also be interesting to examine the redox chemistry of PN in its natural form (without containing hydrochloride).

1.6. Aims and Objectives of Thesis

1.6.1. Rationale of using electrochemical techniques

Electrochemical methods are useful techniques for the study of reactions that involve electron exchange because it can provide considerable amounts of information such as the number and order of electrons transferred, the associated chemical stabilities and redox potentials, and the corresponding kinetic and thermodynamic values involved in the transformations. In addition, because electrochemistry deals with the interplay between chemistry and electricity, voltammetry has the advantage of a precise control over the redox reactions (e.g. reduction or oxidation) by simply varying the electrode potential. Furthermore, with the use and adjustment of appropriate parameters such as temperature and scan rate in the cyclic voltammetry measurements, knowledge about the identities of associated intermediates can be gained. Also, other electrochemical methods like controlled potential electrolysis enables the examination of a molecule's stability over prolong period of time (minutes to hours). Hence, the use of a combination of electrochemical techniques can be helpful for comprehensive examinations of molecular redox species.

1.6.2. Aims of thesis

The advances that have been made in the area of voltammetric mechanistic studies pertaining to the four redox-active compounds to be covered in this thesis (sesamol, vanillin, diethylstilbestrol and pyridoxine) have been disclosed in the preceding sections (Sections 1.2-1.5), with some of the less well-explored areas being identified. Overall, it has been found that although there have been many impressive reports performed in protic systems (e.g. aqueous solution), the corresponding studies in aprotic media remain far fewer. Building on the existing knowledge, it is envisaged that detailed investigations of the electrochemical mechanism of

these compound in organic aprotic solvent can potentially serve as supplementary and/or comparison models, and possibly value add to prevailing works. Additionally, the information gained from these works can be useful for the rational design of electrochemical sensors.

Because the scarcity of protons in an aprotic environment can sometimes help to reduce the tendency of intermediates to undergo coupled chemical reactions (e.g. hydrolysis) immediately following its electro-generation, thereby improving their stability, this may facilitate the voltammetric detection of transient electroactive species or possibly aid in their isolation if the intermediates are long-lived enough. Consequently, this may also allow for a generally simpler elucidation of the mechanistic pathways involved and may serve as an alternative approach for more comprehensive molecular understanding of these electrochemical transformations [35, 230].

Therefore, the focal point of this thesis is directed to gathering mechanistic insights into the redox properties of sesamol, vanillin, diethylstilbestrol and pyridoxine in an aprotic organic solvent, acetonitrile (CH_3CN), and are elaborated in Chapters 2, 3, 4 and 5 respectively. In addition, the interaction of water with these four compounds were also examined and the influence on their voltammetric responses are delineated. Notably, it is worthy to highlight that the full exclusion of all water from the sample solution is not the objective of the current thesis. In cases where the analyte displayed significant changes and/or high sensitivity to water during preliminary scans, additional voltammetric analysis such as higher substrate concentration (so that the concentration of substrate is higher than the water content) CV experiments were performed so as to assess such interactions in further detail.

1.7. References

[1] M.T. Nguyen, E.S. Kryachko, L.G. Vanquickenborne, General and Theoretical Aspects of Phenols, in: Z. Rappoport (Ed.) The Chemistry of Phenols, John Wiley & Sons Ltd, Chichester, England, 2003, pp. 1–198.

[2] N.P. Visavadiya, A.V.R.L. Narasimhacharya, Sesame as a Hypocholesteraemic and Antioxidant Dietary Component, Food Chem. Toxicol., 46 (2008) 1889–1895.

[3] R.H.R. Carvalho, E.L. Galvão, J.Â.C. Barros, M.M. Conceição, E.M.B.D. Sousa, Extraction, Fatty Acid Profile and Antioxidant Activity of Sesame Extract (Sesamum Indium L.), Braz. J. Chem. Eng., 29 (2012) 409–420.

[4] K. Selvarajan, C.A. Narasimhulu, R. Bapputty, S. Parthasarathy, Anti-Inflammatory and Antioxidant Activities of the Nonlipid (Aqueous) Components of Sesame Oil: Potential Use in Atherosclerosis, J. Med. Food, 18 (2015) 393–402.

[5] S.S. Kumar, K.I. Priyadarsini, K.B. Sainis, Inhibition of Peroxynitrite-Mediated Reactions by Vanillin, J. Agric. Food Chem., 52 (2004) 139–145.

[6] A. Tai, T. Sawano, F. Yazama, H. Ito, Evaluation of Antioxidant Activity of Vanillin by Using Multiple Antioxidant Assays, Biochim. Biophys. Acta, Gen. Subj., 1810 (2011) 170–177.

[7] M. Makni, Y. Chtourou, H. Fetoui, E.M. Garoui, M. Barkallah, C. Marouani, C. Kallel, N. Zeghal, Erythrocyte Oxidative Damage in Rat Treated with CCl4: Protective Role of Vanillin, Toxicol. Ind. Health, 28 (2012) 908–916.

[8] M.B. Shimkin, H.G. Grady, Mammary Carcinomas in Mice Following Oral Administration of Stilbestrol, Proc. Soc. Exp. Biol. Med., 45 (1940) 246–248.

[9] C.A. Frye, E. Bo, G. Calamandrei, F. Dessì-Fulgheri, M. Fernández, L. Fusani, O. Kah, M. Kajta, Y. Le Page, H.B. Patisaul, A. Venerosi, A.K. Wojtowicz, G.C. Panzica, Endocrine Disrupters: A Review of Some Sources, Effects, and Mechanisms of Actions on Behaviour and Neuroendocrine Systems, J. Neuroendocrinol., 24 (2012) 144–159.

[10] C. Preda, M.C. Ungureanu, C. Vulpoi, Endocrine Disruptors in the Environment and Their Impact on Human Health, Environ. Eng. Manage. J., 11 (2012) 1697–1706.

[11] A.C. Gore, V.A. Chappell, S.E. Fenton, J.A. Flaws, A. Nadal, G.S. Prins, J. Toppari, R.T. Zoeller, EDC-2: The Endocrine Society's Second Scientific Statement on Endocrine-Disrupting Chemicals, Endocr. Rev., 36 (2015) E1–E150.

[12] M.G. Traber, J. Atkinson, Vitamin E, Antioxidant and Nothing More, Free Radical Biol. Med., 43 (2007) 4–15.

[13] M.W. Clarke, J.R. Burnett, K.D. Croft, Vitamin E in Human Health and Disease, Crit. Rev. Clin. Lab. Sci., 45 (2008) 417–450.

[14] M.S. Fernandez-Panchon, D. Villano, A.M. Troncoso, M.C. Garcia-Parrilla, Antioxidant Activity of Phenolic Compounds: from *In Vitro* Results to *In Vivo* Evidence, Crit. Rev. Food Sci. Nutr., 48 (2008) 649–671.

[15] H. Eickhoff, G. Jung, A. Rieker, Oxidative Phenol Coupling–Tyrosine Dimers and Libraries Containing Tyrosyl Peptide Dimers, Tetrahedron, 57 (2001) 353–364.

[16] G.W. Morrow, Anodic Oxidation of Oxygen-Containing Compounds, in: H. Lung, O. Hammerich (Eds.) Organic Electrochemistry, Marcel Dekker, New York, USA, 2001, pp. 589–620.

[17] R. Francke, T. Quell, A. Wiebe, S.R. Waldvogel, Oxygen-Containing Compounds. Alcohols, Ethers, and Phenols, in: O. Hammerich, B. Speiser (Eds.) Organic Electrochemistry, CRC Press, Boca Raton, Florida, 2016, pp. 982–1033.

[18] L.L. Williams, R.D. Webster, Electrochemically Controlled Chemically Reversible Transformation of α-Tocopherol (Vitamin E) into Its Phenoxonium Cation, J. Am. Chem. Soc., 126 (2004) 12441–12450

[19] G.J. Wilson, C.Y. Lin, R.D. Webster, Significant Differences in the Electrochemical Behavior of the α-, β-, γ-, and δ-Tocopherols (Vitamin E), J. Phys. Chem. B, 110 (2006) 11540–11548.

[20] R.D. Webster, New Insights into the Oxidative Electrochemistry of Vitamin E, Acc. Chem. Res., 40 (2007) 251-257.

[21] W.W. Yao, H.M. Peng, R.D. Webster, P.M.W. Gill, Variable Scan Rate Cyclic Voltammetry and Theoretical Studies on Tocopherol (Vitamin E) Model Compounds, J. Phys. Chem. B, 112 (2008) 6847–6855.

[22] S.B. Lee, A.C. Willis, R.D. Webster, Synthesis of the Phenoxonium Cation of an α-Tocopherol Model Compound Crystallized with Non-Nucleophilic $[B(C_6F_5)_4]^-$ and $(CB_{11}H_6Br_6)^-$ Anions, J. Am. Chem. Soc., 128 (2006) 9332–9333.

[23] H.M. Peng, B.F. Choules, W.W. Yao, Z. Zhang, R.D. Webster, P.M.W. Gill, Long-Lived Radical Cations as Model Compounds for the Reactive One-Electron Oxidation Product of Vitamin E, J. Phys. Chem. B, 112 (2008) 10367–10374.

[24] H.M. Peng, R.D. Webster, Investigation into Phenoxonium Cations Produced During the Electrochemical Oxidation of Chroman-6-ol and Dihydrobenzofuran-5-ol Substituted Compounds, J. Org. Chem., 73 (2008) 2169–2175.

[25] A. Rieker, R. Beisswenger, K. Regier, Syntheses via Anodically Produced Phenoxenium Ions. Applications in the Field of Peptides and Carbohydrates, Tetrahedron, 47 (1991) 645–654.

[26] M. Quan, D. Sanchez, M.F. Wasylkiw, D.K. Smith, Voltammetry of Quinones in Unbuffered Aqueous Solution: Reassessing the Roles of Proton Transfer and Hydrogen Bonding in the Aqueous Electrochemistry of Quinones, J. Am. Chem. Soc., 129 (2007) 12847–12856.

[27] Y. Hui, E.L.K. Chng, C.Y.L. Chng, H.L. Poh, R.D. Webster, Hydrogen-Bonding Interactions between Water and the One and Two-Electron-Reduced Forms of Vitamin K_1: Applying Quinone Electrochemistry To Determine the Moisture Content of Non-Aqueous Solvents, J. Am. Chem. Soc., 131 (2009) 1523–1534.

[28] Y. Hui, E.L.K. Chng, L.P.-L. Chua, W.Z. Liu, W. Richard David, Voltammetric Method for Determining the Trace Moisture Content of Organic Solvents Based on Hydrogen-Bonding Interactions with Quinones, Anal. Chem. (Wash.), 82 (2010) 1928–1934.

[29] Y. Hui, R.D. Webster, Absorption of Water into Organic Solvents Used for Electrochemistry under Conventional Operating Conditions, Anal. Chem. (Wash.), 83 (2011) 976–981.

[30] Y.S. Tan, S. Chen, W.M. Hong, J.M. Kan, E.S.H. Kwek, S.Y. Lim, Z.H. Lim, M.E. Tessensohn, Y. Zhang, W. Richard David, The Role of Low Levels of Water in the

Electrochemical Oxidation of α-Tocopherol (Vitamin E) and Other Phenols in Acetonitrile, Phys. Chem. Chem. Phys., 13 (2011) 12745–12754.

[31] M.E. Tessensohn, H. Hirao, R.D. Webster, Electrochemical Properties of Phenols and Quinones in Organic Solvents are Strongly Influenced by Hydrogen-Bonding with Water, J. Phys. Chem. C, 117 (2013) 1081–1090.

[32] M.E. Tessensohn, M. Lee, H. Hirao, R.D. Webster, Measuring the Relative Hydrogen-Bonding Strengths of Alcohols in Aprotic Organic Solvents, ChemPhysChem, 16 (2015) 160–168.

[33] M.E. Tessensohn, W. Richard David, Using Voltammetry to Measure Hydrogen-Bonding Interactions in Non-Aqueous Solvents: A Mini-Review, Electrochem. Commun., 62 (2016) 38–43.

[34] V. Katovic, M.A. May, C.P. Keszthelyi, Vacuum-Line Techniques, in: P.T. Kissinger, W.R. Heineman (Eds.) Laboratory Techniques in Electroanalytical Chemistry, Marcel Dekker, New York, 1996, pp. 543–567.

[35] H. Lund, Practical Problems in Electrolysis, in: H. Lung, O. Hammerich (Eds.) Organic Electrochemistry, Marcel Dekker, New York, USA, 2001, pp. 223–292.

[36] C. Laurence, M. Berthelot, J. Graton, Hydrogen-Bonded Complexes of Phenols, in: Z. Rappoport (Ed.) The Chemistry of Phenols2003, pp. 529–604.

[37] M. Iwatsuki, J. Tsuchiya, E. Komuro, Y. Yamamoto, E. Niki, Effects of Solvents and Media on the Antioxidant Activity of α-Tocopherol, Biochim. Biophys. Acta, Gen. Subj., 1200 (1994) 19–26.

[38] L. Valgimigli, J.T. Banks, K.U. Ingold, J. Lusztyk, Kinetic Solvent Effects on Hydroxylic Hydrogen Atom Abstractions Are Independent of the Nature of the Abstracting Radical. Two Extreme Tests Using Vitamin E and Phenol, J. Am. Chem. Soc., 117 (1995) 9966–9971.

[39] R. Amorati, M.G. Fumo, S. Menichetti, V. Mugnaini, G.F. Pedulli, Electronic and Hydrogen Bonding Effects on the Chain-Breaking Activity of Sulfur-Containing Phenolic Antioxidants, J. Org. Chem., 71 (2006) 6325–6332.

[40] W. Tantawy, Tuning the Activity of Antioxidants from a Chemical Point of View, Mini-Rev. Org. Chem., 11 (2014) 186–224.

[41] D. Bedigian, Evolution of Sesame Revisited: Domestication, Diversity and Prospects, Genet. Resour. Crop Evol., 50 (2003) 779–787.

[42] D. Bedigian, J.R. Harlan, Evidence for Cultivation of Sesame in the Ancient World, Econ. Bot., 40 (1986) 137–154.

[43] M. Namiki, The Chemistry and Physiological Functions of Sesame, Food Rev. Int., 11 (1995) 281–329.

[44] S. Periasamy, D.-Z. Hsu, V.R.M. Chandrasekaran, M.-Y. Liu, Sesame Oil Accelerates Healing of 2,4,6-Trinitrobenzenesulfonic Acid-Induced Acute Colitis by Attenuating Inflammation and Fibrosis, JPEN, J, Parenter. Enteral Nutr., 37 (2013) 674–682.

[45] C.A. Narasimhulu, K. Selvarajan, D. Litvinov, S. Parthasarathy, Anti-Atherosclerotic and Anti-Inflammatory Actions of Sesame Oil, J. Med. Food, 18 (2015) 11–20.

[46] D. Nigam, C. Singh, U. Tiwari, Evaluation of *in vitro* Study of Antioxidant and Antibacterial Activities of Methanolic Seed Extract of Sesamum Indicum, J. Pharmacogn. Phytochem., 3 (2015) 88–92.

[47] R. Shasmitha, Health Benefits of Sesamum Indicum: A Short Review, Asian J. Pharm. Clin. Res., 8 (2015) 1–3.

[48] D. Sankar, G. Sambandam, M.R. Rao, K.V. Pugalendi, Modulation of Blood Pressure, Lipid Profiles and Redox Status in Hypertensive Patients Taking Different Edible Oil, Clin. Chim. Acta, 355 (2005) 97–104.

[49] S.C.M. Cheung, Y.T. Szeto, I.F.F. Benzie, Antioxidant Protection of Edible Oils, Plant Foods Hum Nutr., 62 (2007) 39–42.

[50] S.K. Veličkovska, L. Brühl, S. Mitrev, H. Mirhosseini, B. Matthäus, Quality Evaluation of Cold-Pressed Edible Oils from Macedonia, Eur. J. Lipid Sci. Technol., 117 (2015) 2023–2035.

[51] D.-Z. Hsu, Y.-H. Li, S.-P. Chien, M.-Y. Liu, Effects of Sesame Oil on Oxidative Stress and Hepatic Injury after Cecal Ligation and Puncture in Rats, Shock, 21 (2004) 466–469.

[52] D.-Z. Hsu, S.-P. Chien, Y.-H. Li, Y.-C. Chuang, Y.-C. Chang, M.-Y. Liu, Sesame Oil Attenuates Hepatic Lipid Peroxidation by Inhibiting Nitric Oxide and Superoxide Anion Generation in Septic Rats, JPEN, J, Parenter. Enteral Nutr., 32 (2008) 154–159.

[53] A. Biswas, P. Dhar, S. Ghosh, Antihyperlipidermic Effect of Sesame (Sesamum indicum L.) Protein Isolate in Rats Fed a Normal and High Cholesterol Diet, J. Food Sci., 75 (2010) H274–H279.

[54] J.B. Morris, Food, Industrial, Nutraceutical, and Pharmaceutical Uses of Sesame Genetic Resources, in: J. Janick, A. Whipkey (Eds.) Trends in New Crops and New Uses, ASHS Press, Alexandria, VA, 2002, pp. 153–156.

[55] T.-S. Hahm, C.-Y. Kuei, Present and Potential Industrial Applications of Sesame: A Mini Review, J. Food Process. Preserv., 39 (2015) 3137–3144.

[56] Y. Wan, H. Li, G. Fu, X. Chen, F. Chen, M. Xie, The Relationship of Antioxidant Components and Antioxidant Activity of Sesame Seed Oil, J. Sci. Food Agric., 95 (2015) 2571–2578.

[57] I. Kim, E. Choe, Effects of Bleaching on the Properties of Roasted Sesame Oil, J. Food Sci., 70 (2005) C48–C52.

[58] K. Kikugawa, M. Arai, T. Kurechi, Participation of Sesamol in Stability of Sesame Oil, J. Am. Oil Chem. Soc., 60 (1983) 1528–1533.

[59] Y. Fukuda, T. Osawa, M. Namiki, T. Ozaki, Studies on Antioxidative Substances in Sesame Seed, Agric. Biol. Chem., 49 (1985) 301–306.

[60] K.P. Suja, A. Jayalekshmy, C. Arumughan, Free Radical Scavenging Behavior of Antioxidant Compounds in Sesame in DPPH System, J. Agric. Food Chem., 52 (2004) 912–915.

[61] S.-H. Park, S.-N. Ryu, Y. Bu, H. Kim, J.E. Simon, K.-S. Kim, Antioxidant Components as Potential Neuroprotective Agents in Sesame (Sesamum Indicum L.), Food Rev. Int., 26 (2010) 103–121.

[62] P.-Y. Chu, P. Srinivasan, J.-F. Deng, M.-Y. Liu, Sesamol Attenuates Oxidative Stress-Mediated Experimental Acute Pancreatitis in Rats, Hum. Exp. Toxicol., 31 (2012) 397–404.

[63] H. Yoshida, S. Takagi, Effects of Seed Roasting Temperature and Time on the Quality Characteristics of Sesame (Sesamum Indicum) Oil, J. Sci. Food Agric., 75 (1997) 19–26.

[64] J. Lee, E. Choe, Extraction of Lignan Compounds from Roasted Sesame Oil and their Effect on the Autoxidation of Methyl Linoleate, J. Food Sci., 71 (2006) C430–C436.

[65] S.W. Lee, M.K. Jeung, M.H. Park, S.Y. Lee, J.H. Lee, Effects of Roasting Conditions of Sesame Seeds on the Oxidative Stability of Pressed Oil during Thermal Oxidation, Food Chem., 118 (2010) 681–685.

[66] R. Joshi, M.S. Kumar, K. Satyamoorthy, M.K. Unnikrisnan, T. Mukherjee, Free Radical Reactions and Antioxidant Activities of Sesamol: Pulse Radiolytic and Biochemical Studies, J. Agric. Food Chem., 53 (2005) 2696–2703.

[67] H.Y. Aboul-Enein, I. Kruk, A. Kładna, K. Lichszteld, T. Michalska, Scavenging Effects of Phenolic Compounds on Reactive Oxygen Species, Biopolymers, 86 (2007) 222–230.

[68] T. Geetha, R. Bhandari, I.P. Kaur, Sesamol: An Efficient Antioxidant with Potential Therapeutic Benefits, Med. Chem., 5 (2009) 367–371.

[69] D.R. Johnson, E.A. Decker, The Role of Oxygen in Lipid Oxidation Reactions: A Review, Annu. Rev. Food Sci. Technol., 6 (2015) 171–190.

[70] V.R.M. Chandrasekaran, S.-P. Chien, D.-Z. Hsu, M.-Y. Liu, Anti-Hepatotoxic Effects of 3,4-Methylenedioxyphenol and N-Acetylcysteine in Acutely Acetaminophen-Overdosed Mice, Hum. Exp. Toxicol., 30 (2011) 1609–1615.

[71] S. Jnaneshwari, M. Hemshekhar, R.M. Thushara, M.S. Sundaram, M.S. Santhosh, K. Sunitha, R.L. Shankar, K. Kemparaju, K.S. Girish, Sesamol Ameliorates Cyclophosphamide-Induced Hepatotoxicity by Modulating Oxidative Stress and Inflammatory Mediators, Anti-Cancer Agents Med. Chem., 14 (2014) 975–983.

[72] V. Kakkar, A.K. Mishra, K. Chuttani, K. Chopra, I.P. Kaur, Delivery of Sesamol-Loaded Solid Lipid Nanoparticles to the Brain for Menopause-related Emotional and Cognitive Central Nervous System Derangements, Rejuvenation Res., 14 (2011) 597–604.

[73] A.K. Sachdeva, S. Misra, I.P. Kaur, K. Chopra, Neuroprotective Potential of Sesamol and its Loaded Solid Lipid Nanoparticles in ICV-STZ-Induced Cognitive Deficits: Behavioral and Biochemical Evidence, Eur. J. Pharmacol., 747 (2015) 132–140.

[74] G.J. Kapadia, M.A. Azuine, H. Tokuda, M. Takasaki, T. Mukainaka, T. Konoshima, H. Nishino, Chemopreventive Effect of Resveratrol, Sesamol, Sesame oil and Sunflower Oil in the Epstein-Barr Virus Early Antigen Activation Assay and the Mouse Skin Two-Stage Carcinogenesis, Pharmacol. Res., 45 (2002) 499–505.

[75] Z. Liu, Q. Xiang, L. Du, G. Song, Y. Wang, X. Liu, The Interaction of Sesamol with DNA and Cytotoxicity, Apoptosis, and Localization in HepG2 Cells, Food Chem., 141 (2013) 289–296.

[76] P.-Y. Chu, D.-Z. Hsu, P.-Y. Hsu, M.-Y. Liu, Sesamol Down-Regulates the Lipopolysaccharide-Induced Inflammatory Response by Inhibiting Nuclear Factor-kappa B Activation, Innate Immunity, 16 (2010) 333–339.

[77] D.-Z. Hsu, P.-Y. Chu, M.-Y. Liu, Sesame Seed (Sesamum Indicum l.) Extracts and their Anti-Inflammatory Effect, ACS Symp. Ser., 1093 (2012) 335–341.

[78] I.P. Kaur, A. Saini, Sesamol Exhibits Antimutagenic Activity against Oxygen Species Mediated Mutagenicity, Mutat. Res., Genet. Toxicol. Environ. Mutagen., 470 (2000) 71–76.

[79] N. Erkan, G. Ayranci, E. Ayranci, Antioxidant Activities of Rosemary (Rosmarinus Officinalis L.) Extract, Blackseed (Nigella sativa L.) Essential Oil, Carnosic Acid, Rosmarinic Acid and Sesamol, Food Chem., 110 (2008) 76–82.

[80] T. Masuda, A. Fujimoto, Y. Oyama, T. Maekawa, Y. Sone, Structures of Cytotoxic Products from Fe-Catalyzed Oxidation of Sesamol in Ethanol, Tetrahedron Lett., 50 (2009) 3905–3908.

[81] T. Masuda, Y. Shingai, A. Fujimoto, M. Nakamura, Y. Oyama, T. Maekawa, Y. Sone, Identification of Cytotoxic Dimers in Oxidation Product from Sesamol, a Potent Antioxidant of Sesame Oil, J. Agric. Food Chem., 58 (2010) 10880–10885.

[82] Y. Shingai, A. Fujimoto, A. Nakajima, M. Saito, K. Kanemaru, T. Masuda, Y. Oyama, Cytotoxic Characteristics of Two Isomeric Dimers Produced by Oxidation of Sesamol, An Antioxidant in Sesame Oil, J. Health Sci., 57 (2011) 425–431.

[83] M.E.S. Mirghani, Y.B. Che Man, S. Jinap, B.S. Baharin, J. Bakar, Application of FTIR Spectroscopy in Determining Sesamol in Sesame Seed Oil, J. Am. Oil Chem. Soc., 80 (2003) 1–4.

[84] W. Sun, R. Xiao, Determination of Sesamol in Sesame Oil by Anion Exchange Solid Phase Extraction Coupled with HPLC, Anal. Methods, 6 (2014) 6432–6436.

[85] A.S. Bhatnagar, J. Hemavathy, A.G. Gopala Krishna, Development of a Rapid Method for Determination of Lignans Content in Sesame Oil, J. Food Sci. Technol. (New Delhi, India), 52 (2015) 521–527.

[86] H. Liu, D. Wu, Y. Liu, H. Zhang, T. Ma, A. Aidaerhan, J. Wang, B. Sun, Application of an Optosensing Chip based on Molecularly Imprinted Polymer Coated Quantum Dots for the Highly Selective and Sensitive Determination of Sesamol in Sesame Oils, J. Agric. Food Chem., 63 (2015) 2545–2549.

[87] S. Shiragami, O.-S. Kim, K. Kusuda, Direct Survey of Redox Active Compounds in Sesame Oil by Cyclic Voltammetry-Studies on Sesaminol, Sesamol and Hydroxyhydroquinone in Nujol, J. Electroanal. Chem., 379 (1994) 315–319.

[88] R. Estévez Brito, J.M. Rodríguez Mellado, P. Maldonado, M. Ruiz Montoya, A. Palma, E. Morales, Elucidation of the Electrochemical Oxidation Mechanism of the Antioxidant Sesamol on a Glassy Carbon Electrode, J. Electrochem. Soc., 161 (2014) G27–G32.

[89] N.J. Walton, M.J. Mayer, A. Narbad, Vanillin, Phytochemistry, 63 (2003) 505–515.

[90] C.C. De Guzman, R.R. Zara, Vanilla, in: K.V. Peter (Ed.) Handbook of Herbs and Spices, Woodhead Publishing Limited, Cambridge, UK, 2012, pp. 547–589.

[91] K. Anuradha, B.N. Shyamala, M.M. Naidu, Vanilla- Its Science of Cultivation, Curing, Chemistry, and Nutraceutical Properties, Crit. Rev. Food Sci. Nutr., 53 (2013) 1250–1276.

[92] M.B. Hocking, Vanillin: Synthetic Flavoring from Spent Sulfite Liquor, J. Chem. Educ., 74 (1997) 1055–1059.

[93] M.D. Sharp, N.A. Kocaoglu-Vurma, V. Langford, L.E. Rodriguez-Saona, W.J. Harper, Rapid Discrimination and Characterization of Vanilla Bean Extracts by Attenuated Total Reflection Infrared Spectroscopy and Selected Ion Flow Tube Mass Spectrometry, J. Food Sci., 77 (2012) C284–C292.

[94] N.J. Gallage, E.H. Hansen, R. Kannangara, C.E. Olsen, M.S. Motawia, K. Jørgensen, I. Holme, K. Hebelstrup, M. Grisoni, B.L. Møller, Vanillin Formation from Ferulic Acid in Vanilla Planifolia is Catalysed by a Single Enzyme, Nat. Commun., 5 (2014) 4037–4050.

[95] S.R. Rao, G.A. Ravishankar, Vanilla Flavour: Production by Conventional and Biotechnological Routes, J. Sci. Food Agric., 80 (2000) 289–304.

[96] J.-A. Jiang, C. Chen, Y. Guo, D.-H. Liao, X.-D. Pan, Y.-F. Ji, A Highly Efficient Approach to Vanillin Starting from 4-Cresol, Green Chem., 16 (2014) 2807–2814.

[97] W. Fu, X. Duan, L. Yue, S. Dai, L. Xu, J. Li, G. Lu, D. Mao, Study on the Oxidation of Vanillymandelic Acid to Vanillin over Mesoporous Copper Oxide, React. Kinet., Mech. Catal., 116 (2015) 191–204.

[98] D. Havkin-Frenkel, F.C. Belanger, Biotechnological Production of Vanillin, in: D. Havkin-Frenkel, F.C. Belanger (Eds.) Biotechnology in Flavor Production, Blackwell Publishing Ltd, Oxford, UK, 2008, pp. 83–103.

[99] B. Kaur, D. Chakraborty, Biotechnological and Molecular Approaches for Vanillin Production: A Review, Appl. Biochem. Biotechnol., 169 (2013) 1353–1372.

[100] T. Furuya, M. Miura, M. Kuroiwa, K. Kino, High-Yield Production of Vanillin from Ferulic Acid by a Coenzyme-Independent Decarboxylase/Oxygenase Two-Stage Process, New Biotechnology, 32 (2015) 335–339.

[101] J.F. Arteaga, M. Ruiz-Montoya, A. Palma, G. Alonso-Garrido, S. Pintado, J.M. Rodrígues-Mellado, Comparison of the Simple Cyclic Voltammetry (CV) and DPPH Assays for the Determination of Antioxidant Capacity of Active Principles, Molecules, 17 (2012) 5126–5138.

[102] D. Srikanth, H.M. Vishma, S. Nischal, U. Rathnakar, P.G. Shiv, D.A. Sahana, S.K. Ashok, A. Udupa, Evaluation of Anti-Inflammatory Property of Vanillin in Carrageenan Induced Paw Edema Model in Rats, Int. J. Bioassays, 2 (2013) 269–271.

[103] J. Niazi, N. Kaur, R.K. Sachdeva, Y. Bansal, V. Gupta, Anti-Inflammatory and Antinociceptive Activity of Vanillin, Drug Dev. Ther., 5 (2014) 145–147.

[104] D.J. Fitzgerald, M. Stratford, A. Narbad, Analysis of the Inhibition of Food Spoilage Yeasts by Vanillin, Int. J. Food Microbiol., 86 (2003) 113–122.

[105] R.M. Cava-Roda, A. Taboada-Rodríguez, M.T. Valverde-Franco, F. Marín-Iniesta, Antimicrobial Activity of Vanillin and Mixtures with Cinnamon and Clove Essential Oils in Controlling *Listeria monocytogenes* and *Escherichia coli* O157:H7 in Milk, Food Bioprocess Technol., 5 (2012) 2120–2131.

[106] A.C. Silveira, G.C. Moreira, F. Artés, E. Aguayo, Vanillin and Cinnamic Acid in Aqueous Solutions or in Active Modified Packaging Preserve the Quality of Fresh-Cut Cantaloupe Melon, Sci. Hortic. (Amsterdam, Neth.), 192 (2015) 271–278.

[107] N.A. Negm, N.G. Kandile, E.A. Badr, M.A. Mohammed, Gravimetric and Electrochemical Evaluation of Environmentally Friendly Nonionic Corrosion Inhibitors for Carbon Steel in 1 M HCl, Corros. Sci., 65 (2012) 94–103.

[108] S.M. Shaban, I. Aiad, M.M. El-Sukkary, E.A. Soliman, M.Y. El-Awady, Inhibition of Mild Steel Corrosion in Acidic Medium by Vanillin Cationic Surfactants, J. Mol. Liq., 203 (2015) 20–28.

[109] S.M. Tawfik, N.A. Negm, Vanillin-Derived Non-Ionic Surfactants as Green Corrosion Inhibitors for Carbon Steel in Acidic Environments, Res. Chem. Intermed., 42 (2016) 3579–3607.

[110] S. Menon, N. Nayeem, Vanilla Planifolia: A Review of a Plant Commonly Used as Flavouring Agent, Int. J. Pharm. Sci. Rev. Res., 20 (2013) 225–228.

[111] E. Anklam, S. Gaglione, A. Müller, Oxidation Behaviour of Vanillin in Dairy Products, Food Chem., 60 (1997) 43–51.

[112] G.I. Panoutsopoulos, C. Beedham, Enzymatic Oxidation of Vanillin, Isovanillin and Protocatechuic Aldehyde with Freshly Prepared Guinea Pig Liver Slices, Cell. Physiol. Biochem., 15 (2005) 89–98.

[113] A.P. Hansen, D.C. Booker, Flavor Interaction with Casein and Whey Protein, in: R.J. McGorrin, J.V. Leland (Eds.) Flavor-Food Interactions, American Chemical Society, Washington, DC, 1996, pp. 75–89.

[114] Z. Li, I.U. Grün, L.N. Fernando, Interaction of Vanillin with Soy and Dairy Proteins in Aqueous Model Systems: A Thermodynamic Study, J. Food Sci., 65 (2000) 997–1001.

[115] W. Chobpattana, I.J. Jeon, J.S. Smith, T.M. Loughin, Mechanisms of Interaction Between Vanillin and Milk Proteins in Model Systems, J. Food Sci., 67 (2002) 973–977.

[116] M. Weerawatanakorn, J.-C. Wu, M.-H. Pan, C.-T. Ho, Reactivity and Stability of Selected Flavor Compounds, J. Food Drug Anal., 23 (2015) 176–190.

[117] A.P. Hansen, J.J. Heinis, Decrease of Vanillin Flavor Perception in the Presence of Casein and Whey Proteins, J. Dairy Sci., 74 (1991) 2936–2940.

[118] E. Graf, K.B. de Roos, Performance of Vanilla Flavor in Low-Fat Ice Cream, in: R.J. McGorrin, J.V. Leland (Eds.) Flavor-Food Interactions, American Chemical Society, Washington, DC, 1996, pp. 24–35.

[119] L.S. De Jager, G.A. Perfetti, G.W. Diachenko, Comparison of Headspace-SPME-GC–MS and LC–MS for the Detection and Quantification of Coumarin, Vanillin, and Ethyl Vanillin in Vanilla Extract Products, Food Chem., 107 (2008) 1701–1709.

[120] Y. Shen, B. Hu, X. Chen, Q. Miao, C. Wang, Z. Zhu, C. Han, Determination of Four Flavorings in Infant Formula by Solid-Phase Extraction and Gas Chromatography-Tandem Mass Spectrometry, J. Agric. Food Chem., 62 (2014) 10881–10888.

[121] D. Farthing, D. Sica, C. Abernathy, I. Fakhry, J.D. Roberts, D.J. Abraham, P. Swerdlow, High-Performance Liquid Chromatographic Method for Determination of Vanillin and Vanillic Acid in Human Plasma, Red Blood Cells and Urine, J. Chromatogr. B: Biomed. Sci. Appl., 726 (1999) 303–307.

[122] Y.-H. Li, Z.-H. Sun, P. Zheng, Determination of Vanillin, Eugenol and Isoeugenol by RP-HPLC, Chromatographia, 60 (2004) 709–713.

[123] J. Guan, F. Yan, S. Shi, Y. Li, Simultaneous Separation and Determination of Vanillin and o-Vanillin by CE compared with HPLC, Adv. Mater. Res. (Durnten-Zurich, Switz.), 236–238 (2011) 2725–2728.

[124] S. Minematsu, G.-S. Xuan, X.-Z. Wu, Determination of Vanillin in Vanilla Perfumes and Air by Capillary Electrophoresis, J. Environ. Sci. (China), 25 (2013) S8–S14.

[125] L. Huang, K. Hou, X. Jia, H. Pan, M. Du, Preparation of Novel Silver Nanoplates/Graphene Composite and their Application in Vanillin Electrochemical Detection, Mater. Sci. Eng., C, 38 (2014) 39–45.

[126] X. Lin, Y. Ni, S. Kokot, Electrochemical Mechanism of Eugenol at a Cu Doped Goldnanoparticles Modified Glassy Carbon Electrode and its Analytical Application in Food Samples, Electrochim. Acta, 133 (2014) 484–491.

[127] P. Deng, Z. Xu, R. Zeng, C. Ding, Electrochemical Behavior and Voltammetric Determination of Vanillin Based on an Acetylene Black Paste Electrode Modified with Graphene–Polyvinylpyrrolidone Composite Film, Food Chem., 180 (2015) 156–163.

[128] T.R. Silva, D. Brondani, E. Zapp, I.C. Vieira, Electrochemical Sensor Based on Gold Nanoparticles Stabilized in Poly(Allylamine hydrochloride) for Determination of Vanillin, Electroanalysis, 27 (2015) 465–472.

[129] W. Giraud, M. Mirabel, M. Comtat, Electroanalysis may be used in the Vanillin Biotechnological Production, Appl. Biochem. Biotechnol., 172 (2014) 1953–1963.

[130] R.T. Kachoosangi, G.G. Wildgoose, R.G. Compton, Carbon Nanotube-based Electrochemical Sensors for Quantifying the 'Heat' of Chilli Peppers: The Adsorptive Stripping Voltammetric Determination of Capsaicin, Analyst, 133 (2008) 888–895.

[131] P.L. Sharma, J.N. Gaur, Electrolytic Reduction of Vanillin to Vanillyl Alcohol at Amalgamated Copper, Lead and Zinc Electrodes, J. Appl. Electrochem., 11 (1981) 173–176.

[132] J.-J. Jow, T.-C. Chou, Product Distributions and Kinetics of Cathodic Reduction of Vanillin in Aqueous Solution, Electrochim. Acta, 32 (1987) 311–317.

[133] M. Chandrasekaran, M. Noel, V. Krishnan, Electroreduction of Vanillin in Aprotic and Protic Media on Glassy Carbon Electrode, Bull. Electrochem., 6 (1990) 524–525.

[134] M. Chandrasekaran, M. Noel, V. Krishnan, Glassy Carbon Surface Effects on the Electroreduction of Aromatic Carbonyl Compounds Part III: Vanillin, J. Appl. Electrochem., 22 (1992) 1072–1076.

[135] E.C. Dodds, L. Goldberg, W. Lawson, R. Robinson, Estrogenic Activity of Certain Synthetic Compounds, Nature, 141 (1938) 247–248.

[136] E.C. Dodds, W. Lawson, R.L. Noble, Biological Effects of The Synthetic Estrogenic Substance, 4,4'-dihydroxy-α,ß-diethylstilbene, Lancet, I (1938) 1389–1391.

[137] S.H. Swan, Intrauterine Exposure to Diethylstilbestrol: Long-term effects in humans, APMIS, 108 (2000) 793–804.

[138] R.R. Newbold, Lessons Learned from Perinatal Exposure to Diethylstilbestrol, Toxicol. Appl. Pharmacol., 199 (2004) 142–150.

[139] R.N. Hoover, M. Hyer, R.M. Pfeiffer, E. Adam, B. Bond, A.L. Cheville, T. Colton, P. Hartge, E.E. Hatch, A.L. Herbst, B.Y. Karlan, R. Kaufman, K.L. Noller, J.R. Palmer, S.J. Robboy, R.C. Saal, W. Strohsnitter, L. Titus-Ermstoff, R. Troisi, Adverse Health Outcomes in Women Exposed in Utero to Diethylstilbestrol, New Engl. J. Med., 365 (2011) 1304–1314.

[140] J. Lewis-Wambi, V.C. Jordan, Diethylstilbestrol: A Tragedy In Reproductive Endocrinology But A Pioneering Cancer Treatment, in: V.C. Jordan (Ed.) Estrogen Action, Selective Estrogen Receptor Modulators and Women's Health. Progress and Promise, Imperial College Press, London, 2013, pp. 31–54.

[141] C.E. Reed, S.E. Fenton, Exposure to Diethylstilbestrol During Sensitive Life Stages: A Legacy of Heritable Health Effects, Birth Defects Res. C. Embryo Today Rev., 99 (2013) 134–146.

[142] W.J. Dieckmann, M.E. Davis, L.M. Rynkiewicz, R.E. Pottinger, Does The Administration of Diethylstilbestrol During Pregnancy Have Therapeutic Value?, Am. J. Obstet. Gynecol., 66 (1953) 1075–1081.

[143] A.L. Herbst, H. Ulfelder, D.C. Poskanzer, Adenocarcinoma of The Vagina. Association of Maternal Stilbestrol Therapy with Tumor Appearance in Young Women, N. Engl. J. Med., 284 (1971) 878–881.

[144] K.E. McMartin, K.A. Kennedy, G. P., S.N. Alam, P. Greiner, J. Yam, Diethylstilbestrol: A Review of Its Toxicity and Use as a Growth Promotant in Food-Producing Animals, J. Environ. Pathol. Toxicol., 1 (1978) 279–313.

[145] A.G. Rico, Metabolism of Endogenous and Exogenous Anabolic Agents in Cattle, J. Anim. Sci., 57 (1983) 226–232.

[146] R.L. Preston, Hormone Containing Growth Promoting Implants in Farmed Livestock, Adv. Drug Del. Rev., 38 (1999) 123–138.

[147] R.M. Giusti, K. Iwamoto, E.E. Hatch, Diethylstilbestrol Revisited: A Review of The Long-Term Health Effects, Annals of Internal Medicine, 122 (1995) 778–788.

[148] S. Schrager, B.E. Potter, Diethylstilbestrol Exposure, Am. Fam. Physician, 69 (2004) 2395–2400.

[149] J.G. Liehr, A.M. Ballatore, J.A. McLachlan, D.A. Sirbasku, Mechanism of Diethylstilbestrol Carcinogenicity as Studied with The Fluorinated Analog E-3',3'',5',5''-Tetrafluorodiethylstilbestrol, Cancer Res., 43 (1983) 2678–2682.

[150] T. Tokumoto, M. Tokumoto, P. Thomas, Interactions of Diethylstilbestrol (DES) and DES Analogs with Membrane Progestin Receptor-α and The Correlation with Their Nongenomic Progestin Activities, Endocrinology, 148 (2007) 3459–3467.

[151] W.N. Sawaya, K.P. Lone, A. Husain, B. Dashti, S. Al-Zenki, Screening for Estrogenic Steroids in Sheep and Chicken by The Application of Enzyme-Linked Immunosorbent Assay

and A Comparison with Analysis by Gas Chromatography-Mass Spectrometry, Food Chem., 63 (1998) 563–569.

[152] L.C. Dickson, J.D. MacNeil, J. Reid, A.C.E. Fesser, Validation of Screening Method for Residues of Diethylstilbestrol, Dienestrol, Hexestrol, and Zeranol in Bovine Urine using Immunoaffinity Chromatography and Gas Chromatography/Mass Spectrometry, J. AOAC Int., 86 (2003) 631–639.

[153] L.C. Dickson, R. Costain, D. McKenzie, A.C.E. Fesser, J.D. MacNeil, Quantitative Screening of Stilbenes and Zeranol and Its Related Residues and Natural Precursors in Veal Liver by Gas Chromatography-Mass Spectrometry, J. Agric. Food Chem., 57 (2009) 6536–6542.

[154] X.-B. Chen, Y.-L. Wu, T. Yang, Simultaneous Determination of Clenbuterol, Chloramphenicol and Diethylstilbestrol in Bovine Milk by Isotope Dilution Ultraperformance Liquid Chromatography-Tandem Mass Spectrometry, J. Chromatogr. B: Anal. Technol. Biomed. Life Sci., 879 (2011) 799–803.

[155] Y. Yang, J. Chen, Y.-P. Shi, Determination of Diethylstilbestrol in Milk using Carbon Nanotube-Reinforced Hollow Fiber Solid-Phase Microextraction Combined with High-Performance Liquid Chromatography, Talanta, 97 (2012) 222–228.

[156] X. Du, Y. Wu, H. Zhou, N. Cheng, M. Feng, J. Zheng, W. Cao, Development of a HPLC-ECD Method for The Simultaneous Determination of Three Synthetic Estrogens in Milk, Anal. Methods, 5 (2013) 2822–2826.

[157] L. Wang, Y. Zhang, G. Liu, C. Zhang, S. Wang, A Time-Resolved Fluorescence Immunoassay for The Ultrasensitive Determination of Diethylstilbestrol Based on the Double-Codified Gold Nanoparticles, Steriods, 89 (2014) 41–46.

[158] J. Wang, C. Cheng, Y. Yang, Determination of Estrogens in Milk Samples by Magnetic-Solid-Phase Extraction Technique Coupled With High-Performance Liquid Chromatography, J. Food Sci., 80 (2015) C2655–C2661.

[159] Q. Qiao, N. Shi, X. Feng, J. Lu, Y. Han, C. Xue, Diethylstilbestrol in Fish Tissue Determined through Subcritical Fluid Extraction and with GC-MS, J. Ocean Univ. China, 15 (2016) 489–494.

[160] Q.-L. Zhang, J. Li, T.-T. Ma, Z.-T. Zhang, Chemiluminescence Screening Assay for Diethylstilbestrol in Meat, Food Chem., 111 (2008) 498–502.

[161] X. Xie, D. Sun, G. Liu, Q. Zeng, Sensitive and Rapid Determination of Diethylstilbestrol Using Mesoporous SBA-15 Modified Electrode, Anal. Methods, 6 (2014) 1640–1644.

[162] X. Zhu, L. Lu, X. Duan, K. Zhang, J. Xu, D. Hu, H. Sun, L. Dong, Y. Gao, Y. Wu, Efficient Synthesis of Graphene–Multiwalled Carbon Nanotubes Nanocomposite and its Application in Electrochemical Sensing of Diethylstilbestrol, J. Electroanal. Chem., 731 (2014) 84–92.

[163] X. Ma, M. Chen, Electrochemical Sensor Based on Graphene Doped Gold Nanoparticles Modified Electrode for Detection of Diethylstilboestrol, Sensors Actuators B: Chem., 215 (2015) 445–450.

[164] Z. Yan, P. Xiong, N. Gan, J. He, N. Long, Y. Cao, F. Hu, T. Li, A Novel Sandwich-Type Noncompetitive Immunoassay of Diethylstilbestrol using β-cyclodextrin Modified Electrode and Polymer-Enzyme Labels, J. Electroanal. Chem., 736 (2015) 30–37.

[165] J.-M. Séquaris, J. Fritz, Voltammetric Detection and Analysis of the Behavior of Diethylstilbestrol Oxidation Products, Electroanalysis, 4 (1992) 121–127.

[166] D. Lu, S. Lin, L. Wang, X. Shi, C. Wang, Y. Zhang, Synthesis of Cyclodextrin-Reduced Graphene Oxide Hybrid Nanosheets for Sensitivity Enhanced Electrochemical Determination of Diethylstilbestrol, Electrochim. Acta, 85 (2012) 131–138.

[167] C. Yu, W. Ji, Y. Wang, N. Bao, H. Gu, Graphene Oxide-Modified Electrodes for Sensitive Determination of Diethylstilbestrol, Nanotechnology, 24 (2013) 115502/115501–115502/115509.

[168] L. Peng, S. Dong, H. Xie, G. Gu, Z. He, J. Lu, T. Huang, Sensitive Simultaneous Determination of Diethylstilbestrol and Bisphenol A based on Bi_2WO_6 Nanoplates Modified Carbon Paste Electrode, J. Electroanal. Chem., 726 (2014) 15–20.

[169] K.S. Korach, M. Metzler, J.A. McLachlan, Estrogenic Activity in vivo and in vitro of Some Diethylstilbestrol Metabolites and Analogs, Proc. Natl. Acad. Sci. U. S. A., 75 (1978) 468–471.

[170] J.G. Liehr, B.B. DaGue, A.M. Ballatore, J. Henkin, Diethylstilbestrol (DES) Quinone: A Reactive Intermediate in DES Metabolism Biochem. Pharmacol., 32 (1983) 3711–3718.

[171] D. Roy, J.G. Liehr, Metabolic Oxidation of Diethylstilbestrol to Diethylstilbestrol-4',4"-quinone in Syrian Hamsters, Carcinogenesis, 10 (1989) 1241–1245.

[172] K. Chae, J. Lindzey, J.A. McLachlan, K.S. Korach, Estrogen-dependent Gene Regulation By An Oxidative Metabolite of Diethylstilbestrol, Diethylstilbestrol-4',4"-quinone, Steriods, 63 (1998) 149–157.

[173] P. Fenichel, N. Chevalier, F. Brucker-Davis, Bisphenol A: An Endocrine and Metabolic Disruptor, Ann. Endocrinol., 74 (2013) 211–220.

[174] L.L. Ferreira, R. Couto, P.J. Oliveira, Bisphenol A as Epigenetic Modulator: Setting the Stage for Carcinogenesis?, Eur. J. Clin. Invest., 45 (2015) 32–36.

[175] F. Rancière, J.G. Lyons, V.H.Y. Loh, J. Botton, T. Galloway, T. Wang, J.E. Shaw, D.J. Magliano, Bisphenol A and The Risk of Cardiometabolic Disorders: A Systematic Review with Meta-Analysis of The Epidemiological Evidence, Environ. Health (London, U. K.), 14 (2015) 1–34.

[176] D.D. Seachrist, K.W. Bonk, S.-M. Ho, G.S. Prins, A.M. Soto, R.A. Keri, A Review of the Carcinogenic Potential of bisphenol A, Reprod. Toxicol., 59 (2016) 167–182.

[177] Y.Y. Chan, Y. Yue, Y. Li, R.D. Webster, Electrochemical/Chemical Oxidation of Bisphenol A in a Four-electron/Two-proton Process in Aprotic Organic Solvents, Electrochim. Acta, 112 (2013) 287–294.

[178] F. Lombardo, M.Y. Shalaeva, K.A. Tupper, F. Gao, ElogD_{oct}: A Tool for Lipophilicity Determination in Drug Discovery. 2. Basic and Neutral Compounds, J. Med. Chem., 44 (2001) 2490–2497.

[179] H. Tapiero, G.N. Ba, K.D. Tew, Estrogens and Environmental Estrogens, Biomed. Pharmacother., 56 (2002) 36–44.

[180] D.A. Bender, Vitamin B_6, in: D.A. Bender (Ed.) Nutritional Biochemistry of The Vitamins, Cambridge University Press, New York, 2003, pp. 232–269.

[181] M. Takagi, T. Fukui, S. Shimomura, Catalytic Mechanism of Glycogen Phosphorylase: Pyridoxal(5')diphospho(1)-α-D-glucose as a Transition-State Analogue, Proc. Natl. Acad. Sci. USA, 79 (1982) 3716–3719.

[182] D. Palm, H.W. Klein, R. Schinzel, M. Buehner, E.J.M. Helmreich, The Role of Pyridoxal 5'-Phosphate in Glycogen Phosphorylase Catalysis, Biochemistry, 29 (1990) 1099–1107.

[183] N.B. Livanova, N.A. Chebotareva, T.B. Eronina, B.I. Kurganov, Pyridoxal 5'-Phosphate as a Catalytic and Conformational Cofactor of Muscle Glycogen Phosphorylase B, Biochemistry (Moscow, Russian Federation), 67 (2002) 1089–1098.

[184] D.B. Tully, V.E. Allgood, J.A. Cidlowski, Modulation of Steroid Receptor-Mediated Gene Expression by Vitamin B_6, FASEB J., 8 (1994) 343–349.

[185] S.R. Davis, E.P. Quinlivan, P.W. Stacpoole, J.F. Gregory III, Plasma Glutathione and Cystathionine Concentrations Are Elevated but Cysteine Flux Is Unchanged by Dietary Vitamin B-6 Restriction in Young Men and Women, J. Nutr., 136 (2006) 373–378.

[186] C.P. Lima, S.R. Davis, A.D. Mackey, J.B. Scheer, J. Williamson, J.F. Gregory III, Vitamin B-6 Deficiency Suppresses The Hepatic Transsulfuration Pathway but Increases Glutathione Concentration in Rats Fed AIN-76A or AIN-93G Diets, J. Nutr., 136 (2006) 2141–2147.

[187] H.F. Nijhout, J.F. Gregory III, C. Fitzpatrick, E. Cho, K.Y. Lamers, C.M. Ulrich, M.C. Reed, A Mathematical Model Gives Insights into the Effects of Vitamin B-6 Deficiency on 1-Carbon and Glutathione Metabolism, J. Nutr., 139 (2009) 784–791.

[188] M. Ehrenshaft, P. Bilkski, M.Y. Li, C.F. Chignell, M.E. Daub, A Highly Conserved Sequence is a Novel Gene Involved in De Novo Vitamin B6 Biosynthesis, Proc. Natl. Acad. Sci. USA, 96 (1999) 9374–9378.

[189] P. Bilkski, M.Y. Li, M. Ehrenshaft, M.E. Daub, C.F. Chignell, Vitamin B_6 (pyridoxine) and Its Derivatives are Efficient Singlet Oxygen Quenchers and Potential Fungal Antioxidants., Photochem. Photobiol., 7 (2000) 129–134.

[190] B.K. Ohta, C.S. Foote, Characterization of Endoperoxide and Hydroperoxide Intermediates in the Reaction of Pyridoxine with Singlet Oxygen, J. Am. Chem. Soc., 124 (2002) 12064–12065.

[191] J.M. Matxain, M. Ristilä, Å. Strid, L.A. Eriksson, Theoretical Study of the Reaction of Vitamin B_6 with $^1O_2$, Chem. Eur. J., 13 (2007) 4636–4642.

[192] S.K. Jain, G. Lim, Pyridoxine and Pyridoxamine Inhibits Superoxide Radicals and Prevents Lipid Peroxidation, Protein Glycosylation, and $(Na^+ + K^+)$-ATPase Activity Reduction in High Glucose-Treated Human Erythrocytes, Free Radical Biol. Med., 30 (2001) 232–237.

[193] S.A. Denslow, A.A. Walls, M.E. Daub, Regulation of Biosynthetic Genes and Antioxidant Properties of Vitamin B_6 Vitamers During Plant Defense Responses, Physiol. Mol. Plant Pathol., 66 (2005) 244–255.

[194] J.M. Matxaon, M. Ristilä, Å. Strid, L.A. Eriksson, Theoretical Study of the Antioxidant Properties of Pyridoxine, J. Phys. Chem. A, 110 (2006) 13068–13072.

[195] J.A. Matxain, D. Padro, M. Ristilä, Å. Strid, L.A. Eriksson, Evidence of High •OH Radical Quenching Efficiency by Vitamin B_6, J. Phys. Chem. B, 113 (2009) 9629–9632.

[196] S. Dakshinamurti, K. Dakshinamurti, Vitamin B_6, in: R.B. Rucker, J. Zempleni, J.W. Suttie, D.B. McCormick (Eds.) Handbook of Vitamins, CRC Press, New York, 2007, pp. 315–360.

[197] V.R. Da Silva, K.A. Russell, J.F. Gregory III, Vitamin B_6, in: J.W. Erdman Jr., I.A. Macdonald, S.H. Zeisel (Eds.) Present knowledge in Nutrition, Wiley-Blackwell, Chichester, 2012, pp. 307–320.

[198] P. György, Vitamin B_2 and the Pellagra-Like Dermatitis of Rats, Nature (London, United Kingdom), 133 (1934) 448–449.

[199] P. György, Crystalline Vitamin B_6, J. Am. Chem. Soc., 60 (1938) 983–984.

[200] P. György, R.E. Eckardt, Vitamin B_6 and Skin Lesions in Rats, Nature, 144 (1939) 512.

[201] J. Zempleni, W. Kübler, The Utilization of Intravenously Infused Pyridoxine in Humans, Clin. Chim. Acta, 229 (1994) 27–36.

[202] J. Zempleni, W. Kübler, Metabolism of Vitamin B_6 by Human Kidney, Nutr. Res. (N. Y., NY, U. S.), 15 (1995) 187–192.

[203] S. Dakshinamutri, K. Dakshinamurti, Vitamin B_6, in: R.B. Rucker, J. Zempleni, J.W. Suttle, D.B. McCormick (Eds.) Handbook of Vitamins, CRC Press, New York, 2007, pp. 315–360.

[204] D.A. Bender, Vitamin B_6: beyond adequacy, J. Evidence-Based Complementary Altern. Med., 16 (2011) 29–39.

[205] S.L. Ink, L.M. Henderson, Vitamin B_6 Metabolism, Annu. Rev. Nutr., 4 (1984) 455–470.

[206] P. Söderhjelm, J. Lindquist, Voltammetric Determination of Pyridoxine by Use of a Carbon Paste Electrode, Analyst (Cambridge UK), 100 (1975) 349–354.

[207] R.C. Barthus, L.H. Mazo, R.J. Poppi, Simultaneous Determination of Vitamins C, B6 and PP in Pharmaceutics using Differential Pulse Voltammetry with a Glassy Carbon Electrode and Multivariate Calibration Tools, J. Pharm. Biomed. Anal., 38 (2005) 94–99.

[208] Y. Wu, F. Song, Voltammetric Investigation of Vitamin B_6 at a Glassy Carbon Electrode and Its Application in Determination, Bull. Korean Chem. Soc., 29 (2008) 38–42.

[209] J. Gonzalez-Rodriguez, J.M. Sevilla, T. Pineda, M. Blazquez, Electrochemical Analysis on Compounds of the Vitamin B_6 Family using Glassy Carbon Electrodes, Int. J. Electrochem. Sci., 7 (2012) 2221–2229.

[210] Z. Cao, Q. Xie, M. Li, S. Yao, Simultaneous EQCM and Fluorescence Detection of Adsorption/Desorption and Oxidation for Pyridoxol in Aqueous KOH on a Gold Electrode, J. Electroanal. Chem., 568 (2004) 343–351.

[211] M.L. Wang, Y.Y. Zhang, Q.J. Xie, S.Z. Yao, In Situ FT-IR Spectroelectrochemical Study of Electrooxidation of Pyridoxol on a Gold Electrode, Electrochim. Acta, 51 (2005) 1059–1068.

[212] M.F.S. Teixeira, A. Segnini, F.C. Moraes, L.H. Marcolino-Júnior, O. Fatibello-Filho, É.T.G. Cavalheiro, Determination of Vitamin B_6 (Pyridoxine) in Pharmaceutical Preparations by Cyclic Voltammetry at a Copper(II) Hexacyanoferrate(III) Modified Carbon Paste Electrode, J. Braz. Chem. Soc., 14 (2003) 316–321.

[213] M.F.S. Teixeira, G. Marino, E.R. Dockal, É.T.G. Cavalheiro, Voltammetric Determination of Pyridoxine (Vitamin B_6) at a Carbon Paste Electrode Modified with Vanadyl(IV)–Salen Complex, Anal. Chim. Acta, 508 (2004) 79–85.

[214] P.B. Desai, R.M. Kotkar, A.K. Srivastava, Electrochemical Behaviour of Pyridoxine Hydrochloride (Vitamin B_6) at Carbon Paste electrode Modified with Crown Ethers, J. Solid State Electrochem., 12 (2008) 1067–1075.

[215] A. Mekonnen, R.C. Saini, A. Tadese, R. Pal, Square Wave Voltammetric Determination of Pyridoxine in Pharmaceutical Preparations using Cobalthexacyanoferrate Modified Carbon Paste Electrode, J. Chem. Pharm. Res., 6 (2014) 544–551.

[216] A. Baghizadeh, H. Karimi-Maleh, Z. Khoshnama, A. Hassankhani, M. Abbasghorbani, A Voltammetric Sensor for Simultaneous Determination of Vitamin C and Vitamin B_6 in Food Samples Using ZrO_2 Nanoparticle/Ionic Liquids Carbon Paste Electrode, Food Anal. Methods, 8 (2015) 549–557.

[217] W. Qu, K. Wu, S. Hu, Voltammetric Determination of Pyridoxine (Vitamin B_6) by use of a Chemically-Modified Glassy Carbon Electrode, J. Pharm. Biomed. Anal., 36 (2004) 631–635.

[218] S.M. Cottica, J. Nozaki, H.S. Nakatani, C.C. Oliveira, N.E. de Souza, J.V. Visentainer, Voltammetric Determination of Pyridoxine (Vitamin B_6) in Drugs using a Glassy Carbon Electrode Modified with Chromium(III) Hexacyanoferrate(II), J. Braz. Chem. Soc., 20 (2009) 496–501.

[219] T. Nie, J.-K. Xu, L.-M. Lu, K.-X. Zhang, L. Bai, Y.-P. Wen, Electroactive Species-Doped Poly(3,4-ethylenedioxythiophene) Films: Enhanced Sensitivity for Electrochemical Simultaneous Determination of Vitamins B_2, B_6 and C, Biosensors Bioelectron., 50 (2013) 244–250.

[220] B. Habibi, H. Phezhhan, M.H. Pournaghi-Azar, Voltammetric Determination of Vitamin B_6 (Pyridoxine) using Multi Wall Carbon Nanotube Modified Carbon-Ceramic Electrode, J. Iran. Chem. Soc., 7 (2010) S103–S112.

[221] H. Razmi, M. Jabbari, R. Mohammad-Rezaei, Electrochemically Reduced Graphene Oxide Modified Carbon Ceramic Electrode for the Determination of Pyridoxine, Anal. Chem. Lett., 4 (2014) 73–85.

[222] M.H. Pournaghi-Azar, H. Dastangoo, M. Ziaei, Electrocatalytic Oxidation of Pyridoxine (Vitamin B_6) on Aluminum Electrode Modified by Metallic Palladium Particles/Iron (III) Hexacyanoferrate (II) Film, J. Solid State Electrochem., 11 (2007) 1221–1227.

[223] B. Brunetti, E. Desimoni, Voltammetric Determination of Vitamin B_6 in Food Samples and Dietary Supplements, J. Food Compos. Anal., 33 (2014) 155–160.

[224] C.A. Fonseca, G.C.S. Vaz, J.P.A. Azevedo, F.S. Semaan, Exploiting Ion-Pair Formation for the Enhancement of Electroanalytical Determination of Pyridoxine (B_6) onto Polyurethane-Graphite Electrodes, Microchem. J., 99 (2011) 186–192.

[225] A.S. Boev, E.I. Korotkova, A.A. Bakibaev, Voltammetric Determination of Pyridoxine (Vitamin B_6) at a Modified Platinum Electrode, Izv. Vyssh. Uchebn. Zaved. Khim. Khim. Tekhnol., 51 (2008) 21–24.

[226] M.A. Raj, N.S.K. Gowthaman, S.A. John, Highly Sensitive Interference-Free Electrochemical Determination of Pyridoxine at Graphene Modified Electrode: Importance in Parkinson and Asthma Treatments, J. Colloid Interface Sci., 474 (2016) 171–178.

[227] S.R. Hernández, G.G. Ribero, H.C. Goicoechea, Enhanced Application of Square Wave Voltammetry with Glassy Carbon Electrode Coupled to Multivariate Calibration Tools for the

Determination of B_6 and B_{12} Vitamins in Pharmaceutical Preparations, Talanta, 61 (2003) 743–753.

[228] T. Pineda, J.M. Sevilla, A.J. Román, M. Blázquez, Electrooxidation of Pyridoxal (PL) on a Polycrystalline Gold Electrode in Alkaline Solutions, J. Electroanal. Chem., 492 (2000) 38–45.

[229] J. Gonzalez-Rodríguez, J.M. Sevilla, T. Pineda, M. Blázquez, A Comparative Study of the Electrochemical Properties of Vitamin B-6 Related Compounds at Physiological pH, Russ. J. Electrochem., 47 (2011) 835–845.

[230] J. Jörissen, B. Speiser, Preparative Electrolysis on the Laboratory Scale, in: O. Hammerich, B. Speiser (Eds.) Organic Electrochemistry, CRC Press, Boca Raton, Florida, 2016, pp. 265–330.

Chapter 2

The Electrochemical Study of Sesamol in Acetonitrile

This page has been intentionally left blank

2.1. Chapter Overview

In this chapter, a detailed investigation on the electrochemical oxidation of sesamol (Scheme 2.1) in an aprotic solvent, acetonitrile (CH_3CN), was performed using a several electrochemical techniques such as cyclic voltammetry (CV) and controlled potential electrolysis (CPE).

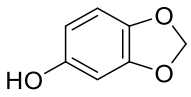

Scheme 2.1. Chemical structure of sesamol.

During the initial stage of the study, preliminary results put forward in the current work revealed that sesamol is highly sensitive to low amounts of water present in the test solution, as evidenced by the significant change in the electrochemical responses after a short time interval (15 minutes). As such, CV measurements conducted with and without the presence of molecular sieves were compared. In addition, the interaction of water with sesamol and its influence on the voltammetric appearances of the redox reactions undergone by sesamol were also described. Notably, however, the complete elimination of all water is not the objective of the present work.

At a platinum electrode, sesamol was found to undergo an electrochemical oxidation reaction at ca. 0.70 vs. $(Fc/Fc^+)/V$ that involves the loss of five moles of electrons per two molecules of sesamol. With the use of a chemical oxidant, nitrosonium hexafluoroantimonate ($NOSbF_6$), sesamol was chemically oxidized to generate a dimer which was subsequently isolated and positively identified. Lastly, using the information gathered, a tentative mechanism was proposed.

2.2. Results and Discussion

2.2.1. Electrochemical oxidation of sesamol in CH_3CN

The cyclic voltammograms collected of sesamol in CH_3CN showed that the oxidized product is sensitive to trace amounts of moisture present in the sample solution. As depicted in Figure 2.1, there is a marked change in electrochemical behavior at the onset (solid line) and after 15 mins (dashed line) of the experiment when absorption of water from the environment into the test solution has occurred [1]. For instance, while the oxidation wave at ca. 0.70 vs. $(Fc/Fc^+)/V$ appeared similar, the reverse cathodic wave at ca. 0.35 vs. $(Fc/Fc^+)/V$ was of significantly reduced magnitude on the return sweep after 15 mins. Nonetheless, after the addition of 3 Å molecular sieves, a well-known drying agent [2-4], the initial voltammetric response could be re-obtained (Figure 2.1, dotted line). Therefore, these preliminary results imply an interaction is occurring between the oxidized form of sesamol with low levels of moisture that is present in the solution. As such, subsequent experiments conducted in the presence and absence of the molecular sieves were compared and discussed. With the use of molecular sieves, both the solvent and electrolyte can be dried, particularly the latter which are generally hydroscopic [3]. In order to ascertain that there is only minimum voltammetric interference from the molecular sieves, a CV background measurements was performed in the absence of sesamol (Figure A2.1 in the Appendix section). At this juncture, it is worth mentioning that the total exclusion of water is not the purpose of the present study.

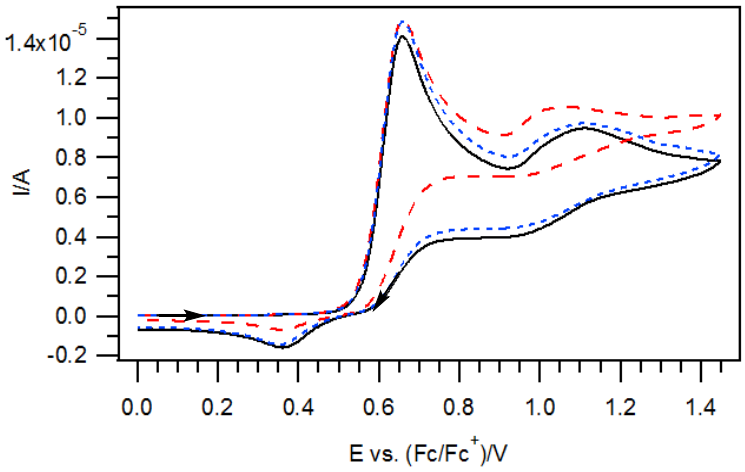

Figure 2.1. Cyclic voltammograms of 2 mM sesamol in CH_3CN with 0.2 M Bu_4NPF_6, recorded using a 1 mm diameter planar Pt electrode at a scan rate of 0.1 V s^{-1} and 22 (±2) °C. (—) Start of the experiment. (- - -) After 15 minutes. (·····) After the addition of molecular sieves.

2.2.2. Voltammetry of sesamol under lower water content conditions

CV scans of sesamol in CH_3CN solutions containing water content between 8 to 13 mM were carried out. Two oxidation peaks at ca. 0.70 and 1.25 vs. (Fc/Fc^+)/V (waves 1 and 2) were observed and when the scan direction was reversed, two reduction peaks were detected at ca. 0.35 and -0.40 vs. (Fc/Fc^+)/V (waves 3 and 4) (Figure 2.2a). Additionally, it was revealed that wave 3 increased in magnitude as the potential window was restricted to only the first anodic step, thus implying the plausible association of the cathodic peak with a reactive intermediate produced via the initial oxidation at ca. 0.70 vs. (Fc/Fc^+)/V (Figure 2.2b). Moreover, a new oxidation peak at ca. 0.40 vs. (Fc/Fc^+)/V (wave 5) which was not observed in the wider potential window (Figure 2.2a) was registered during the second cycle of the narrower scan potential (Figure 2.2b). This additional wave (wave 5) is likely to be attributable to the oxidation of the species generated in wave 3 (i.e. waves 3 and 5 together form a redox couple).

To examine the oxidation reaction occurring at wave 1 in greater detail, the starting potential was changed to ca. 0.00 vs. (Fc/Fc^+)/V (instead of at -0.70 vs. (Fc/Fc^+)/V) and it was found that the current magnitude of wave 5 increased (Figure 2.2c, dotted line). Similarly, this process (wave 5) was also observed by Estévez Brito et al. [5] during their experiments which were performed in aqueous solutions and ascribed this process to stem from the reaction product of the oxidation process occurring at wave 1. However, the species responsible for wave 5 must be different in the present study as compared to the previous case [5] as wave 5 was not observed if the water content of the CH_3CN solution is increased (Section 2.2.3). A comparison of Figures 2.2a and 2.2b indicates that the intermediate species are more long-lived with a smaller potential range (switching potential at ca. 1.10 vs. (Fc/Fc^+)/V), in the sense that waves 3 and 5 display larger peak currents. Therefore, subsequent discussions of sesamol's electrochemical behavior will be focused only on this potential window (Figure 2.2b).

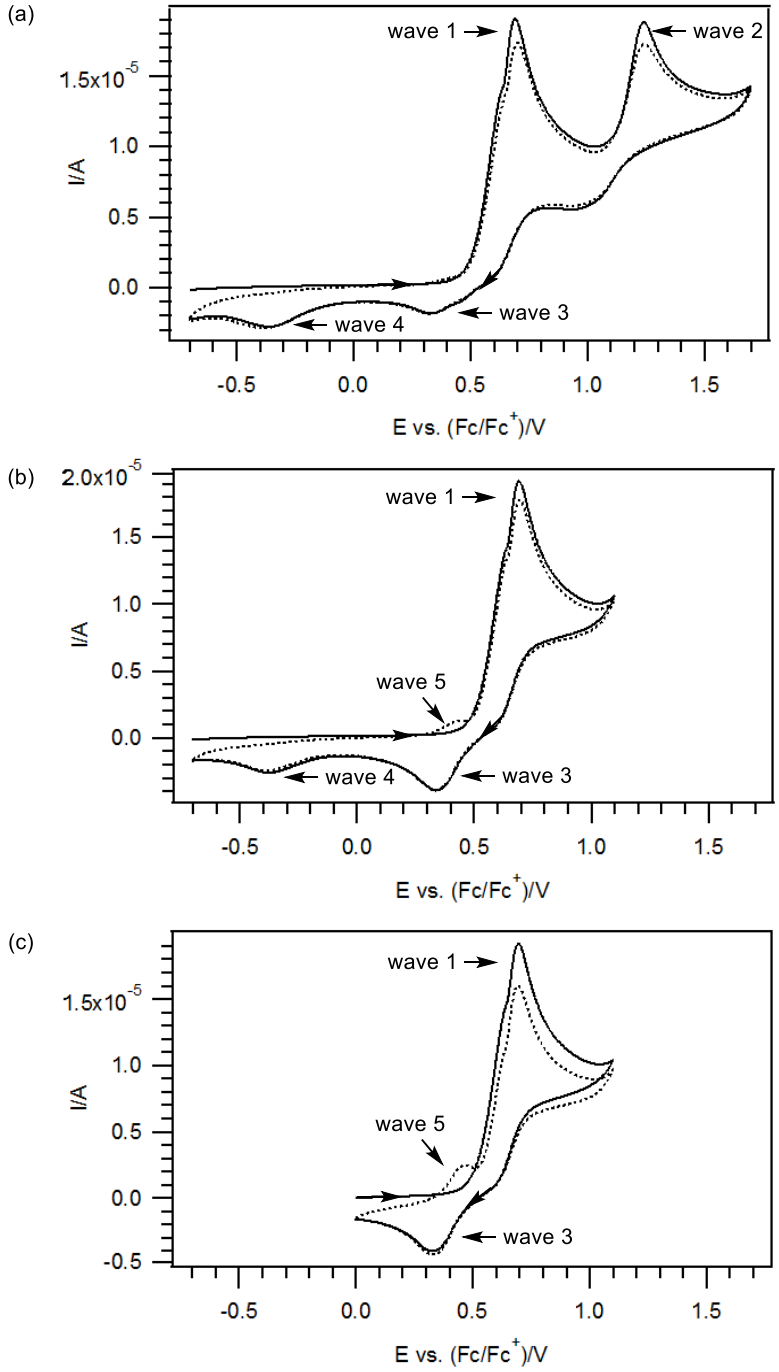

Figure 2.2. Cyclic voltammograms of 2 consecutive scans of 2 mM sesamol in CH_3CN ($[H_2O]_{initial}$ = 8 mM, $[H_2O]_{final}$ = 13 mM) with 0.2 M Bu_4NPF_6, recorded using a 1 mm diameter planar Pt electrode at a scan rate of 0.1 V s^{-1} and 22 (±2) °C. (—) 1st cycle. (·····) 2nd cycle. (a) Start/end potentials: -0.70 vs. (Fc/Fc^+)/V. Switching potential: 1.65 vs. (Fc/Fc^+)/V. (b) Start/end

potentials: -0.70 vs. (Fc/Fc^+)/V. Switching potential: 1.10 vs. (Fc/Fc^+)/V. (c) Start/end potentials: 0.00 vs. (Fc/Fc^+)/V. Switching potential: 1.10 V vs. (Fc/Fc^+)/V.

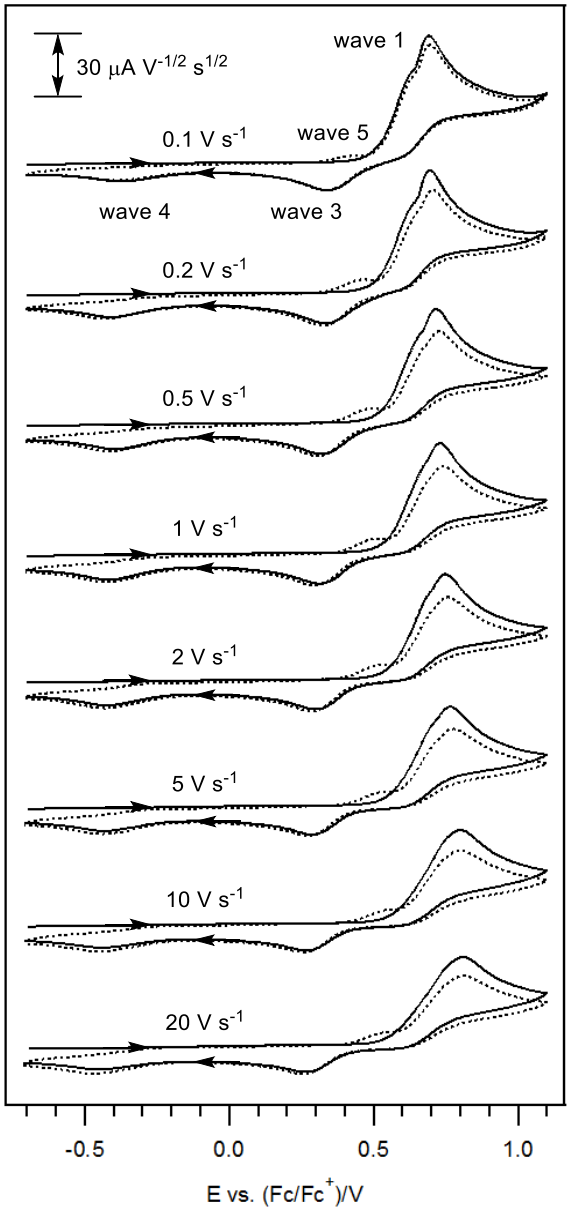

Figure 2.3. Variable scan rates cyclic voltammograms of 2 consecutive scans of 2 mM sesamol in CH_3CN ($[H_2O]_{initial}$ = 8 mM, $[H_2O]_{final}$ = 13 mM) with 0.2 M Bu_4NPF_6, recorded using a 1 mm diameter planar Pt electrode at 22 (±2) °C. (—) 1st cycle. (·····) 2nd cycle. Current data were multiplied by (scan rate)$^{-0.5}$ for normalization.

Figure 2.3 illustrates the CV responses of sesamol in CH_3CN obtained over various scan rates (0.1 V s^{-1} to 20 V s^{-1}). At slower scan rates ≤ 2 V s^{-1}, two closely-spaced peaks were detected at wave 1 whereas only one oxidation peak was observed when higher scan rates (≥ 5 V s^{-1}) were used. In addition, a plot of the normalized current against potential revealed that the ratio of the reduction (i_p^{red}, wave 3) to oxidation (i_p^{ox}, wave 1) peak currents (i_p^{red}/ i_p^{ox}) generally increased with faster scan rates (Figure 2.4). However, it is notable that in spite of the utilization of high scan rates (e.g. 20 V s^{-1}), the i_p^{red}/ i_p^{ox} ratios did not reach unity. Also, the large separation between waves 1 and 3 over the scan rates examined indicates that slow heterogeneous electron transfer is unlikely to be entirely responsible for the wide peak to peak separation (E_{pp}) between both waves. Moreover, the close proximity of wave 5 to wave 3 suggests that wave 3 is not responsible for the regeneration of the starting material (**1**), and instead is associated with another intermediate species that is reduced in wave 3 and chemically reversibly oxidized back in wave 5.

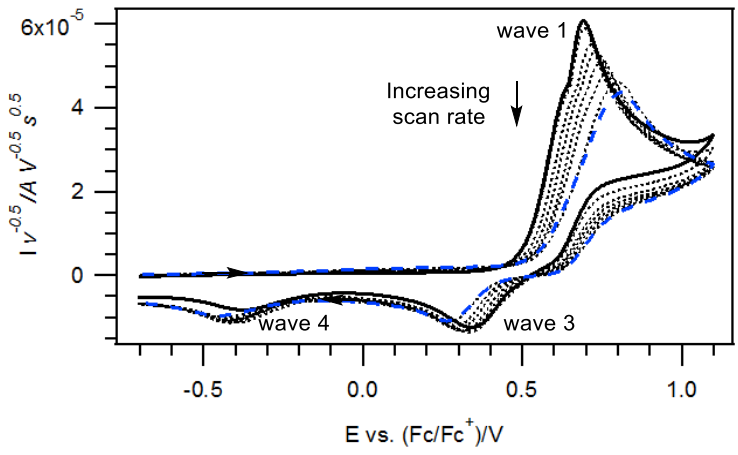

Figure 2.4. Overlaid variable scan rates cyclic voltammograms of 2 mM sesamol in CH_3CN ($[H_2O]_{initial}$ = 8 mM, $[H_2O]_{final}$ = 13 mM) with 0.2 M Bu_4NPF_6, recorded using a 1 mm diameter planar Pt electrode at 22 (±2) °C. Current data were multiplied by (scan rate)$^{-0.5}$ for normalization. (—) 0.1 V s^{-1}. (·····) 0.2, 0.5, 1, 2, 5, and 10 V s^{-1}. (- - -) 20 V s^{-1}.

To further assess the interaction of sesamol with low amounts of water, CVs of varying scan rates were similarly conducted using a larger concentration of sesamol (10 mM instead of 2 mM) under dry conditions (Figure 2.5). In doing so, the analyte concentration (10 mM) is maintained higher than that of trace water ($[H_2O]_{initial}$ = 8 mM). Overall, the voltammetric behavior of sesamol was found to be reminiscent of Figure 2.3, where two closely-spaced peaks were registered at wave 1 at slower scan rates and only one anodic process was observed when the scan rates were increased (≥ 10 V s^{-1}). Apart from that, two additional closely-spaced cathodic peaks were also detected at wave 3 at lower scan rates (≤ 1 V s^{-1}) which were not recorded in the CV experiments conducted using 2 mM of starting material (Figure 2.3). These results can tentatively be interpreted as two forms of sesamol co-existing in solution; the hydrogen bonded (with H_2O) and non-hydrogen bonded forms, of which the latter is promoted at a higher substrate concentration [6].

2.2.3. Voltammetry of sesamol under higher water content conditions

CV experiments under varied scan rates were likewise carried out under a condition of higher water content ($[H_2O]_{initial}$ = 126 mM) where no efforts were made to preclude water (Figure 2.6).

In contrast to earlier findings illustrated in Figure 2.3, a splitting of wave 1 was not observed and the anodic process appeared to be completely chemically irreversible at 0.1 V s^{-1}; the corresponding cathodic peak (wave 3) only became voltammetrically noticeable at faster scan rates (≥ 1 V s^{-1}). The apparent dichotomy illustrated in Figures 2.3 and 2.6 demonstrate a significant interaction between the intermediate oxidized forms of sesamol with trace amounts of water in the test solution. In addition, it was also revealed that although wave 3 increases with higher scan rates, in accordance with expectation, wave 4 decreases in intensity at higher

scan rates. Therefore, the latter heterogeneous step can be reasoned to be due to a secondary process.

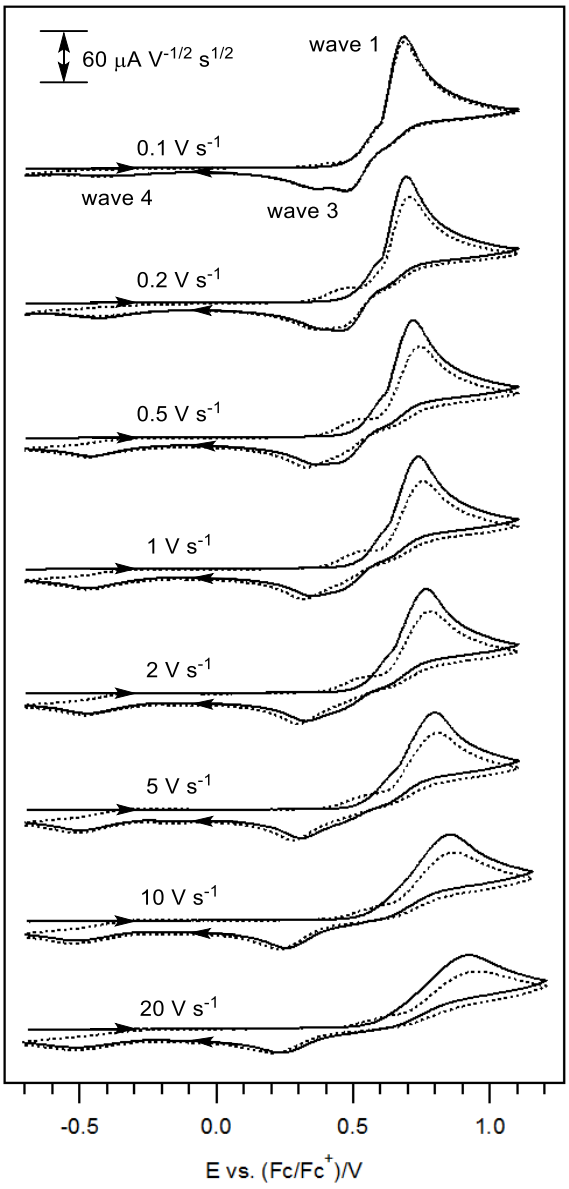

Figure 2.5. Variable scan rates cyclic voltammograms of 2 consecutive scans of 10 mM sesamol in CH_3CN ($[H_2O]_{initial}$ = 8 mM, $[H_2O]_{final}$ = 13 mM) with 0.2 M Bu_4NPF_6, recorded using a 1 mm diameter planar Pt electrode at 22 (±2) °C. (—) 1st cycle. (·····) 2nd cycle. Current data were multiplied by (scan rate)$^{-0.5}$ for normalization.

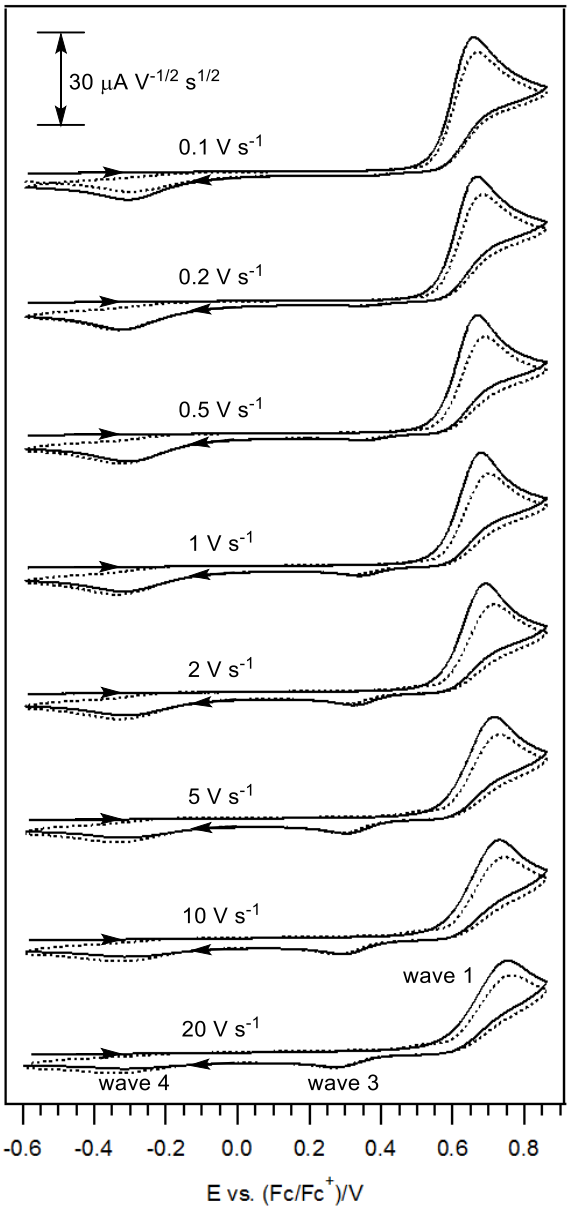

Figure 2.6. Variable scan rates cyclic voltammograms of 2 consecutive scans of 2 mM sesamol in CH_3CN ($[H_2O]_{initial}$ = 126 mM) with 0.2 M Bu_4NPF_6, recorded using a 1 mm diameter planar Pt electrode at 22 (±2) °C. (—) 1st cycle. (·····) 2nd cycle. Current data were multiplied by (scan rate)$^{-0.5}$ for normalization.

2.2.4. Voltammetry of sesamol in variable water content

Results gathered from the preceding sections have demonstrated that the oxidized form of sesamol undergoes interactions with even relatively low levels of water present inside the sample solution. To gain additional insights into this interactions, CV analysis of sesamol in the presence of varied water content was performed where accurately known volumes of water were carefully introduced.

It was revealed that wave 1 and its corresponding reduction peak (wave 3) shifted to less positive potentials with higher water concentration. Similarly, wave 4 translated to more negative potentials when incremental amounts of water were added (Figure 2.7). The magnitude of wave 3 diminished with increasing water content, such that when the water concentration reached ca. 37 mM, only the secondary process (wave 4) was detected at a scan rate of 0.1 V s^{-1}. Therefore, it is posited that the species responsible for wave 3 is relatively unstable and short-lived under high water concentrations which in turn results in the observation of the increase in wave 4. However, the stability of this intermediate species did not improve even though the temperature of the sample solution was decreased (Figure A2.4 in the Appendix section).

At [H_2O] = 37 mM, wave 3 that was not apparent at a scan rate 0.1 V s^{-1} was re-observed again at faster scan rates (Figure 2.8). This further corroborates the assignment of the reduction process in wave 3 to be a result of an intermediate of the oxidized product formed at wave 1, with an improvement in its chemical reversibility achieved at higher scan rates and/or lower moisture content.

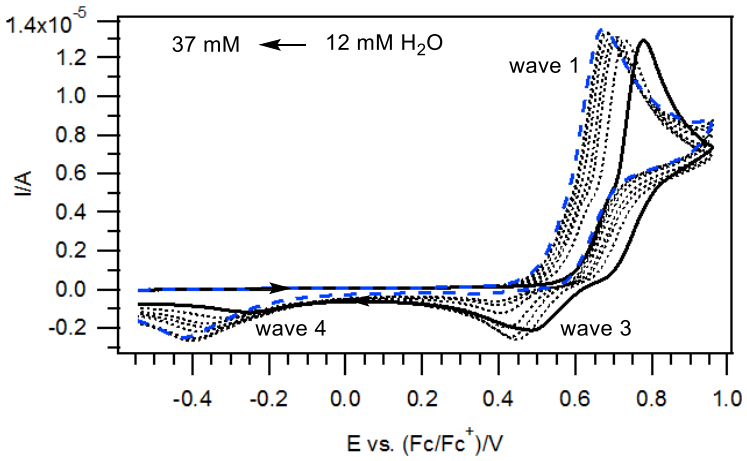

Figure 2.7. Overlaid cyclic voltammograms of 2 mM sesamol in CH_3CN ($[H_2O]_{initial}$ = 12 mM, $[H_2O]_{final}$ = 37 mM) with 0.2 M Bu_4NPF_6, recorded using a 1 mm diameter planar Pt electrode at a scan rate of 0.1 V s^{-1} and 22 (±2) °C, with varying amount of water. (—) 12 mM. (·····) 12-37. (- - -) 37 mM.

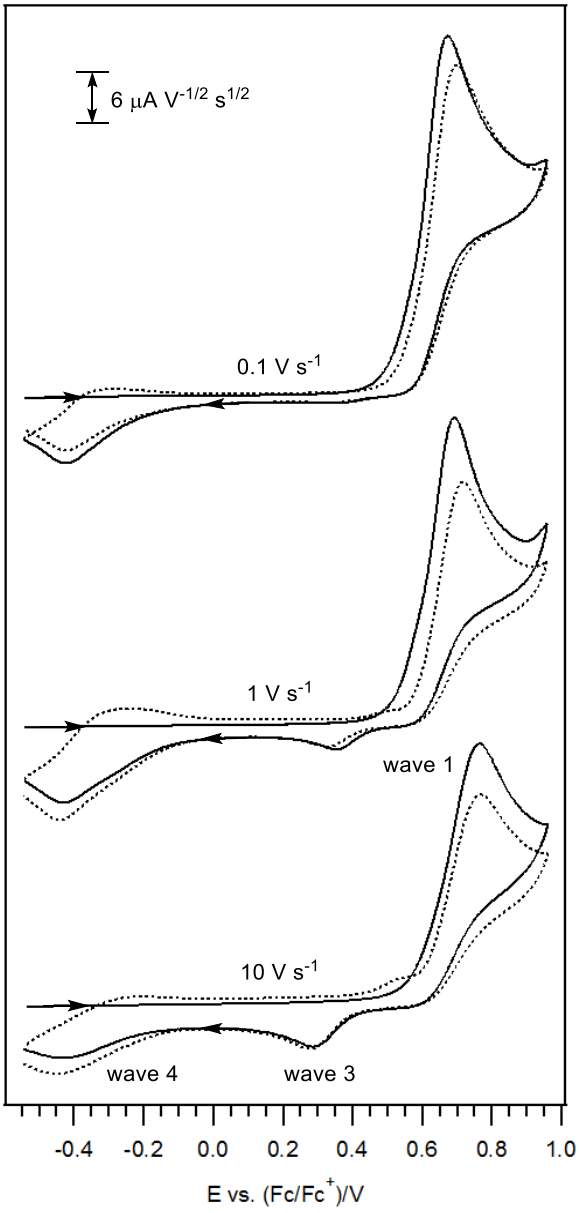

Figure 2.8. Variable scan rates cyclic voltammograms of 2 consecutive scans of 2 mM sesamol in CH_3CN ($[H_2O]_{initial}$ = 37 mM) with 0.2 M Bu_4NPF_6, recorded using a 1 mm diameter planar Pt electrode at 22 (±2) °C. (—) 1st cycle. (·····) 2nd cycle. Current data were multiplied by (scan rate)$^{-0.5}$ for normalization.

2.2.5. Preparative scale oxidation of sesamol

Even though CV is a preeminent technique that is often used for the study of redox transformations, it does not always provide direct and/or conclusive information regarding the number of electrons involved or the degree of chemical reversibility over an extended period (t ≥ minutes). Therefore, exhaustive controlled potential electrolysis (CPE) experiments were carried out to probe the long term stability of the oxidized product and its intermediate(s). The electrolysis results are given in Figure 2.9, together with the associated cyclic voltammograms collected prior to and after the CPE. To ensure a complete oxidation of the starting material is achieved, the potential was applied at 50 mV more positive than the E_p^{ox} value of wave 1 attained during CV experiments. Confirmation of the complete oxidation can be obtained from the disappearance of the initial anodic peak at ca. 0.70 vs. (Fc/Fc^+)/V (wave 1) (Figure 2.9(a), blue dashed line) and the observation of an almost zero faradic current in the coulometry result (Figure 2.9(b), black solid line).

Using Eq. (2.1), the exhaustive oxidation of sesamol was found to involve ca. 2.5 electrons per molecule of analyte, with the initial colorless solution turning dark green via a purple intermediate. This result was verified by repeating the electrolysis experiments at the same concentration (2 mM) three times (Figure A2.5-A2.7 in the Appendix section). In comparison, the CPE of 2 mM ferrocene under similar conditions demonstrated a total of 1.0 electron was transferred per molecule of analyte, in line with expectations (Figure A2.8 in the Appendix section), confirming the validity of the electrolysis cell set-up. In addition, the oxidative CPE of sesamol was also performed at different concentrations. In general, the results showed that the number of electrons transferred per molecule of analyte decreased as the amount of starting material used was increased. More specifically, ca. 3.2, 2.2, and 1.8 electrons were transferred per molecule of sesamol when the electrolysis experiments were conducted at a concentration of 1, 5, and 10 mM respectively (Figure A2.9-A2.11 in the Appendix section). This implys that

the oxidation reaction is highly sensitive to the analyte concentration employed and likely entails dimerization/coupling reactions between the oxidized forms of the compound in addition to multiple electron transfer steps. Moreover, the anodic process appeared to be chemically irreversible over prolong periods of time (t ≥ minutes), with the resultant voltammogram revealing a new redox couple (E_p^{red} at ca. -0.55 vs. (Fc/Fc^+)/V) after the disappearance of the initial anodic peak (wave 1).

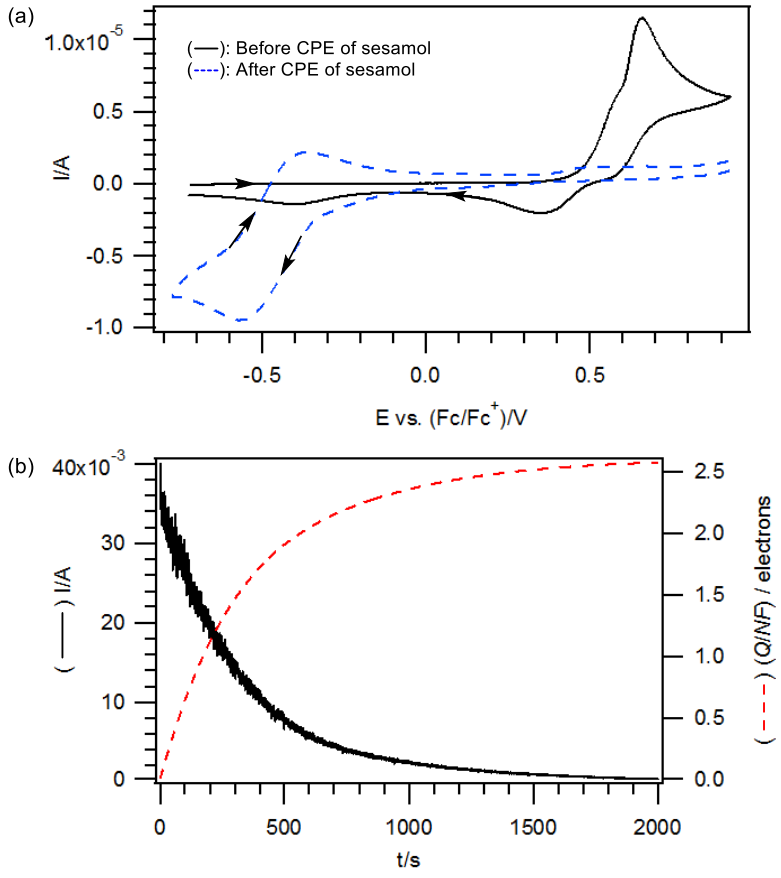

Figure 2.9. Voltammetric and coulometric data recorded during the controlled potential electrolysis of 2 mM sesamol in CH_3CN with 0.2 M Bu_4NPF_6 at 22 (±2) °C. (a) Cyclic voltammograms obtained at a scan rate of 0.1 V s^{-1} using a 1 mm diameter planar Pt electrode. (b) Current vs. time data logged during the exhaustive oxidation of sesamol at 0.70 vs. (Fc/Fc^+)/V.

Besides being an alternative approach for the bulk conversion of the starting material into its final product, chemical oxidation also enables the verification of the number of electrons involved in a redox process. More notably, this expeditious method does not involve the use of any supporting electrolyte which would require removal during product isolation. $NOSbF_6$, a one-electron chemical oxidant [7], was chosen for the current work as it possesses several desirable characteristics including being ^{1}H and ^{13}C NMR silent which allows for convenient NMR spectroscopic analysis of the products. Moreover, the reduction of $NOSbF_6$ results in the generation of NO, a gaseous byproduct, that can be easily excluded from the reaction mixture and has been utilized successfully in earlier studies relating to the chemical/electrochemical oxidation of phenolic compounds [8-11].

The feasibility of oxidizing sesamol using $NOSbF_6$ was examined by carrying out a small CV scale experiment where increasing equivalences of the aforementioned chemical oxidant was added to a solution of sesamol (Figure 2.10). In accordance with expectations, wave 1 decreased in intensity after the addition of each molar equivalent of $NOSbF_6$, and disappeared completely upon reaching 2.5 molar equivalents; which matched the results obtained during the CPE experiments (Figure 2.9). Furthermore, a new redox pair with E_p^{red} at ca. -0.55 vs. $(Fc/Fc^+)/V$ was observed which is also consistent with earlier findings (Figure 2.9) .

After testing the suitability of using $NOSbF_6$ for the chemical oxidation of sesamol, a synthetic scale reaction was conducted by adding 2.5 molar equivalents of $NOSbF_6$ to a CH_3CN (dried over molecular sieves) solution of sesamol. Initially, efforts to isolate the generate product via flash column chromatography were futile. Thus, it was envisioned that the treatment with an appropriate electrophile (e.g. iodomethane) into the reaction mixture could be performed in order to trap the likely formed hydrolyzed product [5], and minimize the likelihood of it undergoing follow-up reactions to form multiple products [11]. After this chemical treatment

step, a dimeric product was isolated using flash column chromatography, and its identity was positively confirmed by X-ray crystallography, as depicted in Figure 2.11.

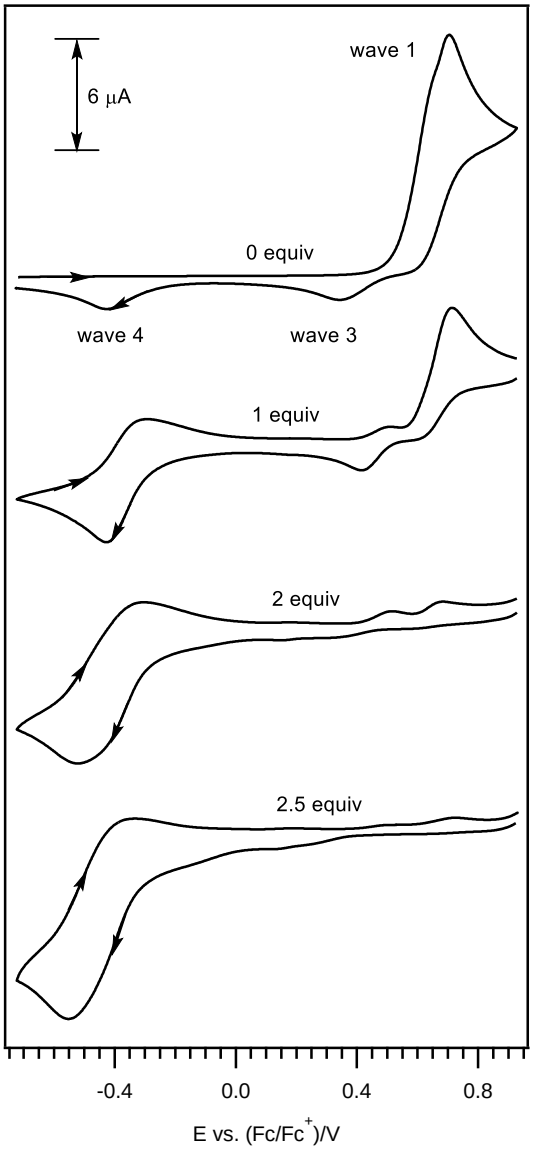

Figure 2.10. Cyclic voltammograms of 2 mM sesamol in CH_3CN with 0.2 M Bu_4NPF_6, recorded at a 1 mm diameter planar Pt electrode at 22 (±2) °C and at a scan rate of 0.1 V s^{-1} with varying equivalents of $NOSbF_6$.

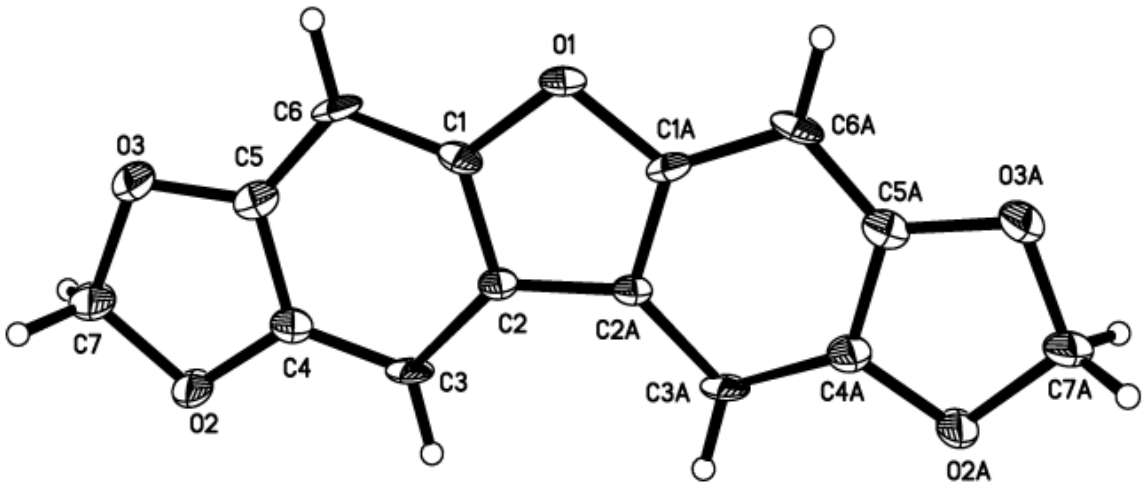

Figure 2.11. ORTEP drawing of the isolated dimeric product **8** with thermal ellipsoids at 50% probability levels.

2.2.6. Proposed electrochemical oxidation mechanism in the presence/absence of water

Based on the results gathered, a mechanism for the electrochemical oxidation of sesamol to form the dimeric product is illustrated in Schemes 2.2 and 2.3. Behaving in a similar fashion as a typical phenol, it is posited that sesamol initially undergoes a two-electron/one-proton ($-2e^-/-H^+$) oxidation via an ECE pathway, where E and C represent an electrochemical and chemical step respectively (Scheme 2.2) to form a reactive diamagnetic cation (compound **6**). Cationic molecules such as compound **6** are often very reactive towards nucleophiles including trace moisture, with the oxidized form of α-tocopherol (vitamin E) being one exception that has been known to be able survive indefinitely in very dry CH_3CN [6, 8].

The presence of wave 1 is consistent with usual observations during the electrochemical oxidation of phenols, where the second electron transfer step (to form the cation) occurs at a less positive potential than the first heterogeneous process (to form the cation radical), and therefore leading in the observation of only a single anodic peak [8-11]. In light of this, wave 3 can be assigned to the reduction of the positively charged compound **6** back to **5** or the reduction

of the dimeric compound **7** that is produced via the rapid coupling of the diamagnetic cation (**6**) with the loss of two protons (Eq. (ii) in Scheme 2.3). In the presence of sufficiently high quantities of water, it is likely that a hydrolysis reaction will occur instead of the dimerization reaction, thereby resulting in the absence of wave 3 as the water content increases. Wave 5 that is evident on the second cycle is assigned as the reverse of the heterogeneous reaction occuring in wave 3.

Subsequently, the further reaction of two molecules of **7** alongside the loss of a molecular oxygen (O_2) leads to the generation of two molecules of **8** (Eq. (iii) in Scheme 2.3), which can undergo a further one-electron oxidation to deliver the radical cation dimer **9**. The presence of compound **9** is supported by electron paramagnetic resonance (EPR) spectroscopy performed in a solution of sesamol that has been treated with 2.5 equivalents of $NOSbF_6$ (Figure A2.12 in the Appendix section). The existence of this cation radical has also previously been reported by Hellberg et al. [12], although its synthesis was carried out through a completely different route than in the present study.

Lastly, the addition of iodomethane, an alkyl iodide that can undergo oxidation readily [13], facilitates the reduction of the double dimerized paramagnetic product into a single diamagnetic dimer. Summarily, two molecules of sesamol can undergo an overall five-electron oxidation reaction via the loss of four protons and O_2.

The presence of the hydrogen bonded forms as put forward in Scheme 2.2 is validated by the translation of wave 1 to less positive potentials in the CV experiments conducted at increasing water concentrationa (Figure 2.7). This is proposed to be attributable to the weakening of the phenolic hydroxyl functionality, specifically the oxygen-hydrogen bond, when interacting with the neighboring water molecules. This results in the phenols' exhibition of some phenolate characteristics such as the tendency to oxidize at less positive potentials as compared its

corresponding phenolic analogue [6, 14]. Furthermore, the observation of an additional oxidation peak near wave 1 under very dry conditions (Figure 2.3 and 2.5) and at lower scan rates of ≤ 2 V s^{-1} is likely to be accountable for by the co-existence of hydrogen and non-hydrogen bonded forms. However, only a single anodic peak was seen when faster scan rates were used, and this could possibly be attributed to the outrun of the hydrogen bond forming steps (from compound **1** to **3** and compound **2** to **4**) or the relatively slower electron transfer rate during the oxidation of the hydrogen bonded forms (compound **3** to **4**) in comparison to the transformation of compound **1** to **2**. On the contrary, in the presence of high concentrations of water (Figure 2.6), where the analyte molecules are expected to mostly exist in their hydrogen bonded forms, only one anodic peak was detected regardless of the scan rate employed.

The moderate yield attained for the dimer **8** in the present study may possibly be due to the instability of the phenoxonium cation **6** or the initially formed oxygenated dimers undergoing other homogeneous reactions (apart from the pathways that are outlined in Scheme 2.3) such as dealkylation or hydrolysis [8, 9] as thin layer chromatography (TLC) analysis revealed several other products that could not be isolated and identified in the current work. Furthermore, a secondary reduction process was also experimentally observed at ca. -0.40 vs. (Fc/Fc^{+})/V (wave 4, Figure 2.3). Nonetheless, the generation of the dimer **8** is suggestive of the existence and stability of the prerequisite compound **7**. It is worthy to note that the mechanism outlined in Schemes 2.2 and 2.3 only applies to CH_3CN solutions containing trace quantities of water. In exclusively aqueous media or in systems comprising of water with low amounts of CH_3CN, the mechanism is likely to vary as many of the oxidized intermediate species will themselves be susceptible to reactions with excess moisture.

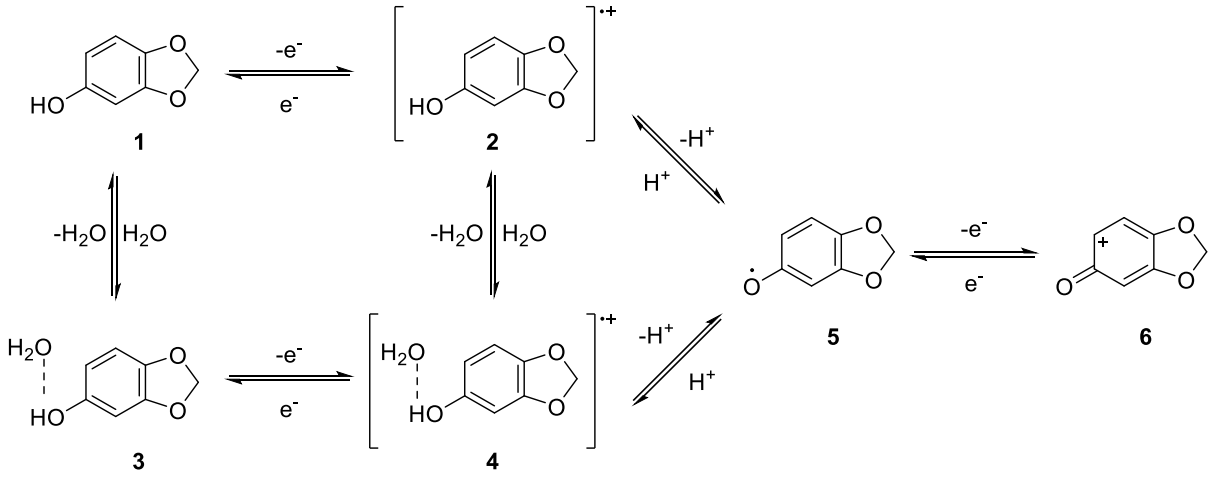

Scheme 2.2. The proposed ECE ($-2e^-/-H^+$) oxidative mechanism of sesamol and its hydrogen bonded forms.

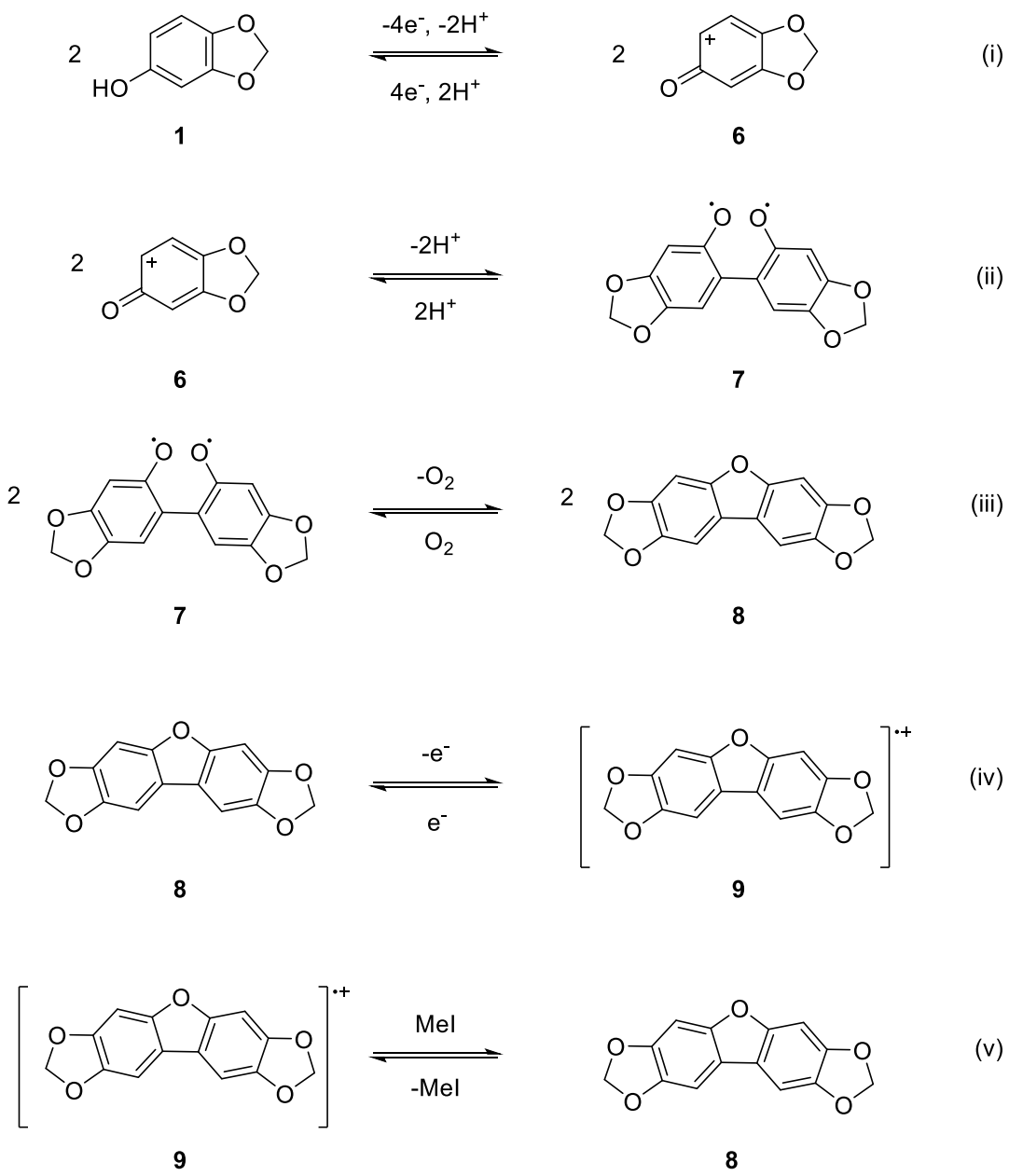

Scheme 2.3. Proposed general mechanistism for the reaction of sesamol in CH_3CN with 2.5 and 1.1 equiv. $NOSbF_6$ and CH_3I respectively.

2.3. Conclusion

In conclusion, the voltammetric responses collected in the present study have clearly established the significance of trace moisture modifying the electrochemical appearances of sesamol. This is likely accountable for by the hydrogen bonding interactions between sesamol and water, where the redox peaks were generally shifted to less positive potentials following the gradual increment in water content. Similarly, this shift in peak potentials, in accordance to the increase in water levels, were recorded during the electrochemical oxidation of other phenolic compounds performed in CH_3CN [6, 15]. At a Pt electrode, sesamol, together with its hydrogen bonded forms, can be electrochemically oxidized at ca. 0.70 vs. (Fc/Fc^+)/V (wave 1) with a corresponding cathodic peak seen at ca. 0.35 vs. (Fc/Fc^+)/V (wave 3) that is related to the reduction of an intermediate species generated after the initial oxidation reaction. The magnitude of wave 3 relative to wave 1 increases with higher scan rates, albeit with only limited improvement as evidenced by the limited peak current ratios attained even with the employment of very fast scan rates (e.g. 20 V s^{-1}). Both the oxidative CPE and chemical oxidation analysis revealed the involvement of multiple electrons, and a dimeric form of sesamol was successfully isolated and positively identified. The proposed mechanism for the oxidation of sesamol is posited to initially involve a two electron/one proton ($-2e^-/-H^+$) loss via an ECE sequence, with two of the generated phenoxonium cations undergoing a coupling reaction with one another alongside the concomitant loss of two protons. Thereafter, a subsequent dimerization reaction takes place through the loss of O_2, followed by a one-electron oxidation to generate a tetrameric radical cation **9** which was characterized by EPR spectroscopy. Interestingly, the treatment with iodomethane, a chemical added in order to trap the generated product, acts as a reductant which enables the isolation of the dimer **8**.

2.4. Experimental

2.4.1. General remarks

All chemicals and reagents were purchased from commercial sources and used as received unless otherwise stated. ^{1}H and ^{13}C NMR spectra were measured on Bruker Avance 500 (500 MHz) NMR spectrometer. Chemical shifts (parts per million) were recorded using tetramethylsilane (TMS, 0.00 ppm) as the internal reference standard and referenced to $CDCl_3$, the solvent used. $CDCl_3$ was acquired from the Cambridge Isotope Laboratories Inc. Multiplicities are given as s (singlet) and the number of protons (*n*) for a given resonance is indicated by *n*H. High resolution mass spectra (HRMS) were obtained on a Waters Q-TOF Premier Mass Spectrometer equipped with Waters Acquity UPLC.

2.4.2. Chemicals and reagents

Sesamol (98%) was obtained from Alfa Aesar and stored at 0 °C. 1/16 inch rods molecular sieves with pore size 3 Å (CAS: 308080-99-1) was purchased from Fluka. Nitrosonium hexafluororoantimonate ($NOSbF_6$, 99.9%) was acquired from Sigma-Aldrich and stored in a glovebox under a nitrogen atmosphere. HPLC purity acetonitrile (CH_3CN) was purchased from Macron. Ultrapure water with resistivity ≥ 18 MΩ cm was obtained from an ELGA Purelab Option-Q water purification system. The supporting electrolyte, tetrabutylammonium hexafluorophosphate (Bu_4NPF_6), was prepared according to a literature procedure by reacting equal molar amount of Bu_4NOH (40%, Alfa Aesar) and HPF_6 (65%, Fluka), washing the precipitate with ultrapure water and recrystallizing three times with hot ethanol followed by drying under vacuum at 140 °C for 6 hours.

2.4.3. Voltammetry

Cyclic Voltammetry (CV) experiments were performed with a computer controlled Eco Chemie Autolab PGSTAT302N potentiostat in a three-electrode cell where a 1 mm diameter planar disk platinum (Pt) working electrode (eDAQ Pty Ltd) was used together with a Pt auxiliary electrode (Metrohm) and an Ag wire miniature reference electrode (eDAQ Pty Ltd) which was connected to the test solution via a salt bridge containing 0.5 M Bu_4NPF_6 in CH_3CN. Accurate potentials were obtained via the addition of ferrocene (Fc) as an internal standard at the end of the measurements. All solutions used for the voltammetric experiments were deoxygenated by purging with high purity argon gas and measurements were performed in a Faraday Cage. Variable temperature CV experiments (-30 to 20 °C) were conducted in a Metrohm jacketed glass cell using a Julabo FP89-HL ultralow refrigerated ethanol circulating bath. Ohmic drop was not compensated for all cyclic voltammograms.

2.4.4. Measurement of water content in analyte solution

Karl Fisher (KF) titrations were performed using a Mettler Toledo DL32 coulometer using (Riedel-deHaën) HYDRANAL- coulomat CG and HYDRANAL- coulomat AG for the cathode and anode compartment respectively. Measurements were carried out inside a humidity control box (122cm × 61cm × 61cm) maintained at a constant humidity (30%) using a dry nitrogen purge gas system from Coy Laboratory Products Inc. Sample solutions in a 5 mL vacuum syringe (SGE Analytical Science) were injected into the coulometer through a silicon/Telfon septum.

2.4.5. Preparations for dry cyclic voltammetry experiments

CV experiments with lower water content (initial [H_2O] ~ 8 mM) were conducted in an electrochemical cell that was dried at 100 °C for at least 1 hour prior to the experiment and cooled under an argon atmosphere before the addition of 3 Å molecular sieves (0.84 g) which were likewise preheated at 160 °C for at least 2 hours. The internal filling solution of the reference electrode was prepared by heating 0.5 M of Bu_4NPF_6 at 160 °C for at least 6 hours and subsequently dissolved in CH_3CN (dried over molecular sieves). The analyte was weighed in a humidity chamber before dissolving in CH_3CN (dried over molecular sieves) and subsequently transferred into the cooled electrochemical cell. Before subjecting to voltammetric measurements, aliquots of the sample solution were measured by KF titration to acquire an estimate of the initial water content present.

2.4.6. Controlled potential electrolysis

Controlled potential electrolysis (CPE) experiments were conducted in a two-compartment electrolysis cell divided by a sintered glass frit of porosity no. 5 (1.0 – 1.7μm). Two identically sized Pt mesh plates, used as working and auxiliary electrodes, were arranged symmetrically with respect to each other with an Ag wire reference electrode (isolated from the sample solution via a salt bridge containing 0.5 M Bu_4NPF_6 in CH_3CN) positioned within 2 mm of the surface of the working electrode. Solutions in both compartments of the cell (25 ml each) were simultaneously stirred and deoxygenated using bubbles of argon gas. All CPE experiments were performed at 22 (±2) °C. The number of electrons transferred during the bulk electrolysis process was calculated using the following equation

$$N = Q/nF \qquad (2.1)$$

where, N = number of moles of starting material used, Q = charge (in coulombs), n = number of moles of electrons, and F is the Faraday constant (96 485 C/mol).

2.4.7. Formation of chemically oxidized sesamol

$NOSbF_6$ (2.5 mol equiv.) was added to a 10 ml solution of sesamol (50 mM) dissolved in CH_3CN (dried over molecular sieves) and subsequently left to stir for ½ hour under a nitrogen atmosphere. Following which, iodomethane (1.1 equiv.) was added to the resulting mixture and stirred for one hour. Upon completion, the crude mixture was concentrated under vacuum and purified by flash column chromatography on silica gel, using eluent made up of *n*-hexane and ethyl acetate in the ratio 9:1. Thin-layer chromatography (TLC) analysis was performed using pre-coated silica gel plates and visualization was achieved by UV light (254 nm). The purified product was dried under vacuum, affording the designated compound (**8**) as a yellow solid in 18% yield. ^{1}H NMR ($CDCl_3$, 500 MHz): δ = 6.02 (1H, s, CH_2), 7.01 (1H, s, aromatic H), 7.16 (1H, s, aromatic H); ^{13}C NMR ($CDCl_3$, 125 MHz): δ = 94.17, 98.70, 101.64, 117.79, 144.37, 146.86, 151.93; HRMS (ESI) calcd. for $C_{14}H_8O_5$ $[M+H]^+$: 257.04; found 257.05.

2.5. References

[1] Y. Hui, R.D. Webster, Absorption of Water into Organic Solvents Used for Electrochemistry under Conventional Operating Conditions, Anal. Chem. (Wash.), 83 (2011) 976–981.

[2] D.R. Burfield, G.-H. Gan, R.H. Smithers, Molecular Sieves - Desiccants of Choice, Journal of Applied Chemistry & Biotechnology, 28 (1978) 23–30.

[3] A.J. Fry, W.E. Britton, Solvents and Supporting Electrolytes, in: P.T. Kissinger, W.R. Heineman (Eds.) Laboratory Techniques in Electroanalytical Chemistry, Marcel Dekker, New York, USA, 1996, pp. 469–485.

[4] D.B.G. Williams, M. Lawton, Drying of Organic Solvents: Quantitative Evaluation of the Efficiency of Several Desiccants, J. Org. Chem., 75 (2010) 8351–8354.

[5] R. Estévez Brito, J.M. Rodríguez Mellado, P. Maldonado, M. Ruiz Montoya, A. Palma, E. Morales, Elucidation of the Electrochemical Oxidation Mechanism of the Antioxidant Sesamol on a Glassy Carbon Electrode, J. Electrochem. Soc., 161 (2014) G27–G32.

[6] Y.S. Tan, S. Chen, W.M. Hong, J.M. Kan, E.S.H. Kwek, S.Y. Lim, Z.H. Lim, M.E. Tessensohn, Y. Zhang, W. Richard David, The Role of Low Levels of Water in the Electrochemical Oxidation of α-Tocopherol (Vitamin E) and Other Phenols in Acetonitrile, Phys. Chem. Chem. Phys., 13 (2011) 12745–12754.

[7] N.G. Connelly, W.E. Geiger, Chemical Redox Agents for Organometallic Chemistry, Chem. Rev., 96 (1996) 877–910.

[8] S.B. Lee, C.Y. Lin, P.M.W. Gill, R.D. Webster, Transformation of α-Tocopherol (Vitamin E) and Related Chromanol Model Compounds into Their Phenoxonium Ions by Chemical Oxidation with the Nitrosonium Cation, J. Org. Chem., 70 (2005) 10466 –10473.

[9] Y.Y. Chan, Y. Yue, Y. Li, R.D. Webster, Electrochemical/Chemical Oxidation of Bisphenol A in a Four-electron/Two-proton Process in Aprotic Organic Solvents, Electrochim. Acta, 112 (2013) 287–294.

[10] Y.Y. Chan, Y. Yue, R.D. Webster, Voltammetric Studies on Vitamins D_2 and D_3 in Organic Solvents, Electrochim. Acta, 138 (2014) 400–409.

[11] J.H.Q. Lee, Y. Yue, R. Ganguly, R.D. Webster, Electrochemical Study of Pyridoxine (Vitamin B_6) in Acetonitrile, ChemElectroChem, 2 (2015) 412–420.

[12] J. Hellberg, G. Ahlgren, S. Söderholm, G. Olovsson, J.U.V. Schutz, A New Cation Radical Salt: $(bMDODBF)_2AsF_6$, Mol. Cryst. Liq. Cryst., 120 (1985) 273–276.

[13] G. Asensio, C. Andreu, C. Boix-Bernardini, R. Mello, M.E. González-Nuñez, Iodomethane Oxidation by Dimethyldioxirane: A New Route to Hypoiodous Acid and Iodohydrines, Org. Lett., 1 (1999) 2125–2128.

[14] I.J. Rhile, T.F. Markle, H. Nagao, A.G. DiPasquale, O.P. Lam, M.A. Lockwood, K. Rotter, J.M. Mayer, Concerted Proton-Electron Transfer in the Oxidation of Hydrogen-Bonded Phenols, J. Am. Chem. Soc., 128 (2006) 6075–6088.

[15] M.E. Tessensohn, H. Hirao, R.D. Webster, Electrochemical Properties of Phenols and Quinones in Organic Solvents are Strongly Influenced by Hydrogen-Bonding with Water, J. Phys. Chem. C, 117 (2013) 1081–1090.

This page has been intentionally left blank

Chapter 3

The Electrochemical Study of Vanillin in Acetonitrile

This page has been intentionally left blank

3.1. Chapter Overview

The current chapter aims at gathering mechanistic insights into the redox properties (both oxidation and reduction) of vanillin (Scheme 3.1) in an aprotic organic solvent, acetonitrile (CH_3CN) using a platinum (Pt) electrode. To achieve that, electrochemical techniques such as cyclic voltammetry (CV) and controlled potential electrolysis (CPE) were used and the CV results gathered were supplemented with digital simulation data which enabled an estimation of the electrochemical and kinetic parameters associated with the electrode reactions. Additionally, the effect of water on the electrochemical processes was also examined.

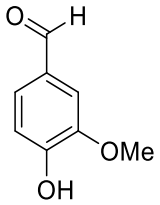

Scheme 3.1. Chemical structure of vanillin.

At a low scan rate of 0.1 V s^{-1}, vanillin displayed an anodic peak at ca. 1.12 vs. (Fc/Fc^+)/V, and a cathodic peak at ca. 0.09 vs. (Fc/Fc^+)/V (on the return scan of CV after the initial oxidation) due to the reduction of a secondary reaction product. Tentative mechanisms for the redox processes of vanillin in CH_3CN and at a Pt surface were disclosed, along with the discussion of their similarity with reported works. Independent of the former oxidation process, vanillin was also found to be electrochemically reduced at ca. -1.58 vs. (Fc/Fc^+)/V, and this cathodic process was demonstrated to require the presence of a catalytic surface.

3.2. Results and Discussion

3.2.1. Electrochemical oxidation of vanillin in CH_3CN

As discussed in Section 1.3.4, vanillin is established to undergo a $-2e^-/-H^+$ oxidation process on the forward cycle of the cyclic voltammogram, which indicated no sign of conversion of the oxidized product (compound **4**) back to the starting material on the reverse sweep. Instead, when the scan direction was reversed, a separate cathodic peak was observed, which gave a corresponding anodic peak on the second cycle of the scan. The cathodic peak was then surmised to be attributable to the reduction of the *ortho*-quinone (compound **6**) which is formed via hydrolysis reaction and subsequent loss of the methoxy substituent of the oxidized product (compound **4**) (Scheme 3.2) [1-4].

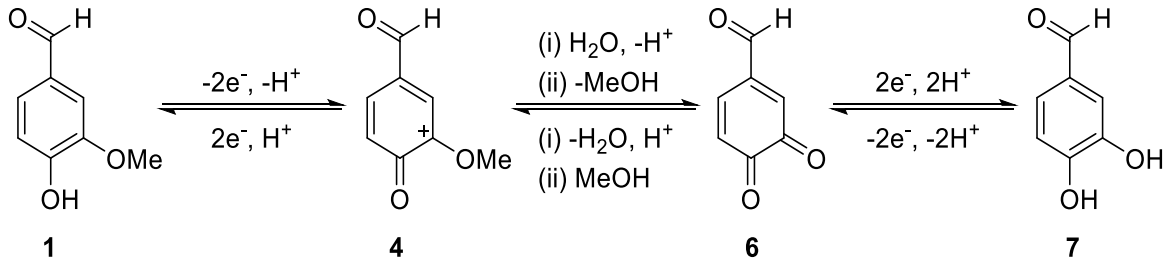

Scheme 3.2. Proposed mechanism for the electrochemical oxidation of vanillin [1-4].

In the current study, CV analysis of vanillin using a Pt electrode at a scan rate of 0.1 V s^{-1} revealed an oxidation peak at ca. 1.12 vs. (Fc/Fc^+)/V (wave 1) and a reduction wave at ca. 0.09 vs. (Fc/Fc^+)/V (wave 2), with no indication of the aforementioned anodic process upon successive scanning (Figure 3.1). The large peak-to-peak separation between waves 1 and 2 decreases the probability that wave 2 is responsible for the regeneration of the starting material, and suggests that it is more likely instead for wave 2 to be associated with the reduction of a secondary product resultant from the oxidized species formed at wave 1. Therefore, it is

conceivable to posit that wave 1 is a chemically irreversible process, as consistent with observations from earlier reports.

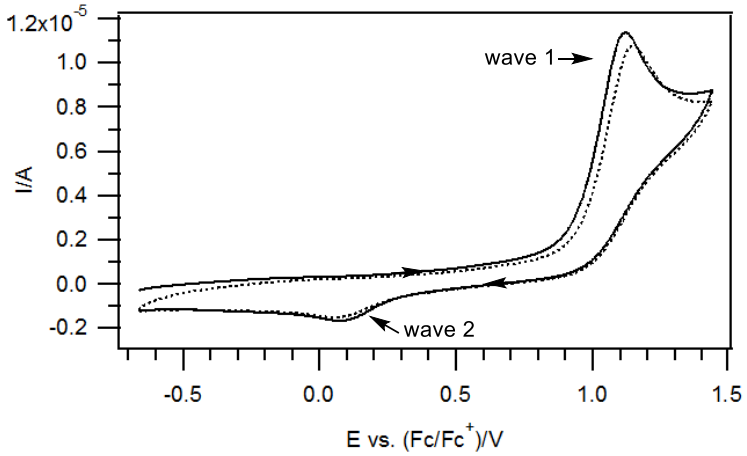

Figure 3.1. Cyclic voltammograms of 2 consecutive scans of 2 mM vanillin in CH_3CN with 0.2 M Bu_4NPF_6, recorded using a 1 mm diameter planar Pt electrode at 22 (±2) °C at a scan rate of 0.1 V s^{-1} and 22 (±2) °C. (—) 1st cycle. (·····) 2nd cycle.

With these preliminary results at hand, variable scan rate (ν) experiments were subsequently performed to assess the effect of shorter experimental time scales on the electrochemical behavior of vanillin (Figure 3.2). As the scan rates were increased, it was found that wave 2 increased in magnitude progressively up to ν = 0.5 V s^{-1}, after which it decreased with increasing scan rates. Concomitantly, a newly formed cathodic wave 3 was observed at ca. -0.28 vs. (Fc/Fc^+)/V, which upon continuous cycling, gave a corresponding anodic wave 4 at ca. -0.20 vs. (Fc/Fc^+)/V (Figure 3.2, dotted line). Furthermore, it was also noted that the ratios of the reduction (i_p^{red}, wave 3) to oxidation (i_p^{ox}, wave 4) peak currents (i_p^{red}/ i_p^{ox}) are generally close to unity, implying a fairly chemically reversible process in this case. However, since this redox couple (waves 3 and 4) can only be observed at ≥ 2 V s^{-1}, along with a decrease in the magnitude of wave 2, it is logical that waves 2 and 3 are associated with competing pathways where the latter (wave 3) is due to an intermediate that is not as long-lived as the species in

wave 2, thus necessitating higher scan rates in order for it to be voltammetrically detected. To the best of our knowledge, the existence of this intermediate (waves 3 and 4) has not yet been reported and is observable in the present study possibly due to the decrease in proton activities present in the current aprotic solvent system. Conversely, wave 2 is rationalized to be due to a long-term, stable product whose formation is promoted at lower scan rates ≤ 1 V s^{-1} (longer timeframes).

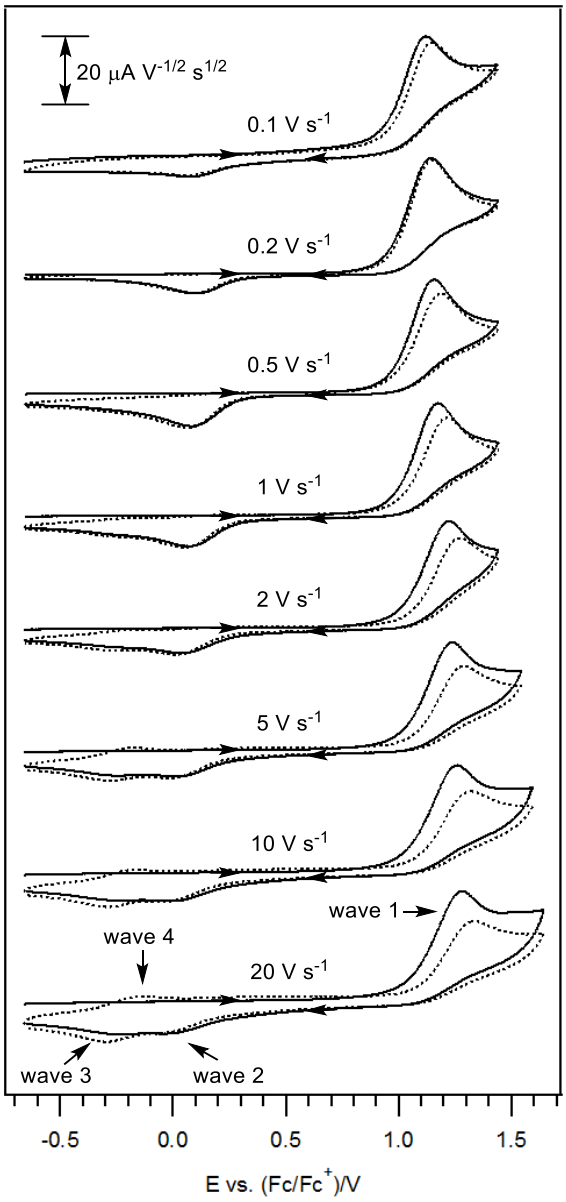

Figure 3.2. Variable scan rates cyclic voltammograms of 2 consecutive scans of 2 mM vanillin in CH_3CN with 0.2 M Bu_4NPF_6, recorded using a 1 mm diameter planar Pt electrode at 22 (±2) °C. (—) 1st cycle. (·····) 2nd cycle. Current data were multiplied by (scan rate)$^{-0.5}$ for normalization.

3.2.2. Voltammetry of vanillin at varied temperatures

Low temperature voltammetry can sometimes help to slow down fast reactions, thus improving the stability and lifetimes of intermediates and consequently enable the capture of these reactive species [5]. As such, varied temperature experiments ranging from -30 to 20 °C were performed in order to further examine the species involved in wave 3 (Figure 3.3). Consistent with earlier findings, the progressive diminish in peak current of wave 2 was found to be accompanied by an increase in the magnitude of wave 3 (and its corresponding wave 4) as the temperature of the sample solution was decreased. However, in spite of the results above illustrating that lowered temperatures ($\leq$ -10 °C) or high scan rates ($\geq$ 2 V s^{-1}) appear to be useful in improving the stability of the intermediate responsible for wave 3 (at least in the voltammetry timeframe of seconds), the sole detection of the intermediate in wave 3 (and wave 4), without the observation of wave 2, could not be achieved in the current system employed.

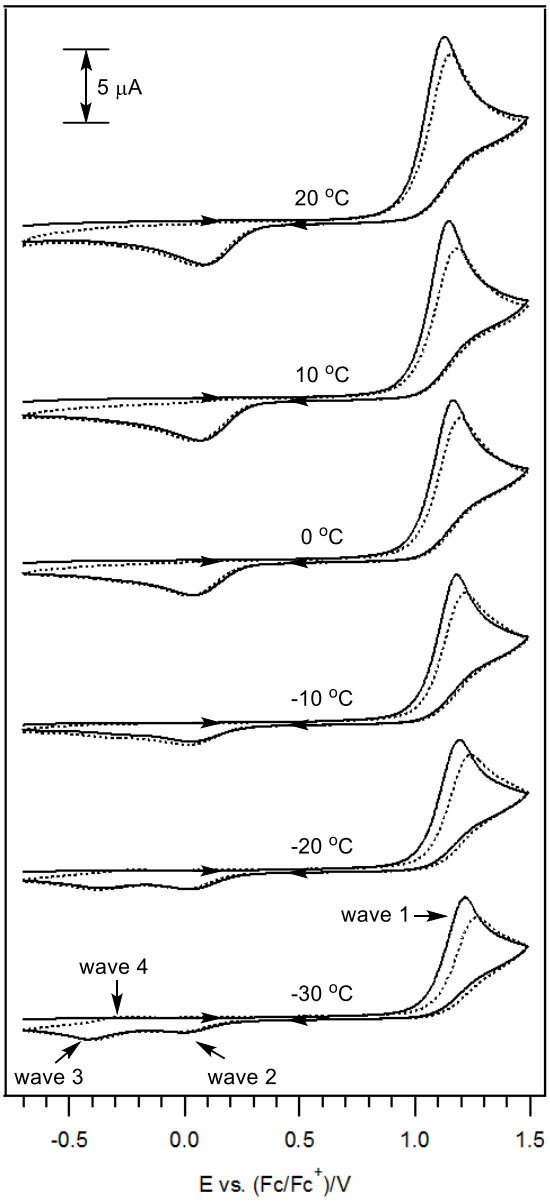

Figure 3.3. Variable temperatures cyclic voltammograms of 2 consecutive scans of 2 mM vanillin in CH_3CN with 0.2 M Bu_4NPF_6, recorded using a 1 mm diameter planar Pt electrode and at a scan rate of 0.1 V s^{-1}. (—) 1st cycle. (·····) 2nd cycle.

3.2.3. Controlled potential electrolysis of vanillin

As CV only offers information regarding a compound's short term chemically reversibility (≤ seconds), CPE experiments, which require longer timeframes (≥ minutes), were conducted. Furthermore, the electrolysis measurements would also allow for the accurate determination of

the number of electrons involved in a redox process. The initial applied potential for the electrolysis was set at ca. 100 mV more positive than that recorded for wave 1 to ensure a complete oxidation of the substrate. Figure 3.4 depicts the coulometric and voltammetric data obtained after 1200 seconds of exhaustive electrolysis. It can be seen that the current logged in the coulometry graph decays from an initial ca. 50 mA to a close to zero current value, together with the disappearance of the initially present (prior to the electrolysis) wave 1 in the voltammogram recorded after the bulk oxidation (Figure 3.4, dotted line).

Using Eq. (3.1), it was calculated that ca. 2.0 moles of electrons (per mole of vanillin) were involved in the oxidation process. In addition, following the disappearance of wave 1, wave 2 became more prominent (with its peak potential shifting to more negative potentials), together with the observation of its corresponding anodic peak at ca. 0.97 vs. $(Fc/Fc^{+})/V$ (wave 5) when the scan direction was reversed. In view of the literature precedence outlined in Scheme 3.2 [1-4], it would be conceivable to ascribe wave 2 as the reduction of the substituted *ortho*-quinone (compound **6**) that is formed after hydrolysis of the oxidized product generated in wave 1. The minimum amount of protons present in the current aprotic system could possibly account for the wide peak to peak separation observed, which differs from those described in the aqueous solutions (where protons are readily available). Moreover, the large separation in peak potential could likely also be attributable to the individual heterogeneous and homogeneous ($2e^{-}/2H^{+}$) steps occurring in a consecutive fashion as well as the possibility of differing pathways taken on by the compound as it oxidizes and reduces [6].

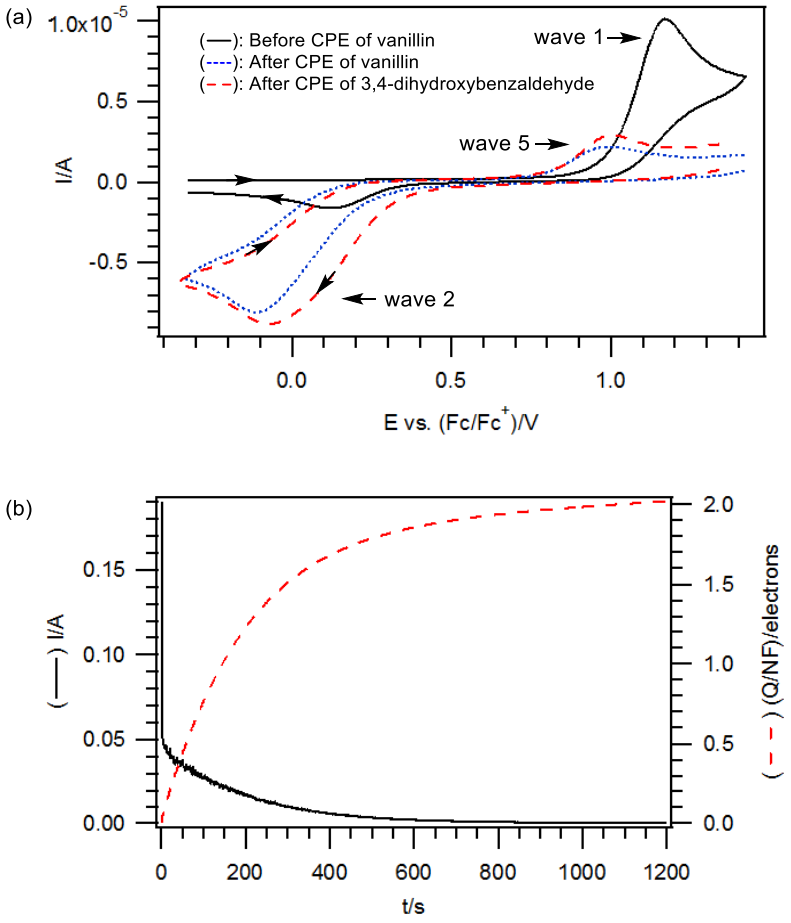

Figure 3.4. Voltammetric and coulometric data recorded during the controlled potential electrolysis of 2 mM vanillin in CH_3CN with 0.2 M Bu_4NPF_6 at 22 (±2) °C. (a) Cyclic voltammograms obtained at a scan rate of 0.1 V s^{-1} using a 1 mm diameter planar Pt electrode. The coulometry data collected during the bulk oxidation of the 3,4-dihydroxybenzaldehyde is given in Figure A3.2 of the Appendix section. (b) Current/coulometry vs. time data logged during the exhaustive oxidation of vanillin at 1.27 vs. $(Fc/Fc^+)/V$.

The shift in potential of wave 2 during the electrolysis experiments can be rationalized based on hydrogen bonding interactions, similar to interactions observed during the oxidation of dopamine to its corresponding *ortho*-quinone which has been the subject of recent studies [7, 8]. Being a structurally similar compound to dopamine, it is reasoned that hydrogen bonding interactions would likewise have an effect on the voltammetric appearance of compound **6** (the substituted *ortho*-quinone formed after bulk oxidation and hydrolysis of vanillin). The presence of this supramolecular effect (e.g. hydrogen bonding) was ascertained by the CV analysis of vanillin with varying amounts of water (Figure 3.5). It was found that the position of wave 2 shifts towards negative potentials with increasing amount of water added, until an almost 200 mV shift (similar to the shift of wave 2 observed in Figure 3.4) was obtained after the addition of 200 equivalents of water ($[H_2O]_{final}$ = 507 mM). Hence, it can be reasoned that the electrogenerated compound **6** after the bulk oxidative electrolysis of vanillin is likely to interact with trace amounts of water present in the sample solution. As no rigorous efforts were made to exclude water during the electrolysis process (which is difficult to achieve due to the design of the multi-compartment cell), the distinctive shift in potential of wave 2 in the voltammogram collected after the electrolysis can be accounted for by the accumulation of water from the surroundings over the prolonged period of electrolysis.

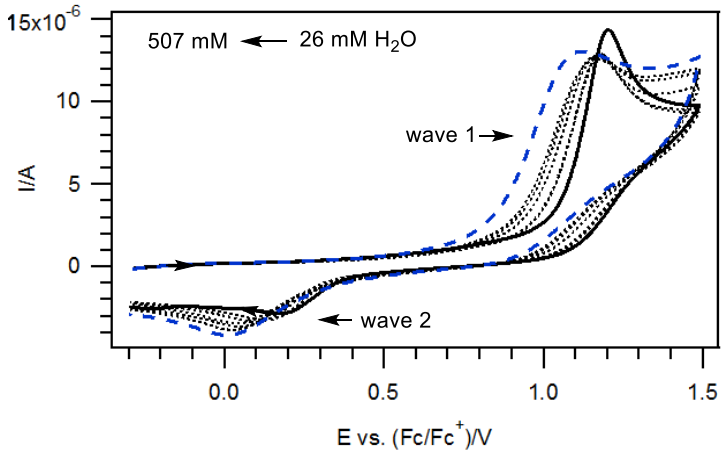

Figure 3.5. Overlaid cyclic voltammograms of 2 mM vanillin in CH_3CN ($[H_2O]_{initial}$ = 26 mM) with 0.2 M Bu_4NPF_6, recorded using a 1 mm diameter planar Pt electrode at a scan rate of 0.1 V s^{-1} and 22 (±2) °C. (—) Prior to the addition of known amount of H_2O. After the addition of (·····) 10-100 equiv. of H_2O (- - -) 200 equiv. of H_2O ($[H_2O]_{final}$ = 507 mM).

To further examine the cathodic reaction occurring in wave 2, a reductive electrolysis set at an applied potential slightly past wave 2 was next conducted on a solution of the oxidized product which was produced immediately upon bulk oxidation of vanillin (Figure A3.1 in the Appendix section). After the transfer of ca. 1.7 moles of electrons, similar cyclic voltammograms were obtained before and after the exhaustive reduction. The slight difference in electron count (ca. 1.7 moles of electrons (Figure A3.1 in the Appendix section) vs. ca. 2.0 moles of electrons (Figure 3.4)) could be due to the loss of some oxidized product during its diffusion into the other compartment of the electrolysis cell [9, 10]. Nevertheless, consistent with the proposed premise, it can be concluded that the oxidized product generated in wave 1 is reducible by 2 electrons (wave 2). Additionally, in order to further corroborate the proposed generation of the substituted *ortho*-quinone (compound **6**) (following the bulk oxidation of vanillin), a CPE oxidation experiment was also performed on a solution of 3,4-dihydroxybenzaldehyde, which was anticipated to produce the aforementioned substituted *ortho*-quinone (compound **6**) upon

oxidation (Figure A3.2 in the Appendix section). In line with expectations, after the transfer of ca. 2.2 moles of electrons (the bulk oxidation of 3,4-dihydroxybenzaldehyde), the cyclic voltammogram of the resultant product gave a relatively close match with the voltammogram recorded after the exhaustive oxidation of vanillin (Figure 3.4, dashed line). Hence, it can be inferred from the results obtained that vanillin likely undergoes a similar oxidation pathway to the mechanism shown in Scheme 3.2. More specifically, the oxidized product formed after the anodic process in wave 1 is likely to undergo a hydrolysis reaction and the loss of its methoxy group to give a substituted *ortho*-quinone (compound **6**) which can subsequently be reduced via a two-electron/two-proton process to provide its corresponding 1,2-dihydroxybenzene (the substituted catechol, compound **7**).

Since the intermediate responsible for wave 3 can be monitored during the low temperature CV measurements (Figure 3.3), it was envisaged that a similar CPE experiment could be performed to investigate its long term stability. As shown in the voltammogram of the oxidized product obtained after the exhaustive oxidation of vanillin at -40 °C (Figure 3.6, dotted line), however, minimal signals of waves 3 and 4 were detected, with majority of the voltammogram revealing wave 2 positioned at a more negative potential along with its corresponding anodic peak (wave 5). As such, even with the further reduction of temperature to -40 °C (as compared to the -30 °C in CV), the colder environment appeared to only be able to improve the stability of the hemiketal intermediate (wave 3) over a short duration (≤ seconds), but not under prolonged periods of time (≥ minutes). The assignment of wave 2 as the stable, long term product is also further substantiated by the similar results obtained in the CPE experiments conducted under both ambient (Figure 3.4) and lowered temperatures (Figure 3.6).

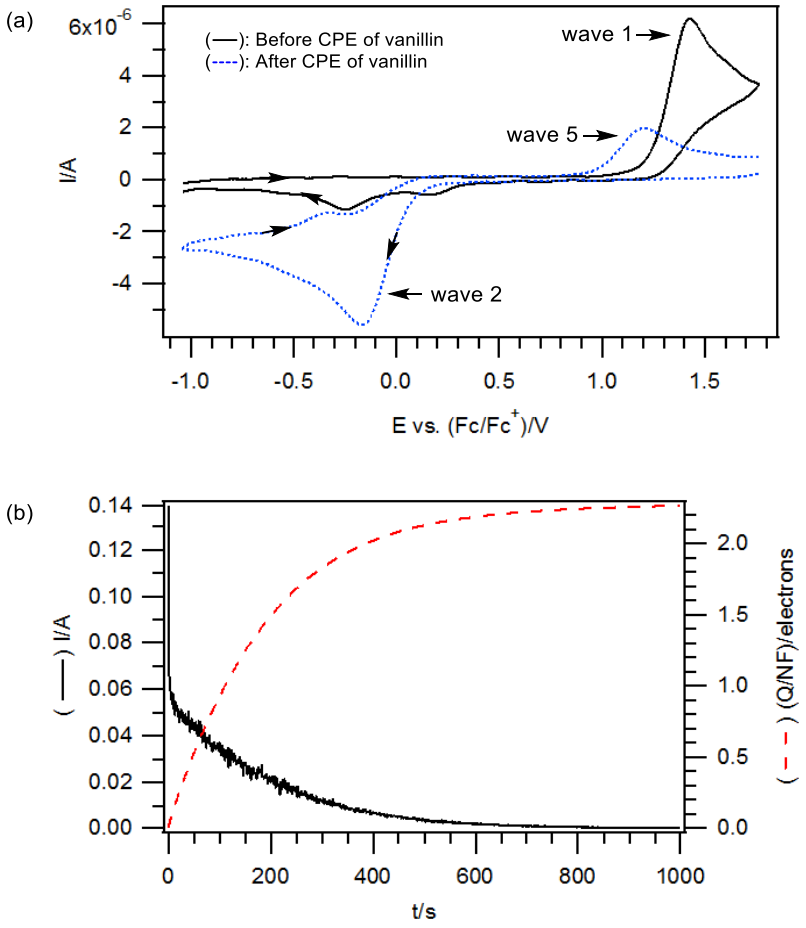

Figure 3.6. Voltammetric and coulometric data recorded during the controlled potential electrolysis of 2 mM vanillin in CH_3CN with 0.2 M Bu_4NPF_6 at -40 (±2) °C. (a) Cyclic voltammograms obtained at a scan rate of 0.1 V s^{-1} using a 1 mm diameter planar Pt electrode. (b) Current/coulometry vs. time data logged during the exhaustive oxidation of vanillin at 1.42 vs. $(Fc/Fc^+)/V$.

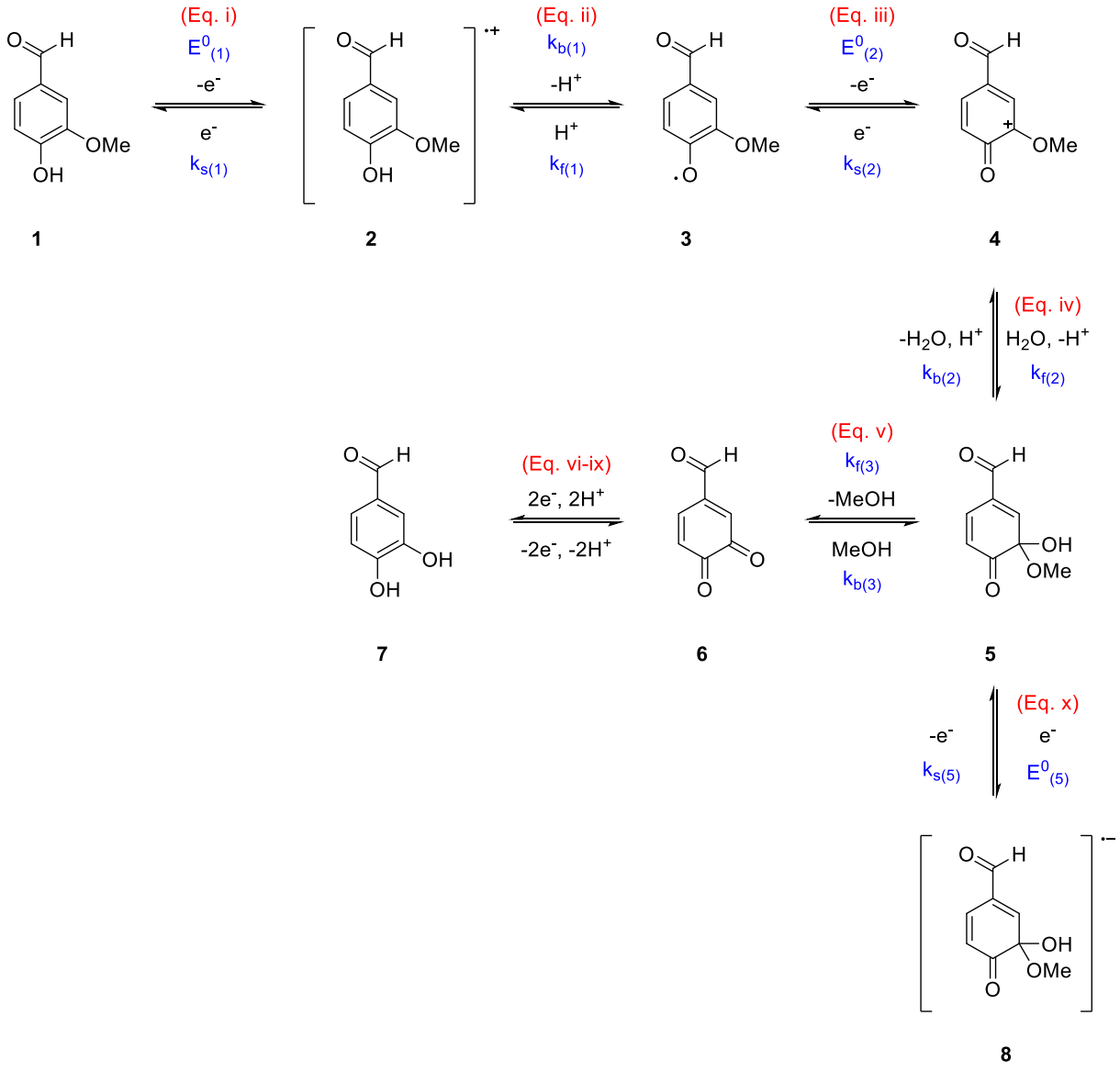

Scheme 3.3. Proposed general mechanism for the electrochemical oxidation of vanillin in CH_3CN, with the conversion of compound **6** to **7** (Eqs. (vi)-(ix)) illustrated in Scheme 3.4. For simplicity, only one resonance structure is displayed.

3.2.4. Proposed electrochemical oxidation mechanism and digital simulations

Overall, the electrochemical responses gathered from the preceding sections can be interpreted based on the mechanism presented in Scheme 3.3. In accordance with the usual electrochemical behavior of a phenol, vanillin is surmised to undergo an initial oxidation via an ECE process (where E and C denote an electrochemical and chemical step respectively) to generate a reactive diamagnetic cation.

Consistent with the mechanism illustrated in Scheme 3.2, and as the second oxidation process takes place at a less positive potential than the first step, compound **3** which is formed after the initial $-e^-/-H^+$ oxidation can be instantaneously oxidized to generate compound **4**, thereby contributing to the observation of a multi-electron wave 1 [11]. Following on, the produced phenoxonium cation (compound **4**) which are generally very reactive and susceptible to further reaction with trace amounts of water [12, 13] will undergo subsequent hydrolysis, together with the loss of its methoxy group, to give a substituted *ortho*-quinone (compound **5** to **6**). Lastly, the substituted *ortho*-quinone (compound **6**) is posited to be rapidly reduced through the gain of two electrons and two protons ($2e^-/2H^+$) to form its substituted 1,2-dihydroxybenzene product (compound **7**), giving rise to the observed wave 2.

As presented in the variable scan rates CV analysis (Figure 3.2), the sole observation of waves 1 and 2 was generally maintained at scan rates ≤ 1 V s^{-1}, with additional redox peaks (waves 3 and 4) registered only at scan rates ≥ 2 V s^{-1}, in conjunction with the decrease in magnitude of wave 2. In this context, and building on the mechanistic premise provided in Scheme 3.2, an additional pathway is rationalized to be accountable for the observed trend (conversion of compound **5** to **8** in Scheme 3.3). Also, the experimental results indicate that the reactions that lead to the products that are reduced in wave 3 are in competition with the reactions associated with the products reduced in wave 2, with the species responsible for wave 3 being clearly more

reactive than the species associated with wave 2. Furthermore, in order for waves 2 and 3 to co-exist at high scan rates and only wave 2 to be detected for low scan rates, the reaction product formed at wave 3 cannot be too dissimilar from compound **5**, thus negating the possibility of a ring-opened structure. Hence, the species involved in wave 3 is assigned as the hemiketal form, which are well-known oxidation products of phenols, such as for α-tocopherol (vitamin E) [9, 12, 14]. At higher scan rates of ≥ 2 V s^{-1}, the formation of compound **6** is partially outrun; thus allowing compound **5** to be concomitantly converted to both compounds **8** and **6**. Notably, a similar outcome was also found on decreasing the solution temperature as depicted in Figure 3.3. The need for low temperatures ($\leq$ -10 °C) or high scan rates (≥ 2 V s^{-1}) in order for wave 3 to be voltammetrically noticeable indicates the high reactivity of its assigned chemical species. Also, this was further supported by the electrolysis experiments performed at -40 °C which revealed minimum observation of wave 3 after the exhaustive oxidation of vanillin (Figure 3.6).

The reduction of the *ortho*-quinone (compound **6**) to its corresponding 1,2-dihydroxybenzene form (compound **7**) is well-established to involve a series of electron and proton transfer steps ($2e^-/2H^+$), as shown in Scheme 3.4 [6]. The observation of this cathodic process is evidenced by the reductive electrolysis conducted after the bulk oxidation of vanillin (Figure A3.1 in the Appendix section). Also, validation of the identity of the *ortho*-quinone (compound **6**) was demonstrated by the similar voltammograms obtained after the exhaustive oxidation of vanillin and after the bulk oxidation of 3,4-dihydroxybenzaldehyde (Figure 3.4); both of which are expected to produce the same substituted *ortho*-quinone (compound **6**) after their respective electrolysis processes. It was also postulated that the broad peak–to-peak separation observed in the CV obtained in the electrolysis experiment (Figure 3.4) is due to the individual chemical and electrochemical steps occurring in a successive manner and possibly by different pathways partaken by the compound in the forward (reduction) and reverse (oxidation) processes. However, as it is very difficult to voltammetrically confirm the sequence of these pathways, a

concerted loss or gain of the electrons and protons (occurring via diagonal arrows in Scheme 3.4) cannot be completely ruled out [6].

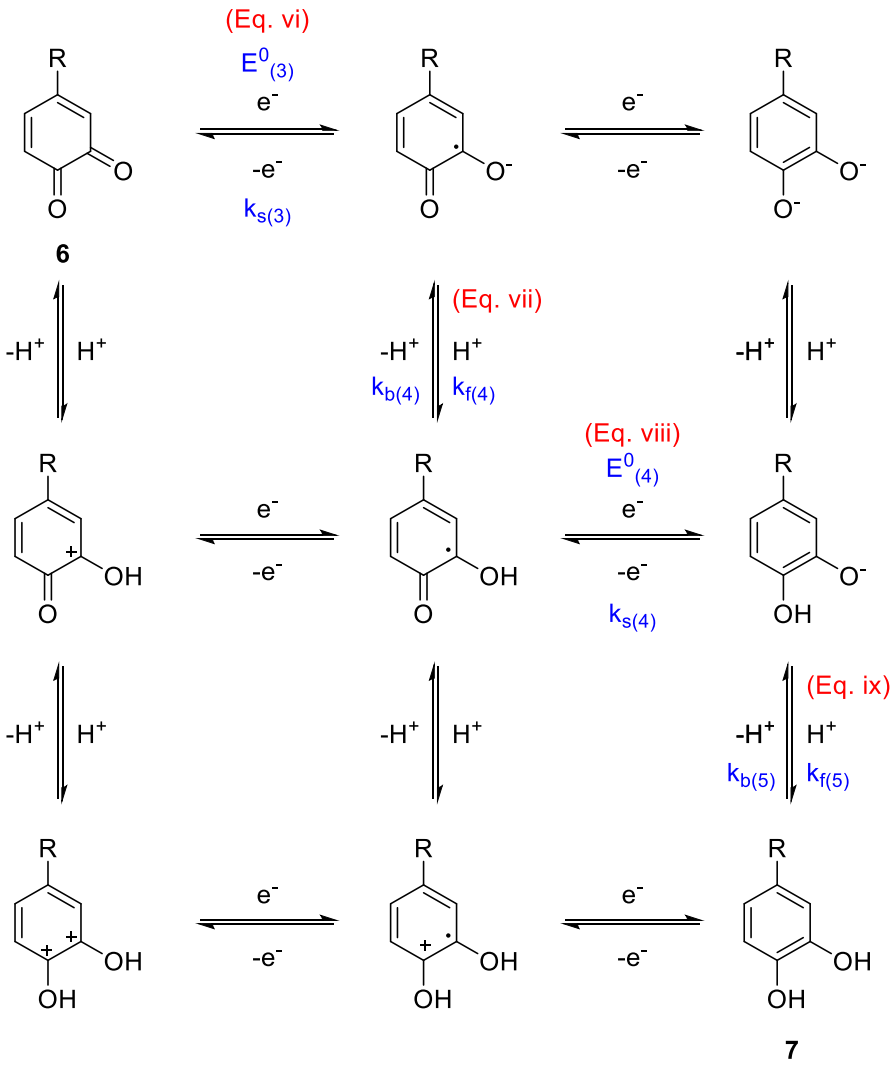

Scheme 3.4. The proposed ECEC ($2e^-/2H^+$) reductive mechanism of compound **6** (substituted *ortho*-quinone) to compound **7** (substituted 1,2-dihydroxybenzene). For simplicity, only one resonance structure is displayed.

To verify the aforementioned pathways outlined in Scheme 3.3, digital simulations (DigiElch 7) were subsequently performed. The use of modelling techniques also enables the extraction of information regarding the kinetics of the electrode reactions. Generally, the simulation work was conducted in a trial and error manner that involves the systematic addition of the different charge transfer and homogeneous chemical steps. Due to the wide possibility of voltammetrically indistinguishable pathways involved in the conversion of compound **6** to

compound **7** as mentioned above, an ECEC mechanism was used during the modelling work for simplicity (Scheme 3.4).

Since it might be possible for a single cyclic voltammogram to be reproduced using several different mechanisms (with the appropriate kinetic values), a fixed set of parameters was used for the different scan rates examined to increase the credibility of the results [15]. In addition, a similar set of parameters was also used for the variable temperature CV experiments where the electrode potential values remained constant while the diffusion coefficients and rate constants were decreased systemically to account for the effects of lowered temperature. Fitting of the experimental and simulated curves were performed by feature analysis based on eye instead of using an automated define error minimization process. As illustrated in Figures 3.7 and 3.8, a comparison of the experimental and simulated voltammograms revealed a reasonably good fit. The various optimized electrochemical and chemical kinetic parameters used for the CV experiments conducted at ambient temperature are tabulated in Tables 3.1 and 3.2, while those used for the variable temperature analyses are listed in Table A3.1-A3.12 in the Appendix section.

Taking into account the chemically irreversible nature of wave 1, the products formed after the initial oxidation of vanillin (compound **4**) are scarcely converted back to the starting material. Hence, it would be expected that the equilibrium and forward rate constants for the chemical reaction (hydrolysis process, Eq. (iv)) following the electrogeneration of compound **4** would be large and in favor of the formation of the secondary product (compound **5**). Also, results gathered from the preceding sections have established that, at the expense of wave 2, wave 3 was observed to increase in magnitude and appear more voltammetrically noticeable at high scan rates. Since wave 2 is attributable to the reduction of compound **6**, in order for wave 2 to decrease relative to wave 3 at high scan rates, the formation of the *ortho*-quinone (compound **6**) via the loss of the methoxy substituent (Eq. (v)), together with the proton-addition steps that

are coupled to compound **6** (Eqs. (vii) and (ix)) must be processes that can be partially outrun at large scan rates. Therefore, the rate constants of the homogeneous reactions in Eqs. (v), (vii) and (ix) must be relatively small in value (forward rate constants (k_f) range from 3 to 10). In doing so, the formation of compound **8** from **5** would be facilitated, thereby leading to an increase in peak height of wave 3.

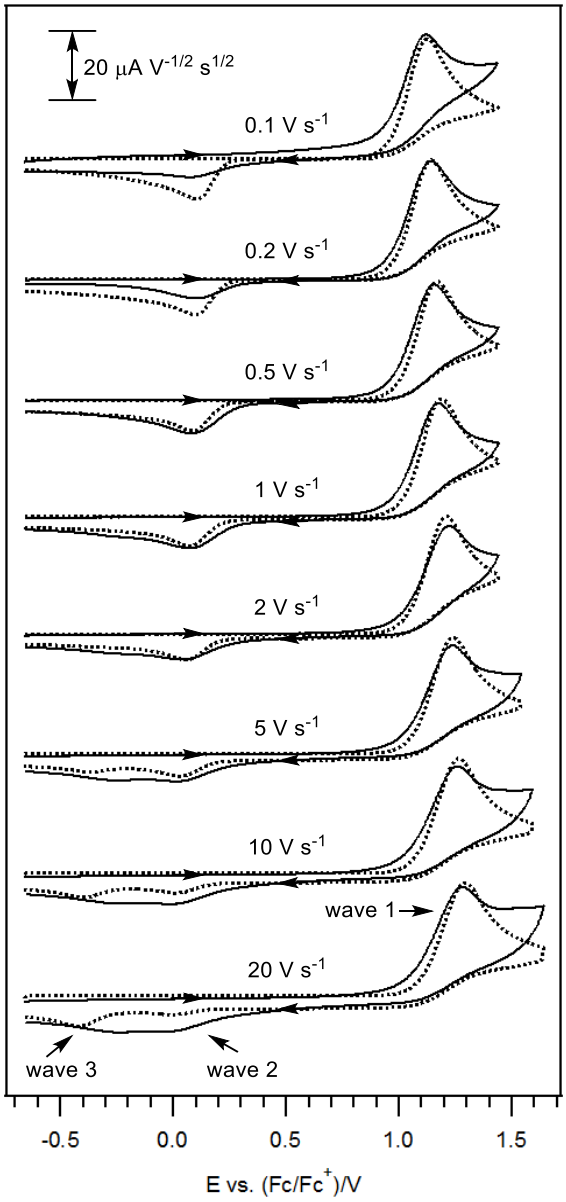

Figure 3.7. Variable scan rates cyclic voltammograms of 2 mM vanillin in CH_3CN with 0.2 M Bu_4NPF_6, recorded using a 1 mm diameter planar Pt electrode at 22 (±2) °C. (—) Experimental voltammograms. (·····) Simulated voltammograms generated based on the mechanism outlined in Schemes 3.3 and 3.4. Current data were multiplied by (scan rate)$^{-0.5}$ for normalization.

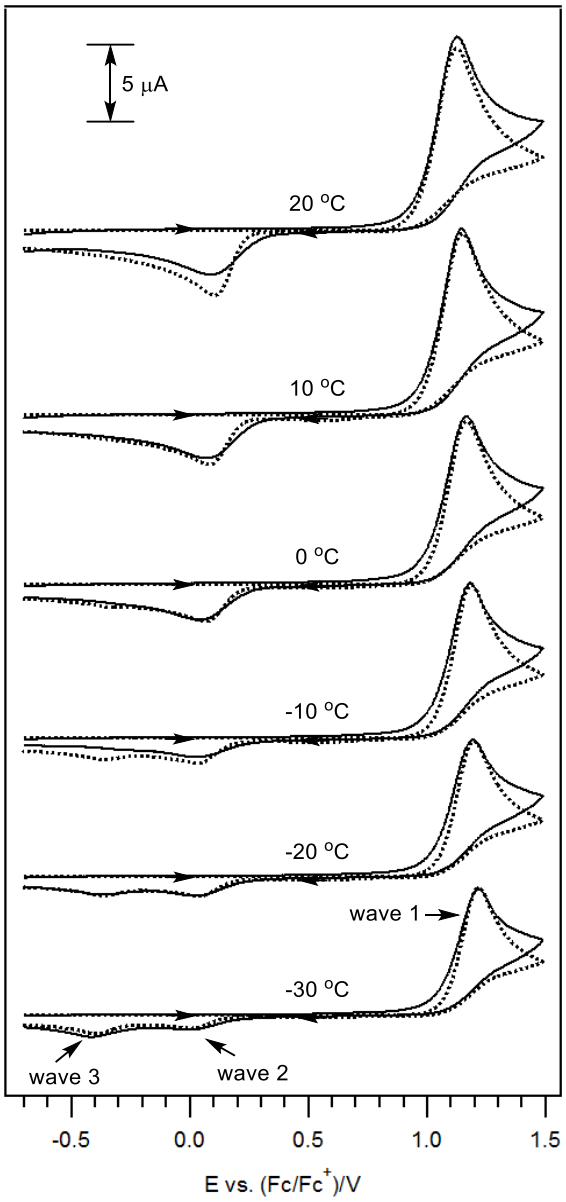

Figure 3.8. Variable temperatures cyclic voltammograms of 2 mM vanillin in CH_3CN with 0.2 M Bu_4NPF_6, recorded using a 1 mm diameter planar Pt electrode. (—) Experimental voltammograms. (·····) Simulated voltammograms generated based on the mechanism outlined in Schemes 3.3 and 3.4.

Table 3.1. Electrochemical parameters[a] obtained by digital simulations of CV data[b] for the reaction mechanisms shown in Schemes 3.3 and 3.4.

Electrochemical Parameters	Eq. i	Eq. iii	Eq. vi	Eq. viii	Eq. x
E^0 (V)	1.100	0.850	0.170	0.320	-0.250
k_s (cm s^{-1})	≤ 0.0100	≤ 0.0100	≤ 0.0080	≤ 0.0080	≤ 0.0080

[a]E^0 = formal oxidation potential vs. (Fc/Fc^+)/V, k_s = heterogeneous electron transfer rate constant. The diffusion coefficients were estimated via simulation techniques to be 2.60 x 10^{-5} cm^2 s^{-1} for vanillin and its oxidized forms and 3.50 x 10^{-5} cm^2 s^{-1} for H_2O, H^+ and MeOH. The transfer coefficient (α) values were assumed to be 0.5. [b]CV data were logged using a 1 mm diameter Pt electrode for solutions of 2 mM vanillin and 0.2 M Bu_4NPF_6 in CH_3CN at 22 (±2) °C. The water and proton concentrations were assumed to be 0.1 M.

Table 3.2. Equilibrium and rate constants[a] obtained by digital simulations of CV data[b] for the reaction mechanisms shown in Schemes 3.3 and 3.4.

Kinetic Parameters	Eq. ii	Eq. iv	Eq. v	Eq. vii	Eq. ix
K_{eq}	1.00 x 10^{-5}	2.50 x 10^3	5.00 x 10^1	1.00 x 10^3	1.00 x 10^3
k_f	5.00 x 10^1	1.00 x 10^5	3.00 x 10^0	1.00 x 10^1	1.00 x 10^1
k_b	5.00 x 10^6	4.00 x 10^1	6.00 x 10^{-2}	1.00 x 10^{-2}	1.00 x 10^{-2}

[a]K_{eq} = equilibrium constant, k_f = forward rate constant, k_b = backward rate constant. The homogeneous rate constants have units of s^{-1} and L mol^{-1} s^{-1} for the first- and second-order reactions, respectively. [b]CV data were logged using a 1 mm diameter Pt electrode for solutions of 2 mM vanillin and 0.2 M Bu_4NPF_6 in CH_3CN at 22 (±2) °C. The water and proton concentrations were assumed to be 0.1 M.

3.2.5. Electrochemical reduction of vanillin in CH_3CN

Apart from being able to undergo electrochemical oxidation reactions, vanillin was also found to display reductive behavior that is independent of the former heterogeneous electron transfer process. This is supported by the similar voltammograms obtained regardless of the initial potential scan direction (e.g. scanning towards the positive or negative potentials first) (Figure 3.9). The cathodic phenomenon was examined further as presented in Figure 3.10 (Solid line), where a chemically reversible cathodic peak at ca. -1.58 vs. $(Fc/Fc^{+})/V$ was observed, with the ratio of its anodic to cathodic peak nearing unity. Moreover, a large peak to peak separation was recorded and continued to increase correspondingly with higher scan rates (Figure A3.3 in the Appendix section). This is likely to be attributable to the relatively slow heterogeneous electron transfer rate. Notably, the requirement of a catalytic surface was demonstrated by the absence of any discernible faradic current detected when a glassy carbon electrode was used (Figure 3.10, dashed line), thus implying the importance of a surface/solute interaction. Hence, consistent with what has been observed during the voltammetric reduction of O-H acids [16-18], it was reasoned that the cathodic wave recorded is likely to be associated with the direct discharge of the phenolic functional group present in vanillin to form hydrogen gas via the adsorption of atomic hydrogen on the Pt electrode.

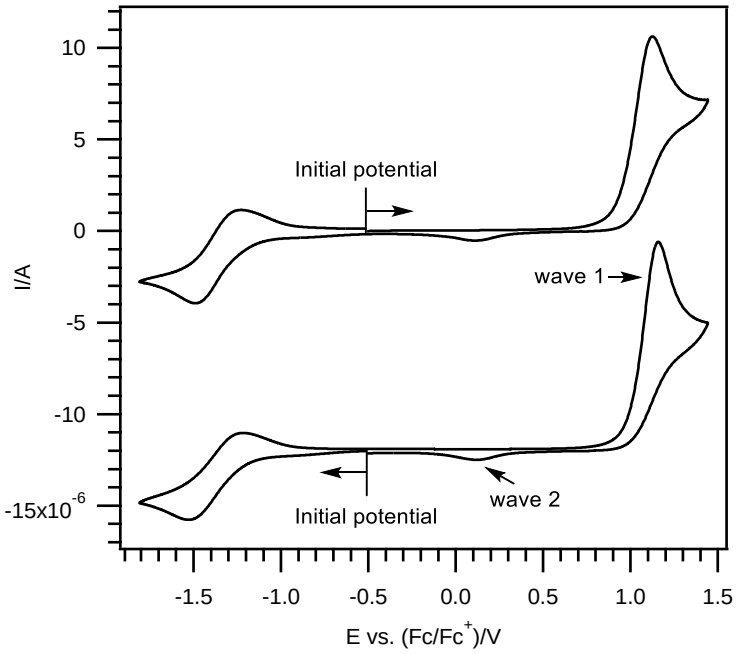

Figure 3.9. Cyclic voltammograms of 2 mM vanillin in CH_3CN with 0.2 M Bu_4NPF_6, recorded using a 1 mm diameter planar Pt electrode at a scan rate of 0.1 V s^{-1} and 22 (±2) °C, commencing at different initial potential scan direction. Start/end potentials: -0.51 vs. (Fc/Fc^+)/V. Switching potentials: 1.44 and -1.81 vs. (Fc/Fc^+)/V.

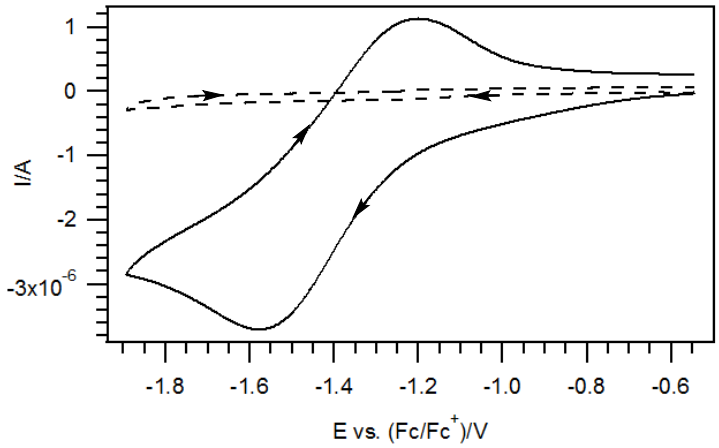

Figure 3.10. Cyclic voltammograms of 2 mM vanillin in CH_3CN with 0.2 M Bu_4NPF_6, recorded at a scan rate of 0.1 V s^{-1} and 22 (±2) °C, obtained using a 1 mm diameter planar (—) Pt electrode. (- - -) GC electrode. Start/end potentials: -0.54 V vs. (Fc/Fc^+)/V. Switching potential: -1.89 V vs. (Fc/Fc^+)/V.

3.3. Conclusion

In summary, vanillin was found to undergo electrochemical oxidation at ca. 1.12 vs. (Fc/Fc^+)/V (wave 1), with a cathodic peak at ca. 0.09 vs. (Fc/Fc^+)/V (wave 2) recorded on the return sweep at low scan rates of ≤ 1 V s^{-1}. After the transfer of two moles equivalences of electrons to a solution of vanillin via CPE, the generated product was found to be able to undergo a subsequent chemically reversible reduction process (waves 2 and 5). Therefore, in agreement with the mechanism that has been previously delineated [1-4], wave 1 was rationalized to be associated with the oxidation of vanillin via a two electron/one proton ($-2e^-/-H^+$) process in an ECE manner. The resultant phenoxonium cation was then hydrolyzed to generate a substituted *ortho*-quinone (compound **6**) which would eventually be reduced in wave 2 to form its corresponding 1,2-dihydroxybenzene (compound **7**, that can be reversibly oxidized back to compound **6** in wave 5). Interestingly, the increase of scan rates or decrease in temperature allows the observation of an additional reduction peak at ca. -0.28 vs. (Fc/Fc^+)/V (wave 3) and its corresponding anodic peak (after a second consecutive scan) at ca. -0.20 vs. (Fc/Fc^+)/V (wave 4). Using the results obtained from the CPE experiments conducted under both the room and lowered temperature, the intermediate associated with wave 3 was determined to be able to survive only in short timeframe of seconds along with the requirement of high scan rates (≥ 2 V s^{-1}) or decreased temperatures ($\leq$ -10 °C) to be employed. Hence, in addition to the aforementioned mechanistic posit, an unprecedented pathway which involves the reduction of a hemiketal form (compound **5**) was proposed. In order to gain kinetic and mechanistic insights into the proposed pathways, digital simulations were used to analyze the voltammetric responses. Vanillin was also observed to exhibit an independent voltammetric reduction behavior at ca. -1.58 vs. (Fc/Fc^+)/V, which was assigned to the direct discharge of its phenolic substituent on a Pt electrode.

3.4. Experimental

3.4.1. General remarks

Unless otherwise stated, all chemicals and reagents were acquired from commercial sources and used as received.

3.4.2. Chemicals and reagents

Vanillin (99%) was purchased from Alfa Aesar, while HPLC grade acetonitrile (CH_3CN) was bought from Macron. Ultrapure water (resistivity ≥ 18 MΩ cm) was obtained from an ELGA Purelab Option-Q water purification system. The supporting electrolyte (tetrabutylammonium hexafluorophosphate, Bu_4NPF_6), was prepared following literature procedures by treating equal molar amounts of a 65% aqueous solution of HPF_6 (Fluka) with a 40% aqueous solution of Bu_4NOH (Alfa Aesar) and subsequently washing the precipitate with ultrapure water, recrystallizing three times with hot ethanol, and drying under vacuum for 6 hours at 140 °C.

3.4.3. Voltammetry

Cyclic voltammetry (CV) experiments were conducted using a computer-controlled Metrohm Autolab PGSTAT302N potentiostat with a three-electrode system. A 1 mm diameter planar disk platinum (Pt) or glassy carbon (GC) working electrode (eDAQ Pty Ltd) was used in conjunction with a Pt counter electrode (Metrohm) and a silver (Ag) wire miniature reference electrode (eDAQ Pty Ltd) that was isolated from the sample solution by a salt bridge containing 0.5 M Bu_4NPF_6 in CH_3CN. Accurate potentials were attained by adding ferrocene (Fc) as an internal standard at the end of the measurements. All voltammetric experiments were performed in a Faraday Cage at 22 (±2) °C with the analyte solutions deoxygenated by purging with high purity argon gas. Variable temperature analyses (-30 to 20 °C) were carried out in a Metrohm

jacketed glass cell, with temperatures controlled by a Julabo FP89-HL ultralow refrigerated ethanol circulating bath. Ohmic drop was not compensated for all cyclic voltammograms.

3.4.4. Measurement of water content in sample solution

Karl Fisher (KF) titrations were carried out using a Mettler Toledo DL32 coulometer containing (Riedel-deHaën) HYDRANAL- coulomat CG and HYDRANAL- coulomat AG as the cathode and anode compartment respectively. All measurements were conducted in a humidity control box (122cm × 61cm × 61cm) that is maintained at a constant humidity (30%) by the use a dry nitrogen purge gas system acquired from Coy Laboratory Products Inc. Analyte solutions that were placed in a 5 mL vacuum syringe (SGE Analytical Science) were injected into the coulometer through a silicon/Telfon septum.

3.4.5. Controlled potential electrolysis

Controlled potential electrolysis (CPE) measurements were performed in a two-compartment electrolysis cell separated by a sintered glass frit of porosity no. 5 (1.0 – 1.7μm). The working and auxiliary electrodes used were two identically sized and symmetrically arranged Pt mesh plates together with an Ag wire reference electrode (connected to the analyte solution through a salt bridge containing 0.5 M Bu_4NPF_6 in CH_3CN) that was positioned within 2 mm of the surface of the working electrode. Each compartment of the cell was filled with 25 ml of solutions that were concurrently stirred and deoxygenated using bubbles of argon gas. The number of electrons involved in the bulk electrolysis process was calculated using the following equation.

$$N = Q/nF \tag{3.1}$$

where, N = number of moles of starting material used, Q = charge (in coulombs), n = number of moles of electrons, and F is the Faraday constant (96 485 C/mol).

3.4.6. Digital simulations

Digital simulations of the cyclic voltammograms were conducted using a DigiElch 7 simulation software acquired from Gamry Instruments.

3.5. References

[1] L. Huang, K. Hou, X. Jia, H. Pan, M. Du, Preparation of Novel Silver Nanoplates/Graphene Composite and their Application in Vanillin Electrochemical Detection, Mater. Sci. Eng., C, 38 (2014) 39–45.

[2] X. Lin, Y. Ni, S. Kokot, Electrochemical Mechanism of Eugenol at a Cu Doped Goldnanoparticles Modified Glassy Carbon Electrode and its Analytical Application in Food Samples, Electrochim. Acta, 133 (2014) 484–491.

[3] P. Deng, Z. Xu, R. Zeng, C. Ding, Electrochemical Behavior and Voltammetric Determination of Vanillin Based on an Acetylene Black Paste Electrode Modified with Graphene–Polyvinylpyrrolidone Composite Film, Food Chem., 180 (2015) 156–163.

[4] T.R. Silva, D. Brondani, E. Zapp, I.C. Vieira, Electrochemical Sensor Based on Gold Nanoparticles Stabilized in Poly(Allylamine hydrochloride) for Determination of Vanillin, Electroanalysis, 27 (2015) 465–472.

[5] S. Creager, Solvents and Supporting Electrolytes, in: C.G. Zoski (Ed.) Handbook of Electrochemistry, Elsevier, Amsterdam, The Netherlands, 2007, pp. 57–72.

[6] S. Chen, K.Y. Tai, R.D. Webster, The Effect of the Buffering Capacity of the Supporting Electrolyte on the Electrochemical Oxidation of Dopamine and 4-Methylcatechol in Aqueous and Nonaqueous Solvents, Chem. Asian J., 6 (2011) 1492–1499.

[7] Y. Li, J. Li, E. Shangguan, Q. Li, The Effect of Acidity, Hydrogen Bond Catalysis and Auxiliary Electrode Reaction on the Oxidation Peak Current for Dopamine, Uric Acid and Tryptophan, Anal. Methods, 7 (2015) 2636–2644.

[8] C. Zhai, D. Li, L. Li, F. Sun, H. Ma, X. Liu, Experimental and Theoretical Study on the Hydrogen Bonding between Dopamine Hydrochloride and N,N-Dimethyl Formamide, Spectrochim. Acta, Part A, 145 (2015) 500–504.

[9] L.L. Williams, R.D. Webster, Electrochemically Controlled Chemically Reversible Transformation of α-Tocopherol (Vitamin E) into Its Phenoxonium Cation, J. Am. Chem. Soc., 126 (2004) 12441–12450

[10] S.L.J. Tan, R.D. Webster, Electrochemically Induced Chemically Reversible Proton-Coupled Electron Transfer Reactions of Riboflavin (Vitamin B_2), J. Am. Chem. Soc., 134 (2012) 5954–5964.

[11] A.J. Bard, L.R. Faulkner, Electrochemical Methods: Fundamentals and Applications, 2nd ed., Wiley, New York, USA, 2001.

[12] S.B. Lee, C.Y. Lin, P.M.W. Gill, R.D. Webster, Transformation of α-Tocopherol (Vitamin E) and Related Chromanol Model Compounds into Their Phenoxonium Ions by Chemical Oxidation with the Nitrosonium Cation, J. Org. Chem., 70 (2005) 10466 –10473.

[13] Y.Y. Chan, Y. Yue, Y. Li, R.D. Webster, Electrochemical/Chemical Oxidation of Bisphenol A in a Four-electron/Two-proton Process in Aprotic Organic Solvents, Electrochim. Acta, 112 (2013) 287–294.

[14] W.W. Yao, H.M. Peng, R.D. Webster, P.M.W. Gill, Variable Scan Rate Cyclic Voltammetry and Theoretical Studies on Tocopherol (Vitamin E) Model Compounds, J. Phys. Chem. B, 112 (2008) 6847–6855.

[15] B. Speiser, Application of Digital Simulation, in: O. Hammerich, B. Speiser (Eds.) Organic Electrochemistry: Revised and Expanded, CRC Press, Boca Raton, Florida, 2016, pp. 205–227.

[16] S.E. Treimer, D.H. Evans, Electrochemical Reduction of Acids in Dimethyl Sulfoxide. CE Mechanisms and Beyond, J. Electroanal. Chem., 449 (1998) 39–48.

[17] S.E. Treimer, D.H. Evans, Electrochemical Reduction of Acids in Dimethyl Sulfoxide. Comparison of Weak C–H, N–H and O–H Acids, J. Electroanal. Chem., 455 (1998) 19–28.

[18] J.H.Q. Lee, Y. Yue, R. Ganguly, R.D. Webster, Electrochemical Study of Pyridoxine (Vitamin B_6) in Acetonitrile, ChemElectroChem, 2 (2015) 412–420.

This page has been intentionally left blank

Chapter 4

The Electrochemical Study of

Diethylstilbestrol (DES) in Acetonitrile

This page has been intentionally left blank

4.1. Chapter Overview

The present chapter revealed the detailed electrochemical study of the former drug diethylstilbestrol (DES, Scheme 4.1) by means of cyclic voltammetry (CV) and controlled potential electrolysis (CPE) techniques. In addition, owing to the similar structure of Bisphenol A (BPA, Scheme 4.1) and DES (both contain two phenolic functionality separated by an alkyl bridge), a comparative study between the voltammetric behaviors of the two compounds is also described.

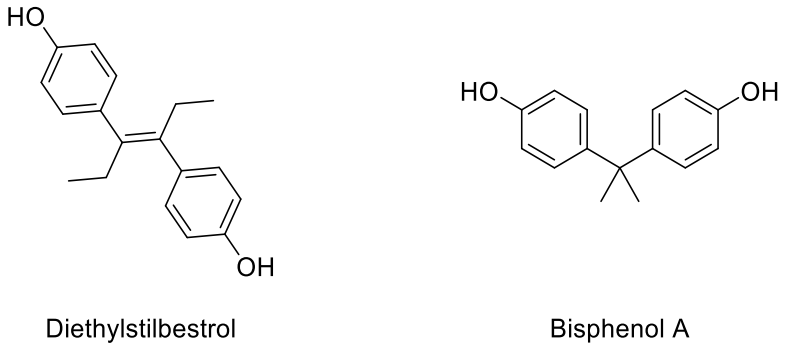

Scheme 4.1. Chemical structures of Diethylstilbestrol (DES) and Bisphenol A (BPA).

Using a glassy carbon (GC) electrode, DES was found to undergo two successive oxidation processes at ca. 0.64 and 0.81 vs. $(Fc/Fc^{+})/V$ in acetonitrile (CH_3CN). In order to investigate the changes in chemical reversibility of the redox processes over shorter time domain, increasingly higher scan rates CV experiments were subsequently performed, and the number of electron involved in the initial oxidation of DES was determined using CPE measurements. Furthermore, the effect of lowered water content was also assessed since hydrolysis was previously proposed to be a possible decomposition pathway undergone by BPA. Taking into account the comparable electrochemical phenomena of DES with that recorded for BPA, a similar electrochemical oxidation mechanism was proposed for DES.

4.2. Results and Discussion

4.2.1. Electrochemical oxidation of BPA and DES in CH_3CN

We had previously found that BPA, when examined in CH_3CN using a GC electrode and a scan rate 0.1 V s^{-1}, displays two consecutive oxidation peaks on the forward scan at ca. 0.99 and 1.44 vs. (Fc/Fc^+)/V (waves I and II), with no corresponding reduction peak when the scan direction was reversed (Figure 4.1(a)). A more thorough examination of the anodic process in wave I further revealed the involvement of a four-electron, two-proton ($-4e^-/-2H^+$) transfer which is eventually followed by a hydrolysis step to generate a hydroxylated bisdienone product [1].

With BPA as a reference compound, attention was turned to assessing the voltammetric behavior of DES under the same conditions (Figure 4.1(b)). Preliminary studies disclosed a comparable phenomenon to that of BPA where two oxidation peaks at ca. 0.64 and 0.81 vs. (Fc/Fc^+)/V (waves 1 and 2) were recorded on the forward scan. More interestingly, however, a diminutive reduction peak was also detected on the return sweep at ca. 0.50 vs. (Fc/Fc^+)/V (wave 3); a cathodic process that was previously unobserved in the system using BPA.

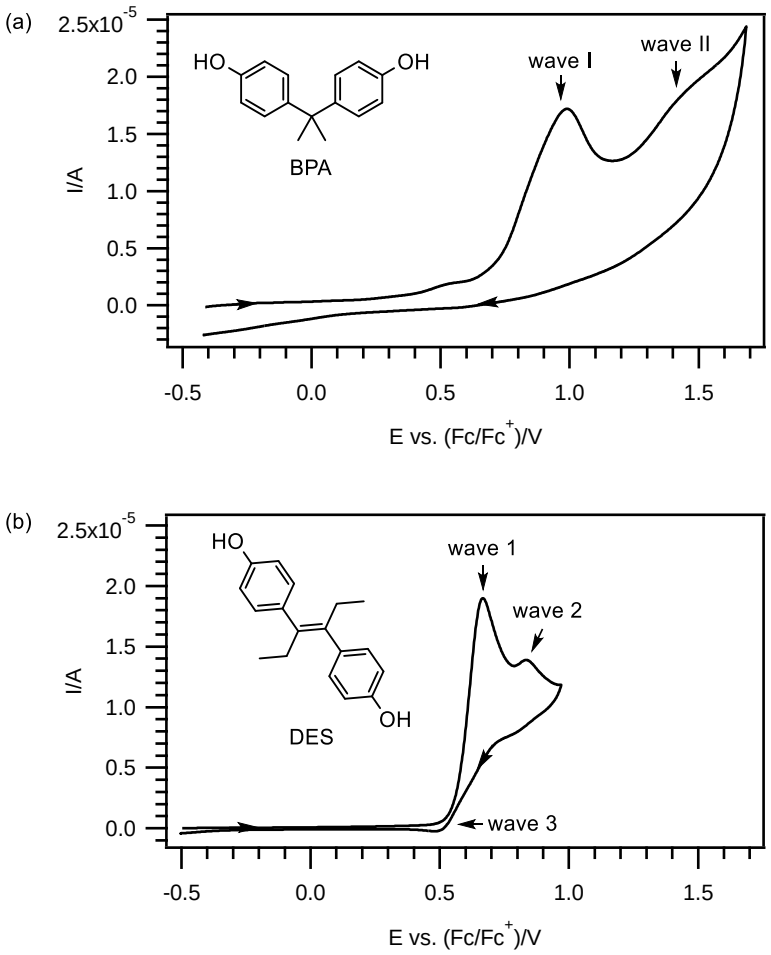

Figure 4.1. Cyclic voltammograms of 2 mM (a) BPA (b) DES in CH_3CN with 0.2 M Bu_4NPF_6, recorded using a 1 mm diameter planar GC electrode at a scan rate of 0.1 V s^{-1} and 22 (±2) °C.

4.2.2. Voltammetry of DES at varied scan rates

In order to assess the effects of shorter experimental time domains on the electrochemical behavior of BPA and DES, varying voltage sweep rate experiments were subsequently conducted on the aforementioned compounds. As shown in Figure 4.2, increasing in scan rates led to the diminishing magnitude of BPA's second oxidation step (wave II) until almost no discernible peak current could be detected at 20 V s^{-1}. Nevertheless, the employment of faster scan rates did not appear to improve the chemical reversibly of its electrochemical oxidation. In comparison, DES similarly showed a decrease in peak current magnitude for wave 2 as the

scan rates were increased (Figure 4.3). Concomitantly, wave 3 became more voltammetrically noticeable at larger scan rates and was also observed to give a corresponding anodic peak at ca. 0.53 vs. $(Fc/Fc^{+})/V$ (wave 4) upon continuous cycling.

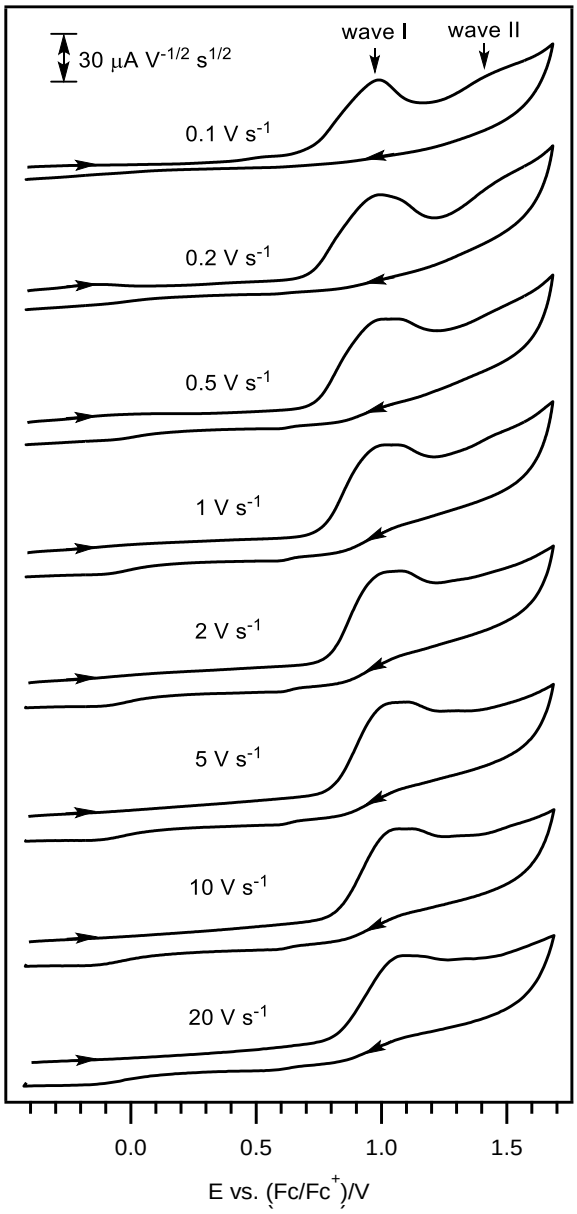

Figure 4.2. Variable scan rate cyclic voltammograms of 2 mM BPA in CH_3CN ($[H_2O]_{initial}$ = 96 mM) with 0.2 M Bu_4NPF_6, recorded using a 1 mm diameter planar GC electrode at 22 (±2) °C. Current data were multiplied by $(\text{scan rate})^{-0.5}$ for normalization.

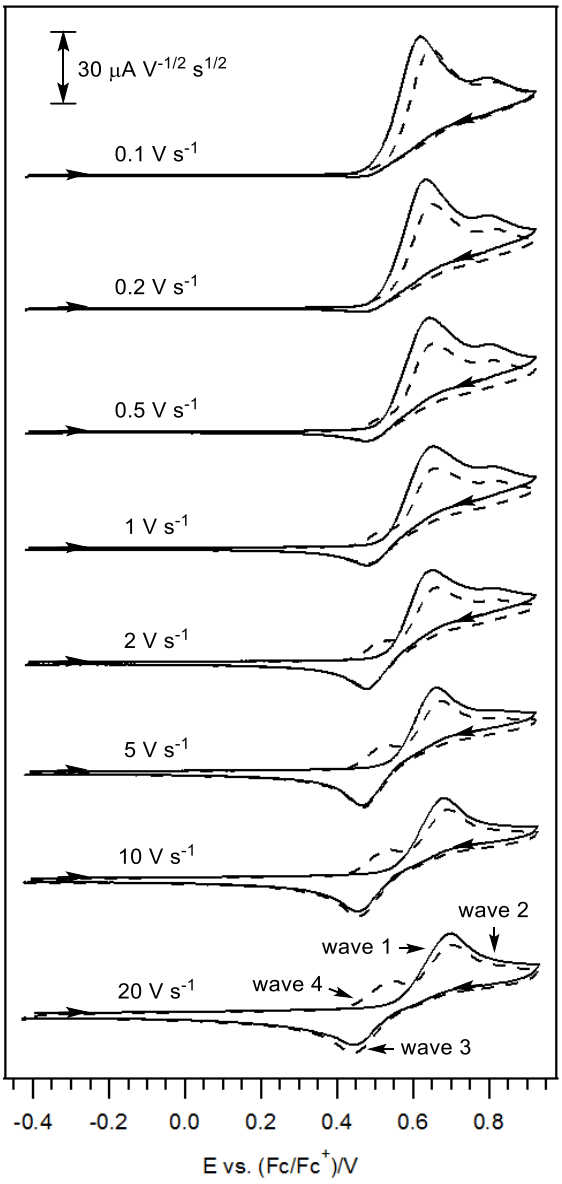

Figure 4.3. Variable scan rate cyclic voltammograms of 2 mM DES in CH_3CN ($[H_2O]_{initial}$ = 80 mM) with 0.2 M Bu_4NPF_6, recorded using a 1 mm diameter planar GC electrode at 22 (±2) °C. (—) 1st cycle. (- - -) 2nd cycle. Current data were multiplied by (scan rate)$^{-0.5}$ for normalization.

Based on the above experimental results, it is posited that waves II and 2 (for BPA and DES respectively) are likely related to the oxidation of secondary product(s) formed after the oxidation of BPA and DES at waves I and 1 respectively. That is, when higher scan rates are employed, the homogeneous reactions that form the secondary products are outrun and therefore are not detected at fast scan rates. In addition, the close proximity of the redox couple waves 3 and 4 with wave 1 (for DES) negates the possibility that wave 3 is associated with the regeneration of the starting material and instead is more probable to be due to the conversion of the oxidized product back into one of its intermediates. Notably, this oxidized species must also only be moderately stable as evidenced by the more marked presence of wave 3 only at larger scan rates (≥ 0.5 V s^{-1}).

4.2.3. Voltammetry of DES at varied temperatures

Because lowering of the temperature can sometimes help in improving the stability and lifetime of transient species, thereby allowing their voltammetric detection [2], variable temperature voltammetry experiments ranging from -30 to 20 °C were also conducted to further investigate the intermediates involved in the electrode reactions of DES (Figure 4.4). In doing so, it was found that waves 3 and 4 appear to become more discernible at ≤ 0 °C (even at a slow scan rate of 0.1 V s^{-1}), and was accompanied by the progressive decrease of wave 2. Hence, it is apparent that the electrode reactions induced at wave 2 will result in a decrease in the amount of species responsible for waves 3 and 4. Additionally, the necessity of lowered temperatures (≤ 0 °C) or higher scan rates (≥ 0.5 V s^{-1}) in order for the detection of waves 3 and 4 implies a limited lifetime of the oxidized product formed at wave 1. Nonetheless, a reduction of temperature only provided modest improvements in the stability of the oxidized product, as evidenced by the limited peak current achieved in waves 3 and 4.

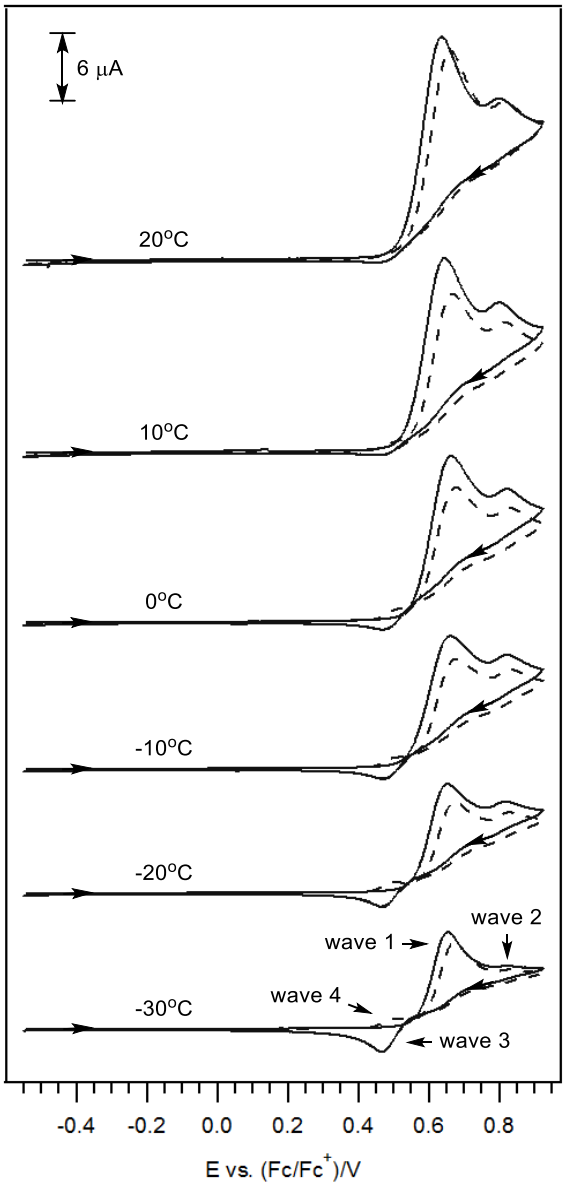

Figure 4.4. Variable temperatures cyclic voltammograms of 2 mM DES in CH_3CN with 0.2 M Bu_4NPF_6, recorded using a 1 mm diameter planar GC electrode at a scan rate of 0.1 V s^{-1}. (—) 1st cycle. (- - -) 2nd cycle.

4.2.4. Voltammetry of DES under lower water content conditions

It was proposed that a hydrolysis reaction is one of the secondary processes partaken by the product formed after the oxidation of BPA at wave I, thereby leading to the redox process being observed as chemically irreversible [1]. As such, it was reasoned that the use of drier conditions might help to mitigate the further reaction of the oxidized form of DES and possibly aid in improving its stability. With this in mind, DES was subjected to a lower amount of water but this revealed only a minimum change in the voltammetric behavior of DES. More specifically, the redox couple of waves 3 and 4 could be more clearly observed at scan rates ≥ 0.2 V s^{-1} ($[H_2O]_{initial}$ = 14 mM, Figure 4.5), instead of requiring higher scan rates of ≥ 0.5 V s^{-1} when examined under a higher trace water content condition ($[H_2O]_{initial}$ = 80 mM, Figure 4.3). As only modest improvements could be attained, this signifies that the oxidized product of DES is likely to be highly reactive in nature and thus relatively short-lived even in a low water environment. Similar attempts to reduce the reactivity of the anodic product of BPA by means of decreasing the concentration of trace water were also found to effect no substantial change (Figure A4.1 in the Appendix section).

Nevertheless, consistent with the earlier findings, waves 3 and 4 in Figure 4.5 were observed to grow at the expense of wave 2 as the scan rate increased. Thus, it stands to reason that the electrode reactions initiated at waves 2 and 3 demonstrate a competing relationship. The dichotomy between waves 2 and 3 arises at higher scan rates as there is less time available for the species responsible for wave 2 to occur which consequently allows more of the oxidized species (formed at wave 1) to undergo the reduction reaction instead, resulting in an increase in magnitude of wave 3 (and corresponding wave 4).

The validity of the association of wave 3 with a species formed after the initial oxidation at wave 1 (rather than wave 2) is demonstrated by restricting the potential range to allow only the

first electron transfer process to occur (Figure 4.6). As compared to the CV recorded from the larger potential range (Figure 4.6, solid line), an almost identical voltammogram was obtained in the narrower potential range (Figure 4.6, dashed line).

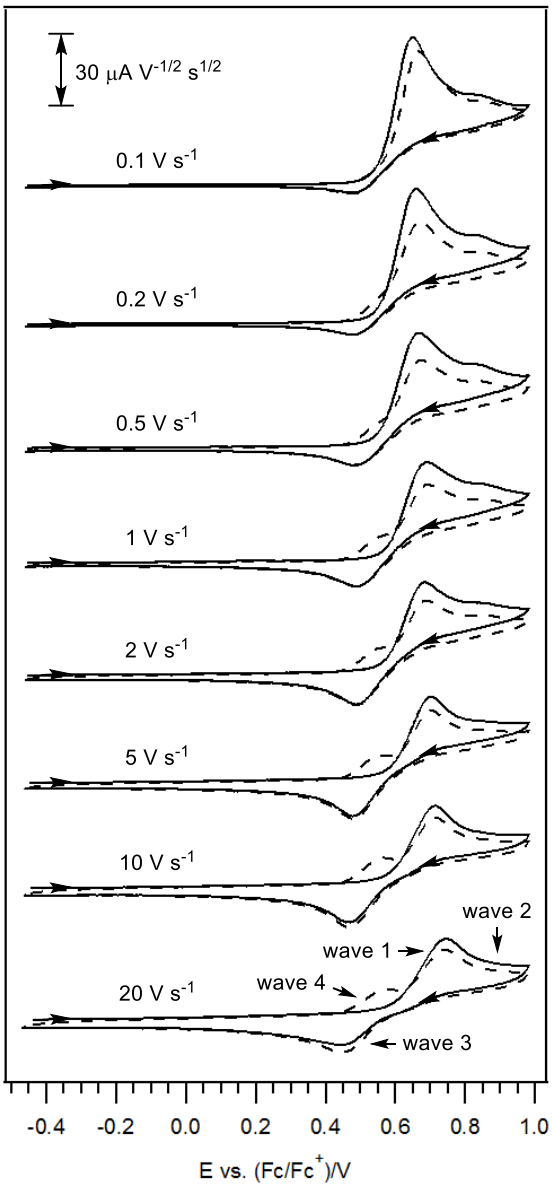

Figure 4.5. Variable scan rates cyclic voltammograms of 2 mM DES in CH_3CN ($[H_2O]_{initial}$ = 14 mM, $[H_2O]_{final}$ = 35 mM) with 0.2 M Bu_4NPF_6, recorded using a 1 mm diameter planar GC electrode at 22 (±2) °C. (—) 1st cycle. (- - -) 2nd cycle. Current data were multiplied by (scan rate)$^{-0.5}$ for normalization.

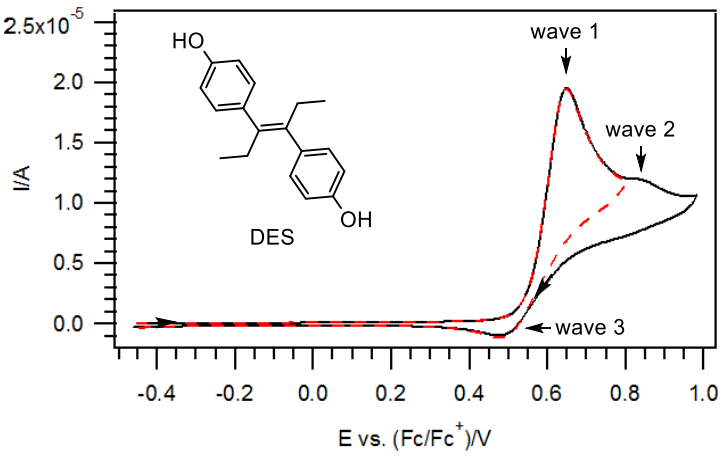

Figure 4.6. Cyclic voltammograms of 2 mM DES in CH_3CN ($[H_2O]_{initial}$ = 14 mM, $[H_2O]_{final}$ = 35 mM) with 0.2 M Bu_4NPF_6, recorded using a 1 mm diameter planar GC electrode at a scan rate of 0.1 V s^{-1} and 22 (±2) °C. (—) Switching potential: 0.98 V vs. (Fc/Fc^+)/V. (- - -) Switching potential: 0.80 V vs. (Fc/Fc^+)/V.

4.2.5. Controlled potential electrolysis of DES

By changing the composition of the solution appreciably, controlled potential electrolysis (CPE) experiments were performed in order to obtain information about the intermediates and long-term oxidation products. In addition, CPE also enables the determination of the number of electrons involved in a redox process. As wave 1 is the first heterogeneous step that DES has to undergo, the potential applied was made sufficiently positive (50 mV more positive than that of wave 1) to allow only a full conversion of the electron transfer process in wave 1 while preventing the simultaneous occurrence of wave 2. Figure 4.7 outlines the coulometric and voltammetric graphs logged after an elapse of 4500 seconds. Verification of the complete oxidation was shown by the absence of wave 1 in the voltammogram obtained after the bulk conversion (Figure 4.7(a), dotted line) as well as the observation of the current decaying from an initial ca.10 mA to an almost zero value, as illustrated in the coulometry data (Figure 4.7(b)).

According to Eq. (4.1), approximately four moles of electron (per mole of DES) were found to be involved in the electron transfer reaction in wave 1. Furthermore, upon the loss of wave 1, a new anodic peak at ca. 0.68 vs. $(Fc/Fc^{+})/V$, together with the previously observed wave 2 were seen (Figure 4.7(a), dotted line). The appearance of wave 2 after the exhaustive electrolysis further corroborates the premise that wave 2 is the subsequent oxidation of the reaction product generated by wave 1. Although the oxidation peak current of the oxidized product is much smaller than for the starting material, it does not necessarily mean that the product is present in very low yield, since its own oxidation may occur by fewer than four electrons.

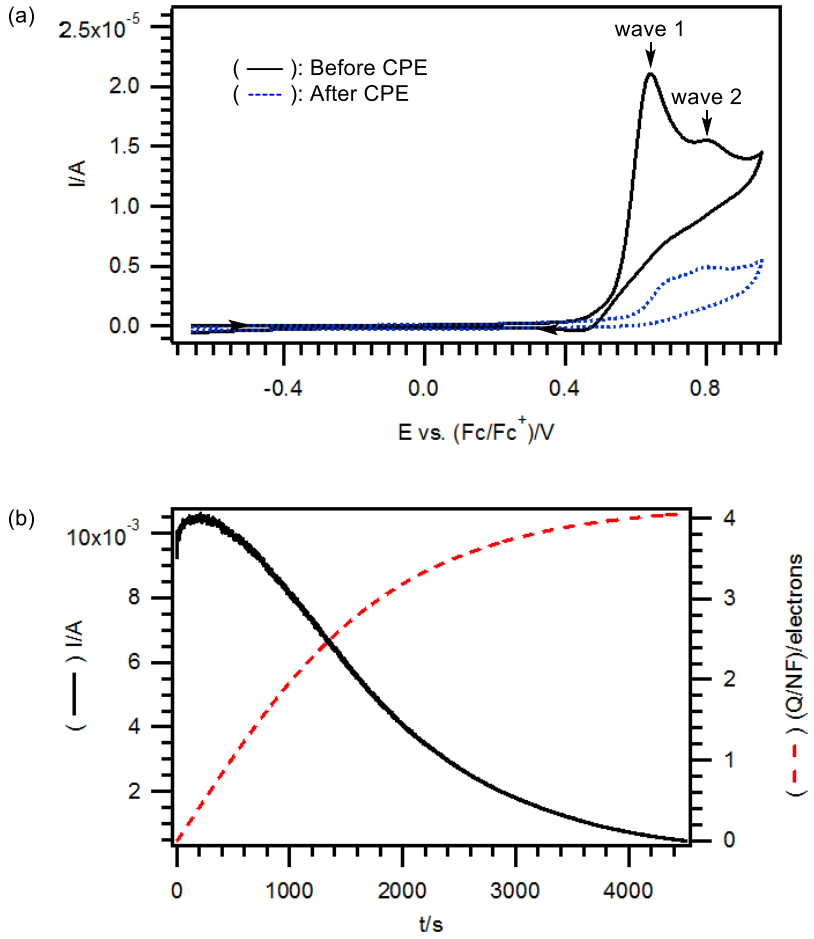

Figure 4.7. Voltammetric and coulometric data recorded during the controlled potential electrolysis of 2 mM DES in CH_3CN with 0.2 M Bu_4NPF_6 at 22 (±2) °C. (a) Cyclic voltammograms obtained at a scan rate of 0.1 V s^{-1} using a 1 mm diameter planar GC electrode. (b) Current vs. time data logged during the exhaustive oxidation of DES at 0.69 vs. $(Fc/Fc^+)/V$.

4.2.6. Proposed electrochemical oxidation mechanism

On the basis of the above results, a tentative mechanism for the electrochemical oxidation of DES is illustrated in Scheme 4.2. Consistent with the proposed mechanism of BPA [1], the oxidation of DES is surmised to proceed via an overall loss of four electrons, two protons in an ECE manner (where E and C represent an electron transfer and chemical step respectively), with a stepwise transfer of an electron in each heterogeneous reaction and a proton involve in

each homogeneous process. Notably, however, because of the highly conjugated structure of DES, as well as the involvement of a large number of steps, it is very difficult to voltammetrically confirm the exact sequence of the electron transfer and homogeneous reactions, thus an alternative order of the electrochemical and chemical transformations cannot be completely ruled out.

Furthermore, with the aim of gaining a better understanding on the mechanistic premise put forward in Scheme 4.2, digital simulations were also conducted to supplement the experimental data. Generally, the simulation work was performed in a trial and error manner that includes the systematic addition of the reaction parameters for the various heterogeneous and homogeneous processes. Additionally, in order to increase the credibility of the simulation results, rather than modeling and fitting to only a single voltammogram, a fixed set of reaction parameters was used for the entire range of scan rates (0.1 to 20 V s^{-1}) examined in the current study [3]. As illustrated in Figure 4.8, a reasonably close fit between the experimental and simulated voltammograms was obtained, and the various optimized electrochemical and chemical kinetic parameters used are tabulated in Tables 4.1 and 4.2.

In line with the behavior of a typical phenol, the initial removal of an electron from DES will produce a cation radical that is more acidic than the parent, thereby allowing the loss of a proton easily (compound **2** to **3**). Consequently, this structural change also enables the second electron transfer process to proceed at a less positive potential thereby producing a multi-electron peak (wave 1) [4]. Due to the presence of two phenolic functional groups in DES, it is conceivable to propose that two ECE processes occurred, with a diamagnetic cation (compound **4** and **8**) formed after every ECE reaction. This was ascertained by the results gathered from the electrolysis experiment where four moles of electrons were involved during the complete oxidation of DES (Figure 4.7). The generated cationic product is well-documented to be highly reactive and can readily undergo follow-up reactions such as hydrolysis (compound **4** to **5** and

8 to **9**) [1, 5]. The possibility of the hydrolysis reactions occurring only after the manifestation of two consecutive ECE processes (i.e. reaction of two molecules of water with the dicationic form of compound **8**) instead of the reaction of one molecule of water with each cationic product that has been formed after every ECE process (compound **4** to **5** and **8** to **9**, as shown in Scheme 4.2) was considered but thought to be less likely based on the simulation analysis. This can be reasoned by the observation of a comparatively lowered peak height of wave 1 at high scan rates, thus implying the occurrence of a less than four-electron process. Therefore, it is rationalized that the hydrolysis reactions take place in a stepwise fashion, with the first hydrolysis process (compound **4** to **5**) being outrun at faster scan rates that will result in only two moles of electrons being transferred, which in turn leads to a dwindling magnitude of wave 1 at high scan rates. As such, the rate constants associated with the first hydrolysis step (Eq. (iv)) are expected to be relatively small in value (forward rate constants (k_f) = 17, backward rate constants (k_b) = 0.017).

With the above information in mind, the species associated with wave 3 which appears near the vicinity of wave 1 is ascribed to be due to the reduction of compound **4** to **3**. The possible involvement of wave 3 as the regeneration of the starting material (DES) (compound **4** to **1**) is discounted based on the observation of the ratio of the peak current of wave 1 and 3 not reaching unity even with the employment of high scan rate such as 20 V s^{-1}. Moreover, this was supported by the presence of a reverse oxidation peak (wave 4) on the second cycle of the CV experiment (i.e. waves 3 and 4 are a redox couple, as shown in Figure 4.3). Therefore, the equilibrium constant for the proton loss in Eq. (ii) would be in favor of the formation of the product (compound **3**) which accounts for only the last E step (Eq. (iii)) of the first ECE sequence (Eqs. (i)-(iii)) of the mechanism to be chemically reversible.

For the variable scan rates experiments carried out under less dry conditions (Figure 4.3), it was observed that the redox couple (waves 3 and 4) became more experimentally detectable at scan

rates ≥ 0.5 V s^{-1}, in conjunction with the decrease in peak current of wave 2. Notably, a similar trend was also observed when the solution temperature was lowered as displayed in Figure 4.4. Despite multiple attempts to isolate the oxidized product of DES after electrolysis, thin layer chromatography analysis revealed that the end product appeared to form several other products that were very difficult to separate and purify using preparative flash column chromatography. This is all the more so given the need to remove the electrolyte, which is usually added in large quantities (at least 10-100 fold excess of the analyte) during electrochemical experiments. In view of the results gathered, it is posited that wave 2 is a secondary process that takes place via an oxidation of compound **9** to **10** which can subsequently decompose into other products. This follow-up chemical reaction therefore accounts for the chemically irreversible nature of wave 2.

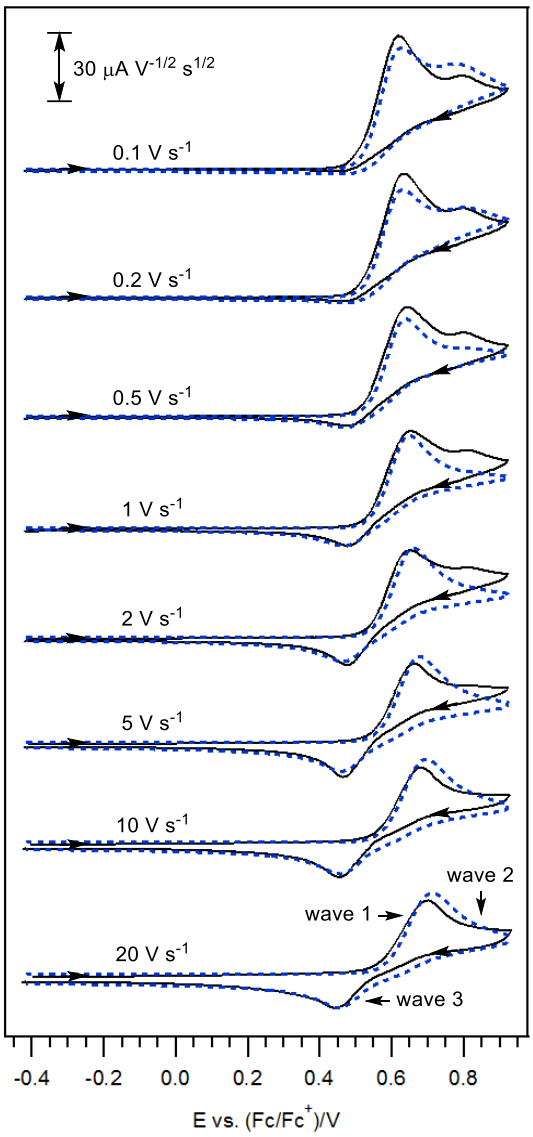

Figure 4.8. Variable scan rates cyclic voltammograms of 2 mM DES in CH_3CN with 0.2 M Bu_4NPF_6, recorded at a 1 mm diameter planar GC electrode at 22 (±2) °C. (—) Experimental voltammograms. (·····) Simulated voltammograms generated based on the mechanism outlined in Scheme 4.2. Current data were scaled by multiplying by (scan rates)$^{-0.5}$.

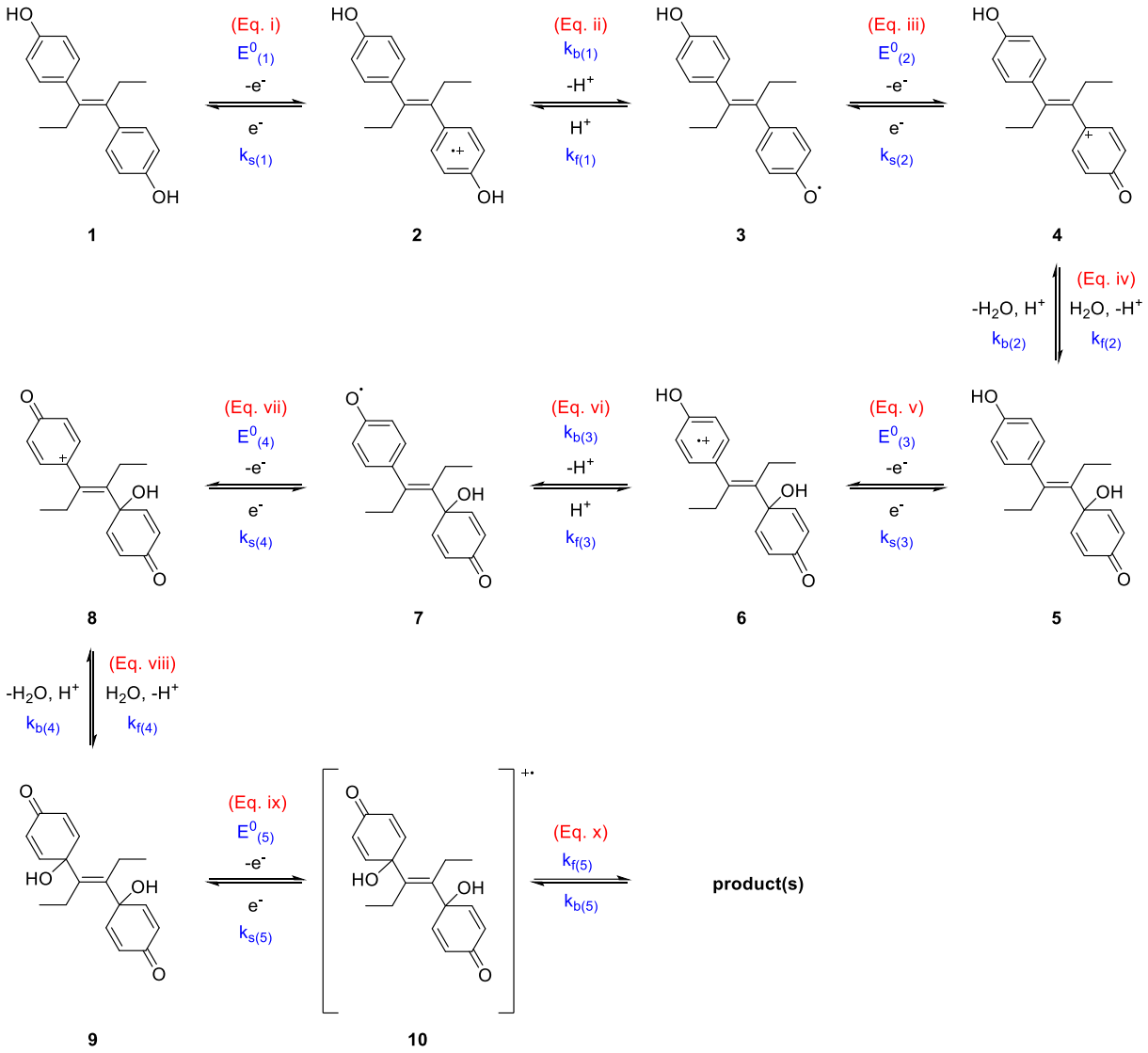

Scheme 4.2. Proposed mechanism for the electrochemical oxidation of DES.

Table 4.1. Electrochemical parameters[a] obtained by digital simulations of CV data[b] for the reaction mechanisms shown in Scheme 4.2.

Electrochemical Parameters	Eq. i	Eq. iii	Eq. v	Eq. vii	Eq. ix
E^0 (V)	0.74	0.49	0.71	0.46	0.92
k_s (cm s^{-1})	0.70	0.60	0.70	0.60	0.20

[a]E^0 = formal oxidation potential vs. (Fc/Fc^+)/V, k_s = heterogeneous electron transfer rate constant. The diffusion coefficients were estimated via simulation techniques to be 2.20 x 10^{-5} cm^2 s^{-1} for DES and its oxidized forms and 3.50 x 10^{-5} cm^2 s^{-1} for H_2O and H^+. The transfer coefficient (α) values were assumed to be 0.5. [b]CV data were logged using a 1 mm diameter GC electrode for solutions of 2 mM DES with 0.2 M Bu_4NPF_6 in CH_3CN at 22 (±2) °C. The water and proton concentrations used were 0.08 M.

Table 4.2. Equilibrium and rate constants[a] obtained by digital simulations of CV data[b] for the reaction mechanisms shown in Scheme 4.2.

Kinetic Parameters	Eq. ii	Eq. iv	Eq. vi	Eq. viii	Eq. x
K_{eq}	8.00 x 10^{-7}	1.00 x 10^{3}	1.00 x 10^{-5}	2.50 x 10^{5}	1.00 x 10^{4}
k_f	1.00 x 10^{0}	1.70 x 10^{1}	5.00 x 10^{-1}	5.00 x 10^{5}	1.00 x 10^{7}
k_b	1.25 x 10^{6}	1.70 x 10^{-2}	5.00 x 10^{4}	2.00 x 10^{0}	1.00 x 10^{3}

[a]K_{eq} = equilibrium constant, k_f = forward rate constant, k_b = backward rate constant. The homogeneous rate constants have units of s^{-1} and L mol^{-1} s^{-1} for the first- and second-order reactions, respectively. [b]CV data were logged using a 1 mm diameter GC electrode for solutions of 2 mM DES with 0.2 M Bu_4NPF_6 in CH_3CN at 22 (±2) °C. The water and proton concentrations used were 0.08 M.

4.3. Conclusion

Overall, the electro-oxidation of DES in CH_3CN revealed a comparable voltammetric behavior to BPA. The concurrence of these results indicates a similar mechanistic premise for the oxidation of DES. Interestingly, in contrast with the chemically irreversible oxidative process recorded for BPA, a reduction peak (wave 3) was observed after the initial oxidation of DES. The cathodic process was reasoned to be due to the reduction of the oxidized product (compound **4**) back to the intermediate compound **3** (wave 3), which gave a corresponding anodic peak (wave 4) on the subsequent cycle. However, the short-lived redox couple (waves 3 and 4) is only experimentally detected at fast scan rates ($\geq$ 0.5 V s^{-1}) during the CV measurements, thus implying the limited stability of compound **4**. Conversely, at low scan rates, an additional anodic peak was seen at ca. 0.81 vs. (Fc/Fc^{+})/V (wave 2) on the forward scan. The latter oxidation process was observed to be outrun at high scan rates, while waves 3 and 4 concomitantly increased in magnitude. Likewise, a similar trend was found on reducing the solution temperature. In light of the aforementioned results, wave 2 is rationalized to be the oxidation of a secondary product. Through careful analysis of the gathered voltammetric responses, a tentative mechanism for the electrochemical oxidation of DES was postulated and digital simulation studies were performed to in order to verify the validity of the proposed mechanism as well as to extract kinetic information regarding its involved pathways.

4.4. Experimental

4.4.1. General remarks

Unless otherwise stated, all chemicals and reagents were purchased from commercial sources and used as received.

4.4.2. Chemicals and reagents

DES (> 98%), BPA (≥ 99%) and HPLC grade acetonitrile (CH_3CN) were obtained from Tokyo Chemical Industry Co., Ltd., Sigma-Aldrich and Macron respectively. Molecular sieves that are made up of 1/16 inch rods with pore size 3 Å (CAS: 308080-99-1) were bought from Fluka. Tetrabutylammonium hexafluorophosphate (Bu_4NPF_6), the supporting electrolyte, was prepared according to a literature procedure [46] by reacting equal molar amounts of a 40% aqueous solution of Bu_4NOH (Alfa Aesar) and a 65% aqueous solution of HPF_6 (Alfa Aesar), washing the resulting precipitate with ultrapure water and recrystallizing three times with hot ethanol, with subsequent drying under vacuum at 140 °C for 6 hours.

4.4.3. Voltammetry

Cyclic Voltammetry (CV) experiments were carried out using a computer controlled Eco Chemie Autolab PGSTAT302N potentiostat with a three-electrode system. The working electrode was a 1 mm diameter planar disk glassy carbon (GC) working electrode (eDAQ Pty Ltd), used along with a platinum (Pt) counter electrode (Metrohm) and a silver (Ag) wire miniature reference electrode (eDAQ Pty Ltd) that was separated from the sample solution via a salt bridge containing 0.5 M Bu_4NPF_6 in CH_3CN. Prior to each scan, all sample solutions used for the voltammetric experiments were deoxygenated by purging with high purity argon gas, with the measurements performed in a Faraday Cage. At the end of the experiments, accurate potentials were obtained by the addition of ferrocene (Fc) as an internal standard. Variable

temperature voltammetric experiments (-30 to 20 °C) were conducted in a Metrohm jacketed glass cell, with the temperatures controlled by a Julabo FP89-HL ultralow refrigerated ethanol circulating bath. Ohmic drop was not compensated for all cyclic voltammograms.

4.4.4. Measurement of Water Content in Sample Solutions

Karl Fischer titrations was conducted inside a humidity control box (122cm × 61cm × 61cm, Coy Laboratory Products Inc) using a Mettler Toledo DL32 coulometer where the HYDRANAL- coulomat CG (Riedel-deHaën) and HYDRANAL- coulomat AG were employed in the cathode and anode compartment respectively. Measurements were performed by injecting analyte solutions that are contained in a 5 mL vacuum syringe (SGE Analytical Science) into the coulometer through a silicon/Teflon septum.

4.4.5. Preparations for Dry Voltammetry Experiments

Voltammetric experiments with lower water content were performed in dried CH_3CN (over 3 Å molecular sieves) that was transferred into an electrochemical cell that was heated at 100 °C in an oven for at least 1 hour prior to the experiment and allowed to cool under an argon atmosphere. Aliquots of the analyte solution were measured by Karl Fischer titration, before subjecting to any CV analysis, to obtain an estimate of the initial water content directly inside the electrochemical cell (initial $[H_2O]$ = 14-17 mM).

4.4.6. Controlled Potential Electrolysis

Controlled potential electrolysis (CPE) measurements were performed in a two-compartment electrolysis cell divided by a sintered glass frit of porosity no. 5 (1.0 – 1.7μm) [47]. Two identically sized GC cylinders were used as the working and counter electrodes, which were arranged symmetrically with respect to each other, and used in conjunction with the aforementioned reference electrode that was positioned within 2 mm of the surface of the

working electrode. Sample solutions (25 ml each) in both compartments of the cell were simultaneously deoxygenated and stirred using bubbles of argon gas. The number of electrons transferred during the bulk electrolysis process was calculated using the Faraday's equation.

$$N = Q/nF \quad (4.1)$$

where, N = number of moles of starting material used, Q = charge (in coulombs), n = number of moles of electrons, and F is the Faraday constant (96 485 C/mol).

4.4.7. Digital Simulations

Digital simulations of the cyclic voltammograms were carried out using a DigiElch 7 simulation software purchased from Gamry Instruments.

4.5. References

[1] Y.Y. Chan, Y. Yue, Y. Li, R.D. Webster, Electrochemical/Chemical Oxidation of Bisphenol A in a Four-electron/Two-proton Process in Aprotic Organic Solvents, Electrochim. Acta 112 (2013) 287–294.

[2] S. Creager, Solvents and Supporting Electrolytes, in: C.G. Zoski (Ed.), Handbook of Electrochemistry, Elsevier, Amsterdam, The Netherlands, 2007, pp. 57–72.

[3] B. Speiser, Application of Digital Simulation, in: O. Hammerich, B. Speiser (Eds.), Organic Electrochemistry: Revised and Expanded, CRC Press, Boca Raton, Florida, 2016, pp. 205–227.

[4] A.J. Bard, L.R. Faulkner, Electrochemical Methods: Fundamentals and Applications, 2nd ed., Wiley, New York, USA, 2001.

[5] H.M. Peng, R.D. Webster, Investigation into Phenoxonium Cations Produced During the Electrochemical Oxidation of Chroman-6-ol and Dihydrobenzofuran-5-ol Substituted Compounds, J. Org. Chem. 73(6) (2008) 2169–2175.

This page has been intentionally left blank

Chapter 5

The Electrochemical Study of Pyridoxine (PN) in Acetonitrile

This page has been intentionally left blank

5.1. Chapter Overview

In the present chapter, a detailed study on the electrochemical behaviour of pyridoxine (PN, scheme 5.1), a member of the vitamin B_6 family, was performed in non-aqueous solvents. As compared to the other aprotic solvents that were examined, PN generally displayed more definitive voltammetric wave shapes in acetonitrile (CH_3CN), and was thus chosen as the main solvent used.

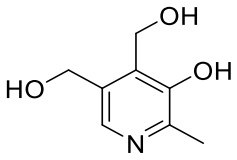

Scheme 5.1. Chemical structure of pyridoxine (PN).

Using a platinum (Pt) electrode, it was revealed that PN undergoes a one-electron chemically irreversible oxidation at ca. 0.50 vs. (Fc/Fc^+)/V and this anodic process appeared to suffer from electrode fouling, which could be detected with repeated scans during cyclic voltammetry (CV) and preparative scale controlled potential electrolysis (CPE) oxidation experiments. Nonetheless, these undesirable adsorption effects were able to be overcome by oxidizing PN using a chemical oxidant ($NOSbF_6$) instead.

Separately, a cathodic peak associated with the reduction of PN was observed at ca. -1.60 vs. (Fc/Fc^+)/V. Unlike the former electron-transfer reaction (oxidation), the reduction process was found to be chemically reversible on the comparatively shorter timescale of CV and does not display any adsorptive phenomena. Also, the cathodic process was shown to require a catalytic surface (e.g. Pt) in order to be voltammetrically observable.

5.2. Results and Discussion

5.2.1. Voltammetry of PN in aprotic solvents

Hitherto, examination of the electrochemistry of PN have generally been directed toward aqueous systems, possibly due to its restricted solubility in non-polar solvents. With this information in mind, the initial voltammetric studies on PN were conducted in the polar aprotic organic solvents acetonitrile (CH_3CN), *N*,*N*-dimethylformamide (DMF), and dimethylsulfoxide (DMSO), and their cyclic voltammograms are shown in Figure 5.1.

In all solutions, PN gave a chemically irreversible anodic peak at ca. 0.50 vs. (Fc/Fc^+)/V and a chemically reversible cathodic wave at ca. -1.60 to -1.80 vs. (Fc/Fc^+)/V. Notably, however, the oxidation peak was less noticeable in DMF and DMSO solutions, due to the oxidation peak occurring in close proximity to the potential window of the aforementioned solvents. Since an overall more well-defined cyclic voltammogram was recorded in CH_3CN, experiments were subsequently conducted in this solvent.

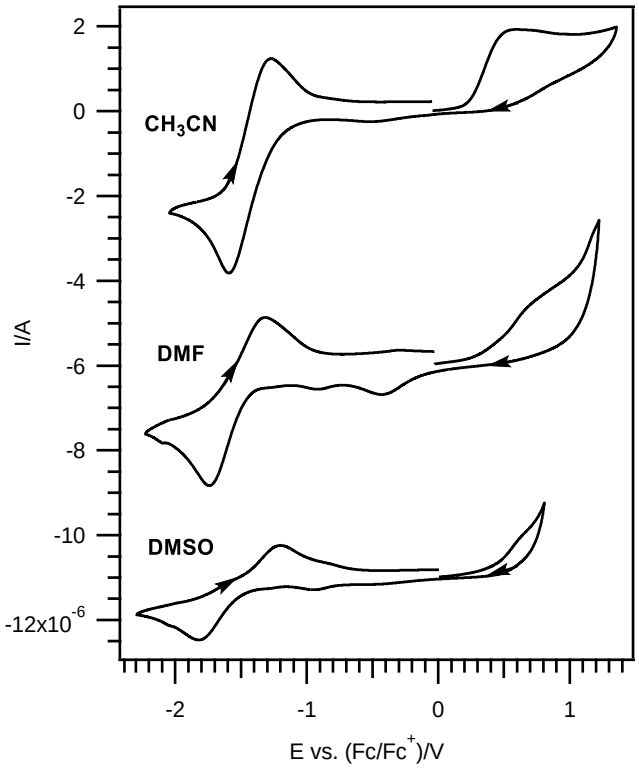

Figure 5.1. Cyclic voltammograms of 2 mM PN in CH_3CN, DMF and DMSO solution with 0.2 M Bu_4NPF_6 recorded using a 1 mm diameter planar Pt electrode at a scan rate of 0.1 V s^{-1} and 22 (±2) °C.

In order to determine the effect of trace water on the voltammetric behavior of PN, CV measurements were therefore performed using two different types of CH_3CN solutions, one that was pre-dried over molecular sieves ($[H_2O]_{initial}$ = 34 mM), whereas the other was not pre-dried, and obtained directly from the solvent bottle ($[H_2O]_{initial}$ = 107 mM; approximately three times higher). As depicted in Figure 5.2, PN displayed a chemically irreversible oxidation process at ca. 0.50 vs. (Fc/Fc^+)/V and a chemically reversible cathodic peak at ca. -1.60 vs. (Fc/Fc^+)/V in both cases. Since the two sample solutions generally resulted in similar voltammograms, subsequent experiments were carried out using the undried CH_3CN solvent.

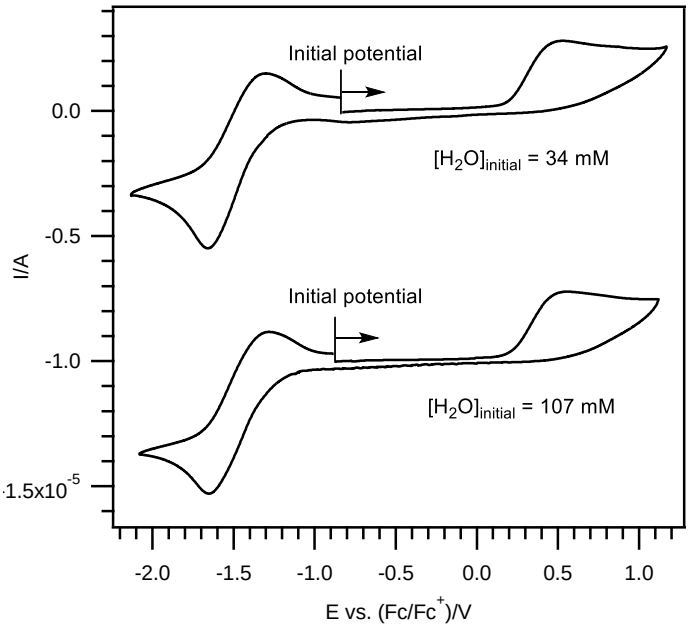

Figure 5.2. Cyclic voltammograms of 2 mM PN in CH_3CN solution with 0.2 M Bu_4NPF_6, containing different water content, recorded using a 1 mm diameter planar Pt electrode at a scan rate of 0.1 V s^{-1} and 22 (±2) °C.

5.2.2. Electrochemical oxidation of PN in CH_3CN

As illustrated above (Figure 5.2), the electrochemical oxidation of PN at ca. 0.50 vs. (Fc/Fc^+)/V appeared to be chemically irreversible in the sense that besides the presence of a small reduction peak at ca. -0.80 vs. (Fc/Fc^+)/V, which is likely to be attributable to a reaction product of the oxidation reaction, no noticeable corresponding cathodic peak was seen on the return sweep, when recorded at a scan rate of 0.1 V s^{-1} (Figure 5.3).

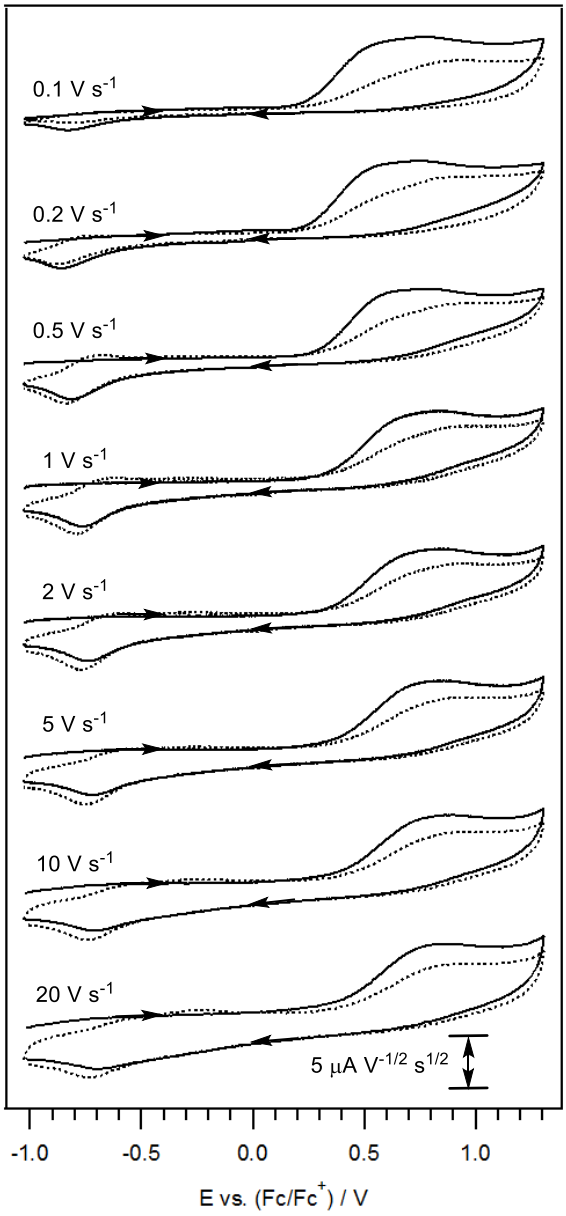

Figure 5.3. Variable scan rate cyclic voltammograms of 2 consecutive scans of 2 mM PN in CH_3CN with 0.2 M Bu_4NPF_6, recorded using a 1 mm diameter planar Pt electrode at 22 (±2) °C. (—) 1st cycle. (·····) 2nd cycle. Current data were multiplied by (scan rate)$^{-0.5}$ for normalization.

As the scan rate was increased from 0.1 to 0.5 V s^{-1}, the reduction peak that was observed at ca. -0.80 vs. (Fc/Fc^{+})/V became more voltammetrically detectable and remained approximately the same magnitude (with respect to the initial oxidation process) as the scan rate was further increased up to 20 V s^{-1} (Figure 5.3). This could possibly be accounted by the longer time domain provided by the slower scan rates (< 0.5 V s^{-1}), thus enabling the oxidized product to have more time to diffuse away from the electrode surface into the bulk solution. Furthermore, due to the wide separation between the oxidation and reduction peaks (~1.30 V), it is not immediately apparent whether the cathodic peak is responsible for the reduction of the oxidized product back to the starting material, or attributable to the reduction of some other intermediate species. Interestingly, experiments performed by continuous cycling (dotted lines in Figure 5.3) revealed that the reduction process at ca. -0.80 vs. (Fc/Fc^{+})/V itself gave a small reverse oxidation peak on the second cycle, which negates the probability of the reduction peak to be involved in the regeneration of the starting material.

In isolation, voltammetry results do not directly provide information on the number of electrons transferred during the oxidation of PN or the long-term chemical stability of the oxidized product and/or its associated intermediate(s). Hence, CPE experiments were performed, with its progress being monitored via CV. The voltammograms recorded prior to and upon cessation of the oxidative electrolysis are depicted in Figure 5.4(a), while the corresponding coulometric results are displayed in Figure 5.4(b). In order to ensure an exhaustive oxidation of the analyte, the applied oxidative potential was set at approximately 200 mV more positive than the oxidation peak value observed in the cyclic voltammogram put forward in Figure 5.4(a).

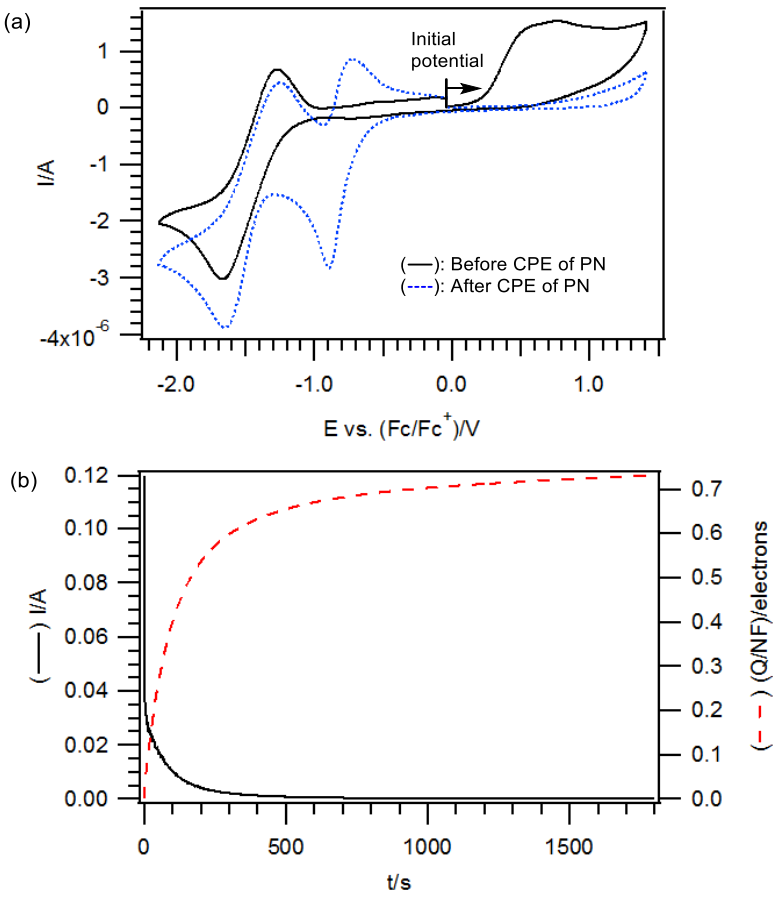

Figure 5.4. Voltammeric and coulometric data recorded during the oxidative CPE of 2 mM PN in CH_3CN with 0.2 M Bu_4NPF_6 at 22 (±2) °C. (a) Cyclic voltammograms obtained at scan rate of 0.1 V s^{-1} using a 1 mm diameter planar Pt electrode. (b) Current vs time data obtained during exhaustive oxidation of PN at 0.87 vs. $(Fc/Fc^+)/V$.

Based on the results outlined in Figure 5.4, the oxidation of PN was found to involve ca. one electron per molecule (n = 0.7) and appeared chemically irreversible. As compared to the colorless solution observed before the commencement of the electrolysis, the resultant solution was bright yellow in color. The complete oxidation of the analyte was confirmed by the disappearance of the initially present oxidation peak (solid line in Figure 5.4(a)), and the observation of a new redox couple with reduction peak at ca. -0.90 vs. $(Fc/Fc^+)/V$. As CPE invokes a bulk oxidation of PN, it is reasoned that this newly formed redox couple is likely to

stem from the same species which is responsible for the cathodic peak (at ca. -0.80 vs. (Fc/Fc^+)/V) seen during the varied scan rates CV measurements (Figure 5.3), and is more pronounced in size plausibly because it is produced in larger quantities during the exhaustive electrolysis. Also, it is noteworthy to highlight that the reduction peak detected at ca. -1.60 vs. (Fc/Fc^+)/V remains even after the exhaustive electrolysis of PN (Figure 5.4(a)). This phenomenon further suggests that the initial reduction of PN occurs at a different site of the molecule that is independent of the oxidation reaction, and is further discussed in section 5.2.4.

With the intention of isolating the oxidized product for identification/characterization, an additional CPE experiment was conducted at a larger starting material concentration of 6 mM (as compared to the 2 mM in Figure 5.4). Unfortunately, the oxidized product appeared to adsorb on the electrode surface, as demonstrated by the charge and current measurements not being able to reach complete oxidation values (Figure 5.5). For instance, over the same timeframe of ca. 30 mins, only a total of ca. 0.5 electrons per molecule of PN (as compared to the 0.7 electrons obtained for 2 mM PN in Figure 5.4) were accumulated. This finding was also supported by the CV results, which illustrated that with continuous cycling at a fixed scan rate, the magnitude of the oxidation current decreased substantially with each sequential scan (Figure 5.6).

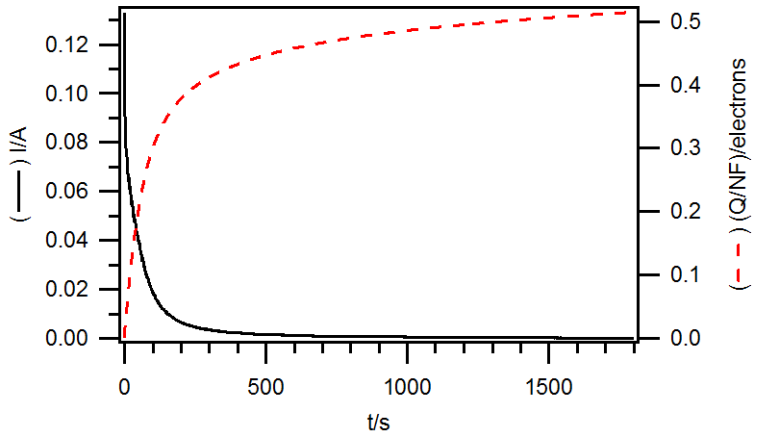

Figure 5.5. Current vs time data obtained during the oxidative CPE of 6 mM pyridoxine in CH_3CN with 0.2 M Bu_4NPF_6 at 22 (±2) °C.

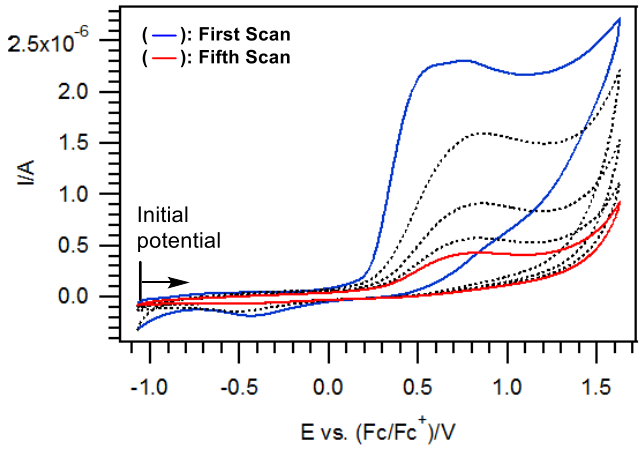

Figure 5.6. Cyclic voltammograms of 5 consecutive scans of 2 mM PN in CH_3CN with 0.2 M Bu_4NPF_6, recorded using a 1 mm diameter planar Pt electrode at a scan rate of 0.1 V s^{-1} and 22 (±2) °C.

5.2.3. Reaction of PN with a chemical oxidant in CH_3CN

To circumvent the adsorption effects encountered during the exhaustive electrochemical oxidation of PN, an alternative strategy of employing a chemical oxidant, nitrosonium hexafluoroantimonate ($NOSbF_6$), was used instead. A significant advantage of using a chemical oxidant is the absence of any supporting electrolyte that would necessitate eventual removal (which is often added in a large excess so as to suppress migration effects and minimize solution resistance in electrochemical solutions). For the current study, $NOSbF_6$ was chosen for various reasons: (a) $NOSbF_6$ is a one-electron chemical oxidant. (b) Its reduction potential in CH_3CN occurs at 0.87 vs. (Fc/Fc^+)/V [1], which is ca. 0.37 V more positive than PN's oxidation potential, and should therefore be able to function as an suitable oxidizing agent. (c) $NOSbF_6$ is ^1H and ^{13}C NMR silent. (d) It forms NO which is a gaseous by-product which can be readily excluded from the reaction mixture [2].

Initially, a small scale treatment of 2 mM PN with $NOSbF_6$ was monitored by CV in order to assess the suitability of using the aforementioned chemical oxidant. As depicted in Figure 5.7, after the reaction with one molar equivalence of $NOSbF_6$, the oxidation peak at ca. 0.50 vs. (Fc/Fc^+)/V was observed to disappear which is consistent with the expectation that the complete oxidation of PN involves a one-electron transfer. The newly observed peaks seen after the addition of $NOSbF_6$, at ca. -0.40 to -0.60 and -0.70 to -1.00 vs. (Fc/Fc^+)/V, are likely to be attributable to a combination of the chemically oxidized product and excess $NOSbF_6$ that is present in the test solution as increasing concentrations of the chemical oxidant was introduced, along with other presently unknown species that are possibly generated via reactions with excess $NOSbF_6$ [3, 4]. This was further supported by the CV scans that were collected without the presence of any PN (Figure 5.7 dotted lines).

After verifying the feasibility of using $NOSbF_6$, a preparative scale oxidation of PN was carried out by reacting one molar equivalence of $NOSbF_6$ to a solution of PN dissolved in CH_3CN. Attempts to isolate the final oxidized product via flash column chromatography were unsuccessful because the end-product appeared to decompose on the column (forming multiple products which were very difficult to isolate). The instability of the oxidized product was further demonstrated by the multiple unsuccessful efforts to crystallize the compound from the reaction solution despite the use of a bulky, non-nucleophilic anion $[B(C_6F_5)_4]^-$ which has previously been reported to be useful in stabilizing several cationic compounds [5, 6]. Nevertheless, since $NOSbF_6$ is NMR silent, ^1H and ^{13}C NMR analysis (Figure A5.6-A5.7 in the Appendix section) could be conducted on the crude reaction mixture. The NMR spectra appeared to be clean (i.e. free of secondary decomposition products), thus signifying a relatively high yield reaction. Additionally, both the ^1H and ^{13}C NMR spectra of the chemically oxidized product were highly reminiscent of PN; both exhibiting the same number of resonances, albeit with slightly more downfield chemical shifts suggesting an increased positive charge. The close similarity of the NMR spectra of the starting material and product implies only a minor change in the structure, with the product remaining in a diamagnetic state despite the transfer of only one electron. The NMR and IR results also did not indicate the presence of any newly formed carbonyl functional groups, thus minimizing the probability of PA or PL being formed in the present study as compared to previous reports [7-9]. Furthermore, the mixture obtained directly after the chemical oxidation of PN using $NOSbF_6$ was also analyzed by mass spectrometry. A comparison of the mass spectra between the chemically oxidized product and the starting material indicate the presence of an additional low intensity peak at m/z = 574.52 (approximately 5% of the size of the base peak) and it is surmised that this peak can arise due to the formation of a positively charged dimeric product with SbF_6^- as the counter anion ($[2M + SbF_6]^+$, where M is the molecular weight of the monomer, PN). Furthermore, the base peak

observed at m/z = 170.05 in the mass spectrum of the product is reasoned to be due to the fragmentation of the unstable dimeric product into two equal monomers of PN during the analysis.

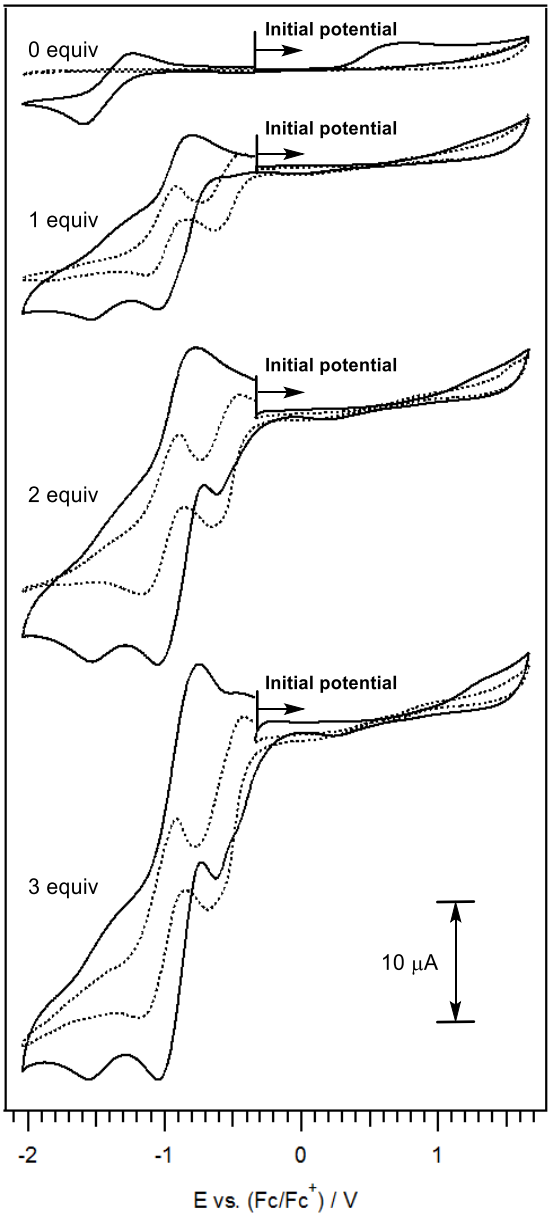

Figure 5.7. Cyclic voltammograms of CH_3CN with 0.2 M Bu_4NPF_6, recorded using a 1 mm diameter planar Pt electrode and at a scan rate of 0.1 V s^{-1} and 22 (±2) °C, with varying amounts of $NOSbF_6$. (—) In the presence of 2 mM PN. (·····) In the absence of PN.

In view of the results gathered, PN is tentatively postulated to undergo a one electron oxidation, delivering a symmetrical dimeric dication product that can be connected either through the aromatic carbon atom (Eq. (ii)) or the nitrogen atom on PN (Eq. (iii)) as shown in Scheme 5.2. The possibility of a C-N coupled dimeric product can be discounted on the basis of the number of resonances observed in the ^{1}H and ^{13}C NMR spectra which suggest that the product must be symmetrical about the coupling bond. Also, the oxidized product would be anticipated to be relatively reactive towards nucleophiles, and therefore poses challenges during the isolation process due to the product's weak connecting bond and high susceptibility to other follow-up reactions such as hydrolysis. As observed earlier during the CPE experiment using a higher concentration (6 mM, Figure 5.5), the adsorption phenomena of PN on the Pt electrode surface appeared to be more significant when larger quantities of the starting material are used, thus hindering the ability to accurately carry out varying concentration dependent voltammetric analyses. The new reduction process that was detected after the bulk oxidation at ca. -0.90 vs. $(Fc/Fc^{+})/V$ as displayed in Figure 5.7 is likely associable with the reduction of the dimeric dication.

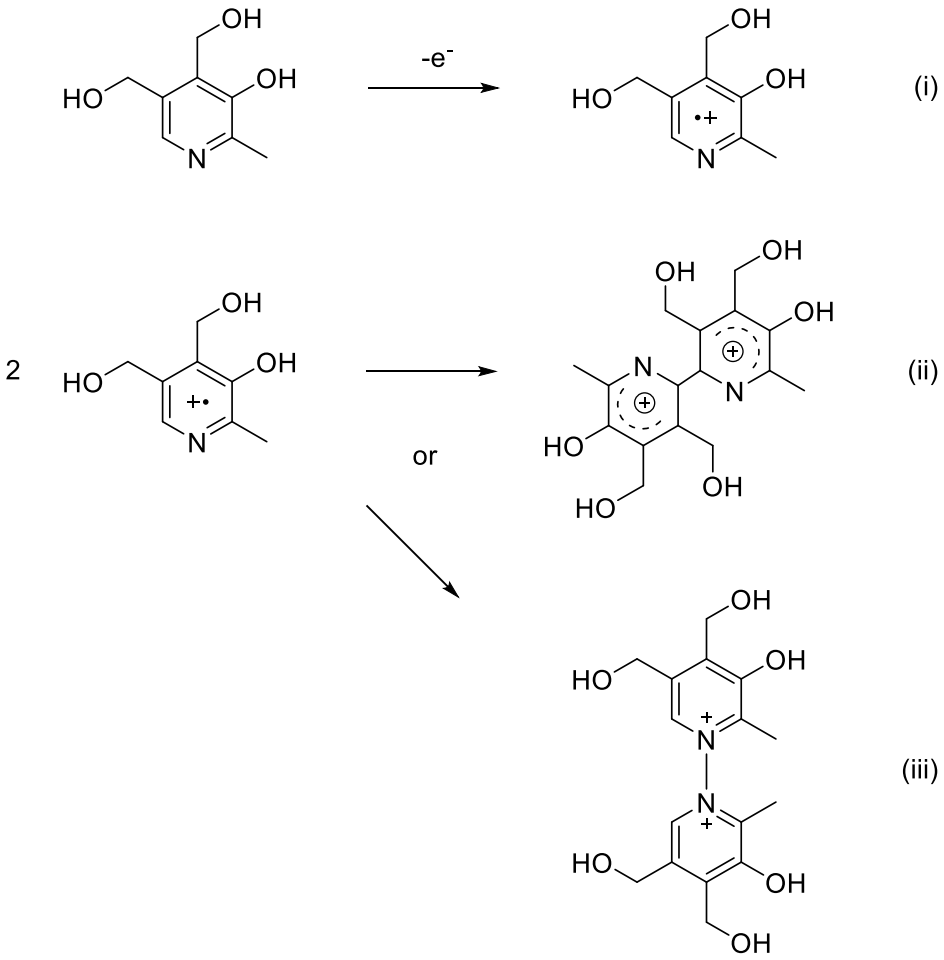

Scheme 5.2. Proposed mechanism for the electrochemical oxidation of PN.

5.2.4. Electrochemical reduction of PN in CH_3CN

In contrast to its electrochemical oxidation which was described in the preceding section, the reduction of PN in CH_3CN (E_p^{red} occurs at ca. -1.60 vs. (Fc/Fc^+)/V) was found to be chemically reversible and possessed I_p^{red}/I_p^{ox} ratios of ca. 1. Additionally, the voltammograms were able to overlap each other very well (i.e. had peak currents of very similar magnitudes), even after repeated cycling, therefore implying an adsorption-free process (Figure 5.8).

Varied scan rates CV experiments were likewise conducted and it was shown that as the scan rates were increased, substantially wider peak-to-peak separations were obtained which is

suggestive of the redox process is to be likely electrochemically quasi-reversible (Figure A5.1 in the Appendix section).

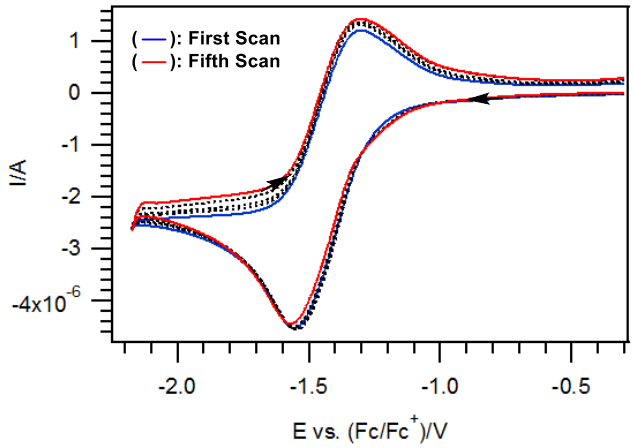

Figure 5.8. Cyclic voltammograms of 5 consecutive scans of 2 mM PN in CH_3CN with 0.2 M Bu_4NPF_6, recorded using a 1 mm diameter planar Pt electrode at a scan rate of 0.1 V s^{-1} and 22 (±2) °C. Start/end potentials: -0.30 vs. (Fc/Fc^+)/V. Switching potential: -2.17 vs. (Fc/Fc^+)/V.

CPE experiments were similarly performed to examine the lifetime of the reduced species as well as to determine the number of electrons transferred during the electrochemical reduction process. The voltammetry and coulometry results are illustrated in Figure 5.9, and it was established that ca. one electron per molecule (n = 1.17) was involved (Figure 5.9(b)). With the loss of the initial reduction peak at ca. -1.60 vs. (Fc/Fc^+)/V, a new oxidation peak was observed at ca. -0.05 vs. (Fc/Fc^+)/V (Figure 5.9(a), dotted line). Therefore, it can be inferred that the reduction of PN is only chemically reversible in the shorter time span of CV (≤ seconds) but not over a longer time domain (≥ minutes) such as in CPE. Notably, no adsorption phenomena and electrode fouling (as observed during the electrochemical oxidation of PN) were experienced.

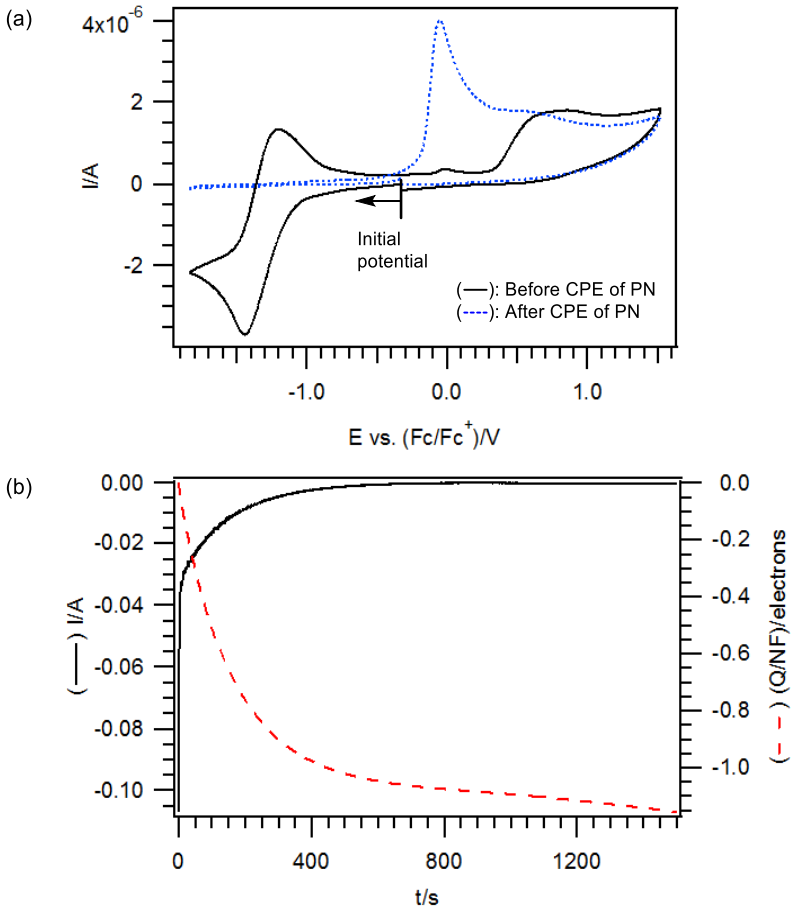

Figure 5.9. Voltammeric and coulometric data recorded during the reductive CPE of 2 mM PN in CH_3CN with 0.2 M Bu_4NPF_6. (a) Cyclic voltammograms obtained at a scan rate of 0.1 V s^{-1} using a 1 mm diameter planar Pt electrode. (b) Current vs. time data obtained during exhaustive reduction of PN at -1.63 vs. $(Fc/Fc^+)/V$.

On the basis of the gathered results, a mechanism is proposed for the electrochemical reduction of PN (Scheme 5.3). It was postulated that PN undergoes reduction via a direct discharge on the Pt electrode by the transfer of an electron which concomitantly resulted in an adsorbed hydrogen atom on the Pt surface (Eq. (iv)). Generation of hydrogen gas (H_2) subsequently occurs either via a discharge of another molecule of PN (Eq. (v)) or through a combination of the surface-adsorbed hydrogen atoms (Eq. (vi)) [10-13]. The formation (and subsequently loss) of the H_2 therefore is attributable for by the chemically irreversible behavior observed in the

CPE measurements. The reverse anodic peak corresponds to the oxidation of the surface-adsorbed hydrogen atoms (reverse of Eq. (iv)) [14]. Notably, a new anodic wave was also registered at ca. -0.05 vs. (Fc/Fc^+)/V after the CPE was completed (Figure 5.9(a)). As an oxide anion product is expected to be generated after the reductive electrolysis (Eq. (v)), it is therefore likely that the new anodic wave is assignable to the oxidation of the oxide anion. The requirement of a catalytic surface (e.g. Pt) for the observed reduction process to occur was highlighted by the absence of any cathodic peak when a glassy carbon electrode was employed (Figure 5.10).

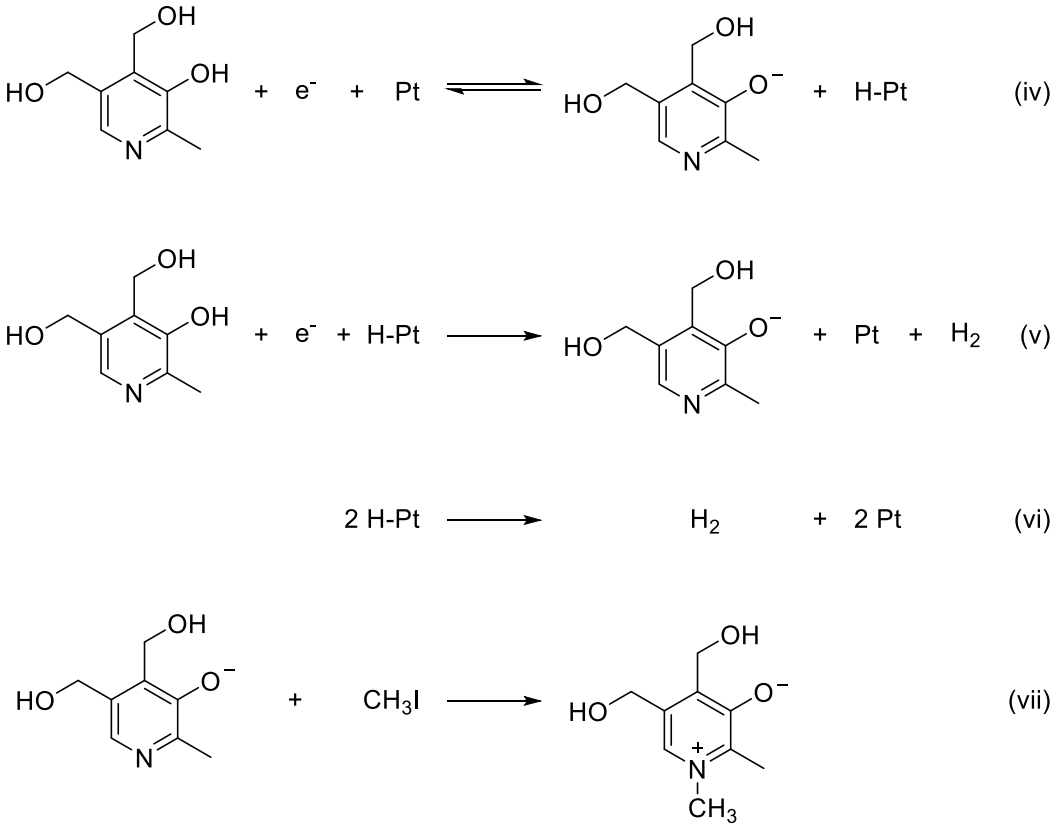

Scheme 5.3. Proposed mechanism for the electrochemical reduction of PN.

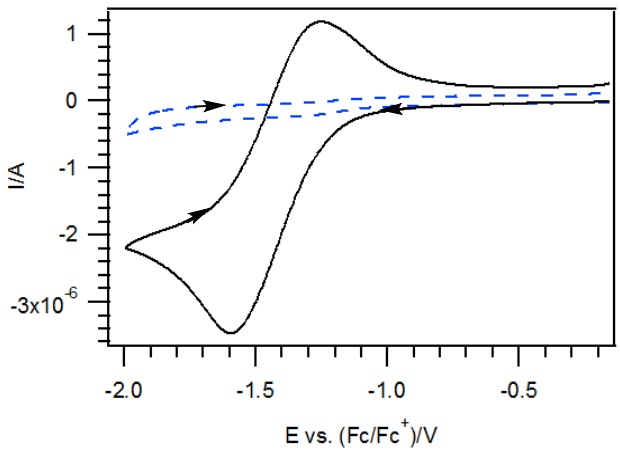

Figure 5.10. Cyclic voltammograms of 2 mM PN in CH_3CN with 0.2 M Bu_4NPF_6, recorded at a scan rate of 0.1 V s^{-1} using a 1 mm diameter planar (—) Pt electrode. (- - -) GC electrode. Start/end potentials: -0.16 vs. (Fc/Fc^+)/V. Switching potential: -2.00 vs. (Fc/Fc^+)/V.

Synthetic scale CPE experiments were conducted by electrolyzing PN in CH_3CN using a Pt mesh working electrode. As a oxide anion was the expected end-product following the reduction of PN, it was surmised that this molecule might be trapped by the addition of an electrophile such as iodomethane (CH_3I) to generate a methoxy functionality after the completion of the electrolysis. Although a diamagnetic methylated product was detected, a nitrogen-methylated PN was produced instead of the expected oxygen-methylated analogue in high yield (Eq. (vii)). This product was unequivocally characterized by high resolution mass spectroscopy (HRMS), NMR, and X-ray crystallography analysis (Figure 5.11 and supporting information provided in Figures A5.10-A5.13 in the Appendix section).

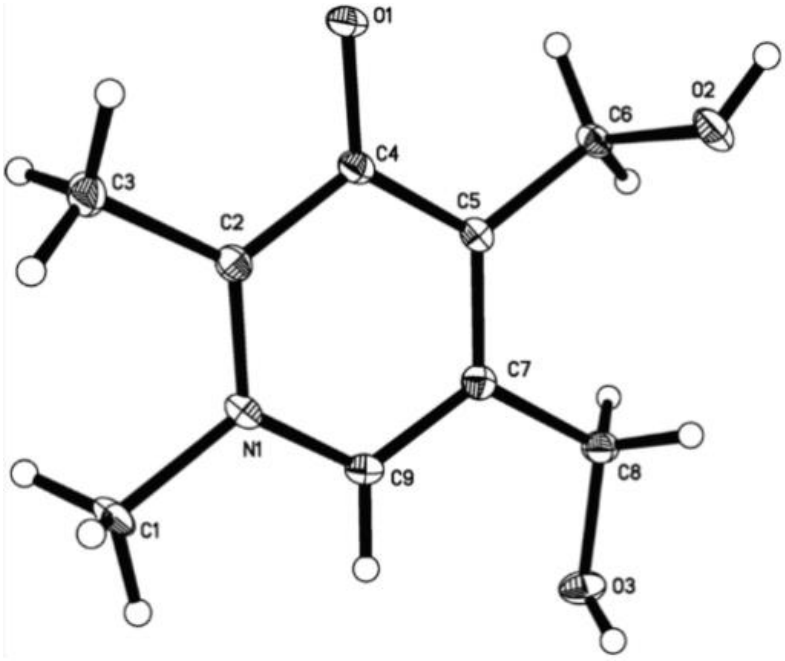

Figure 5.11. ORTEP drawing of nitrogen-methylated PN with thermal ellipsoids at 50% probability levels.

5.3. Conclusion

In CH_3CN solutions, PN was established to undergo a one-electron oxidation at ca. 0.50 vs. (Fc/Fc^+)/V, at unmodified Pt electrodes. CV and CPE experiments demonstrated that the electrochemical oxidation of PN is chemically irreversible, and that this process likely involves an adsorption step which leads to electrode fouling. The adsorption process subsequently prevented the CPE experiments from occurring exhaustively especially when high quantities of analyte were used, and also resulted in diminishing anodic peaks currents during CV experiments when continuous cycling were conducted. In order to overcome these adsorption effects, bulk chemical oxidation was performed using $NOSbF_6$. NMR and mass spectroscopic analysis of the reaction products negated the possibility of pyridoxic acid or pyridoxal as the oxidized product, as previously suggested from voltammetric works using aqueous systems. Instead, the chemically oxidized product was posited to be a dimer dication, linked through either a C-C or N-N coupled bond. Independent of the former oxidation reaction, a separate cathodic peak was also observed at ca. -1.60 vs. (Fc/Fc^+)/V, which was found to be chemically reversible on the shorter timeframe of CV but not over the longer timescales of CPE. This reduction phenomenon was previously not seen in reports performed using aqueous media [7-9, 15-30], as the relatively high potential cannot be achieved in aqueous systems and possibly due to the difference in electrode materials used. Separately, at the Pt electrode surface, PN can undergo an electrochemical reduction reaction via a direct discharge mechanism, forming an oxide anion and hydrogen gas which after treatment with iodomethane, was found to yield a nitrogen-methylated PN.

5.4. Experimental

5.4.1. General remarks

All chemicals were purchased from commercial sources and used as received unless otherwise stated. ^{1}H and ^{13}C NMR spectra were measured on Bruker AV 500 (500 MHz) NMR spectrometer, with tetramethylsilane (TMS, 0.00 ppm) as the internal reference standard and referenced to deuterated methanol (CD_3OD), the solvent used. CD_3OD was obtained from commercial source and used without further purification. Multiplicity is given as s (singlet) and the number of protons (*n*) for a given resonance is indicated by *n*H. Low resolution mass spectra were obtained on a ThermoFinnigan LCQ Fleet Mass Spectrometer equipped with Thermo Accela LC while the high resolution mass spectra (HRMS) were determined on a Waters Q-TOF Premier Mass Spectrometer equipped with Waters Acquity UPLC. Infrared (IR) spectral analysis were performed using a Shimadzu IR Prestige-21 FT-IR spectrometer with solid samples in nujol oil examined as a thin film between NaCl salt plates.

5.4.2. Chemicals and reagents

Pyridoxine (≥ 98%), nitrosonium hexafluoroantimonate ($NOSbF_6$, 99%) and iodomethane (99%) were obtained from Sigma-Aldrich. Solvents used were all ACS grade. 1/16" rods molecular sieves with pore size 3 Å (CAS: 308080-99-1) were acquired from Fluka. Acetonitrile (CH_3CN) with lower water content was dried over 3 Å molecular sieves whereas CH_3CN with higher water content was used directly from the bottle obtained from Tedia. Dichloromethane (DCM) was obtained from Merck and methanol (CH_3OH) from Anaqua Chemicals Supply. The supporting electrolyte, tetrabutylammonium hexafluorophosphate (Bu_4NPF_6), was prepared following standard procedures by reacting equal molar amounts of an aqueous solution of Bu_4OH (40%) with an aqueous solution of HPF_6 (65%), washing the

precipitate with hot water, recrystallizing three times using hot ethanol, subsequently drying under vacuum at 140 °C for 6 h and was stored under vacuum.

5.4.3. Measurements of water content

Karl Fischer (KF) titrations were conducted using a Mettler Toledo DL32 coulometer with (Riedel-deHaën) HYDRANAL-coulomat AG for the anode compartment and the HYDRANAL-coulomat CG for the cathode compartment. Constant humidity (30%) measurements were performed in a (122 cm x 61 cm x 61 cm) humility control box using a dry nitrogen purge gas system from Coy Laboratory Products Inc. Samples in plastic disposable syringes were injected through a silicon/Teflon septum.

5.4.4. Voltammetry

Cyclic voltammetry (CV) experiments were conducted with a computer-controlled Metrohm Autolab PGSTAT302N potentiostat using a three electrode system. Working electrodes used were 1 mm diameter planar platinum (Pt) or glassy carbon (GC) disks (eDAQ Pty Ltd) together with a Pt auxiliary electrode (Metrohm). A silver (Ag) wire miniature reference electrode (eDAQ Pty Ltd) was connected to the test solution via a salt bridge containing a CH_3CN solution of 0.5 M Bu_4NPF_6 and accurate potentials were obtained using ferrocene (Fc) as an internal standard. Solutions of pyridoxine used for voltammetry experiments were deoxygenated by purging the solutions with high purity argon gas and all voltammetric measurements were performed at 22 (±2) °C in a Faraday cage. Ohmic drop was not compensated for all cyclic voltammograms.

5.4.5. Controlled potential electroylsis

Controlled potential electrolysis (CPE) was conducted in a two-compartment electrolysis cell separated by a sintered glass frit of porosity no. 5 (1.0 – 1.7μm). The volumes of solution used

in both the auxiliary and working electrode compartments were ca. 25 ml. Two identical sized Pt mesh plates were used as working and auxiliary electrodes and were arranged symmetrically, with an Ag wire reference electrode (separated from the sample solution by a glass membrane containing 0.5 M Bu_4NPF_6 in CH_3CN) placed within 2 mm of the surface of the working electrode. Solutions in both compartment of the cell were simultaneously stirred and deoxygenated using bubbles of argon gas. All CPE experiments were performed at 22 (±2) °C. The number of electrons transferred during the bulk electrolysis process was calculated using the following equation.

$$N = Q/nF \tag{5.1}$$

where, N = number of moles of starting material used, Q = charge (in coulombs), n = number of moles of electrons, and F is the Faraday constant (96 485 C/mol).

5.4.6. Formation of chemically oxidized pyridoxine

PN (50 mg) was dissolved in 50 mL of CH_3CN and then sonicated at ca. 35 °C for 30 mins. $NOSbF_6$ (1 equiv) was subsequently added and the mixture was left to stir for 1 h under a nitrogen atmosphere. Upon completion, the solvent was removed from the resulting mixture under vacuum. The product was later left to dry under vacuum. ^{1}H NMR (CD_3OD, 500 MHz) δ 2.59 (s, 3H), 4.70 (s, 2H), 5.07 (s, 2H), 8.05 (s, 1H); ^{13}C NMR (CD_3OD, 125 MHz) δ 14.52, 59.26, 60.02, 129.84, 138.57, 141.05, 143.00, 154.90.

5.4.7. Formation of nitrogen-methylated pyridoxine

In the preparative scale experiments, 50 mL of CH_3CN was added to PN (50 mg) and Bu_4NPF_6 (0.1 M) and subsequently sonicated at ca. 35 °C for 30 mins. The solution was then subjected to bulk electrochemical reduction by controlled potential electrolysis, before iodomethane (1.5 equiv) was added and stirred for 1 h under a nitrogen atmosphere. The resultant reaction mixture

was concentrated under reduced pressure and purified by flash column chromatography over silica gel, using an eluent made up of DCM and CH_3OH in the ratio 1:1. Thin-layer chromatography (TLC) analysis was conducted using pre-coated silica gel plates and visualization was achieved using UV light (254 nm). The purified product was then dried under vacuum, affording the titled compound as a white solid in 45% yield. m.p. = 186- 189 ^oC; ^1H NMR (CD_3OD, 500 MHz) δ 2.55 (s, 3H), 4.08 (s, 3H), 4.67 (s, 2H), 4.80 (s, 2H), 7.62 (s, 1H); ^{13}C NMR (CD_3OD, 125 MHz) δ 13.05, 58.38, 60.08, 126.75, 137.78, 140.45, 145.91, 165.80; HRMS (ESI) calculated for $C_9H_{13}NO_3$ $[M + H]^+$ 184.0974, found 184.0977.

5.5. References

[1] N.G. Connelly, W.E. Geiger, Chemical Redox Agents for Organometallic Chemistry, Chem. Rev., 96 (1996) 877–910.

[2] S.B. Lee, C.Y. Lin, P.M.W. Gill, R.D. Webster, Transformation of α-Tocopherol (Vitamin E) and Related Chromanol Model Compounds into Their Phenoxonium Ions by Chemical Oxidation with the Nitrosonium Cation, J. Org. Chem., 70 (2005) 10466 –10473.

[3] Y.Y. Chan, Y. Yue, Y. Li, R.D. Webster, Electrochemical/Chemical Oxidation of Bisphenol A in a Four-electron/Two-proton Process in Aprotic Organic Solvents, Electrochim. Acta, 112 (2013) 287–294.

[4] Y.Y. Chan, Y. Yue, R.D. Webster, Voltammetric Studies on Vitamins D_2 and D_3 in Organic Solvents, Electrochim. Acta, 138 (2014) 400–409.

[5] I. Krossing, I. Raabe, Noncoordination Anions - Fact or Fiction? A Survey of Likely Candidates, Angew. Chem. Int. Ed., 43 (2004) 2066–2090.

[6] S.B. Lee, A.C. Willis, R.D. Webster, Synthesis of the Phenoxonium Cation of an α-Tocopherol Model Compound Crystallized with Non-Nucleophilic $[B(C_6F_5)_4]^-$ and $(CB_{11}H_6Br_6)^-$ Anions, J. Am. Chem. Soc., 128 (2006) 9332–9333.

[7] Z. Cao, Q. Xie, M. Li, S. Yao, Simultaneous EQCM and Fluorescence Detection of Adsorption/Desorption and Oxidation for Pyridoxol in Aqueous KOH on a Gold Electrode, J. Electroanal. Chem., 568 (2004) 343–351.

[8] M.L. Wang, Y.Y. Zhang, Q.J. Xie, S.Z. Yao, In Situ FT-IR Spectroelectrochemical Study of Electrooxidation of Pyridoxol on a Gold Electrode, Electrochim. Acta, 51 (2005) 1059–1068.

[9] M.H. Pournaghi-Azar, H. Dastangoo, M. Ziaei, Electrocatalytic Oxidation of Pyridoxine (Vitamin B_6) on Aluminum Electrode Modified by Metallic Palladium Particles/Iron (III) Hexacyanoferrate (II) Film, J. Solid State Electrochem., 11 (2007) 1221–1227.

[10] S.E. Treimer, D.H. Evans, Electrochemical Reduction of Acids in Dimethyl Sulfoxide. Comparison of Weak C-H, N-H and O-H acids, J. Electroanal. Chem., 455 (1998) 19–28.

[11] S.E. Treimer, D.H. Evans, Electrochemical Reduction of Acids in Dimethyl Sulfoxide. CE mechanisms and Beyond., J. Electroanal. Chem., 449 (1998) 39–48.

[12] S.J.L. Lauw, R. Ganguly, R.D. Webster, The Electrochemical Reduction of Biotin (Vitamin B7) and Conversion into Its Ester, Electrochim. Acta, 114 (2013) 514–520.

[13] Y.S. Tan, D. Urbančok, R.D. Webster, Contrasting Voltammetric Behavior of Different Forms of Vitamin A in Aprotic Organic Solvents, J. Phys. Chem. B, 118 (2014) 8591–8600.

[14] Y. Meng, S. Norman, C. Hardacre, R.G. Compton, The Electroreduction of Benzoic Acid: Voltammetric Observation of Adsorbed Hydrogen at a Platinum Microelectrode in Room Temperature Ionic Liquids, Phys. Chem. Chem. Phys., 15 (2013) 2031–2036.

[15] P. Söderhjelm, J. Lindquist, Voltammetric Determination of Pyridoxine by Use of a Carbon Paste Electrode, Analyst (Cambridge UK), 100 (1975) 349–354.

[16] M.F.S. Teixeira, A. Segnini, F.C. Moraes, L.H. Marcolino-Júnior, O. Fatibello-Filho, É.T.G. Cavalheiro, Determination of Vitamin B_6 (Pyridoxine) in Pharmaceutical Preparations by Cyclic Voltammetry at a Copper(II) Hexacyanoferrate(III) Modified Carbon Paste Electrode, J. Braz. Chem. Soc., 14 (2003) 316–321.

[17] W. Qu, K. Wu, S. Hu, Voltammetric Determination of Pyridoxine (Vitamin B_6) by use of a Chemically-Modified Glassy Carbon Electrode, J. Pharm. Biomed. Anal., 36 (2004) 631–635.

[18] M.F.S. Teixeira, G. Marino, E.R. Dockal, É.T.G. Cavalheiro, Voltammetric Determination of Pyridoxine (Vitamin B_6) at a Carbon Paste Electrode Modified with Vanadyl(IV)–Salen Complex, Anal. Chim. Acta, 508 (2004) 79–85.

[19] R.C. Barthus, L.H. Mazo, R.J. Poppi, Simultaneous Determination of Vitamins C, B6 and PP in Pharmaceutics using Differential Pulse Voltammetry with a Glassy Carbon Electrode and Multivariate Calibration Tools, J. Pharm. Biomed. Anal., 38 (2005) 94–99.

[20] P.B. Desai, R.M. Kotkar, A.K. Srivastava, Electrochemical Behaviour of Pyridoxine Hydrochloride (Vitamin B_6) at Carbon Paste electrode Modified with Crown Ethers, J. Solid State Electrochem., 12 (2008) 1067–1075.

[21] Y. Wu, F. Song, Voltammetric Investigation of Vitamin B_6 at a Glassy Carbon Electrode and Its Application in Determination, Bull. Korean Chem. Soc., 29 (2008) 38–42.

[22] S.M. Cottica, J. Nozaki, H.S. Nakatani, C.C. Oliveira, N.E. de Souza, J.V. Visentainer, Voltammetric Determination of Pyridoxine (Vitamin B_6) in Drugs using a Glassy Carbon Electrode Modified with Chromium(III) Hexacyanoferrate(II), J. Braz. Chem. Soc., 20 (2009) 496–501.

[23] B. Habibi, H. Phezhhan, M.H. Pournaghi-Azar, Voltammetric Determination of Vitamin B_6 (Pyridoxine) using Multi Wall Carbon Nanotube Modified Carbon-Ceramic Electrode, J. Iran. Chem. Soc., 7 (2010) S103–S112.

[24] C.A. Fonseca, G.C.S. Vaz, J.P.A. Azevedo, F.S. Semaan, Exploiting Ion-Pair Formation for the Enhancement of Electroanalytical Determination of Pyridoxine (B_6) onto Polyurethane-Graphite Electrodes, Microchem. J., 99 (2011) 186–192.

[25] J. Gonzalez-Rodriguez, J.M. Sevilla, T. Pineda, M. Blazquez, Electrochemical Analysis on Compounds of the Vitamin B_6 Family using Glassy Carbon Electrodes, Int. J. Electrochem. Sci., 7 (2012) 2221–2229.

[26] T. Nie, J.-K. Xu, L.-M. Lu, K.-X. Zhang, L. Bai, Y.-P. Wen, Electroactive Species-Doped Poly(3,4-ethylenedioxythiophene) Films: Enhanced Sensitivity for Electrochemical Simultaneous Determination of Vitamins B_2, B_6 and C, Biosensors Bioelectron., 50 (2013) 244–250.

[27] B. Brunetti, E. Desimoni, Voltammetric Determination of Vitamin B_6 in Food Samples and Dietary Supplements, J. Food Compos. Anal., 33 (2014) 155–160.

[28] A. Mekonnen, R.C. Saini, A. Tadese, R. Pal, Square Wave Voltammetric Determination of Pyridoxine in Pharmaceutical Preparations using Cobalthexacyanoferrate Modified Carbon Paste Electrode, J. Chem. Pharm. Res., 6 (2014) 544–551.

[29] H. Razmi, M. Jabbari, R. Mohammad-Rezaei, Electrochemically Reduced Graphene Oxide Modified Carbon Ceramic Electrode for the Determination of Pyridoxine, Anal. Chem. Lett., 4 (2014) 73–85.

[30] A. Baghizadeh, H. Karimi-Maleh, Z. Khoshnama, A. Hassankhani, M. Abbasghorbani, A Voltammetric Sensor for Simultaneous Determination of Vitamin C and Vitamin B_6 in Food Samples Using ZrO_2 Nanoparticle/Ionic Liquids Carbon Paste Electrode, Food Anal. Methods, 8 (2015) 549–557.

Chapter 6

The Electrochemical Reduction of Carbon Dioxide (CO_2) to Methanol in the Presence of Pyridoxine (PN)

This page has been intentionally left blank

6.1. Chapter Overview

After having examined the in depth electrochemical behavior of pyridoxine (PN, Scheme 6.1) as detailed in the previous chapter (Chapter 5), in the current section of the thesis, the application of this vitamin compound was explored in the area of converting carbon dioxide (CO_2) into methanol, whereby PN was exploited as a co-reagent to enhance the reduction process.

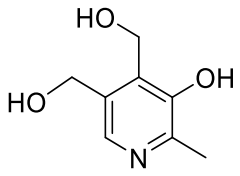

Scheme 6.1. Chemical structure of pyridoxine (PN).

Behaving in a similar manner as previous reports on pyridinium-catalyzed electrochemical reduction of CO_2, at a platinum electrode, an aqueous solution (pH ≈ 5) of PN showed a quasi-reversible redox couple with the cathodic peak detected at ca. -0.55 V vs. Ag/AgCl (3 M KCl) in the presence of CO_2. Furthermore, the significance of the presence of PN was highlighted by the observation of only a very small reduction current in a CO_2-purged solution not containing any PN.

Verification of methanol formation during the pyridoxine-assisted CO_2 reduction was conducted by using gas chromatography analysis of the electrolyzed solutions, using both constant current chronopotentiometry and controlled potential electrolysis techniques. Overall, the encouraging results indicate a potential utility of PN as an alternative reagent to the more toxic pyridine during the electrochemical reduction of CO_2.

6.2. Introduction

Carbon dioxide (CO_2), a well-known ubiquitous greenhouse gas, has garnered increasing concern due to the global warming problems caused by its excessive emission from anthropogenic sources [1-3]. As such, several mitigation approaches such as the capture and storage of CO_2 (CCS) [4-7] or the conversion of CO_2 into value-added products have been widely examined. In particular, growing attention has been focused on the latter method which can be achieved by various ways ranging from chemical transformation [8-10] to photocatalytic [11-14] and electrocatalytic reduction [15-18].

Although the use of electrochemistry as a means of reducing the global atmospheric levels of CO_2 arguably remains an idealistic endeavor [19], with most of the systems studied to date stymied by a combination of high overpotential, low faradic efficiency, and poor product selectivity [20-24], efforts aimed at the electrochemical reduction of CO_2 may be useful in producing a variety of highly valuable reduced carbon-based products such as carbon monoxide, formic acid, formaldehyde, methane and methanol (CH_3OH) [16, 23, 25, 26].

Bearing only a single carbon atom, CH_3OH has been demonstrated to be a useful feedstock for the production of commodity chemicals such as acetic acid, formaldehyde, and dimethyl ether (DME), which can subsequently be used in the manufacture of numerous products like polymers, pharmaceuticals materials and paints [27-30]. In addition, due to its high octane rating and excellent combustion ability, CH_3OH is also used in internal combustion engines and in direct CH_3OH fuel cells (DMFC) [30-32]. Therefore, as a result of the diverse utility of CH_3OH, an approximately 65 million tons of CH_3OH is produced annually [29]. Moreover, the attractiveness of CH_3OH has also given rise to the concept of "Methanol Economy", with many aspects relating to CH_3OH such as state of the art methods used in producing, and utilizing it

as well as the storage and transportation of energy in the form of CH_3OH being disclosed in many accounts [27-30, 33, 34].

For the abovementioned reasons, a myriad of research work has been directed to the electrochemical reduction of CO_2 for the generation of CH_3OH. Notably, however, there exists only few examples of efficient conversion achieved for the CH_3OH formation [35-37]. Among them, the recent use of pyridinium (protonated pyridine) as an electrocatalyst for the electrochemical reduction of CO_2 has emerged as an efficient method for the conversion process due to its low overpotential required and moderate to excellent faradic yields obtained [38-40]. These seminal works were disclosed by Bocarsly and coworkers whose initial study employed hydrogenated palladium electrodes [38], thereafter extending to the utilization of illuminated p-Gap semi-conductors [39], and more recently, onto platinum (Pt) electrodes [40]. Further exploration of this field has also led to the examination of various metallic (iron pyrite [41], copper indium sulfide [42, 43], iridium (Ir) [44], and gold [45]) and non-metallic (glassy carbon [46, 47]) electrode materials as well as alternative nitrogen-containing aromatic molecules (imidazole [41], pyridazine [48], mercaptopteridine [47]). Hence, the search for alternative materials, in terms of both the electrode and reagents used, remains highly pertinent.

In addition, a deeper understanding of the mechanism involved in the pyridinium electro-catalyzed reaction has also been actively pursued [49-54]. For instance, at a Pt electrode, Bocarsly and coworkers previously suggested that the conversion of CO_2 was initiated by the one electron reduction of the pyridinium ion into a pyridinyl radical, which subsequently reacted with CO_2, yielding a carbamate radical intermediate [40, 55]. This mechanistic posit, however did not agree with several theoretical calculation and modelling works [49, 51, 56-58]. In light of the discrepancies, and based on further investigation works, Bocarsly and coworkers followed up with more recent reports [52, 54, 59] of the revised mechanism where the reduction of the pyridinium ions was proposed to first occur via the generation of a platinum bound

hydride intermediate that can facilitate the electrochemical reduction of CO_2 via a proton-coupled hydride transfer pathway, which was found to be consistent with a previously reported analysis [51]. Although the formation of the surface bound hydride intermediate was agreeable with an account described by Costentin et al. [50], the idea of generating CO_2-reduced products using pyridinium was at the same time confuted by the detection of neither formate nor CH_3OH in the latter work, and it was proposed that the pyridinium ions undergo dissociation to generate hydrated protons which were subsequently reduced to only generate hydrogen gas (the sole product detected). Therefore, the role of the pyridinium in the reduction of CO_2 remains uncertain and knowledge on the associated mechanistic pathways are highly sought after as it can allow more efficient CO_2 conversion strategies to be developed.

Inspired by the biological importance of pyridoxine (PN, a member of the vitamin B_6 family), a detailed examination on the electrochemistry of PN in acetonitrile was delineated in the previous chapter [60]. In addition, as part of continuous efforts to examine the electrochemical reactions and applications of this vitamin, it is envisaged that PN, a pyridine-based molecule, can be exploited as a co-reagent for the application of CO_2 reduction into CH_3OH at a Pt electrode.

6.3. Results and Discussion

6.3.1. Cyclic voltammetry of CO_2 reduction in the presence of PN

Previous studies using pyridinium as the electrocatalyst for the electrochemical reduction of CO_2, were conducted in aqueous solutions of pH 5.2-5.4 [38, 40, 44, 48], corresponding to the pKa of pyridine (5.2) [61]. Under these conditions, pyridinium exists in a higher concentration than the free proton, and thus enables the former to function as both the proton source as well as its suggested role of stabilizing the intermediate via hydrogen bonding interactions [51]. It

has also been disclosed that larger currents are obtained in a CO_2-saturated solutions as compared to Ar-purged solutions, and that the current enhancement was observed to decrease with increasing scan rates owing to the relatively slow heterogeneous electron transfer rates [44].

In view of the precedent, preliminary cyclic voltammetry experiments were performed at varied scan rates, and at ca. pH 5, which matches the first pKa value of PN [62] in aqueous solutions. As illustrated in Figures 6.1(a)-(c), a quasi-reversible process with a reduction (half-wave) potential at ca. -0.55 V vs. Ag/AgCl (3 M KCl) was detected in the presence of PN solutions (saturated with CO_2 (solid line) and Ar (dashed line)), whereas only a relatively small cathodic current was observed in the absence of PN (dotted line). Hence, this underlines the importance of PN in order for the reduction process to occur. In addition, akin to the results observed using pyridinium [44], a current increment was registered (as compared to the solution with Ar) in the CO_2-saturated solution with PN; particularly at very low scan rates. Though speculative, the observation of the similar phenomena between the voltammetric responses obtained using protonated PN and pyridinium possibly implies that a similar reduction mechanism is involved in both systems.

During the electrocatalytic study of pyridinium, the presence of a catalytic surface (e.g. Pt) was also emphasized [40, 44]. For instance, Lebégue et al. [44] observed an irreversible reduction peak at ca. -1.50 V vs. Ag/AgCl at a glassy carbon (GC) electrode, a significantly more negative potential than that recorded on a Pt surface (ca. -0.60 V vs. Ag/AgCl). As hydrogen is documented to bind more weakly on a GC electrode than on Pt, the contrasting electrochemical responses obtained was reasoned to be due to the differing reduction pathways occurring on both electrode materials which was accounted for by their different affinities for hydrogen [29]. Notably, for studies utilizing Pt electrode that has been documented thus far (including this present study) [40, 44], the importance of a catalytic surface that has a strong affinity for

hydrogen is highlighted, which therefore implies the significance of a surface/solute interaction. Likewise, in the current study, no distinctive faradic processes were detected in the present potential range when a GC electrode was used for all the scan rates examined (Figure 6.2).

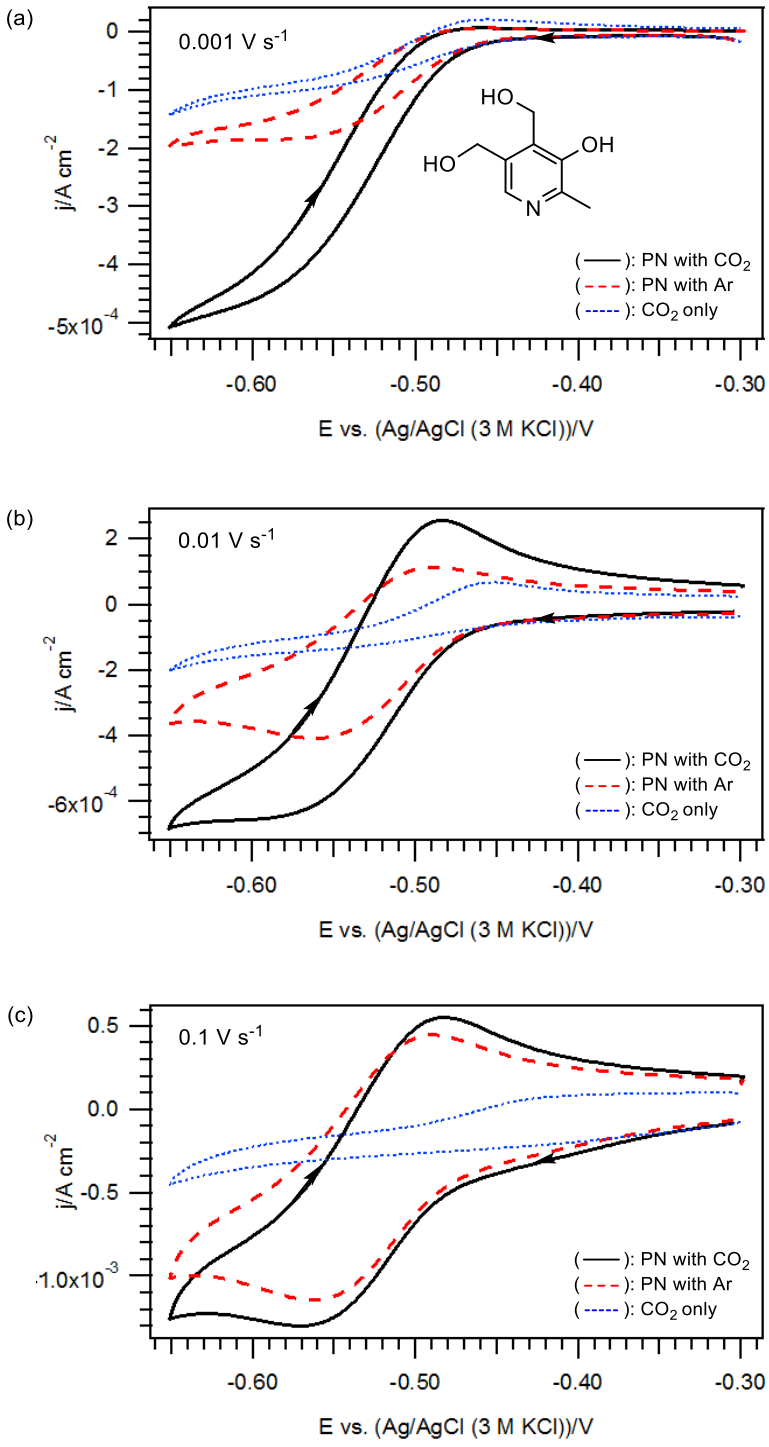

Figure 6.1. Variable scan rates cyclic voltammograms of 10 mM PN with 0.5 M KCl, recorded using a 1 mm diameter planar Pt electrode at pH 5.03. (—) Presence of PN and CO_2. (- - -) Presence of PN and Ar. (·····) Absence of PN, CO_2 only.

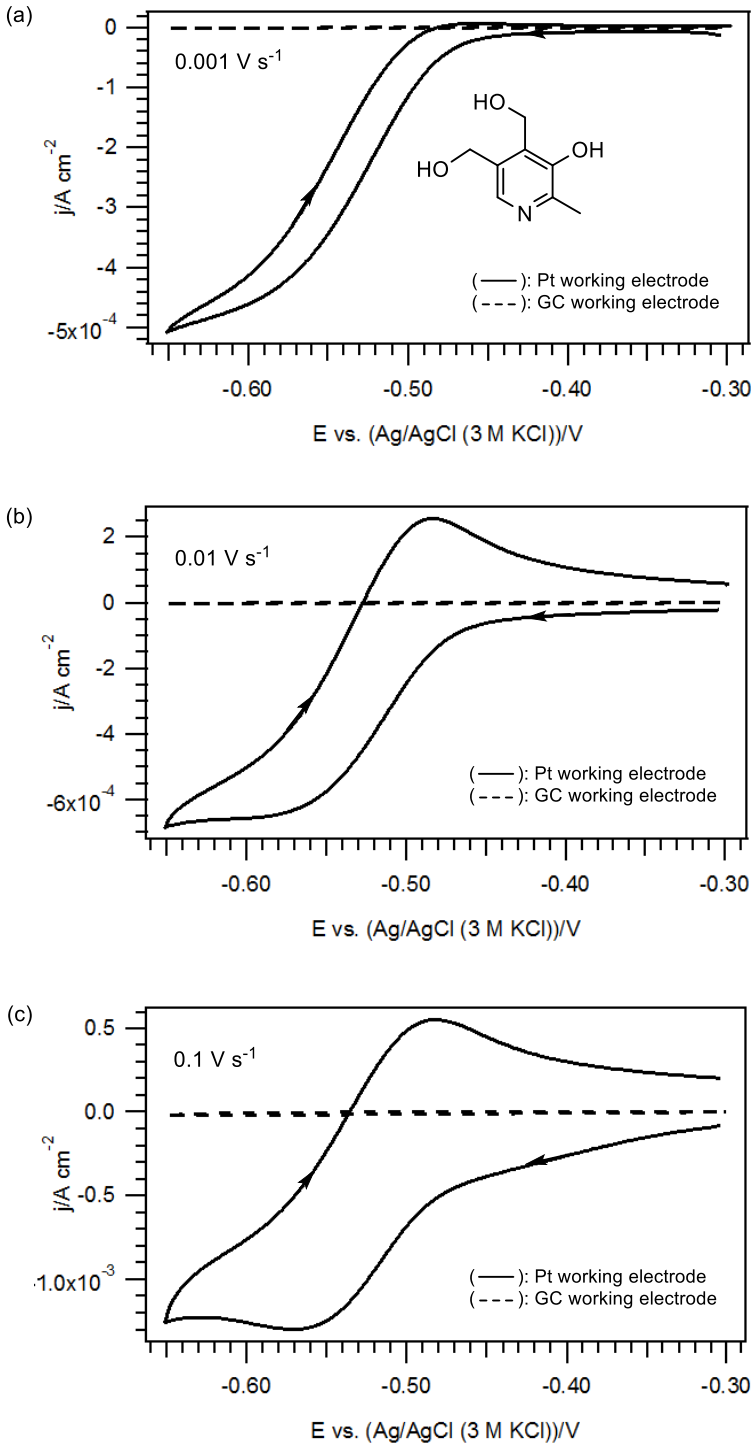

Figure 6.2. Variable scan rates cyclic voltammograms of 10 mM PN with 0.5 M KCl, recorded at pH 5.03 using a 1 mm diameter planar (—) Pt working electrode. (- - -) GC working electrode.

6.3.2. Electrolysis and proposed mechanism of CO_2 reduction in the presence of PN

After voltammetrically assessing the feasibility of using PN, preparative scale electrolysis experiments for the reduction of CO_2 (in the presence of PN) were next performed to corroborate the generation of CH_3OH. In order to ascertain whether there was a significant difference in the type of conversion methods, both the constant current and controlled potential electrolysis methods were attempted over a period of 2 h. Product analysis using gas chromatography revealed faradic yields of CH_3OH of ca. 5% for solutions obtained using both techniques. The collected chromatograms are displayed in Figure A6.1-A6.2 in the Appendix Section. In spite of the relatively low yields obtained, these results are comparable to the faradic efficiencies (4-25%) that have been reported in other works using pyridinium and related aromatic nitrogen-heterocycles as electrocatalysts [48, 54]. As little efforts have been directed to system optimization in the current study, substantially higher yield may be possible.

Taking into account the structural similarities between PN and pyridine, it is likely therefore, that the mechanism involved in the present study is similar to the pathways proposed previously [50, 51, 54] (Scheme 6.2). More specifically, based on a combination of experimental and computational results [51, 52, 54, 59], it was posited that the generation of CH_3OH initially involves a one-electron reduction of pyridinium to form a Pt-bound adsorbed hydrogen intermediate (Eq. (i)). Consequently, the requirement of a catalytic Pt surface is highlighted by this mechanistic posit, and is consistent with the observations shown in Figure 6.2. Thereafter, this intermediate can facilitate the first step of the CH_3OH formation via a proton-coupled hydride transfer pathway with the CO_2-pyridinium adduct (Eq. (ii)). The formic acid produced then undergoes further reductions with pyrdinium (Eqs. (iii)-(v)) to generate CH_3OH as an overall six-electron reduced product. Notwithstanding, because of the relatively low faradic yield obtained for CH_3OH formation, it is probable that a major competing reaction is hydrogen gas (H_2) evolution (a well-documented reaction in aqueous acidic solutions) which involves the

hydrogen adsorbate reacting with a free proton that is dissociated by either pyridinium or carbonic acid (formed by hydrated CO_2) [50] (Eq. (vi)).

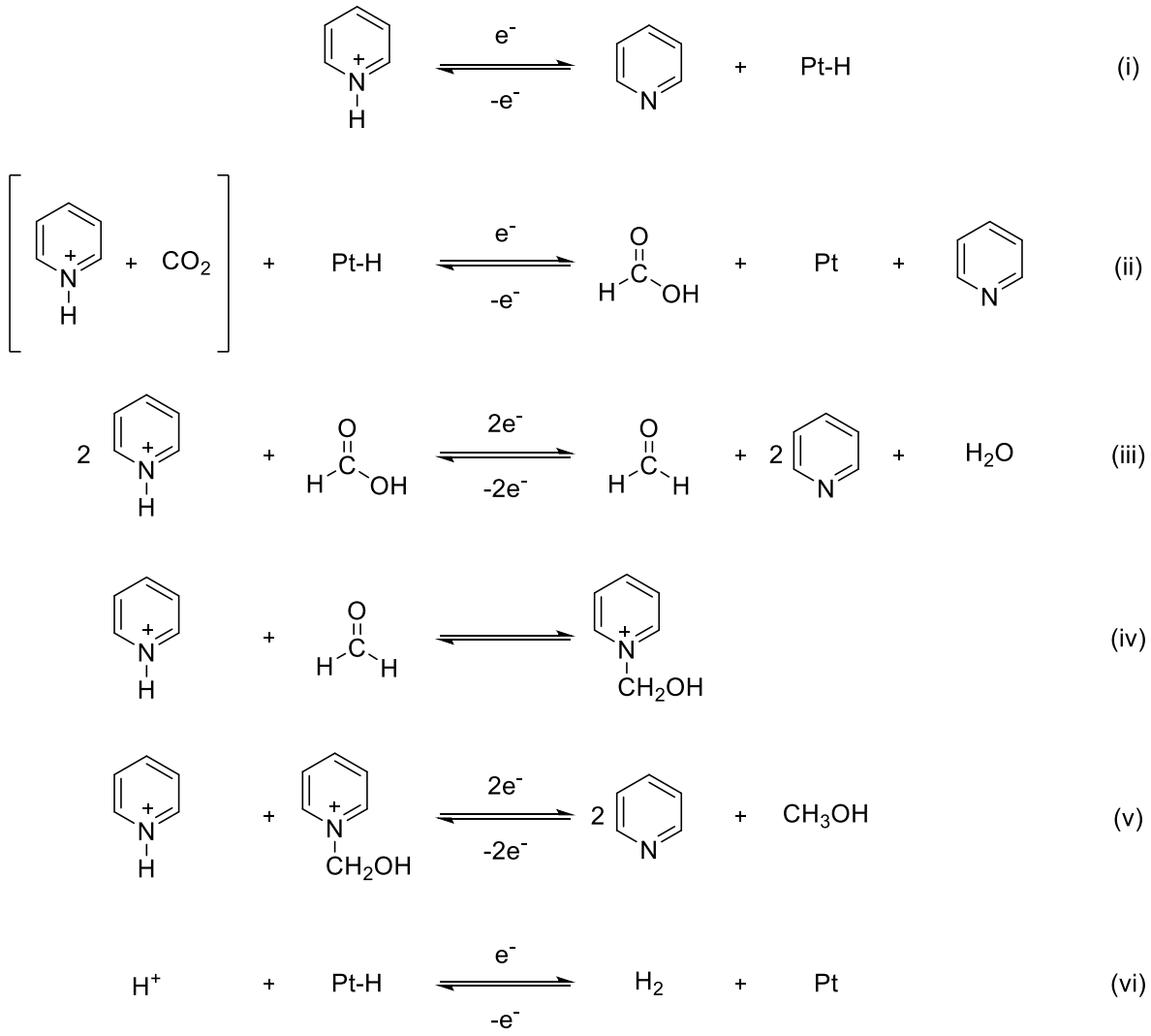

Scheme 6.2. Previously proposed reductive mechanism for the competitive formation of H_2 gas and CH_3OH on a Pt working electrode using pyridinium as the electrocatalyst [50, 51, 54].

As shown in Figure 6.3(a), the voltammetric responses obtained under galvanostatic conditions displayed a reduction process which onsets at ca. -0.55 V vs. Ag/AgCl (equivalent to ca. -0.58 V vs. SCE [63]), thus corresponding to a relatively small overpotential of ca. 60 mV more than the thermodynamic potential for CH_3OH formation (-0.52 V vs. SCE at pH 5.4 [38, 64]). Moreover, over a time span of 2 h, the electrolysis results revealed that the overpotential did

not increase by more than ca. 200 mV. This increase in potential over time was initially suspected to be attributable to the consumption of the acid during the reduction process due to the increase in measured pH values after electrolysis (from ca. 5.01 (start) to 6.21 (end)).

As such, the electrolyzed solution was adjusted back to the initial pH value of 5.01, which resulted in a voltammogram (Figure 6.3(b) dashed green line) that is highly reminiscent of the voltammogram that was recorded for the initial solution of PN before any electrolysis was performed (Figure 6.3(b) solid black line). The close similarity between the voltammograms recorded prior to the electrolysis and at the end of the electrolysis (after pH adjustment) suggests that PN itself undergoes minimal decomposition. Notably, however, the second electrolysis resulted in a slightly greater overpotential to achieve the same overall charge (compare Figure 6.3(a) and 6.3(c)) which can possibly be due to the change in background after the electrolysis or the partial loss of the electrocatalyst.

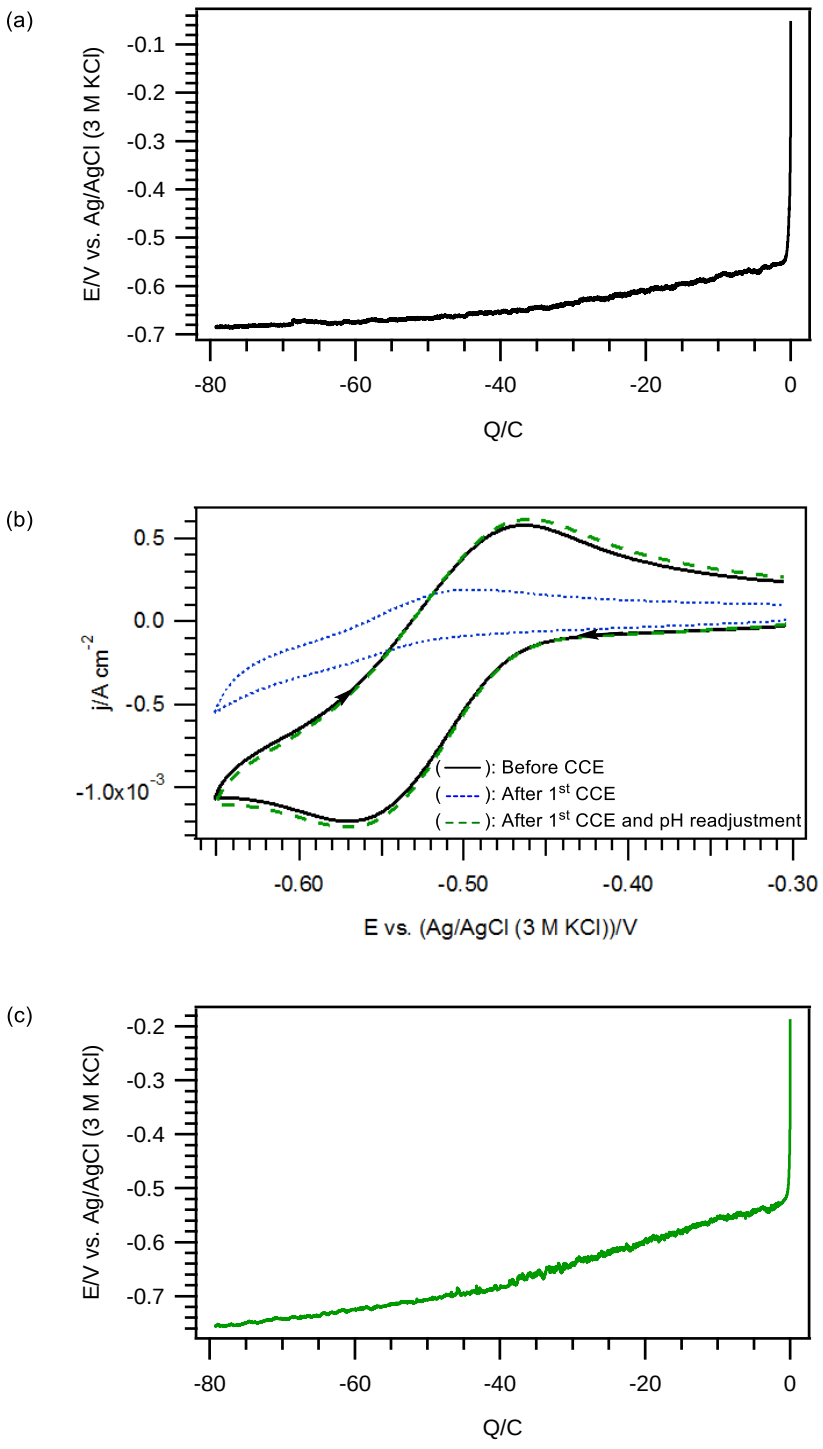

Figure 6.3. (a) Constant current electrolysis (CCE) data recorded over 2 h during the first galvanostatic analysis of PN at pH 5.01. (b) Cyclic voltammograms obtained at 0.1 V s^{-1} using 1 mm diameter planar Pt electrode. (c) CCE data recorded over 2 h during the second galvanostatic analysis (after readjusting the pH back to 5.01).

6.4. Conclusion

In summary, the electrochemical responses gathered have outlined the potential use of PN as an alternative electrocatalyst for the reduction of CO_2 to CH_3OH. At a Pt electrode, a quasi-reversible reduction process was recorded at ca. -0.55 V vs. Ag/AgCl (3 M KCl) in an aqueous solution of PN (pH ≈ 5). Akin to the results recorded using pyridinium, a current enhancement (as compared to the Ar-purged solutions) was observed upon CO_2 saturation along with the disclosure of the importance of a catalytic Pt surface as no appreciative current was detected when a GC electrode was employed. The consistency in the voltammetric results obtained in both systems (pyridinium and PN) suggests a similar mechanistic premise. Verification of CH_3OH formation was achieved by a gas chromatography analysis of the electrolyzed solutions and a faradic yield of ca. 5% was calculated. Additionally, the overpotential for the reduction process was found to be ≤ 200 mV for a two-hour duration. The evolution of H_2 gas appears to be in competition with CH_3OH formation, thereby resulting in the limited yield obtained. Hence, efforts to optimize the faradic efficiency and enhancement of the CH_3OH formation pathway over its competing reaction (H_2 generation) can be subjects of future studies. Despite the limited yield obtained, the use of PN raises the possibility of using other nitrogen-containing, biologically-active and environmentally friendly compounds as molecular electrocatalysts for CO_2 reduction into other value-added products.

6.5. Experimental

6.5.1. General remarks

All chemicals were purchased from commercial sources and used as received unless otherwise stated.

6.5.2. Chemicals and reagents

Unless otherwise stated, all chemicals and reagents were obtained from commercial sources and used as received. PN (≥ 98%), sulfuric acid (H_2SO_4), potassium chloride (KCl), Amberlite IRN-150 ion-exchange resin were acquired from Sigma-Aldrich, Honeywell, Goodrich Chemical Enterprise and Alfa Aesar respectively. Ultrapure water (≥ 18 MΩ cm), was obtained from an ELGA Purelab Option-Q water purification system.

6.5.3. Cyclic voltammetry experiments

Cyclic Voltammetry (CV) experiments were performed using a computer-controlled Metrohm Autolab PGSTAT302N potentiostat in a three-electrode cell. A 1-mm diameter planar platinum (Pt) and glassy carbon (GC) disks working electrodes (eDAQ Pty Ltd) were used along with a Pt counter electrode (Metrohm) and a silver/silver chloride (Ag/AgCl) reference electrode (Metrohm) containing 3 M KCl. Voltammetric measurements of the analyte solutions (10 mM PN, 0.5 M KCl) were performed in a Faraday cage after first saturating with argon (Ar) or CO_2 gas, and then adjusting to the appropriate pH using 1 M H_2SO_4. Ohmic drop was not compensated for all cyclic voltammograms.

6.5.4. Gas chromatography

Before injecting into the gas chromatograph (Agilent 7890A) that was equipped with a flame ionization detector (FID) and a DB-FFAP column (Agilent Technologies), the electrolyzed

sample solutions were filtered through an ion-exchange resin (Amberlite IRN-150) to remove the supporting electrolyte. The injector and detector temperature were fixed at 260 ºC, while temperature programming was used in the oven where it was held at 80 ºC for 1 minute, followed by an increase of 20 ºC/min to 120 ºC for 3 minutes and a further increase to 220 ºC for 3 minutes with a heating rate of 20 ºC/min. The injection volume was 0.2 µL.

6.5.5. Electrolysis experiments

Constant potential and current electrolysis experiments were performed in a two-compartment electrolysis cell separated by a sintered glass frit with a porosity no. 5 (1.0 – 1.7µm). Two symmetrically arranged and identically sized Pt meshes (working and auxiliary electrodes) were arranged symmetrically with respect to each other, along with an Ag wire reference electrode (isolated from the sample solution via a salt bridge containing 3 M KCl) positioned within 2 mm of the surface of the working electrode. Sample solutions (10 mM PN, 0.1 M KCl) were continuously stirred and bubbled with CO_2 throughout the entire experiment. Calculation of faradic yields were based on the generation of methanol via a six-electron reduction process [40].

6.6. References

[1] T.M.L. Wigley, R. Richels, J.A. Edmonds, Economic and Environmental Choices in The Stabilization of Atmospheric CO_2 Concentrations, Nature, 379 (1996) 240–243.

[2] M.I. Hoffert, K. Caldeira, A.K. Jain, E.F. Haites, L.D.D. Harvey, S.D. Potter, M.E. Schlesinger, S.H. Schneider, R. G.Watts, T. M.L.Wigley, D. J.Wuebbles, Energy Implications of Future Stabilization of Atmospheric CO_2 Content, Nature, 395 (1998) 881–884.

[3] K. Caldeira, A.K. Jain, M.I. Hoffert, Climate Sensitivity Uncertainty and the Need for Energy Without CO_2 Emission, Science, 299 (2003) 2052–2054.

[4] S. Bachu, CO_2 Storage in Geological Media: Role, Means, Status and Barriers to Deployment, Prog. Energy Combust. Sci., 34 (2008) 254–273.

[5] D.M. D'Alessandro, B. Smit, J.R. Long, Carbon Dioxide Capture: Prospects for New Materials, Angew. Chem. Int. Ed., 49 (2010) 6058–6082.

[6] R.S. Middleton, G.N. Keating, P.H. Stauffer, A.B. Jordan, H.S. Viswanathan, Q.J. Kang, J.W. Carey, M.L. Mulkey, E.J. Sullivan, S.P. Chu, R. Espositod, T.A. Meckel, The Cross-scale Science of CO_2 Capture and Storage: From Pore Scale to Regional Scale, Energy Environ. Sci., 5 (2012) 7328–7345.

[7] D. Andirova, C.F. Cogswell, Y. Lei, S. Choi, Effect of the Structural Constituents of Metal Organic Frameworks on Carbon Dioxide Capture, Microporous Mesoporous Mater., 219 (2016) 276–305.

[8] C. Maeda, Y. Miyazaki, T. Ema, Recent Progress in Catalytic Conversions of Carbon Dioxide, Catal. Sci. Technol., 4 (2014) 1482–1497.

[9] G. Fiorani, W. Guo, A.W. Kleij, Sustainable Conversion of Carbon Dioxide: The Advent of Organocatalysis, Green Chem., 17 (2015) 1375–1389.

[10] Q. Liu, L. Wu, R. Jackstell, M. Beller, Using Carbon Dioxide as a Building Block in Organic Synthesis, Nat. Commun., 6 (2015) 5933–5947.

[11] A. Corma, H. Garcia, Photocatalytic Reduction of CO_2 for Fuel Production: Possibilities and Challenges, J. Catal., 308 (2013) 168.

[12] S. Das, W.M.A.W. Daud, A Review on Advances in Photocatalysts Towards CO_2 Conversion, RSC Adv., 4 (2014) 20856–20893.

[13] L. Yuan, Y.-J. Xu, Photocatalytic Conversion of CO_2 into Value-Added and Renewable Fuels, Appl. Surf. Sci., 342 (2015) 154.

[14] J.L. White, M.F. Baruch, J.E.P. III, Y. Hu, I.C. Fortmeyer, J.E. Park, T. Zhang, K. Liao, J. Gu, Y. Yan, T.W. Shaw, E. Abelev, A.B. Bocarsly, Light-Driven Heterogeneous Reduction of Carbon Dioxide: Photocatalysts and Photoelectrodes, Chem. Rev., 115 (2015) 12888–12935.

[15] N.S. Spinner, J.A. Vega, W.E. Mustain, Recent Progress in the Electrochemical Conversion and Utilization of CO_2, Catal. Sci. Technol., 2 (2012) 19–28.

[16] D.A. Lowy, M. Jitaru, Electroreduction of Carbon Dioxide, in: K.-Y. Chan, C.-Y.V. Li (Eds.) Electrochemically Enabled Sustainability. Devices, Materials and Mechanisms for Energy Conversion, CRC Press, Boca Raton, 2014, pp. 1–54.

[17] M. Bevilacqua, J. Filippi, H.A. Miller, F. Vizza, Recent Technological Progress in CO_2 Electroreduction to Fuels and Energy Carriers in Aqueous Environments, Energy Technol. (Weinheim, Ger.), 3 (2015) 197–210

[18] I. Ganesh, Electrochemical Conversion of Carbon Dioxide into Renewable Fuel Chemicals - The Role of Nanomaterials and the Commercialization, Renewable Sustainable Energy Rev., 59 (2016) 1269–1297.

[19] D. Pletcher, The Cathodic Reduction of Carbon Dioxide—What Can It Realistically Achieve? A Mini Review, Electrochem. Commun., 61 (2015) 97–101.

[20] Y. Hiro, H. Wakebe, T. Tsukamoto, O. Koga, Electrocatalytic Process of CO Selectivity in Electrochemical Reduction of CO_2 at Metal Electrodes in Aqueous Media, Electrochim. Acta, 39 (1994) 1833–1839.

[21] Y. Hori, Electrochemical CO_2 Reduction on Metal Electrodes, in: C.G. Vayenas, R.E. White, M.E. Gamboa-Aldeco (Eds.) Modern Aspects of Electrochemistry, Springer, New York, 2008, pp. 89–189.

[22] C. Finn, S. Schnittger, L.J. Yellowlees, J.B. Love, Molecular Approaches to the Electrochemical Reduction of Carbon Dioxide, Chem. Commun., 48 (2012) 1392–1399.

[23] J. Qiao, Y. Liu, F. Hong, J. Zhang, A Review of Catalysts for the Electroreduction of Carbon Dioxide to Produce Low-Carbon Fuels, Chem. Soc. Rev., 43 (2014) 631–675.

[24] R. Kortlever, J. Shen, K.J.P. Schouten, F. Calle-Vallejo, M.T.M. Koper, Catalysts and Reaction Pathways for the Electrochemical Reduction of Carbon Dioxide, J. Phys. Chem. Lett., 6 (2015) 4073–4082.

[25] J. Durst, A. Rudnev, A. Dutta, Y. Fu, J. Herranz, V. Kaliginedi, A. Kuzume, A.A. Permyakova, Y. Paratcha, P. Broekmann, T.J. Schmidt, Electrochemical CO_2 Reduction - A Critical View on Fundamentals, Materials and Applications, Chimia, 69 (2015) 769–776.

[26] Q. Lu, F. Jiao, Electrochemical CO_2 Reduction: Electrocatalyst, Reaction Mechanism, and Process Engineering, Nano Energy, (2016) DOI:10.1016/j.nanoen.2016.1004.1009.

[27] G.A. Olah, A. Goeppert, G.K.S. Prakash, Chemical Recycling of Carbon Dioxide to Methanol and Dimethyl Ether: From Greenhouse Gas to Renewable, Environmentally Carbon Neutral Fuels and Synthetic Hydrocarbons, J. Org. Chem., 74 (2009) 487–498.

[28] A. Goeppert, G.K.S. Prakash, G.A. Olah, Carbon Dioxide Recycling to Methanol, Dimethyl Ether and Derived Products for a Sustainable Future, Actual. Chim., 371–372 (2013) 78–83.

[29] A. Goeppert, M. Czaun, J.-P. Jones, G.K.S. Prakash, G.A. Olah, Recycling of Carbon Dioxide to Methanol and Derived Products - Closing the Loop, Chem. Soc. Rev., 43 (2014) 7995–8048.

[30] J. Albo, M. Alvarez-Guerra, P. Castaño, A. Irabien, Towards the Electrochemical Conversion of Carbon Dioxide into Methanol, Green Chem., 17 (2015) 2304–2324.

[31] K.M. McGrath, G.K.S. Prakash, G.A. Olah, Direct Methanol Fuel Cells, J. Ind. Eng. Chem. (Seoul, Repub. Korea), 10 (2004) 1063–1080.

[32] I. Ganesh, Conversion of Carbon Dioxide into Methanol – A Potential Liquid Fuel: Fundamental Challenges and Opportunities (A Review), Renewable Sustainable Energy Rev., 31 (2014) 221–257.

[33] G.A. Olah, A. Goeppert, G.K.S. Prakash, Beyond Oil and Gas: The Methanol Economy, 2nd ed., Wiley-VCH, Weinheim, Germany, 2009.

[34] G.A. Olah, G.K.S. Prakash, A. Goeppert, Anthropogenic Chemical Carbon Cycle for a Sustainable Future, J. Am. Chem. Soc., 133 (2011) 12881–12898.

[35] J. Qu, X. Zhang, Y. Wang, C. Xie, Electrochemical Reduction of CO_2 on RuO_2/TiO_2 Nanotubes Composite Modified Pt Electrode, Electrochim. Acta, 50 (2005) 3576–3580.

[36] J.F. De Brito, A.A. Da Silva, A.J. Cavalheiro, M.V.B. Zanoni, Evaluation of the Parameters Affecting the Photoelectrocatalytic Reduction of CO_2 to CH_3OH at Cu/Cu_2O Electrode, Int. J. Electrochem. Sci., 9 (2014) 5961–5973.

[37] P. Li, H. Hu, J. Xu, H. Jing, H. Peng, J. Lu, C. Wu, S. Ai, New Insights into The Photo-Enhanced Electrocatalytic Reduction of Carbon Dioxide on MoS_2-rods/TiO_2 NTs with Unmatched Energy Band, Appl. Catal., B, 147 (2014) 912–919.

[38] G. Seshadri, C. Lin, A.B. Bocarsly, A New Homogeneous Electrocatalyst for the Reduction of Carbon Dioxide to Methanol at Low Overpotential, J. Electroanal. Chem., 372 (1994) 145–150.

[39] E.E. Barton, D.M. Rampulla, A.B. Bocarsly, Selective Solar-Driven Reduction of CO_2 to Methanol Using a Catalyzed p-GaP Based Photoelectrochemical Cell, J. Am. Chem. Soc., 130 (2008) 6342–6344.

[40] E.B. Cole, P.S. Lakkaraju, D.M. Rampulla, A.J. Morris, E. Abelev, A.B. Bocarsly, Using a One-Electron Shuttle for the Multielectron Reduction of CO_2 to Methanol: Kinetic, Mechanistic, and Structural Insights, J. Am. Chem. Soc., 132 (2010) 11539–11551.

[41] A.B. Bocarsly, Q.D. Gibson, A.J. Morris, R.P. L'Esperance, Z.M. Detweiler, P.S. Lakkaraju, E.L. Zeitler, T.W. Shaw, Comparative Study of Imidazole and Pyridine Catalyzed Reduction of Carbon Dioxide at Illuminated Iron Pyrite Electrodes, ACS Catal., 2 (2012) 1684–1692.

[42] J. Yuan, C. Hao, Solar-Driven Photoelectrochemical Reduction of Carbon Dioxide to Methanol at $CuInS_2$ Thin Film Photocathode, Sol. Energy Mater. Sol. Cells, 108 (2013) 170–174.

[43] J. Yuan, L. Zheng, C. Hao, Role of Pyridine in Photoelectrochemical Reduction of CO_2 to Methanol at a $CuInS_2$ Thin Film Electrode, RSC Adv., 4 (2014) 39435–39438.

[44] E. Lebégue, J. Agullo, M. Morin, D. Bélanger, The Role of Surface Hydrogen Atoms in the Electrochemical Reduction of Pyridine and CO_2 in Aqueous Electrolyte, ChemElectroChem, 1 (2014) 1013–1017.

[45] A.J. Lucio, S.K. Shaw, Pyridine and Pyridinium Electrochemistry on Polycrystalline Gold Electrodes and Implications for CO_2 Reduction, J. Phys. Chem. C, 119 (2015) 12523–12530.

[46] D.J. Boston, Y.M.F. Pachon, R.O. Lezna, N.R.d. Tacconi, F.M. MacDonnell, Electrocatalytic and Photocatalytic Conversion of CO_2 to Methanol using Ruthenium Complexes with Internal Pyridyl Cocatalysts, Inorg. Chem., 53 (2014) 6544–6553.

[47] D. Xiang, D. Magana, R.B. Dyer, CO_2 Reduction Catalyzed by Mercaptopteridine on Glassy Carbon, J. Am. Chem. Soc., 136 (2014) 14007–14010.

[48] E. Portenkirchner, C. Enengl, S. Enengl, G. Hinterberger, S. Schlager, D. Apaydin, H. Neugebauer, G. Knör, N.S. Sariciftci, A Comparison of Pyridazine and Pyridine as Electrocatalysts for the Reduction of Carbon Dioxide to Methanol, ChemElectroChem, 1 (2014) 1543–1548.

[49] J.A. Keith, E.A. Carter, Theoretical Insights into Pyridinium-Based Photoelectrocatalytic Reduction of CO_2, J. Am. Chem. Soc., 134 (2012) 7580–7583.

[50] C. Costentin, J.C. Canales, B. Haddou, J.-M. Savéant, Electrochemistry of Acids on Platinum. Application to the Reduction of Carbon Dioxide in the Presence of Pyridinium Ion in Water, J. Am. Chem. Soc., 135 (2013) 17671–17674.

[51] M.Z. Ertem, S.J. Konezny, C.M. Araujo, V.S. Batista, Functional Role of Pyridinium during Aqueous Electrochemical Reduction of CO_2 on Pt(111), J. Phys. Chem. Lett., 4 (2013) 745–748.

[52] Y. Yan, E.L. Zeitler, J. Gu, Y. Hu, A.B. Bocarsly, Electrochemistry of Aqueous Pyridinium: Exploration of a Key Aspect of Electrocatalytic Reduction of CO_2 to Methanol, J. Am. Chem. Soc., 135 (2013) 14020–14023.

[53] K. Dhar, C. Cavallotti, Investigation of the Initial Steps of the Electrochemical Reduction of CO_2 on Pt Electrodes, J. Phys. Chem. A, 118 (2014) 8676–8688.

[54] E.E.B. Cole, M.F. Baruch, R.P. L'Esperance, M.T. Kelly, P.S. Lakkaraju, E.L. Zeitler, A.B. Bocarsly, Substituent Effects in the Pyridinium Catalyzed Reduction of CO_2 to Methanol: Further Mechanistic Insights, Top. Catal., 58 (2015) 15–22.

[55] A.J. Morris, R.T. McGibbon, A.B. Bocarsly, Electrocatalytic Carbon Dioxide Activation: The Rate-Determining Step of Pyridinium-Catalyzed CO_2 Reduction, ChemSusChem, 4 (2011) 191196.

[56] J.A. Tossell, Calculation of the Properties of Molecules in the Pyridine Catalyst System for the Photochemical Conversion of CO_2 to Methanol, Comput. Theor. Chem., 977 (2011) 123–127.

[57] J.A. Keith, E.A. Carter, Electrochemical Reactivities of Pyridinium in Solution: Consequences for CO_2 Reduction Mechanisms, Chem. Sci., 4 (2013) 1490–1496.

[58] C.-H. Lim, A.M. Holder, C.B. Musgrave, Mechanism of Homogeneous Reduction of CO2 by Pyridine: Proton Relay in Aqueous Solvent and Aromatic Stabilization, J. Am. Chem. Soc., 135 (2013) 142–154.

[59] K. Liao, M. Askerka, E.L. Zeitler, A.B. Bocarsly, V.S. Batista, Electrochemical Reduction of Aqueous Imidazolium on Pt(111) by Proton Coupled Electron Transfer, Top. Catal., 58 (2015) 23–29.

[60] J.H.Q. Lee, Y. Yue, R. Ganguly, R.D. Webster, Electrochemical Study of Pyridoxine (Vitamin B_6) in Acetonitrile, ChemElectroChem, 2 (2015) 412–420.

[61] T. Hanai, K. Koizumi, T. Kinoshita, R. Arora, F. Ahmed, Prediction of pKa Values of Phenolic and Nitrogen-Containing Compounds by Computational Chemical Analysis Compared to Those Measured by Liquid Chromtography, J. Chromatogr. A, 762 (1997) 55–61.

[62] D.E. Metzler, E.E. Snell, Spectra and Ionization Constants of the Vitamin B_6 Group and Related 3-Hydroxypyridine Derivatives, J. Am. Chem. Soc., 77 (1955) 2431–2437.

[63] T.J. Smith, K.J. Stevenson, Reference Electrodes, in: C.G. Zoski (Ed.) Handbook of Electrochemistry, Elsevier, Amsterdam, The Netherlands, 2007, pp. 73–110.

[64] I. Taniguchi, Electrochemical and Photoelectrochemical Reduction of Carbon Dioxide, in: J.O.M. Bockris, R.E. White, B.E. Conway (Eds.) Modern Aspects of Electrochemistry, Plenum Press, New York, USA, 1989, pp. 327–400.

This page has been intentionally left blank

Chapter 7

Summary

This page has been intentionally left blank

7.1. Summary

Phenols are an important class of molecules that serve as basic structural units in a myriad of natural and synthetic compounds and are exploited in numerous applications ranging from food, polymer, medical, pharmaceutical, cosmetics, and chemical uses.

The current thesis encompasses in-depth investigations on the redox chemistry of four phenolic and phenolic-type compounds, sesamol, vanillin, diethylstilbestrol and pyridoxine. In view of the general lack of electrochemical studies conducted in aprotic media as compared to the corresponding works in protic systems (for the aforementioned molecules), the present work focused on the voltammetric behavior of these compounds in an aprotic organic solvent, acetonitrile (CH_3CN) employing the cyclic voltammetry (CV) technique conducted under varied scan rates, temperatures, and water content, as well as using bulk conversion methods such as controlled potential electrolysis (CPE) and chemical oxidation.

In Chapter 2, the voltammetric oxidation of sesamol was addressed, where the anodic process was found to involve the transfer of five electrons per two molecules of sesamol to generate a dimeric product which was subsequently isolated and positively identified. As a result of the dimerization reaction, the number of electrons transfer was observed to vary depending on the exact concentration of sesamol used. Furthermore, the oxidation process was also observed to be influenced by hydrogen bonding interactions with trace amounts of water present in the sample solution.

In Chapter 3, vanillin displayed an anodic peak on the CV measurement, with a cathodic peak detected on the return scan due to the reduction of a secondary product formed after the initial oxidation reaction. Using the voltammetric responses gathered, the oxidation of vanillin is surmised to generate a substituted 1,2-benzoquinone that is electro-reducible. Digital

simulations were used to quantitatively model the collected CV data which enabled an estimation of the electrochemical and kinetic parameters associated with the different heterogeneous and homogeneous reactions. Independently, vanillin can also be electrochemically reduced which involves the direct discharge of its phenolic functionality.

In Chapter 4, the electrochemical oxidation of diethylstilbestrol (DES) was shown to behave in a comparable manner as the oxidative phenomena recorded for bisphenol A (BPA). Under longer time domain (e.g. CV measurements performed at slow scan rates), the initial oxidation of DES was proposed to undergo an overall four-electron oxidation, whereas at fast scan rates the oxidation of DES was found to only involve two electrons. The CV data were modeled using digital simulations which provides insight into the electrochemical and kinetic parameters affiliated with the electrode reactions.

In Chapter 5, pyridoxine (PN) was established to give a one-electron chemically irreversible oxidation peak that suffered from electrode fouling, as evidence from the marked decrease in anodic peak current upon continuous cycling. As a result, this adsorption effect negates the use of preparative scale electrolysis and was resolved by the use of a chemical oxidant, nitrosonium hexafluoroantimonate ($NOSbF_6$). In contrast to the aforementioned oxidation process, PN was also found to undergo electrochemical reduction reaction that is chemically reversible on the shorter timeframe of CV and does not adsorb on the electrode surface. After reductive electrolysis and treatment with iodomethane, the nitrogen-methylated PN was furnished.

In Chapter 6, the potential utility of PN as a molecular electrocatalyst for the amelioration of carbon dioxide (CO_2) into methanol was disclosed. At a platinum electrode, an aqueous solution ($pH \approx 5$) of PN gave a quasi-reversible cathodic peak in the presence of CO_2, whereas only a very small reduction current was detected in the absence of PN. Furthermore, the importance of a catalytic surface was highlighted by the observation of no detectable reduction current

recorded at a glassy carbon electrode under the same conditions. Confirmation of methanol formation during the pyridoxine-assisted CO_2 reduction was conducted by using gas chromatography analysis of the electrolyzed solutions and faradic yields of ca. 5% were afforded.

Although the electrochemical studies presented in the current thesis were primarily conducted using cyclic voltammetry (performed under varied conditions such as scan rates, temperature), controlled potential electrolysis, and digital simulations, alternative techniques such as square wave voltammetry, rotating disk electrode voltammetry, and impedance spectroscopy may also be useful for further mechanistic analysis. Moreover, as all experimental results shown in the present thesis were not treated for IR drop, the large decrease in capacitive current provided by ultramicroelectrode might help in decreasing these ohmic distortion, which can allow for investigation of very rapid kinetic processes. Therefore, the collective use of other techniques (such as those mentioned above) can potentially supplement existing voltammetric works and can be the subject of future studies.

This page has been intentionally left blank

Appendix

Chapter 2

The Electrochemical Study of Sesamol in Acetonitrile

This page has been intentionally left blank

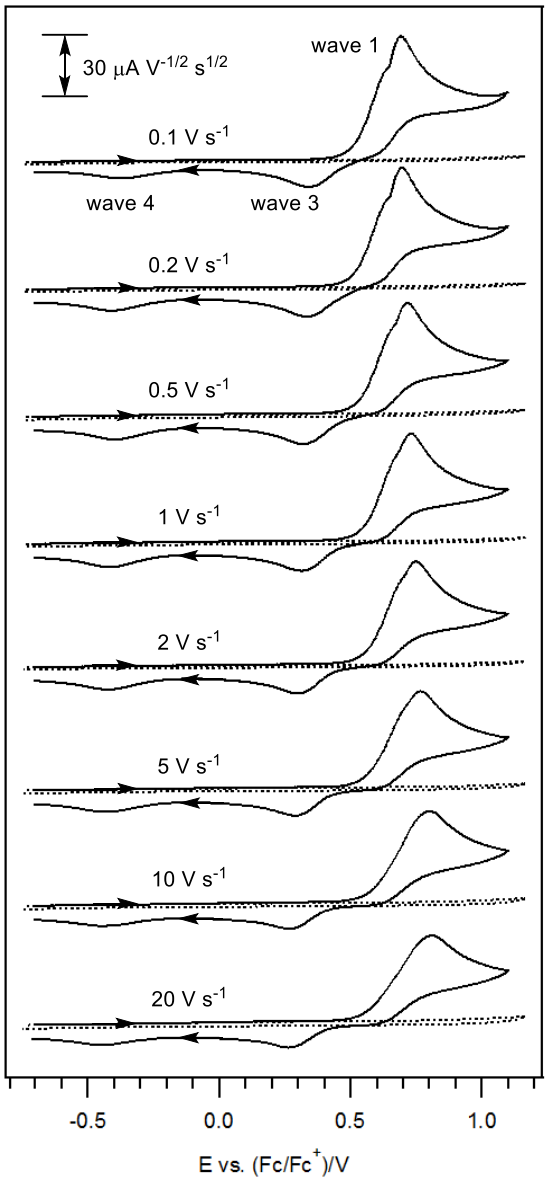

Figure A2.1. Variable scan rates cyclic voltammograms of 2 consecutive scans of 0.2 M Bu_4NPF_6 in CH_3CN, recorded using a 1 mm diameter planar Pt electrode at 22 (±2) °C. (—) With sesamol. (·····) Without sesamol. Current data were multiplied by (scan rate)$^{-0.5}$ for normalization.

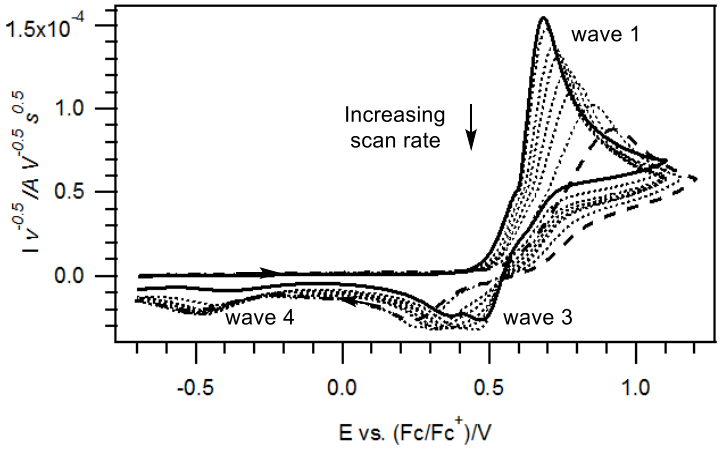

Figure A2.2. Overlaid variable scan rates cyclic voltammograms of 10 mM sesamol in CH_3CN ($[H_2O]_{initial}$ = 8 mM, $[H_2O]_{final}$ = 13 mM) with 0.2 M Bu_4NPF_6, recorded using a 1 mm diameter planar Pt electrode at 22 (±2) °C. Current data were multiplied by (scan rate)$^{-0.5}$ for normalization. (—) 0.1 V s^{-1}. (·····) 0.2, 0.5, 1, 2, 5, and 10 V s^{-1}. (- - -) 20 V s^{-1}.

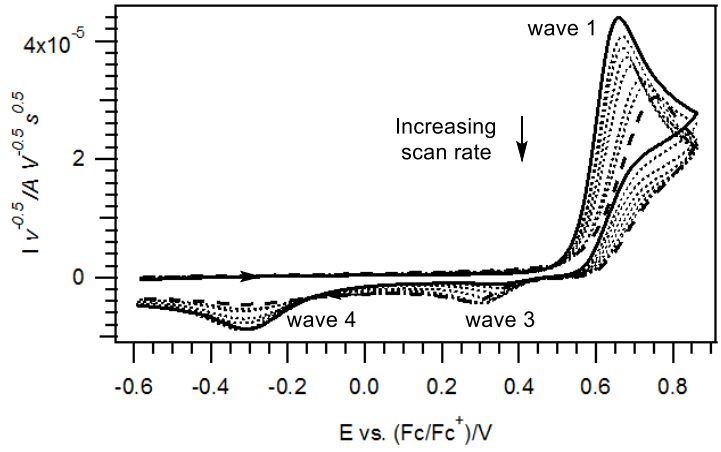

Figure A2.3. Overlaid variable scan rates cyclic voltammograms of 2 mM sesamol in CH_3CN ($[H_2O]_{initial}$ = 126 mM) with 0.2 M Bu_4NPF_6, recorded using a 1 mm diameter planar Pt electrode at 22 (±2) °C. Current data were multiplied by (scan rate)$^{-0.5}$ for normalization. (—) 0.1 V s^{-1}. (·····) 0.2, 0.5, 1, 2, 5, and 10 V s^{-1}. (- - -) 20 V s^{-1}.

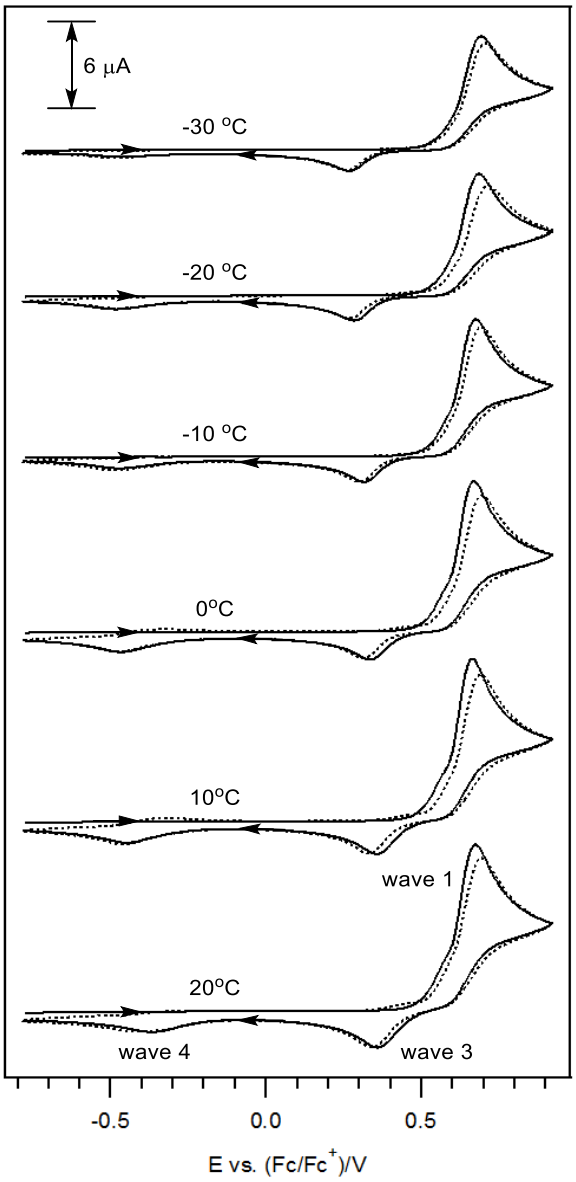

Figure A2.4. Variable temperatures cyclic voltammograms of 2 consecutive scans of 2 mM sesamol in CH_3CN with 0.2 M Bu_4NPF_6, recorded using a 1 mm diameter planar Pt electrode and at a scan rate of 0.1 V s^{-1}. (—) 1st cycle. (·····) 2nd cycle.

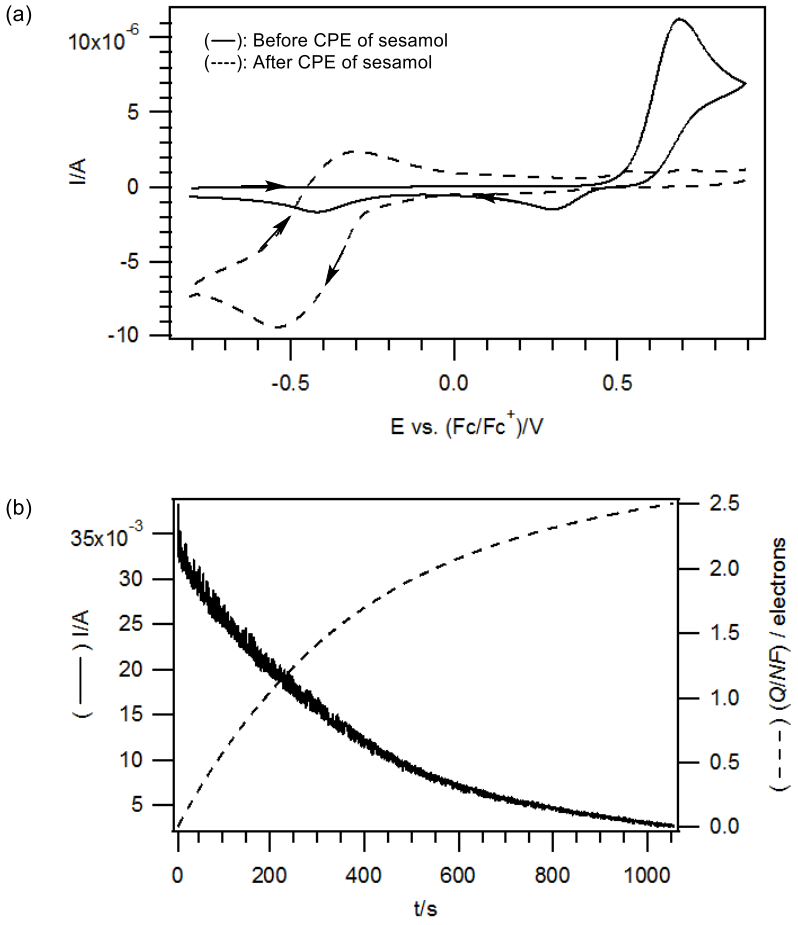

Figure A2.5. Voltammetric and coulometric data recorded during the first of the triplicate repeats of the controlled potential electrolysis of 2 mM sesamol in in CH_3CN with 0.2 M Bu_4NPF_6 at 22 (±2) °C. (a) Cyclic voltammograms obtained at a scan rate of 0.1 V s^{-1} using a 1 mm diameter planar Pt electrode. (b) Current vs. time logged during the exhaustive oxidation of sesamol.

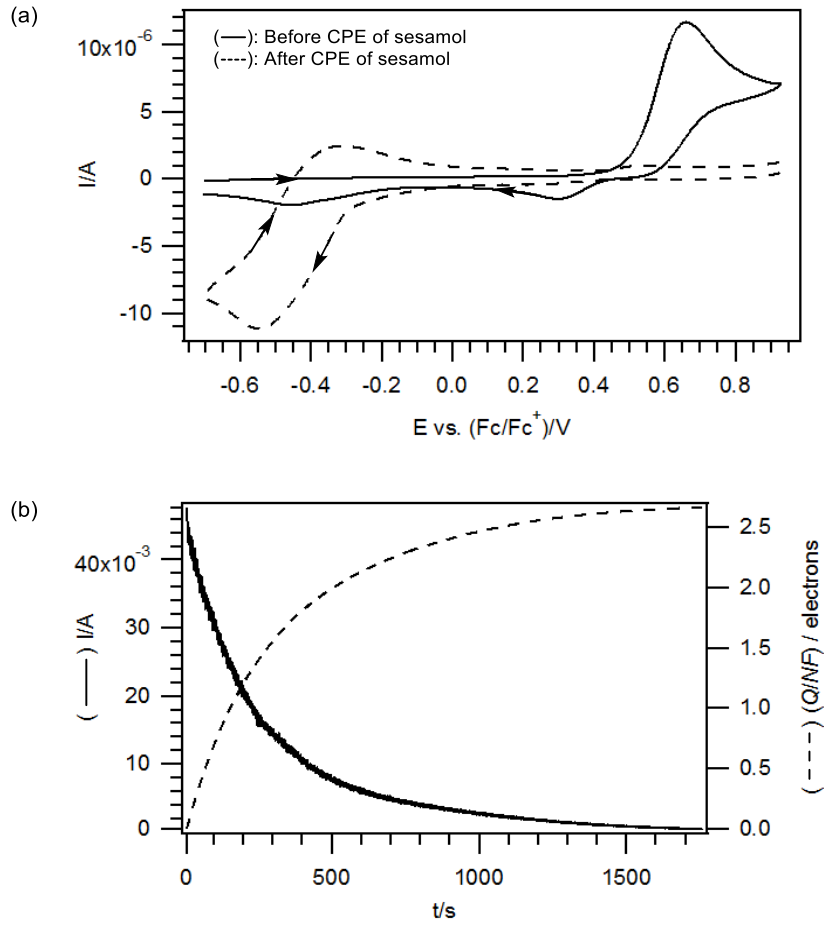

Figure A2.6. Voltammetric and coulometric data recorded during the second of the triplicate repeats of the controlled potential electrolysis of 2 mM sesamol in in CH_3CN with 0.2 M Bu_4NPF_6 at 22 (±2) °C. (a) Cyclic voltammograms obtained at a scan rate of 0.1 V s^{-1} using a 1 mm diameter planar Pt electrode. (b) Current vs. time logged during the exhaustive oxidation of sesamol.

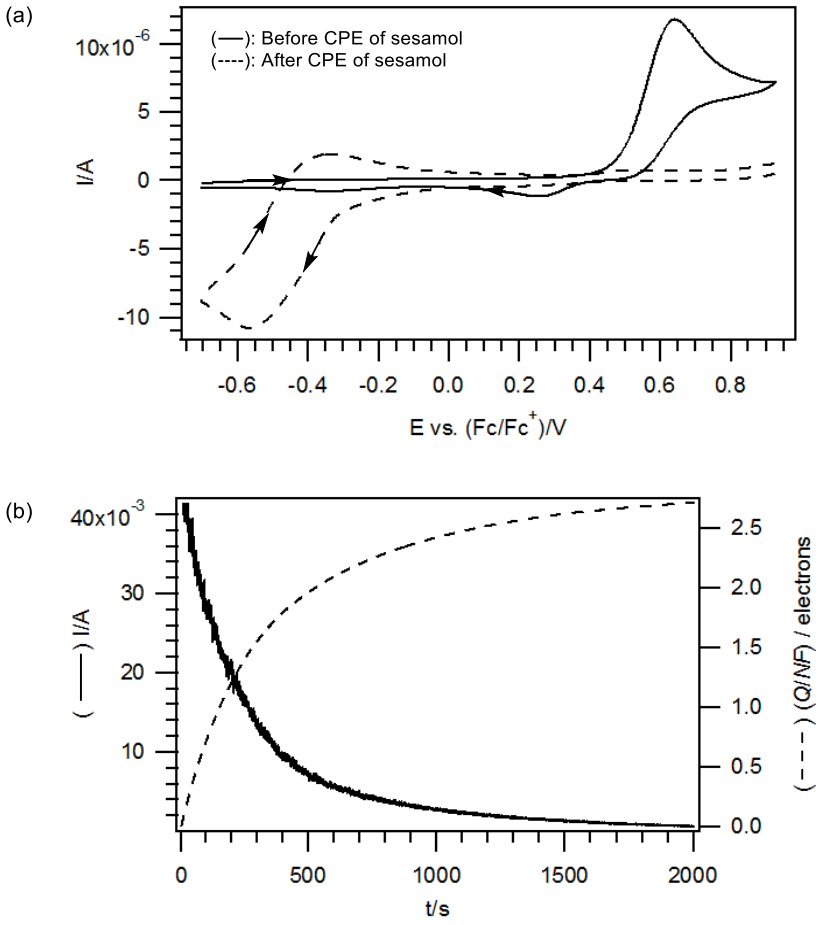

Figure A2.7. Voltammetric and coulometric data recorded during the third of the triplicate repeats of the controlled potential electrolysis of 2 mM sesamol in in CH_3CN with 0.2 M Bu_4NPF_6 at 22 (±2) °C. (a) Cyclic voltammograms obtained at a scan rate of 0.1 V s^{-1} using a 1 mm diameter planar Pt electrode. (b) Current vs. time logged during the exhaustive oxidation of sesamol.

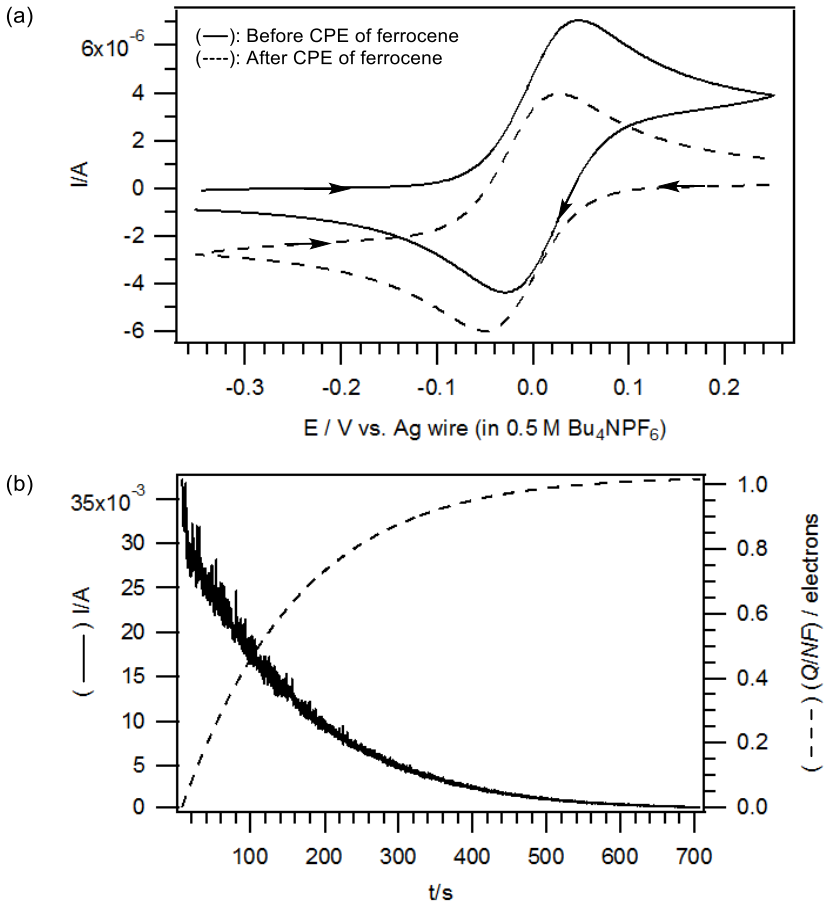

Figure A2.8. Voltammetric and coulometric data recorded during the controlled potential electrolysis of 2 mM ferrocene in CH_3CN with 0.2 M Bu_4NPF_6 at 22 (±2) °C. (a) Cyclic voltammograms obtained at a scan rate of 0.1 V s^{-1} using a 1 mm diameter planar Pt electrode. (b) Current vs. time logged during the exhaustive oxidation of ferrocene.

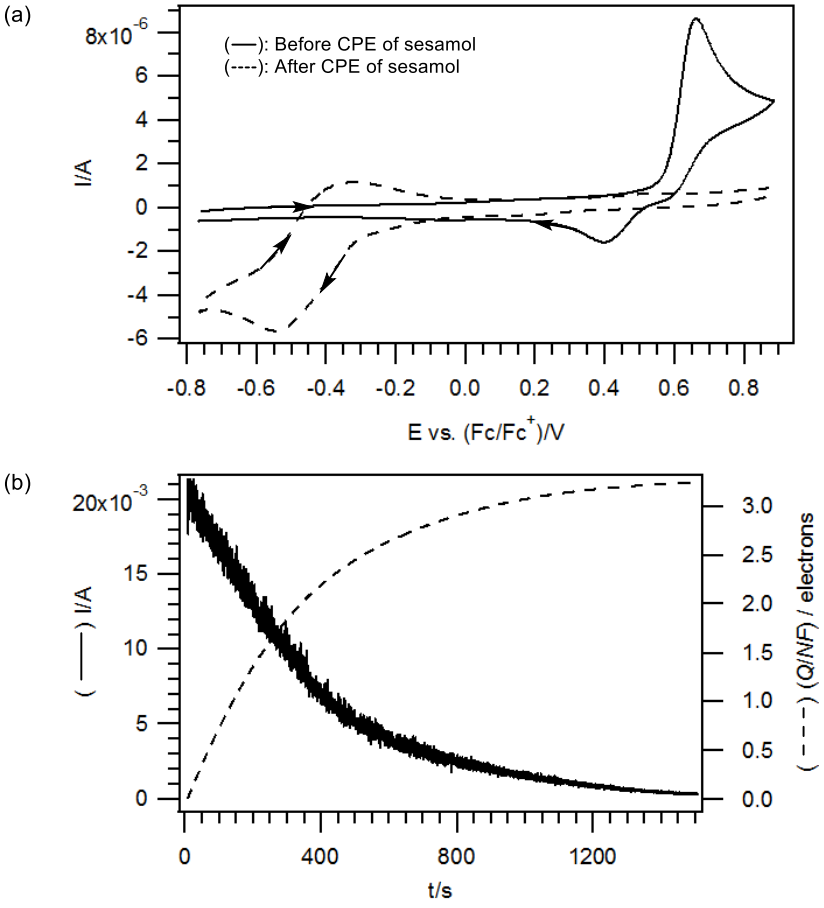

Figure A2.9. Voltammetric and coulometric data recorded during the controlled potential electrolysis of 1 mM sesamol in CH_3CN with 0.2 M Bu_4NPF_6 at 22 (±2) °C. (a) Cyclic voltammograms obtained at a scan rate of 0.1 V s^{-1} using a 1 mm diameter planar Pt electrode. (b) Current vs. time logged during the exhaustive oxidation of sesamol.

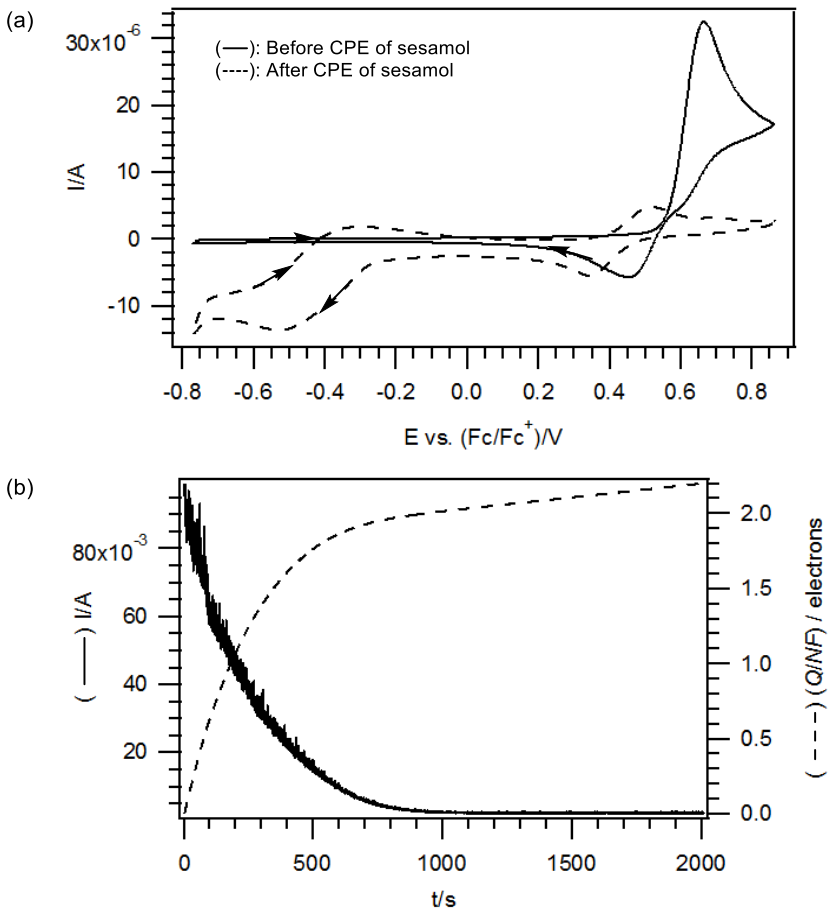

Figure A2.10. Voltammetric and coulometric data recorded during the controlled potential electrolysis of 5 mM sesamol in CH_3CN with 0.2 M Bu_4NPF_6 at 22 (±2) °C. (a) Cyclic voltammograms obtained at a scan rate of 0.1 V s^{-1} using a 1 mm diameter planar Pt electrode. (b) Current vs. time logged during the exhaustive oxidation of sesamol.

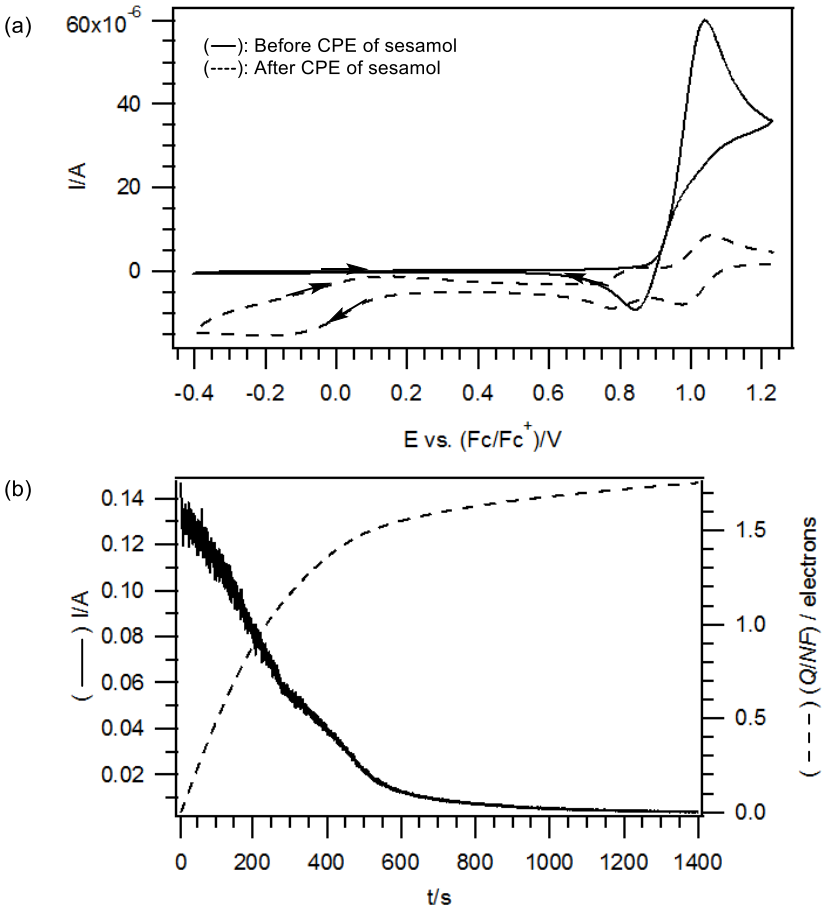

Figure A2.11. Voltammetric and coulometric data recorded during the controlled potential electrolysis of 10 mM sesamol in CH_3CN with 0.2 M Bu_4NPF_6 at 22 (±2) °C. (a) Cyclic voltammograms obtained at a scan rate of 0.1 V s^{-1} using a 1 mm diameter planar Pt electrode. (b) Current vs. time logged during the exhaustive oxidation of sesamol.

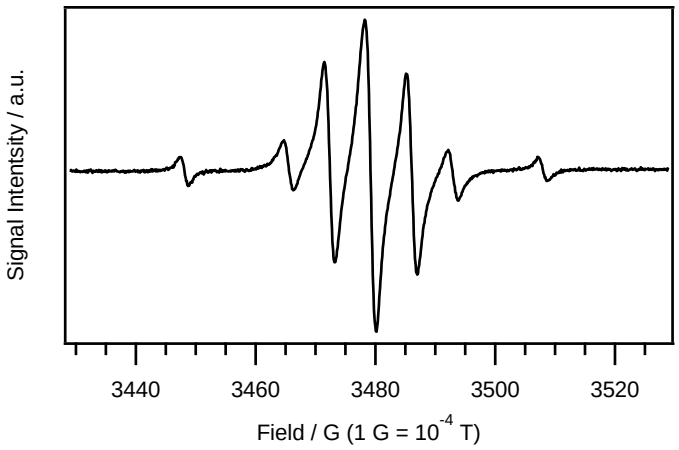

Figure A2.12. EPR Spectrum of the reaction solution of 1 mM sesamol with 2.5 equiv. $NOSbF_6$ obtained after 10 cumulative scans using microwave power = 20 mW (attenuation =10 dB) and modulation amplitude = 1 G.

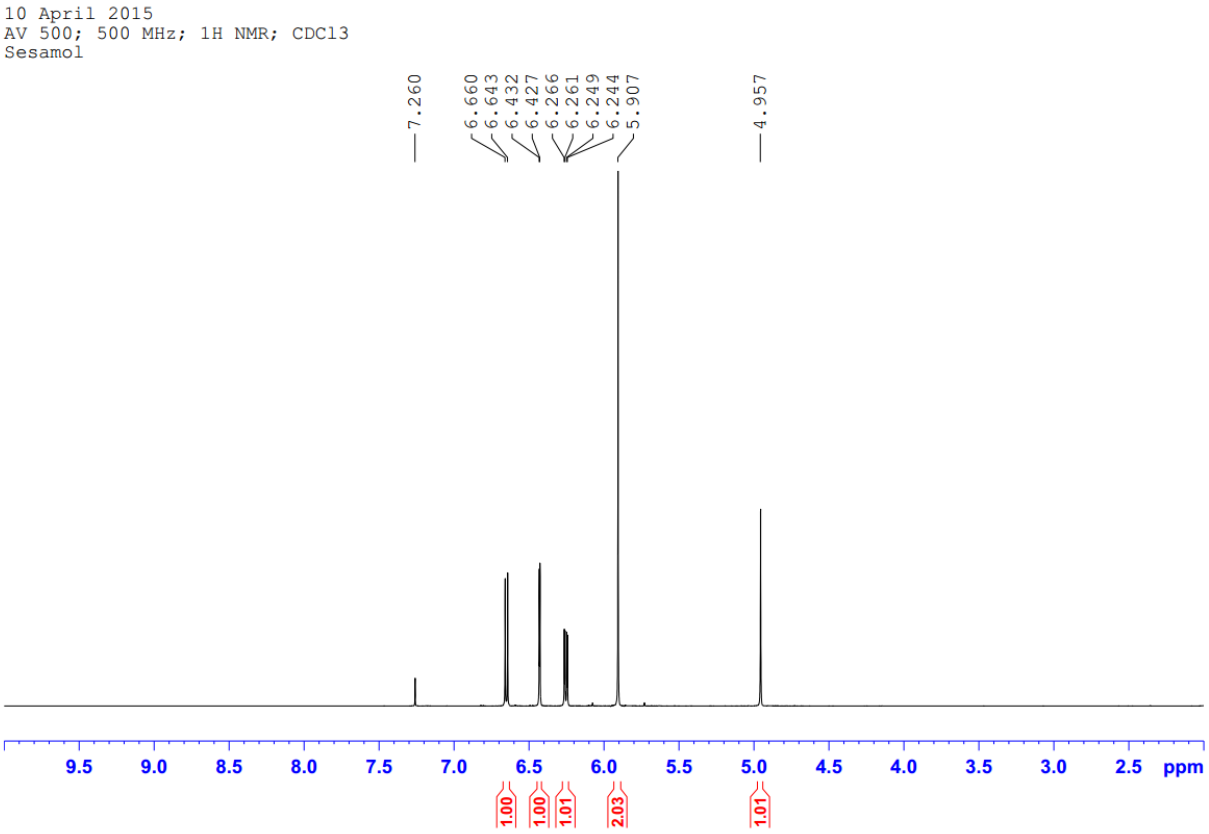

Figure A2.13. ^{1}H NMR Spectrum of sesamol.

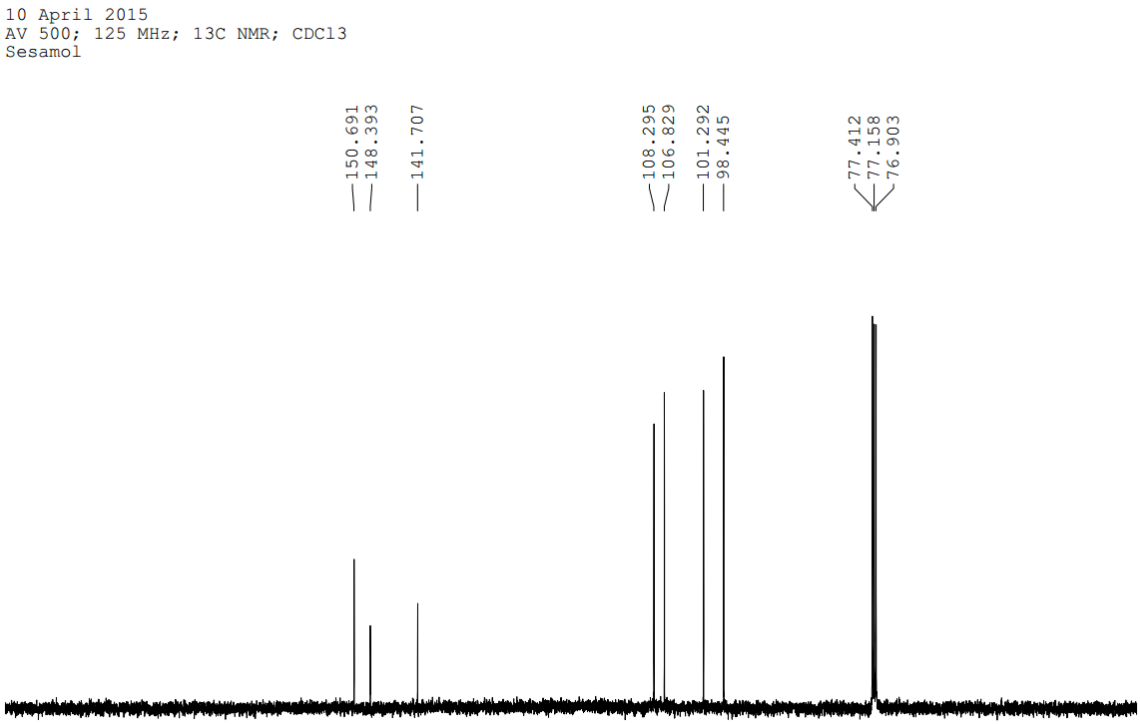

Figure A2.14. ^{13}C NMR Spectrum of sesamol.

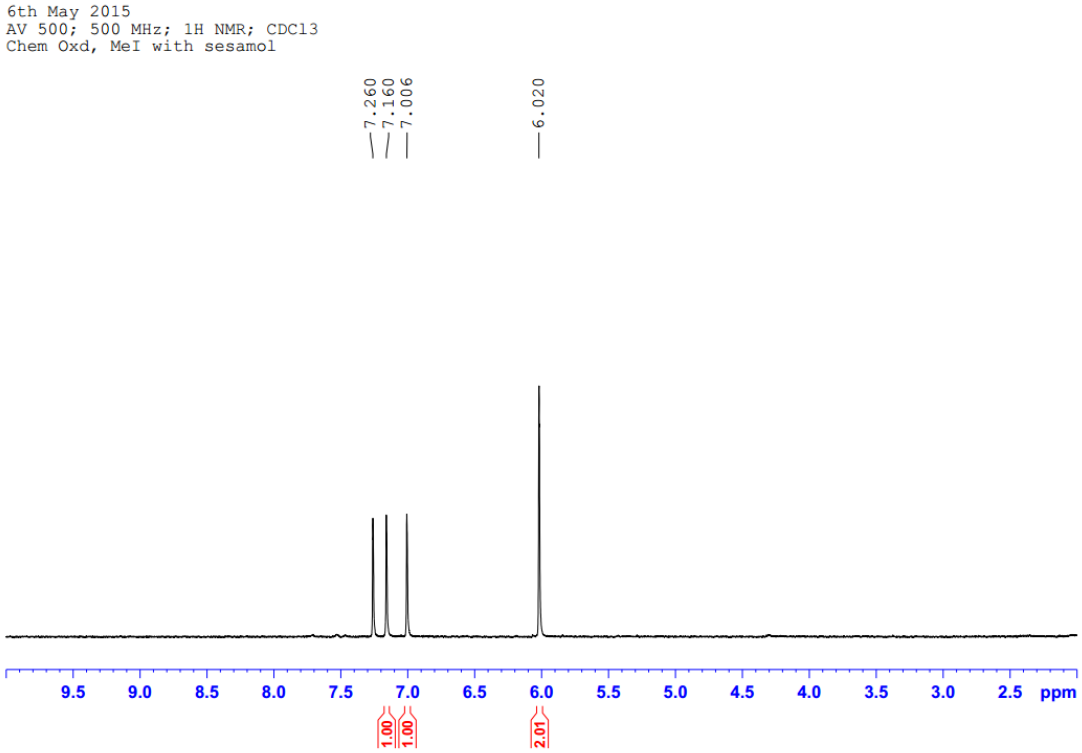

Figure A2.15. ^{1}H NMR Spectrum of dimer **8**.

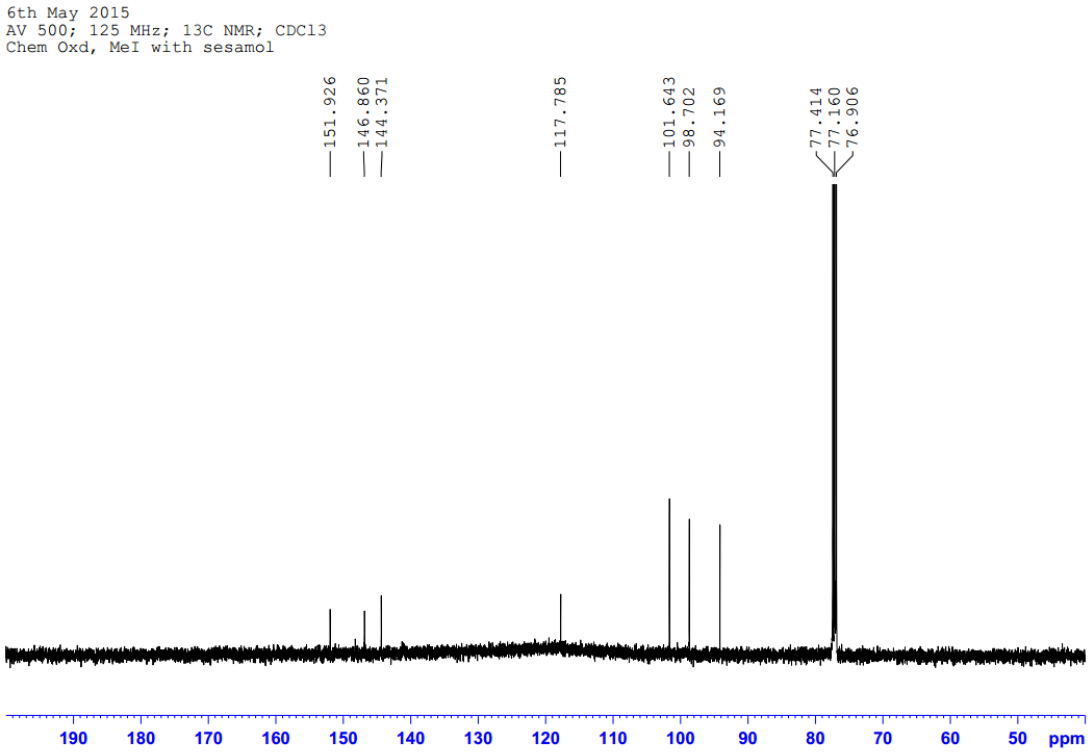

Figure A2.16. ^{13}C NMR Spectrum of dimer **8**.

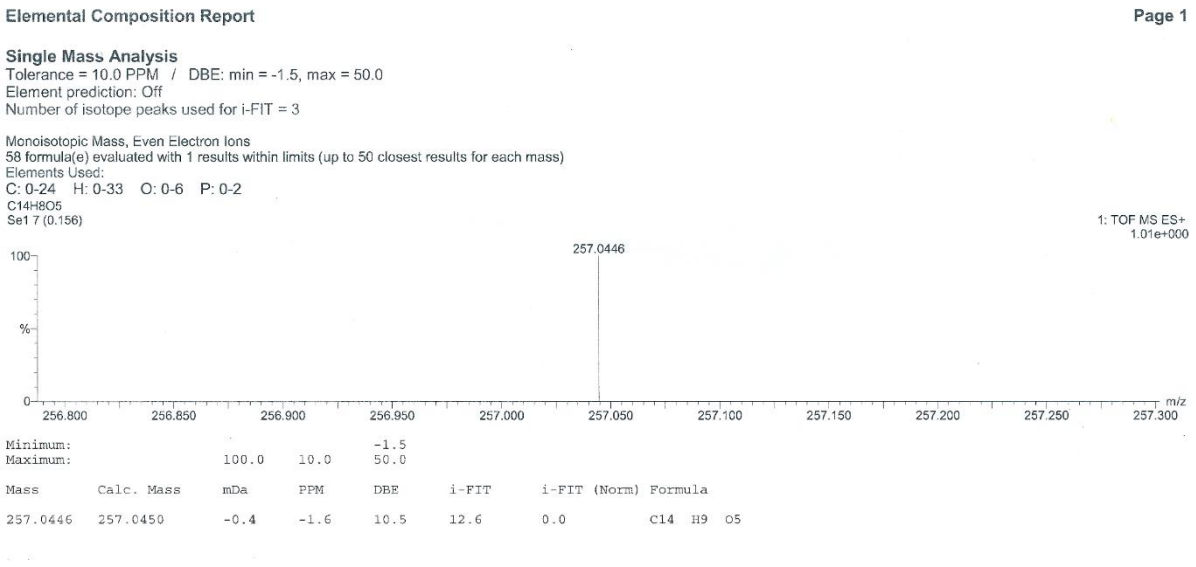

Figure A2.17. HRMS Spectrum of dimer **8**.

Crystal structure report of dimer 8.

A light yellow plate-like specimen of $C_{14}H_8O_5$, approximate dimensions 0.010 mm x 0.040 mm x 0.420 mm, was used for the X-ray crystallographic analysis. The X-ray intensity data were measured.

The total exposure time was 1.12 h. The frames were integrated with the Bruker SAINT software package using a narrow-frame algorithm. The integration of the data using an orthorhombic unit cell yielded a total of 4085 reflections to a maximum θ angle of 25.88° (0.81 Å resolution), of which 992 were independent (average redundancy 4.118, completeness = 99.2%, Rint = 15.24%, Rsig = 14.36%) and 494 (49.80%) were greater than $2\sigma(F^2)$. The final cell constants of a = 20.892(15) Å, b = 4.009(3) Å, c = 12.353(11) Å, volume = 1034.6(15) Å3, are based upon the refinement of the XYZ-centroids of 274 reflections above 20 σ(I) with $6.596° < 2\theta < 40.36°$. Data were corrected for absorption effects using the multi-scan method (SADABS). The ratio of minimum to maximum apparent transmission was 0.616. The calculated minimum and maximum transmission coefficients (based on crystal size) are 0.9490 and 0.9990.

The final anisotropic full-matrix least-squares refinement on F^2 with 87 variables converged at R1 = 7.07%, for the observed data and wR2 = 15.05% for all data. The goodness-of-fit was 1.040. The largest peak in the final difference electron density synthesis was 0.316 e-/Å3 and the largest hole was -0.402 $e^-/Å^3$ with an RMS deviation of 0.083 $e^-/Å^3$. On the basis of the final model, the calculated density was 1.645 g/cm^3 and F(000), 528 e^-.

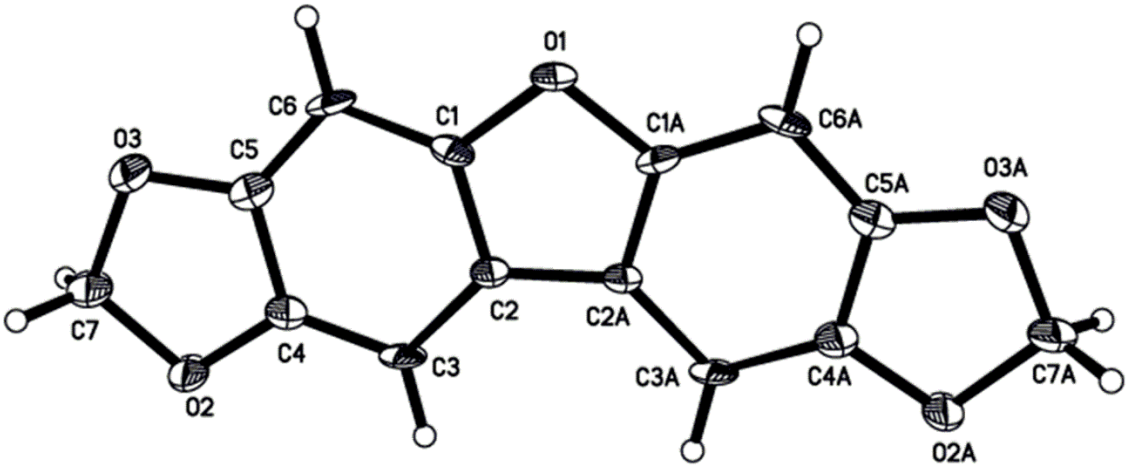

Figure A2.18. ORTEP drawing of dimer **8** with thermal ellipsoids at 50% probability levels.

Table A2.1. Sample and crystal data of dimer **8**.

Identification code	Dimer **8**	
Chemical formula	$C_{14}H_8O_5$	
Formula weight	256.20 g/mol	
Temperature	103(2) K	
Wavelength	0.71073 Å	
Crystal size	0.010 x 0.040 x 0.420 mm	
Crystal habit	light yellow plate	
Crystal system	orthorhombic	
Space group	P c c n	
Unit cell dimensions	a = 20.892(15) Å	α = 90°
	b = 4.009(3) Å	β = 90°
	c = 12.353(11) Å	γ = 90°
Volume	1034.6(15) $Å^3$	
Z	4	
Density (calculated)	1.645 g/cm^3	
Absorption coefficient	0.127 mm^{-1}	
F(000)	528	

Table A2.2. Data collection and structure refinement of dimer **8**.

Theta range for data collection	1.95 to 25.88°	
Index ranges	-20<=h<=25, -4<=k<=4, -14<=l<=15	
Reflections collected	4085	
Independent reflections	992 [R(int) = 0.1524]	
Coverage of independent reflections	99.2%	
Absorption correction	multi-scan	
Max. and min. transmission	0.9990 and 0.9490	
Refinement method	Full-matrix least-squares on F^2	
Refinement program	SHELXL-2014/6 (Sheldrick, 2014)	
Function minimized	$\Sigma\ w(F_o^2 - F_c^2)^2$	
Data / restraints / parameters	992 / 0 / 87	
Goodness-of-fit on F^2	1.040	
Final R indices	494 data; I>2σ(I)	R1 = 0.0707, wR2 = 0.1147
	all data	R1 = 0.1699, wR2 = 0.1505
Weighting scheme	$w=1/[\sigma^2(Fo^2)+(0.0336P)^2+0.8744P]$ where $P=(Fo^2+2Fc^2)/3$	
Largest diff. peak and hole	0.316 and -0.402 $eÅ^{-3}$	
R.M.S. deviation from mean	0.083 $eÅ^{-3}$	

Table A2.3. Atomic coordinates and equivalent isotropic atomic displacement parameters ($Å^2$) of dimer **8**.

U(eq) is defined as one third of the trace of the orthogonalized U_{ij} tensor.

	x/a	y/b	z/c	U(eq)
C1	0.29620(17)	0.3841(10)	0.2373(4)	0.0167(10)
C2	0.28035(16)	0.3342(10)	0.3451(3)	0.0159(10)
C3	0.32224(17)	0.4493(10)	0.4272(4)	0.0196(11)
C4	0.37702(18)	0.6018(11)	0.3915(4)	0.0208(11)
C5	0.39058(18)	0.6498(11)	0.2817(4)	0.0190(11)
C6	0.35133(17)	0.5423(10)	0.1993(4)	0.0204(11)
C7	0.47188(19)	0.8618(12)	0.3781(3)	0.0266(12)
O1	0.25	0.25	0.1684(3)	0.0205(11)
O2	0.42611(12)	0.7300(8)	0.4534(2)	0.0295(10)
O3	0.44775(11)	0.8138(8)	0.2703(2)	0.0271(9)

Table A2.4. Bond lengths (Å) of dimer **8**.

C1-C2	1.387(6)	C1-O1	1.395(4)
C1-C6	1.396(5)	C2-C3	1.416(5)
C2-C2	1.437(7)	C3-C4	1.370(5)
C4-O2	1.378(5)	C4-C5	1.399(6)
C5-O3	1.371(5)	C5-C6	1.376(6)
C7-O2	1.435(5)	C7-O3	1.437(5)
O1-C1	1.395(4)		

Table A2.5. Bond angles (°) of dimer **8**.

C2-C1-O1	111.4(4)	C2-C1-C6	125.8(4)
O1-C1-C6	122.8(4)	C1-C2-C3	119.5(4)
C1-C2-C2	106.2(2)	C3-C2-C2	134.3(2)
C4-C3-C2	115.6(4)	C3-C4-O2	127.6(4)
C3-C4-C5	122.8(4)	O2-C4-C5	109.6(3)
O3-C5-C6	126.4(4)	O3-C5-C4	110.0(4)
C6-C5-C4	123.6(4)	C5-C6-C1	112.7(4)
O2-C7-O3	108.5(3)	C1-O1-C1	104.8(5)
C4-O2-C7	105.9(3)	C5-O3-C7	105.9(3)

Table A2.6. Anisotropic atomic displacement parameters ($Å^2$) for of dimer **8**.

The anisotropic atomic displacement factor exponent takes the form: $-2\pi^2[h^2 a^{*2} U_{11} + ... + 2 h k a^* b^* U_{12}]$

	U_{11}	U_{22}	U_{33}	U_{23}	U_{13}	U_{12}
C1	0.021(2)	0.019(3)	0.010(3)	-0.004(2)	-0.0035(19)	0.0025(19)
C2	0.0181(19)	0.021(3)	0.009(3)	-0.0008(19)	0.0008(19)	0.000(2)
C3	0.027(2)	0.027(3)	0.005(3)	0.0003(19)	0.000(2)	0.002(2)
C4	0.022(2)	0.028(3)	0.013(3)	0.000(2)	-0.001(2)	-0.001(2)
C5	0.024(2)	0.017(3)	0.016(3)	0.001(2)	0.004(2)	0.002(2)
C6	0.028(2)	0.025(3)	0.008(3)	0.006(2)	0.006(2)	0.004(2)
C7	0.028(2)	0.040(3)	0.012(3)	-0.003(2)	0.002(2)	-0.003(2)
O1	0.025(2)	0.030(3)	0.007(3)	0	0	-0.001(2)
O2	0.0245(16)	0.053(3)	0.010(2)	-0.0003(16)	0.0009(14)	-0.0127(16)
O3	0.0238(15)	0.042(2)	0.015(2)	0.0010(16)	0.0036(14)	-0.0067(15)

Table A2.7. Hydrogen atomic coordinates and isotropic atomic displacement parameters ($Å^2$) of dimer **8**.

	x/a	y/b	z/c	U(eq)
H3	0.3130	0.4225	0.5020	0.024
H6	0.3607	0.5724	0.1247	0.025
H7A	0.5134	0.7455	0.3866	0.032
H7B	0.4787	1.1025	0.3920	0.032

This page has been intentionally left blank

Appendix

Chapter 3

The Electrochemical Study of Vanillin in Acetonitrile

This page has been intentionally left blank

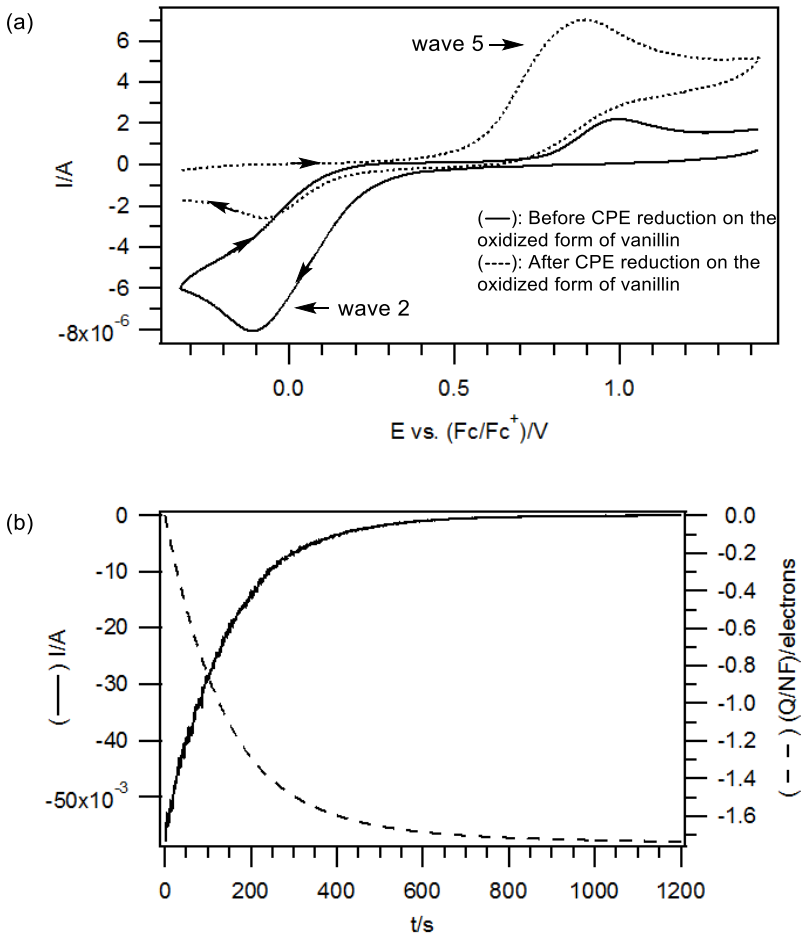

Figure A3.1. Voltammetric and coulometric data recorded during the controlled potential electrolysis of the oxidized form of 2 mM vanillin in CH_3CN with 0.2 M Bu_4NPF_6 at 22 (±2) °C. (a) Cyclic voltammograms obtained at a scan rate of 0.1 V s^{-1} using a 1 mm diameter planar Pt electrode. (b) Current/coulometry vs. time data logged during the exhaustive reduction of the oxidized form of vanillin at -0.20 vs. $(Fc/Fc^+)/V$.

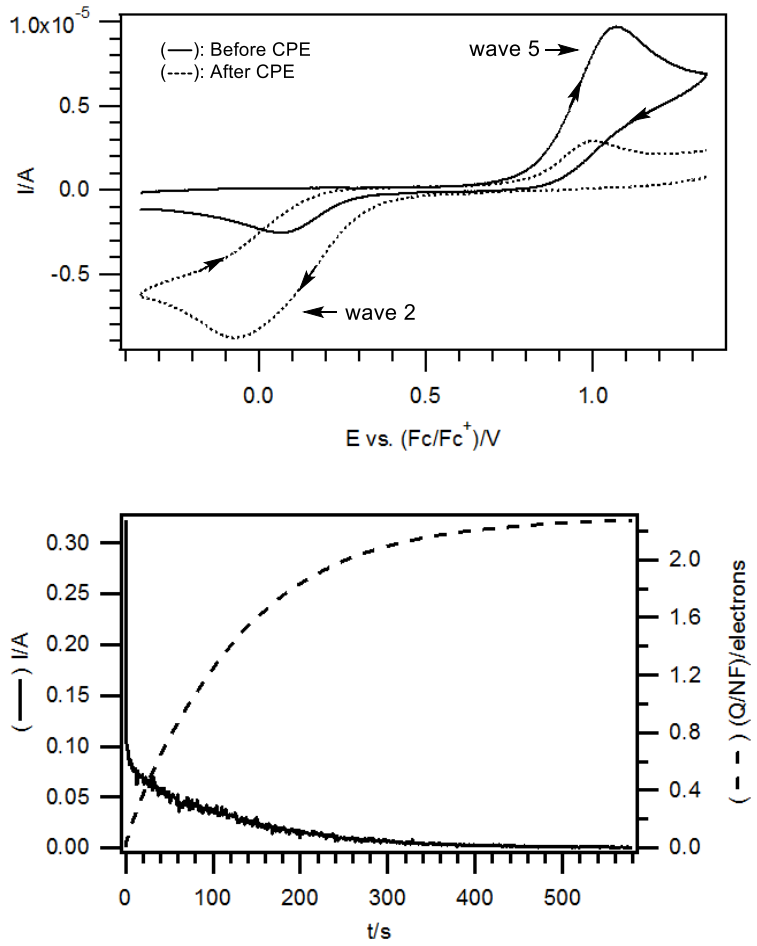

Figure A3.2. Voltammetric and coulometric data recorded during the controlled potential electrolysis of 2 mM 3,4-dihydroxybenzaldehyde in CH_3CN with 0.2 M Bu_4NPF_6 at 22 (±2) °C. (a) Cyclic voltammograms obtained at a scan rate of 0.1 V s^{-1} using a 1 mm diameter planar Pt electrode. (b) Current/coulometry vs. time data logged during the exhaustive oxidation of 3,4-dihydroxybenzaldehyde at 1.15 vs. $(Fc/Fc^+)/V$.

Table A3.1. Electrochemical parameters[a] obtained by digital simulations of CV data[b] for the reaction mechanisms shown in Schemes 3.3 and 3.4.

Electrochemical Parameters	Eq. i	Eq. iii	Eq. vi	Eq. viii	Eq. x
E^0 (V)	1.100	0.850	0.170	0.320	-0.250
k_s (cm s^{-1})	0.0100	0.0100	0.0080	0.0080	0.0080

[a]E^0 = formal oxidation potential vs. (Fc/Fc^+)/V, k_s = heterogeneous electron transfer rate constant. The diffusion coefficients were estimated via simulation techniques to be 2.60 x 10^{-5} cm^2 s^{-1} for vanillin and its oxidized forms and 3.50 x 10^{-5} cm^2 s^{-1} for H_2O, H^+ and MeOH. The transfer coefficient (α) values were assumed to be 0.5. [b]CV data were logged using a 1 mm diameter Pt electrode for solutions of 2 mM vanillin and 0.2 M Bu_4NPF_6 in CH_3CN at 20 (±2) °C. The water and proton concentrations were assumed to be 0.1 M.

Table A3.2. Equilibrium and rate constants[a] obtained by digital simulations of CV data[b] for the reaction mechanisms shown in Schemes 3.3 and 3.4.

Kinetic Parameters	Eq. ii	Eq. iv	Eq. v	Eq. vii	Eq. ix
K_{eq}	1.00 x 10^{-5}	2.50 x 10^3	5.00 x 10^1	1.00 x 10^3	1.00 x 10^3
k_f	5.00 x 10^1	1.00 x 10^5	3.00 x 10^0	1.00 x 10^1	1.00 x 10^1
k_b	5.00 x 10^6	4.00 x 10^1	6.00 x 10^{-2}	1.00 x 10^{-2}	1.00 x 10^{-2}

[a]K_{eq} = equilibrium constant, k_f = forward rate constant, k_b = backward rate constant. The homogeneous rate constants have units of s^{-1} and L mol^{-1} s^{-1} for the first- and second-order reactions, respectively. [b]CV data were logged using a 1 mm diameter Pt electrode for solutions of 2 mM vanillin and 0.2 M Bu_4NPF_6 in CH_3CN at 20 (±2) °C. The water and proton concentrations were assumed to be 0.1 M.

Table A3.3. Electrochemical parameters[a] obtained by digital simulations of CV data[b] for the reaction mechanisms shown in Schemes 3.3 and 3.4.

Electrochemical Parameters	Eq. i	Eq. iii	Eq. vi	Eq. viii	Eq. x
E^0 (V)	1.100	0.850	0.170	0.320	-0.250
k_s (cm s^{-1})	0.0060	0.0060	0.0035	0.0035	0.0035

[a]E^0 = formal oxidation potential vs. $(Fc/Fc^+)/V$, k_s = heterogeneous electron transfer rate constant. The diffusion coefficients were estimated via simulation techniques to be 2.50 x 10^{-5} cm^2 s^{-1} for vanillin and its oxidized forms and 3.00 x 10^{-5} cm^2 s^{-1} for H_2O, H^+ and MeOH. The transfer coefficient (α) values were assumed to be 0.5. [b]CV data were logged using a 1 mm diameter Pt electrode for solutions of 2 mM vanillin and 0.2 M Bu_4NPF_6 in CH_3CN at 10 (±2) °C. The water and proton concentrations were assumed to be 0.1 M.

Table A3.4. Equilibrium and rate constants[a] obtained by digital simulations of CV data[b] for the reaction mechanisms shown in Schemes 3.3 and 3.4.

Kinetic Parameters	Eq. ii	Eq. iv	Eq. v	Eq. vii	Eq. ix
K_{eq}	9.50 x 10^{-6}	2.45 x 10^3	1.50 x 10^1	9.50 x 10^2	9.50 x 10^2
k_f	2.00 x 10^1	9.00 x 10^4	1.50 x 10^{-1}	7.00 x 10^0	7.00 x 10^0
k_b	2.11 x 10^6	3.67 x 10^1	1.00 x 10^{-2}	7.37 x 10^{-3}	7.37 x 10^{-3}

[a]K_{eq} = equilibrium constant, k_f = forward rate constant, k_b = backward rate constant. The homogeneous rate constants have units of s^{-1} and L mol^{-1} s^{-1} for the first- and second-order reactions, respectively. [b]CV data were logged using a 1 mm diameter Pt electrode for solutions of 2 mM vanillin and 0.2 M Bu_4NPF_6 in CH_3CN at 10 (±2) °C. The water and proton concentrations were assumed to be 0.1 M.

Table A3.5. Electrochemical parameters[a] obtained by digital simulations of CV data[b] for the reaction mechanisms shown in Schemes 3.3 and 3.4.

Electrochemical Parameters	Eq. i	Eq. iii	Eq. vi	Eq. viii	Eq. x
E^0 (V)	1.100	0.850	0.170	0.320	-0.250
k_s (cm s^{-1})	0.0035	0.0035	0.0020	0.0020	0.0020

[a]E^0 = formal oxidation potential vs. (Fc/Fc^+)/V, k_s = heterogeneous electron transfer rate constant. The diffusion coefficients were estimated via simulation techniques to be 1.95 x 10^{-5} cm^2 s^{-1} for vanillin and its oxidized forms and 2.35 x 10^{-5} cm^2 s^{-1} for H_2O, H^+ and MeOH. The transfer coefficient (α) values were assumed to be 0.5. [b]CV data were logged using a 1 mm diameter Pt electrode for solutions of 2 mM vanillin and 0.2 M Bu_4NPF_6 in CH_3CN at 0 (±2) °C. The water and proton concentrations were assumed to be 0.1 M.

Table A3.6. Equilibrium and rate constants[a] obtained by digital simulations of CV data[b] for the reaction mechanisms shown in Schemes 3.3 and 3.4.

Kinetic Parameters	Eq. ii	Eq. iv	Eq. v	Eq. vii	Eq. ix
K_{eq}	9.00 x 10^{-6}	2.43 x 10^3	1.10 x 10^1	9.00 x 10^2	9.00 x 10^2
k_f	1.70 x 10^1	1.00 x 10^4	1.00 x 10^{-1}	6.50 x 10^0	6.50 x 10^0
k_b	1.89 x 10^6	4.12 x 10^0	9.09 x 10^{-3}	7.22 x 10^{-3}	7.22 x 10^{-3}

[a]K_{eq} = equilibrium constant, k_f = forward rate constant, k_b = backward rate constant. The homogeneous rate constants have units of s^{-1} and L mol^{-1} s^{-1} for the first- and second-order reactions, respectively. [b]CV data were logged using a 1 mm diameter Pt electrode for solutions of 2 mM vanillin and 0.2 M Bu_4NPF_6 in CH_3CN at 0 (±2) °C. The water and proton concentrations were assumed to be 0.1 M.

Table A3.7. Electrochemical parameters[a] obtained by digital simulations of CV data[b] for the reaction mechanisms shown in Schemes 3.3 and 3.4.

Electrochemical Parameters	Eq. i	Eq. iii	Eq. vi	Eq. viii	Eq. x
E^0 (V)	1.100	0.850	0.170	0.320	-0.250
k_s (cm s^{-1})	0.0020	0.0020	0.0008	0.0008	0.0008

[a]E^0 = formal oxidation potential vs. (Fc/Fc^+)/V, k_s = heterogeneous electron transfer rate constant. The diffusion coefficients were estimated via simulation techniques to be 1.65 x 10^{-5} cm^2 s^{-1} for vanillin and its oxidized forms and 1.67 x 10^{-5} cm^2 s^{-1} for H_2O, H^+ and MeOH. The transfer coefficient (α) values were assumed to be 0.5. [b]CV data were logged using a 1 mm diameter Pt electrode for solutions of 2 mM vanillin and 0.2 M Bu_4NPF_6 in CH_3CN at -10 (±2) °C. The water and proton concentrations were assumed to be 0.1 M.

Table A3.8. Equilibrium and rate constants[a] obtained by digital simulations of CV data[b] for the reaction mechanisms shown in Schemes 3.3 and 3.4.

Kinetic Parameters	Eq. ii	Eq. iv	Eq. v	Eq. vii	Eq. ix
K_{eq}	7.00 x 10^{-6}	2.40 x 10^3	6.50 x 10^0	8.50 x 10^2	8.50 x 10^2
k_f	1.20 x 10^1	6.00 x 10^3	5.50 x 10^{-2}	6.00 x 10^0	6.00 x 10^0
k_b	1.71 x 10^6	2.50 x 10^0	8.46 x 10^{-3}	7.06 x 10^{-3}	7.06 x 10^{-3}

[a]K_{eq} = equilibrium constant, k_f = forward rate constant, k_b = backward rate constant. The homogeneous rate constants have units of s^{-1} and L mol^{-1} s^{-1} for the first- and second-order reactions, respectively. [b]CV data were logged using a 1 mm diameter Pt electrode for solutions of 2 mM vanillin and 0.2 M Bu_4NPF_6 in CH_3CN at -10 (±2) °C. The water and proton concentrations were assumed to be 0.1 M.

Table A3.9. Electrochemical parameters[a] obtained by digital simulations of CV data[b] for the reaction mechanisms shown in Schemes 3.3 and 3.4.

Electrochemical Parameters	Eq. i	Eq. iii	Eq. vi	Eq. viii	Eq. x
E^0 (V)	1.100	0.850	0.170	0.320	-0.250
k_s (cm s^{-1})	0.0013	0.0013	0.00075	0.00075	0.00075

[a]E^0 = formal oxidation potential vs. (Fc/Fc^+)/V, k_s = heterogeneous electron transfer rate constant. The diffusion coefficients were estimated via simulation techniques to be 1.25 x 10^{-5} cm^2 s^{-1} for vanillin and its oxidized forms and 1.60 x 10^{-5} cm^2 s^{-1} for H_2O, H^+ and MeOH. The transfer coefficient (α) values were assumed to be 0.5. [b]CV data were logged using a 1 mm diameter Pt electrode for solutions of 2 mM vanillin and 0.2 M Bu_4NPF_6 in CH_3CN at -20 (±2) °C. The water and proton concentrations were assumed to be 0.1 M.

Table A3.10. Equilibrium and rate constants[a] obtained by digital simulations of CV data[b] for the reaction mechanisms shown in Schemes 3.3 and 3.4.

Kinetic Parameters	Eq. ii	Eq. iv	Eq. v	Eq. vii	Eq. ix
K_{eq}	6.25 x 10^{-6}	2.35 x 10^{3}	5.40 x 10^{0}	7.97 x 10^{2}	7.97 x 10^{2}
k_f	1.00 x 10^{1}	5.00 x 10^{3}	4.50 x 10^{-2}	5.50 x 10^{0}	5.50 x 10^{0}
k_b	1.60 x 10^{6}	2.13 x 10^{0}	8.33 x 10^{-3}	6.90 x 10^{-3}	6.90 x 10^{-3}

[a]K_{eq} = equilibrium constant, k_f = forward rate constant, k_b = backward rate constant. The homogeneous rate constants have units of s^{-1} and L mol^{-1} s^{-1} for the first- and second-order reactions, respectively. [b]CV data were logged using a 1 mm diameter Pt electrode for solutions of 2 mM vanillin and 0.2 M Bu_4NPF_6 in CH_3CN at -20 (±2) °C. The water and proton concentrations were assumed to be 0.1 M.

Table A3.11. Electrochemical parameters[a] obtained by digital simulations of CV data[b] for the reaction mechanisms shown in Schemes 3.3 and 3.4.

Electrochemical Parameters	Eq. i	Eq. iii	Eq. vi	Eq. viii	Eq. x
E^0 (V)	1.100	0.850	0.170	0.320	-0.250
k_s (cm s^{-1})	0.0007	0.0007	0.0003	0.0003	0.0003

[a]E^0 = formal oxidation potential vs. (Fc/Fc^+)/V, k_s = heterogeneous electron transfer rate constant. The diffusion coefficients were estimated via simulation techniques to be 1.05 x 10^{-5} cm^2 s^{-1} for vanillin and its oxidized forms and 1.50 x 10^{-5} cm^2 s^{-1} for H_2O, H^+ and MeOH. The transfer coefficient (α) values were assumed to be 0.5. [b]CV data were logged using a 1 mm diameter Pt electrode for solutions of 2 mM vanillin and 0.2 M Bu_4NPF_6 in CH_3CN at -30 (±2) °C. The water and proton concentrations were assumed to be 0.1 M.

Table A3.12. Equilibrium and rate constants[a] obtained by digital simulations of CV data[b] for the reaction mechanisms shown in Schemes 3.3 and 3.4.

Kinetic Parameters	Eq. ii	Eq. iv	Eq. v	Eq. vii	Eq. ix
K_{eq}	3.33 x 10^{-6}	2.30 x 10^{3}	3.68 x 10^{0}	7.50 x 10^{2}	7.50 x 10^{2}
k_f	5.00 x 10^{0}	1.00 x 10^{3}	3.00 x 10^{-2}	5.00 x 10^{0}	5.00 x 10^{0}
k_b	1.50 x 10^{6}	4.35 x 10^{-1}	8.15 x 10^{-3}	6.67 x 10^{-3}	6.67 x 10^{-3}

[a]K_{eq} = equilibrium constant, k_f = forward rate constant, k_b = backward rate constant. The homogeneous rate constants have units of s^{-1} and L mol^{-1} s^{-1} for the first- and second-order reactions, respectively. [b]CV data were logged using a 1 mm diameter Pt electrode for solutions of 2 mM vanillin and 0.2 M Bu_4NPF_6 in CH_3CN at -30 (±2) °C. The water and proton concentrations were assumed to be 0.1 M.

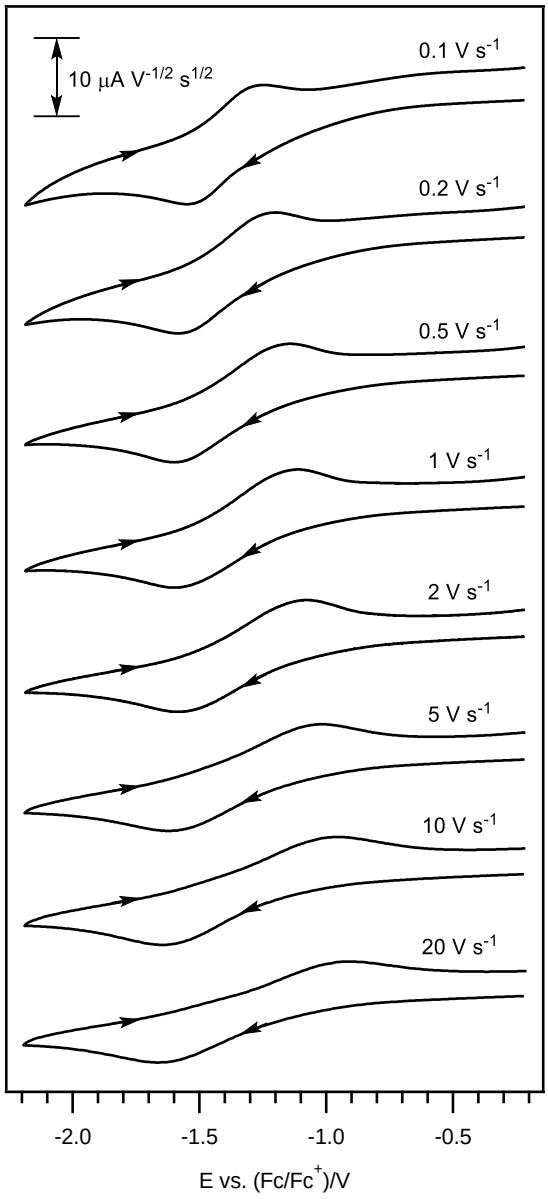

Figure A3.3. Variable scan rates cyclic voltammograms of 2 mM vanillin in CH_3CN with 0.2 M Bu_4NPF_6, recorded using a 1 mm diameter planar Pt electrode at 22 (±2) °C. Current data were multiplied by (scan rate)$^{-0.5}$ for normalization. Start/end potentials: -0.22 vs. (Fc/Fc$^+$)/V. Switching potential: -2.19 vs. (Fc/Fc$^+$)/V.

This page has been intentionally left blank

Appendix

Chapter 4

The Electrochemical Study of

Diethylstilbestrol (DES) in Acetonitrile

This page has been intentionally left blank

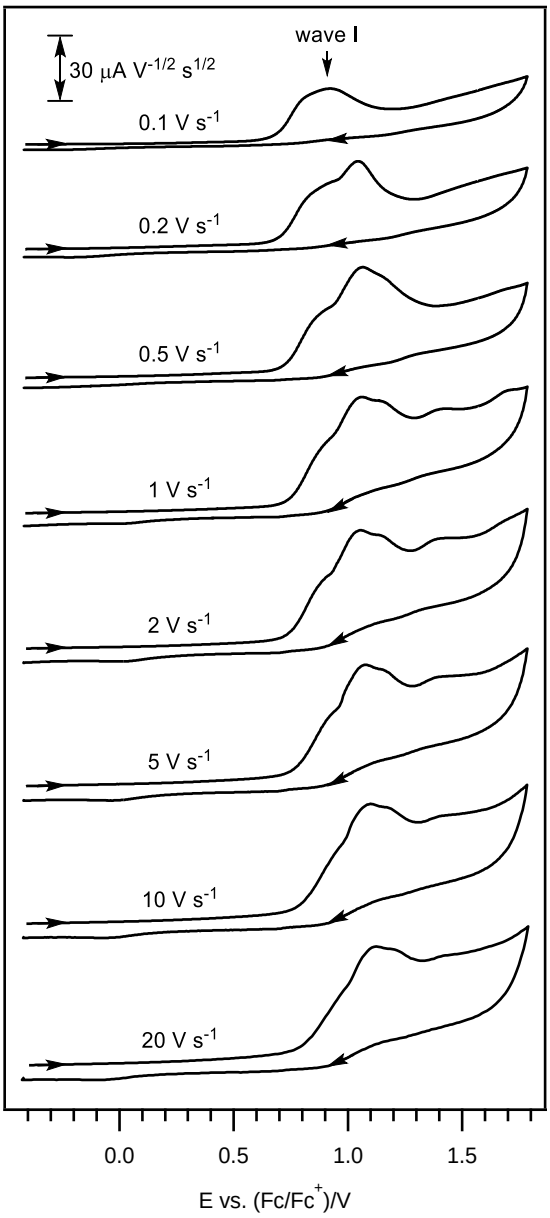

Figure A4.1. Variable scan rates cyclic voltammograms of 2 mM BPA in CH_3CN ($[H_2O]_{initial}$ = 17 mM, $[H_2O]_{final}$ = 38 mM) with 0.2 M Bu_4NPF_6, recorded using a 1 mm diameter planar GC electrode at 22 (±2) °C. Current data were multiplied by (scan rate)$^{-0.5}$ for normalization.

This page has been intentionally left blank

Appendix

Chapter 5

The Electrochemical Study of Pyridoxine (PN) in Acetonitrile

This page has been intentionally left blank

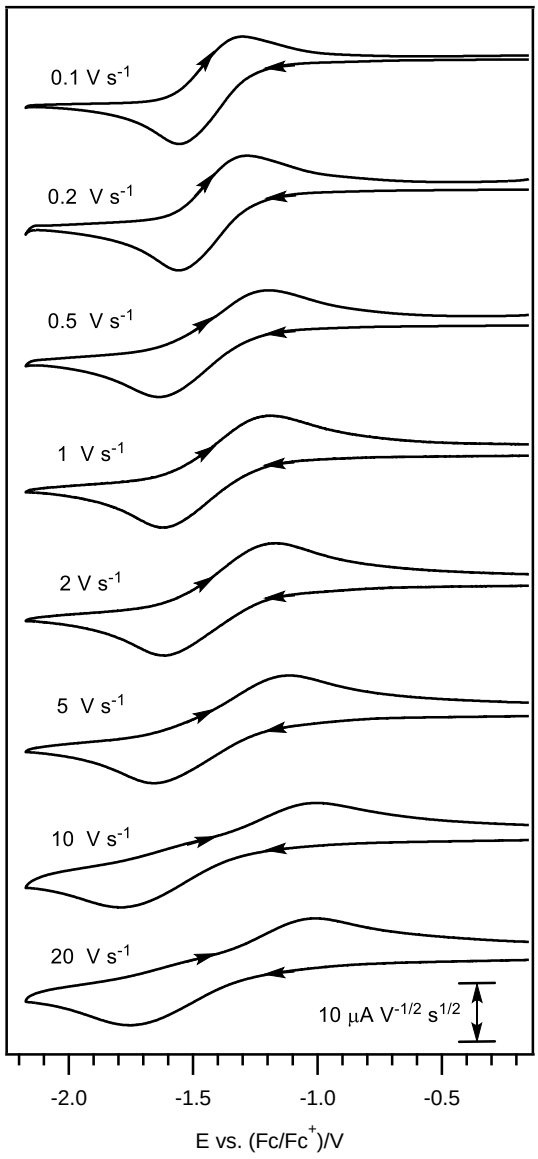

Figure A5.1. Variable scan rate cyclic voltammograms of 2 mM pyridoxine in CH_3CN with 0.2 M Bu_4NPF_6, recorded using a 1 mm diameter planar Pt electrode at 22 (±2) °C. Current data were multiplied by (scan rate)$^{-0.5}$ for normalization. Start/end potentials: -0.30 vs. (Fc/Fc$^+$)/V. Switching potential: -2.17 vs. (Fc/Fc$^+$)/V.

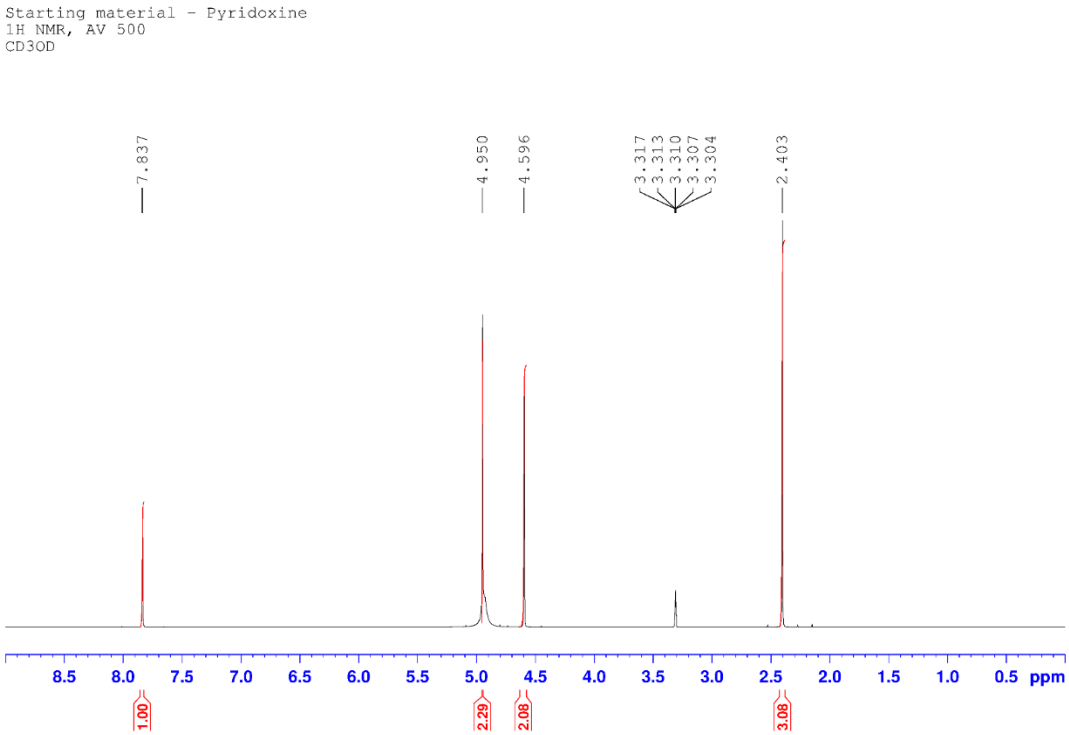

Figure A5.2. ^{1}H NMR Spectrum of PN.

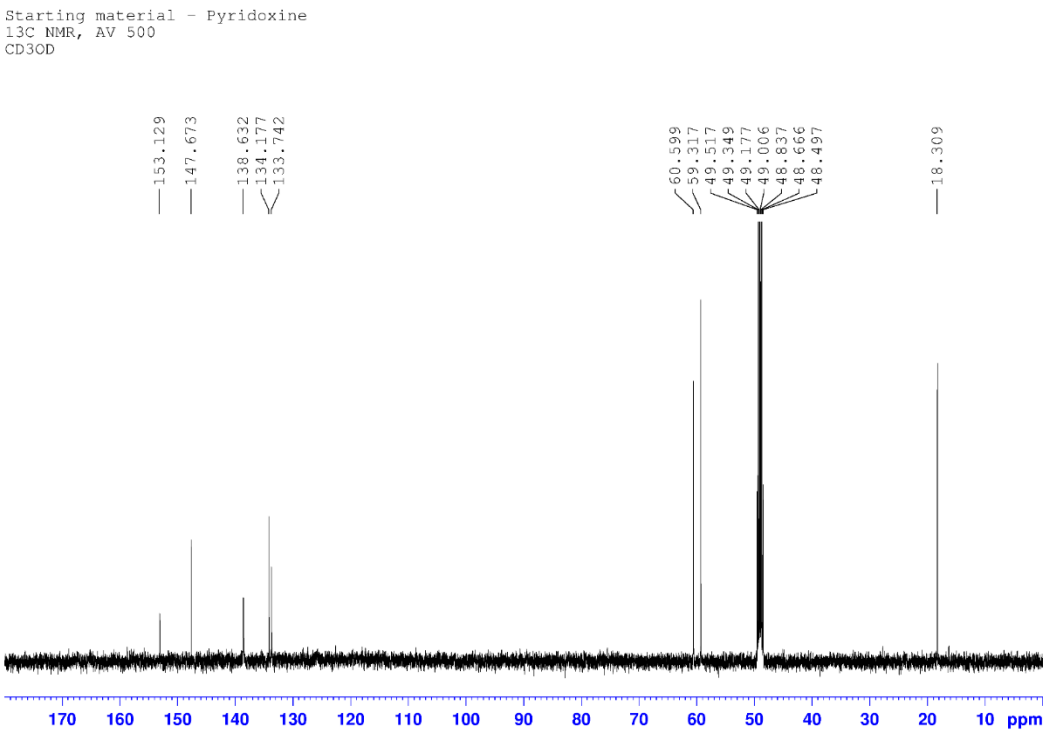

Figure A5.3. ^{13}C NMR Spectrum of PN.

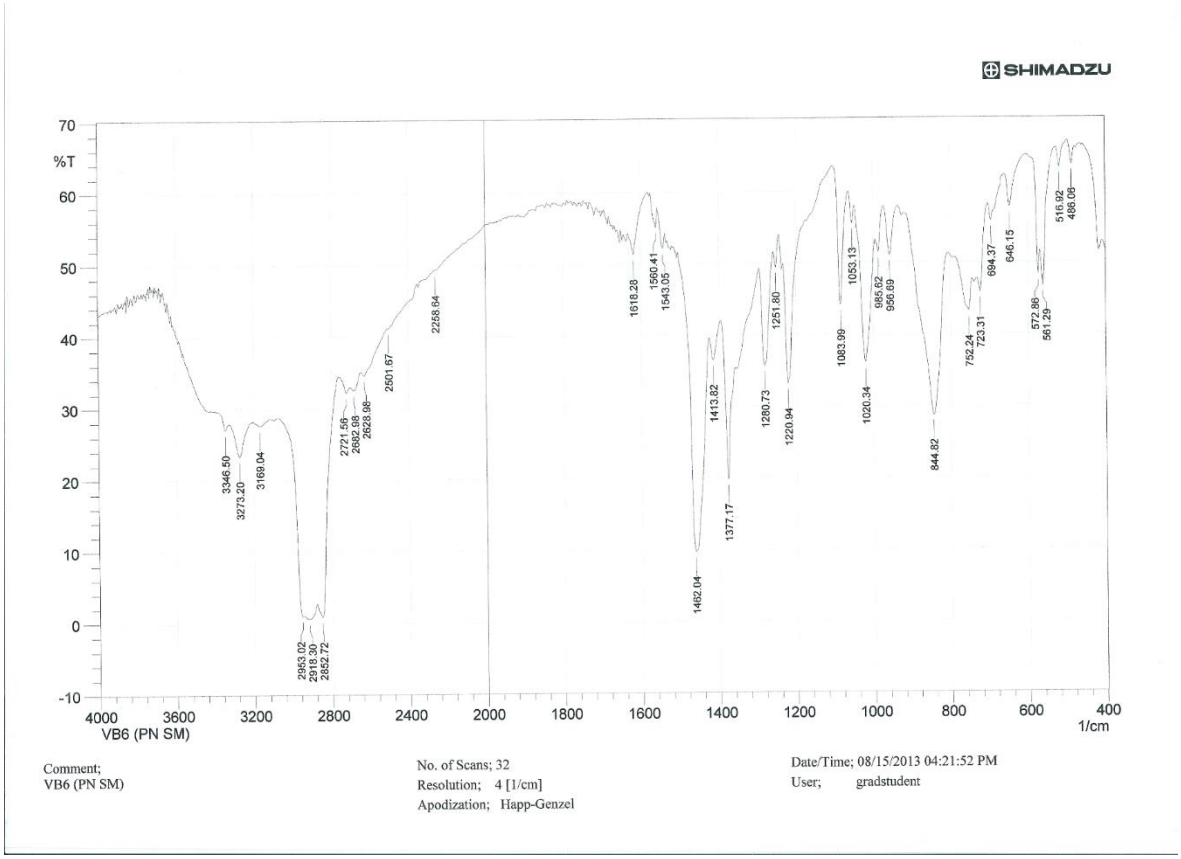

Figure A5.4. IR Spectrum of PN.

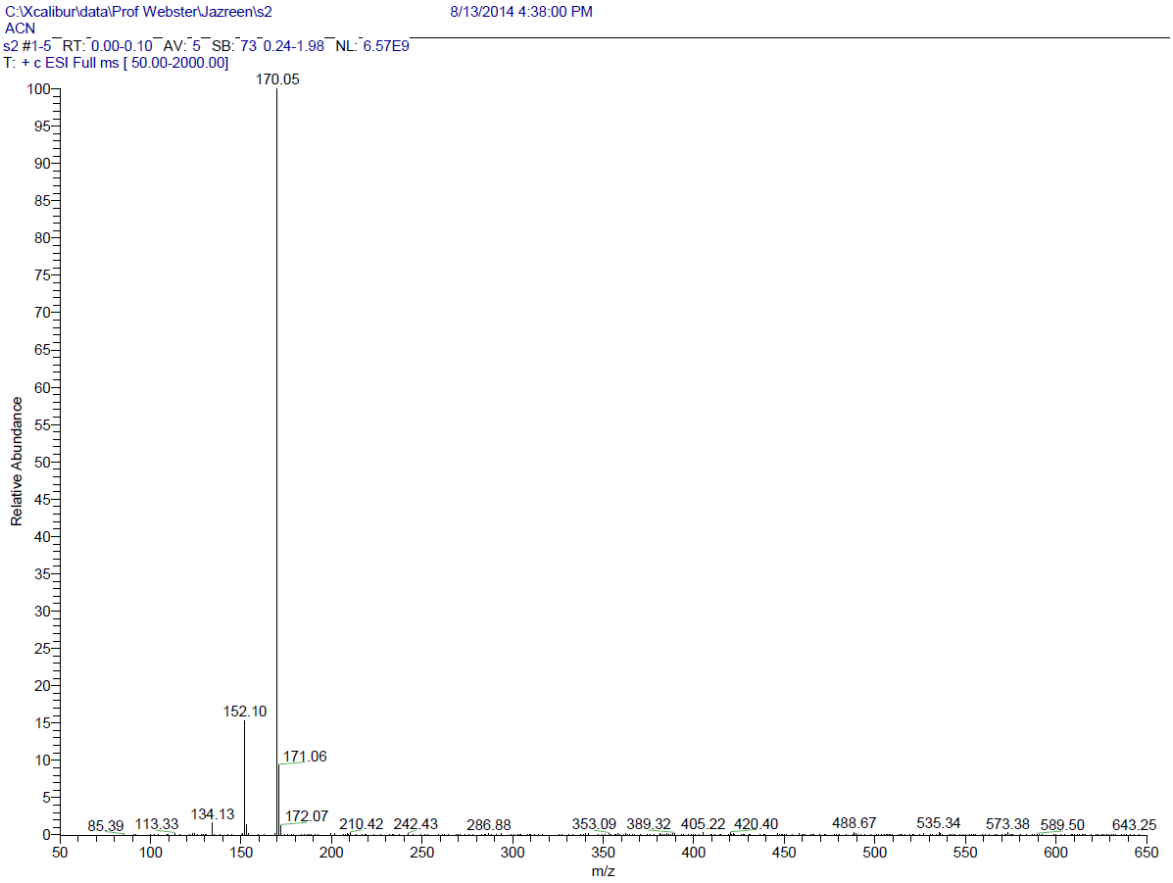

Figure A5.5. LCMS Spectrum of PN.

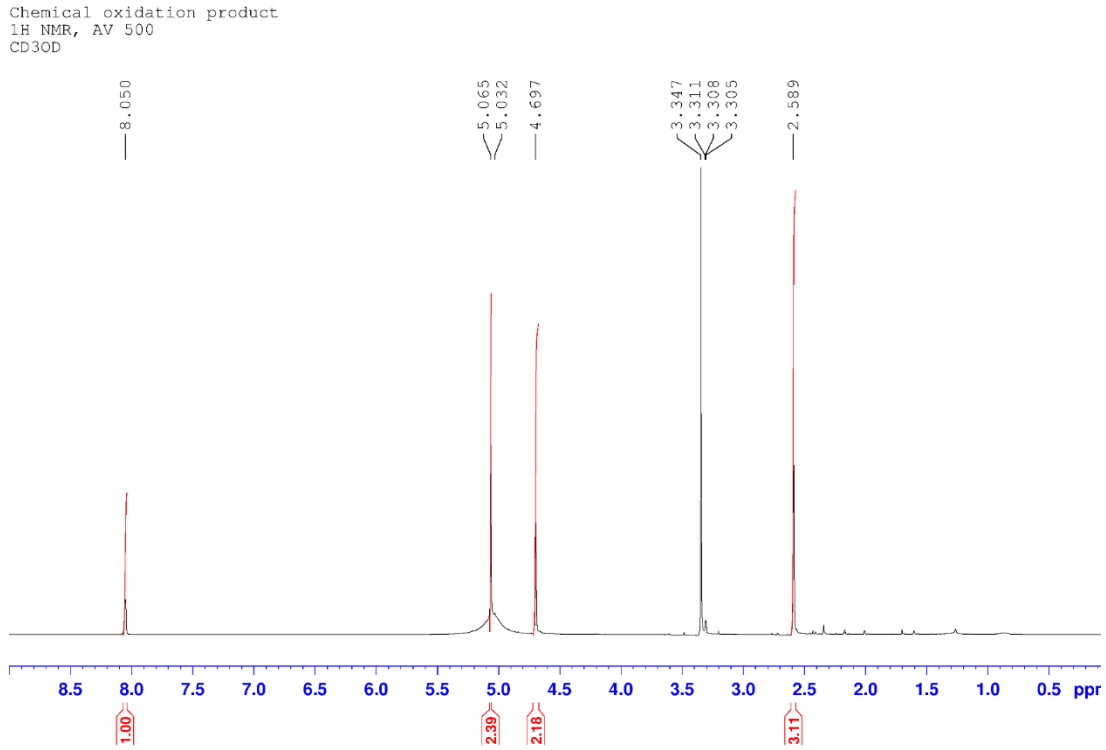

Figure A5.6. ^{1}H NMR Spectrum of chemically oxidized PN.

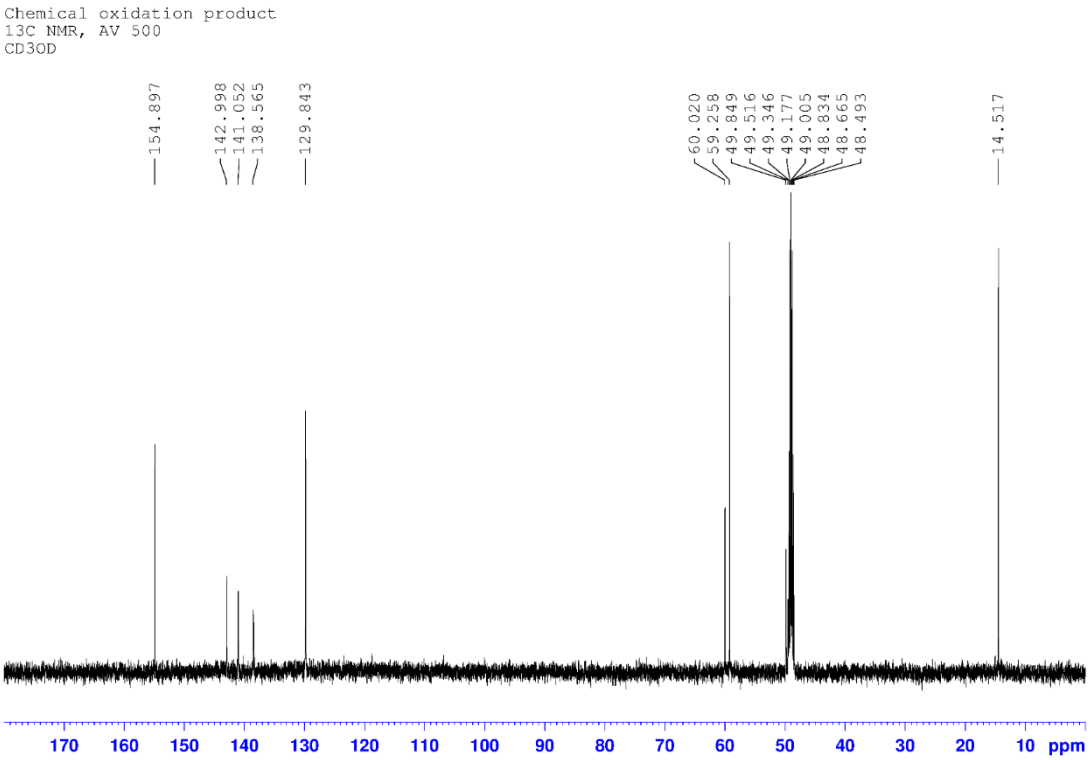

Figure A5.7. ^{13}C NMR Spectrum of chemically oxidized PN.

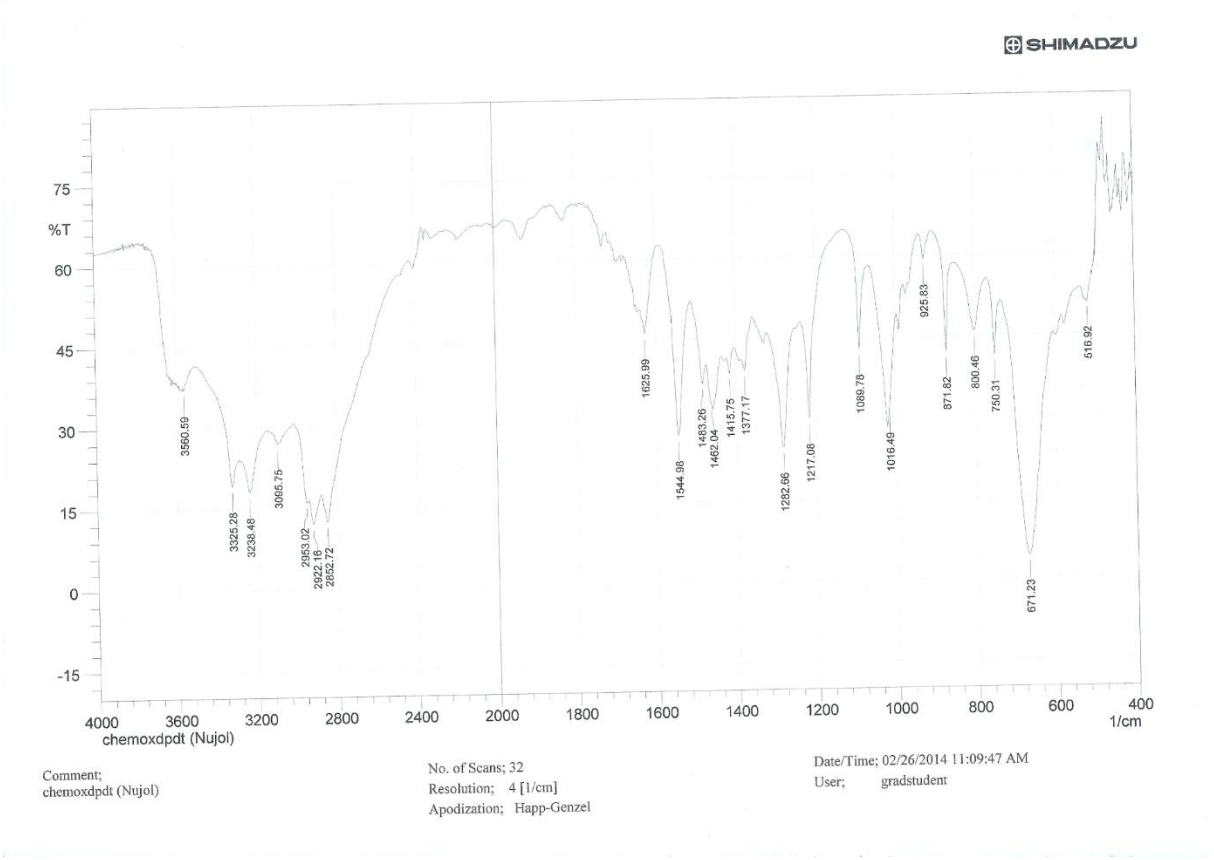

Figure A5.8. IR Spectrum of chemically oxidized PN.

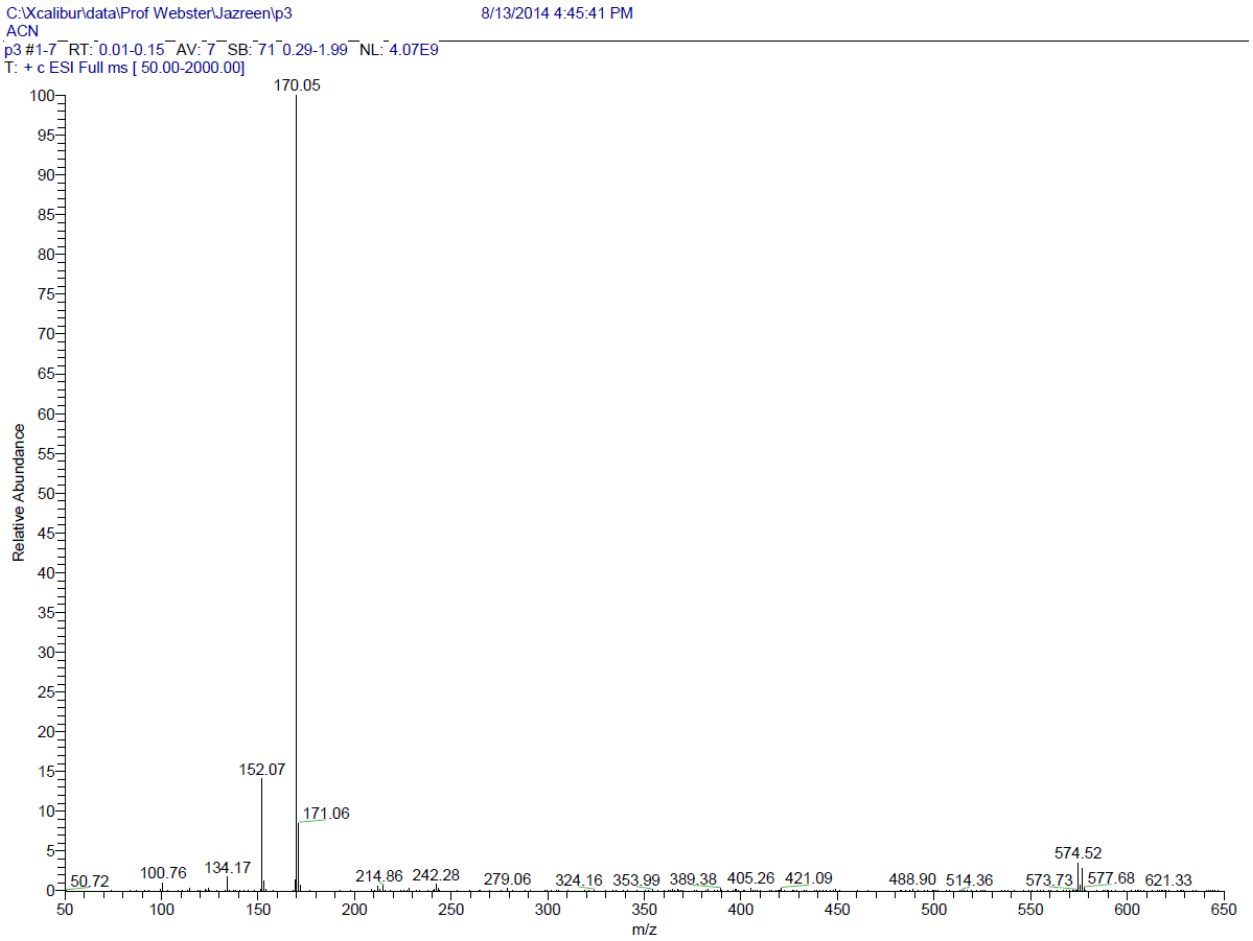

Figure A5.9. LCMS Spectrum of chemically oxidized PN.

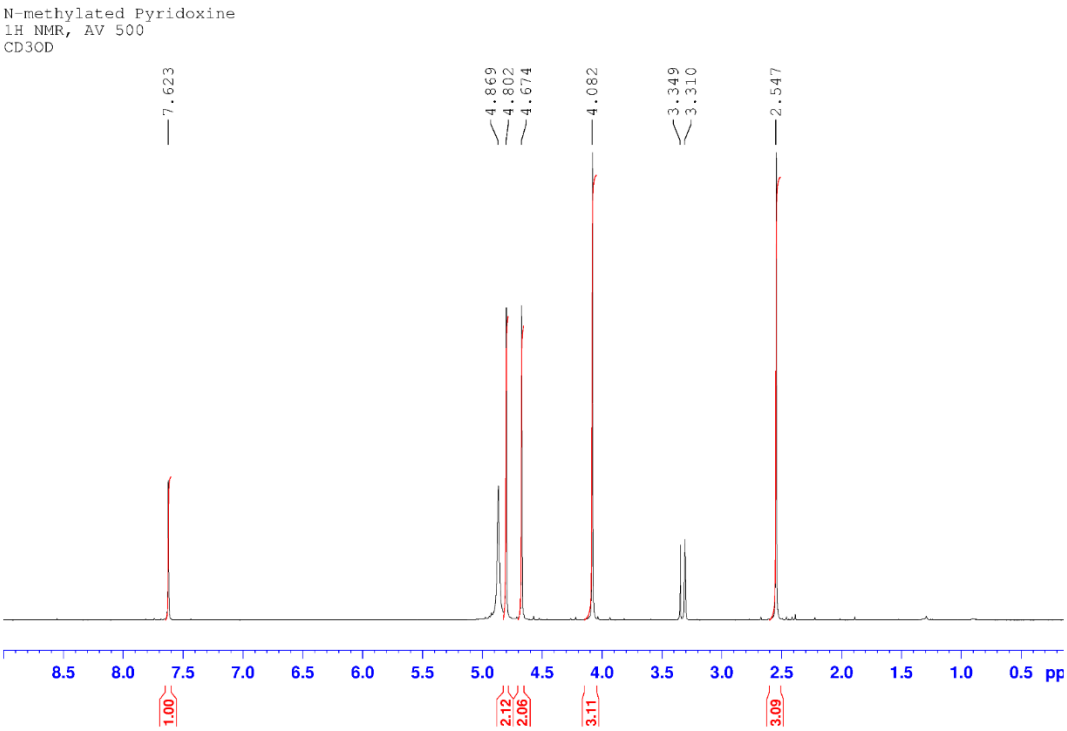

Figure A5.10. ^{1}H NMR Spectrum of nitrogen-methylated PN.

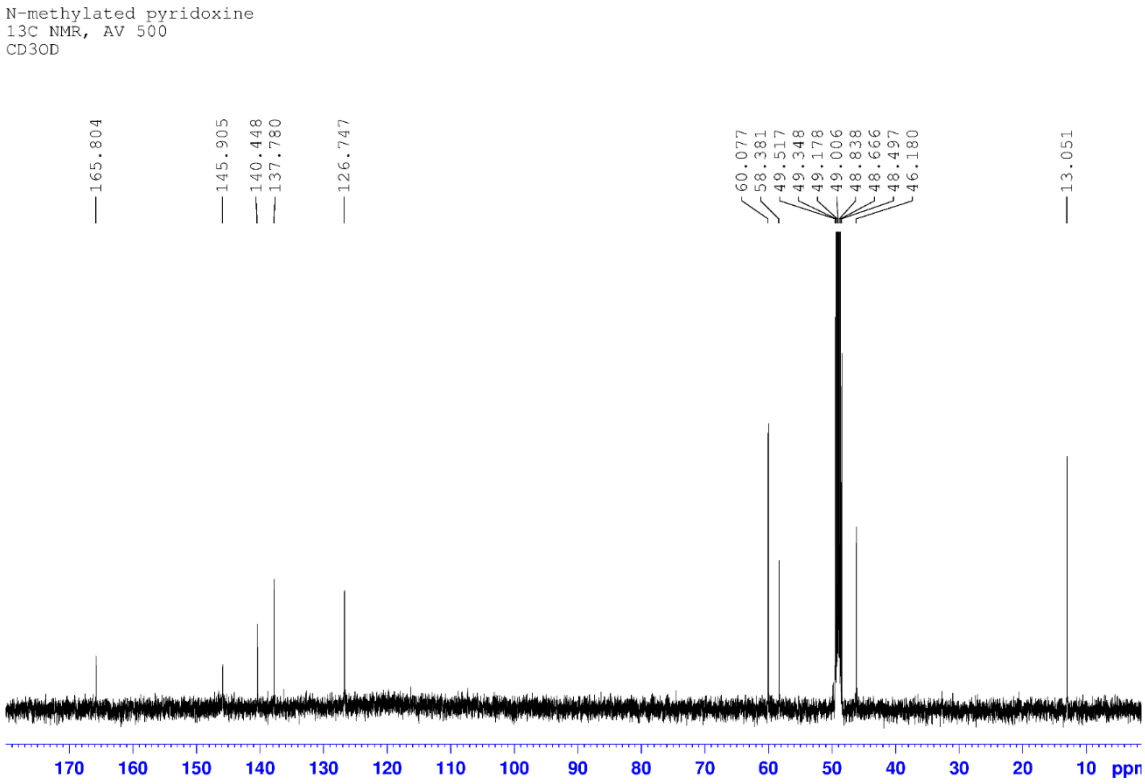

Figure A5.11. ^{13}C NMR Spectrum of nitrogen-methylated PN.

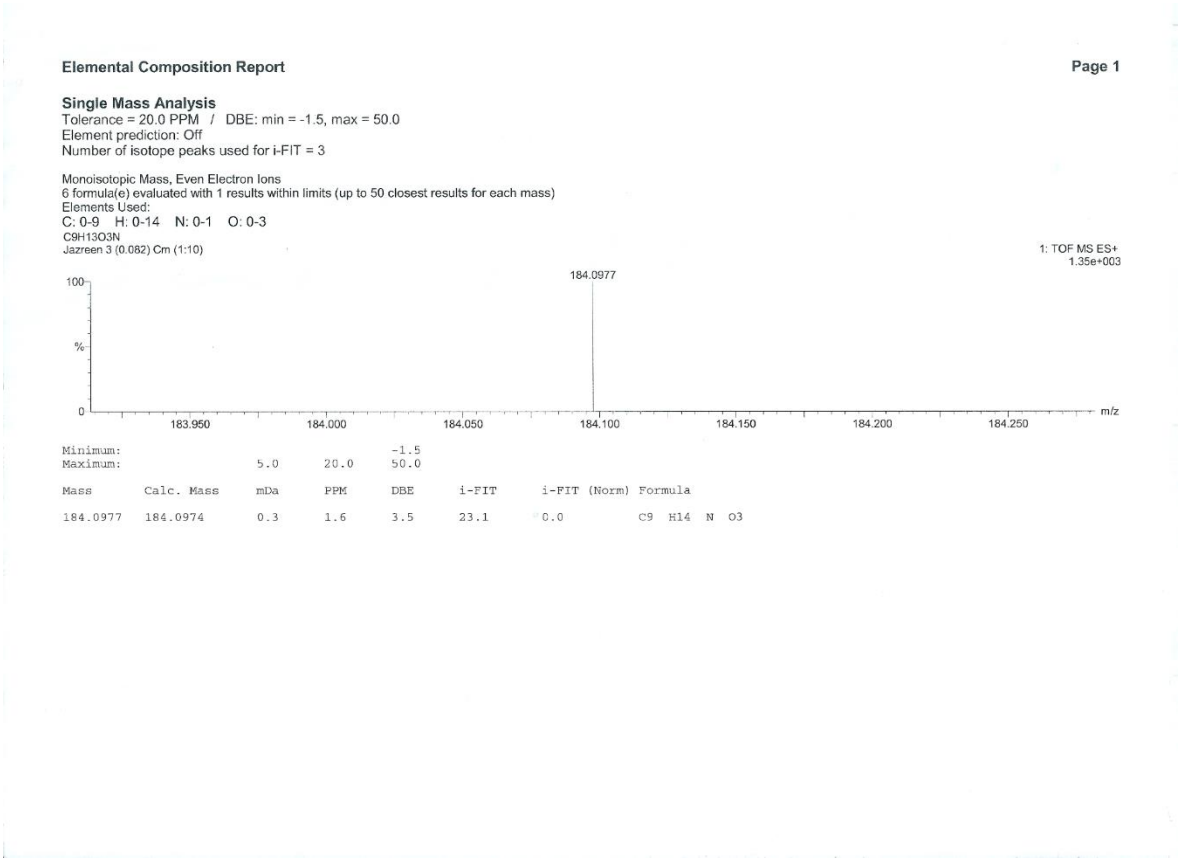

Figure A5.12. HRMS Spectrum of nitrogen-methylated PN.

Crystal structure report for nitrogen-methylated PN

A colorless block-like specimen of $C_9H_{13}NO_3$, approximate dimensions 0.040 mm x 0.080 mm x 0.120 mm, was used for the X-ray crystallographic analysis. The X-ray intensity data were measured.

The total exposure time was 3.21 h. The frames were integrated with the Bruker SAINT software package using a narrow-frame algorithm. The integration of the data using a triclinic unit cell yielded a total of 12136 reflections to a maximum θ angle of 29.28° (0.73 Å resolution), of which 2273 were independent (average redundancy 5.339, completeness = 99.6%, R_{int} = 4.44%) and 1720 (75.67%) were greater than $2\sigma(F^2)$. The final cell constants of a = 7.2810(6) Å, b = 7.3045(7) Å, c = 8.7407(7) Å, α = 93.373(3)°, β =113.496(3)°, γ = 97.120(3)°, volume = 420.03(6) $Å^3$, are based upon the refinement of the XYZ-centroids of 2298 reflections above 20 σ(I) with 5.118° < 2θ < 58.21°. Data were corrected for absorption effects using the multi-scan method (SADABS). The ratio of minimum to maximum apparent transmission was 0.879. The calculated minimum and maximum transmission coefficients (based on crystal size) are 0.9870 and 0.9960.

The final anisotropic full-matrix least-squares refinement on F^2 with 122 variables converged at R1 = 4.10%, for the observed data and wR2 = 12.68% for all data. The goodness-of-fit was 1.056. The largest peak in the final difference electron density synthesis was 0.364 $e^-/Å^3$ and the largest hole was -0.270 $e^-/Å^3$ with an RMS deviation of 0.077 $e^-/Å^3$. On the basis of the final model, the calculated density was 1.449 g/cm^3 and F(000), 196 e^-.

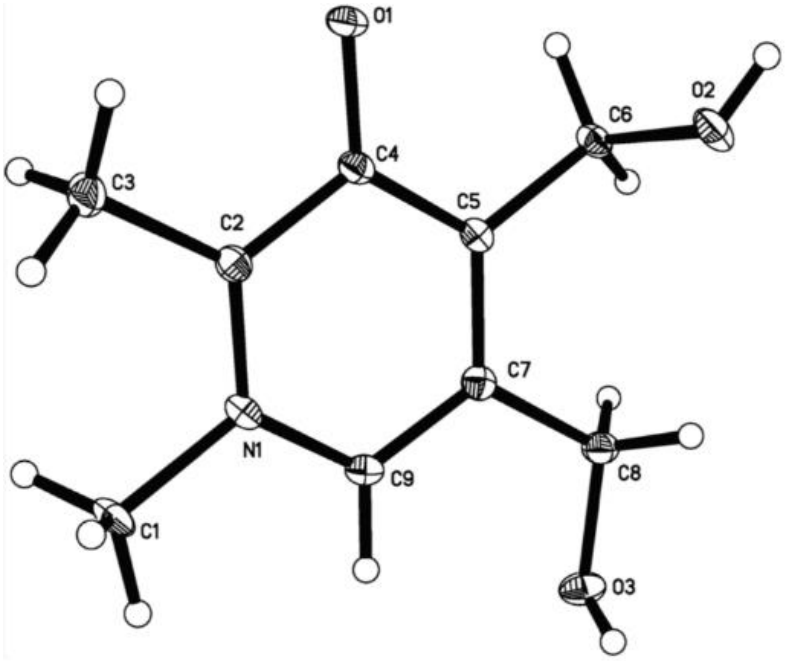

Figure A5.13. ORTEP drawing of nitrogen-methylated PN with thermal ellipsoids at 50% probability levels.

Table A5.1. Sample and crystal data for nitrogen-methylated PN.

Identification code	Nitrogen-methylated PN	
Chemical formula	$C_9H_{13}NO_3$	
Formula weight	183.20	
Temperature	103(2) K	
Wavelength	0.71073 Å	
Crystal size	0.040 x 0.080 x 0.120 mm	
Crystal habit	colorless block	
Crystal system	triclinic	
Space group	P -1	
Unit cell dimensions	a = 7.2810(6) Å	α = 93.373(3)°
	b = 7.3045(7) Å	β = 113.496(3)°
	c = 8.7407(7) Å	γ = 97.120(3)°
Volume	420.03(6) $Å^3$	
Z	2	
Density (calculated)	1.449 g/cm^3	
Absorption coefficient	0.109 mm^{-1}	
F(000)	196	

Table A5.2. Data collection and structure refinement for nitrogen-methylated PN.

Theta range for data collection	3.09 to 29.28°	
Index ranges	-10<=h<=9, -10<=k<=10, -11<=l<=12	
Reflections collected	12136	
Independent reflections	2273 [R(int) = 0.0444]	
Coverage of independent reflections	99.6%	
Absorption correction	multi-scan	
Max. and min. transmission	0.9960 and 0.9870	
Refinement method	Full-matrix least-squares on F^2	
Refinement program	SHELXL-2013 (Sheldrick, 2013)	
Function minimized	$\Sigma\ w(F_o^2 - F_c^2)^2$	
Data / restraints / parameters	2273 / 0 / 122	
Goodness-of-fit on F^2	1.056	
Final R indices	1720 data; I>2σ(I)	R1 = 0.0410, wR2 = 0.1145
	all data	R1 = 0.0602, wR2 = 0.1268
Weighting scheme	$w=1/[\sigma^2(F_o^2)+(0.0743P)^2+0.0226P]$ where $P=(F_o^2+2F_c^2)/3$	
Largest diff. peak and hole	0.364 and -0.270 eÅ^{-3}	
R.M.S. deviation from mean	0.077 eÅ^{-3}	

Table A5.3. Atomic coordinates and equivalent isotropic atomic displacement parameters ($Å^2$) for nitrogen-methylated PN.

U(eq) is defined as one third of the trace of the orthogonalized U_{ij} tensor.

	x/a	y/b	z/c	U(eq)
C1	0.76370(19)	0.69389(19)	0.23633(15)	0.0140(3)
C2	0.09870(19)	0.79196(17)	0.46837(15)	0.0105(3)
C3	0.1860(2)	0.83399(19)	0.34341(16)	0.0144(3)
C4	0.22942(18)	0.81752(17)	0.64341(15)	0.0104(3)
C5	0.14100(18)	0.76938(17)	0.75727(15)	0.0102(3)
C6	0.27711(19)	0.79132(17)	0.94197(15)	0.0113(3)
C7	0.93310(19)	0.70548(17)	0.69750(15)	0.0106(3)
C8	0.83437(19)	0.66354(19)	0.81776(16)	0.0132(3)
C9	0.81448(19)	0.68323(17)	0.52691(15)	0.0110(3)
N1	0.90001(16)	0.72452(14)	0.41798(13)	0.0104(2)
O1	0.42052(13)	0.88048(13)	0.69072(11)	0.0141(2)
O2	0.27668(14)	0.97121(13)	0.01278(11)	0.0158(2)
O3	0.62501(14)	0.59368(13)	0.73683(12)	0.0165(2)

Table A5.4. Bond lengths (Å) for nitrogen-methylated PN.

C1-N1	1.4841(15)	C1-H1A	0.98
C1-H1B	0.98	C1-H1C	0.98
C2-N1	1.3488(16)	C2-C4	1.4293(16)
C2-C3	1.4952(17)	C3-H3A	0.98
C3-H3B	0.98	C3-H3C	0.98
C4-O1	1.2956(15)	C4-C5	1.4229(17)
C5-C7	1.3956(17)	C5-C6	1.5061(16)
C6-O2	1.4201(15)	C6-H6A	0.99
C6-H6B	0.99	C7-C9	1.3804(17)
C7-C8	1.5170(17)	C8-O3	1.4104(15)
C8-H8A	0.99	C8-H8B	0.99
C9-N1	1.3584(16)	C9-H9	0.95
O2-H2	0.84	O3-H3	0.84

Table A5.5. Bond angles (°) for nitrogen-methylated PN.

N1-C1-H1A	109.5	N1-C1-H1B	109.5
H1A-C1-H1B	109.5	N1-C1-H1C	109.5
H1A-C1-H1C	109.5	H1B-C1-H1C	109.5
N1-C2-C4	119.61(11)	N1-C2-C3	120.97(11)
C4-C2-C3	119.39(11)	C2-C3-H3A	109.5
C2-C3-H3B	109.5	H3A-C3-H3B	109.5
C2-C3-H3C	109.5	H3A-C3-H3C	109.5
H3B-C3-H3C	109.5	O1-C4-C5	123.33(11)
O1-C4-C2	119.25(11)	C5-C4-C2	117.42(11)
C7-C5-C4	120.19(11)	C7-C5-C6	121.58(11)
C4-C5-C6	118.22(11)	O2-C6-C5	108.32(10)
O2-C6-H6A	110.0	C5-C6-H6A	110.0
O2-C6-H6B	110.0	C5-C6-H6B	110.0
H6A-C6-H6B	108.4	C9-C7-C5	119.75(11)
C9-C7-C8	119.34(11)	C5-C7-C8	120.89(11)
O3-C8-C7	113.70(10)	O3-C8-H8A	108.8
C7-C8-H8A	108.8	O3-C8-H8B	108.8
C7-C8-H8B	108.8	H8A-C8-H8B	107.7
N1-C9-C7	119.99(11)	N1-C9-H9	120.0
C7-C9-H9	120.0	C2-N1-C9	122.99(11)
C2-N1-C1	120.06(10)	C9-N1-C1	116.95(10)
C6-O2-H2	109.5	C8-O3-H3	109.5

Table A5.6. Anisotropic atomic displacement parameters ($Å^2$) for nitrogen-methylated PN.

The anisotropic atomic displacement factor exponent takes the form: $-2\pi^2[h^2 a^{*2} U_{11} + ... + 2 h k a^* b^* U_{12}]$

	U_{11}	U_{22}	U_{33}	U_{23}	U_{13}	U_{12}
C1	0.0114(6)	0.0168(6)	0.0082(6)	0.0017(5)	-0.0009(5)	-0.0015(5)
C2	0.0110(6)	0.0090(6)	0.0102(6)	0.0005(4)	0.0035(5)	0.0009(4)
C3	0.0154(6)	0.0161(6)	0.0113(6)	0.0015(5)	0.0061(5)	-0.0010(5)
C4	0.0092(6)	0.0097(6)	0.0104(6)	-0.0002(4)	0.0025(5)	0.0006(4)
C5	0.0104(6)	0.0099(6)	0.0088(6)	0.0005(4)	0.0026(5)	0.0012(5)
C6	0.0108(6)	0.0128(6)	0.0080(5)	0.0017(4)	0.0019(4)	-0.0003(5)
C7	0.0110(6)	0.0088(6)	0.0114(6)	0.0009(4)	0.0044(5)	0.0011(4)
C8	0.0098(6)	0.0173(6)	0.0117(6)	0.0022(5)	0.0041(5)	0.0008(5)
C9	0.0081(6)	0.0113(6)	0.0123(6)	0.0012(5)	0.0031(5)	0.0006(4)
N1	0.0100(5)	0.0098(5)	0.0085(5)	0.0009(4)	0.0011(4)	0.0003(4)
O1	0.0082(4)	0.0194(5)	0.0118(4)	0.0001(4)	0.0027(3)	-0.0022(3)
O2	0.0152(5)	0.0159(5)	0.0102(4)	-0.0025(4)	-0.0001(4)	0.0012(4)
O3	0.0098(5)	0.0172(5)	0.0217(5)	0.0023(4)	0.0066(4)	-0.0011(4)

Table A5.7. Hydrogen atomic coordinates and isotropic atomic displacement parameters ($Å^2$) for nitrogen-methylated PN.

	x/a	y/b	z/c	U(eq)
H1A	-0.3712	0.6332	0.2212	0.021
H1B	-0.1809	0.6146	0.1767	0.021
H1C	-0.2468	0.8137	0.1911	0.021
H3A	0.2243	0.7211	0.3064	0.022
H3B	0.3063	0.9302	0.3956	0.022
H3C	0.0846	0.8782	0.2464	0.022
H6A	0.2271	0.6953	0.9977	0.014
H6B	0.4168	0.7764	0.9582	0.014
H8A	-0.0964	0.5717	0.8896	0.016
H8B	-0.1458	0.7788	0.8918	0.016
H9	-0.3270	0.6391	0.4857	0.013
H2	0.3782	0.9997	1.1049	0.024
H3	-0.4407	0.6826	0.7158	0.025

This page has been intentionally left blank

Appendix

Chapter 6

The Electrochemical Reduction of Carbon Dioxide (CO_2) to Methanol in the Presence of Pyridoxine (PN)

This page has been intentionally left blank

Data File C:\CHEM32\1\DATA\JAZREEN\JAZREEN 2015-08-26 11-07-34\078F0301.D
Sample Name: GAL

Acq. Operator : Jazreen Seq. Line : 3
Acq. Instrument : Instrument 1 Location : Vial 78
Injection Date : 8/26/2015 11:42:36 AM Inj : 1
Inj Volume : 0.2 µl
Acq. Method : C:\CHEM32\1\DATA\JAZREEN\JAZREEN 2015-08-26 11-07-34\JAZREEN - 1.M
Last changed : 8/26/2015 10:57:08 AM by Jazreen
Analysis Method : C:\CHEM32\1\DATA\JAZREEN\JAZREEN 2015-08-26 11-07-34\JAZREEN - 1.M (Sequence Method)
Last changed : 8/26/2015 12:47:51 PM by Jazreen
(modified after loading)

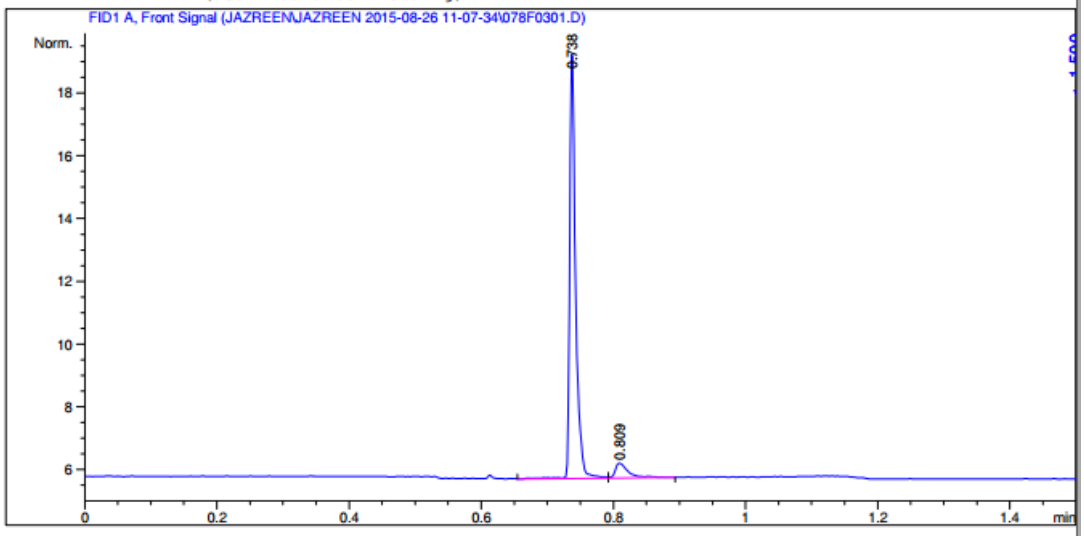

Area Percent Report

Sorted By : Signal
Multiplier: : 1.0000
Dilution: : 1.0000
Use Multiplier & Dilution Factor with ISTDs

Signal 1: FID1 A, Front Signal

Peak #	RetTime [min]	Type	Width [min]	Area [pA*s]	Height [pA]	Area %
1	0.738	BV	9.23e-3	8.47542	13.66834	92.80462
2	0.809	VB	0.0203	6.57121e-1	4.71096e-1	7.19538
Totals :				9.13254	14.13944	

Figure A6.1. Gas chromatogram of constant current electrolyzed sample. Using the procedures described in the experimental section (Section 6.5), the methanol peak was detected at ca. 0.809 min as evidence from its increment in intensity following the increase in concentration of the standards, while the other peak which was eluted earlier (observed at ca. 0.738 min) is reasoned to be attributable to the atmospheric air present (refer to Figure A6.3).

Data File C:\CHEM32\1\DATA\JAZREEN\JAZREEN 2015-08-26 11-07-34\077F0201.D
Sample Name: spl

Acq. Operator : Jazreen Seq. Line : 2
Acq. Instrument : Instrument 1 Location : Vial 77
Injection Date : 8/26/2015 11:25:44 AM Inj : 1
Inj Volume : 0.2 µl
Acq. Method : C:\CHEM32\1\DATA\JAZREEN\JAZREEN 2015-08-26 11-07-34\JAZREEN - 1.M
Last changed : 8/26/2015 10:57:08 AM by Jazreen
Analysis Method : C:\CHEM32\1\DATA\JAZREEN\JAZREEN 2015-08-26 11-07-34\JAZREEN - 1.M (Sequence Method)
Last changed : 8/26/2015 12:47:51 PM by Jazreen
(modified after loading)

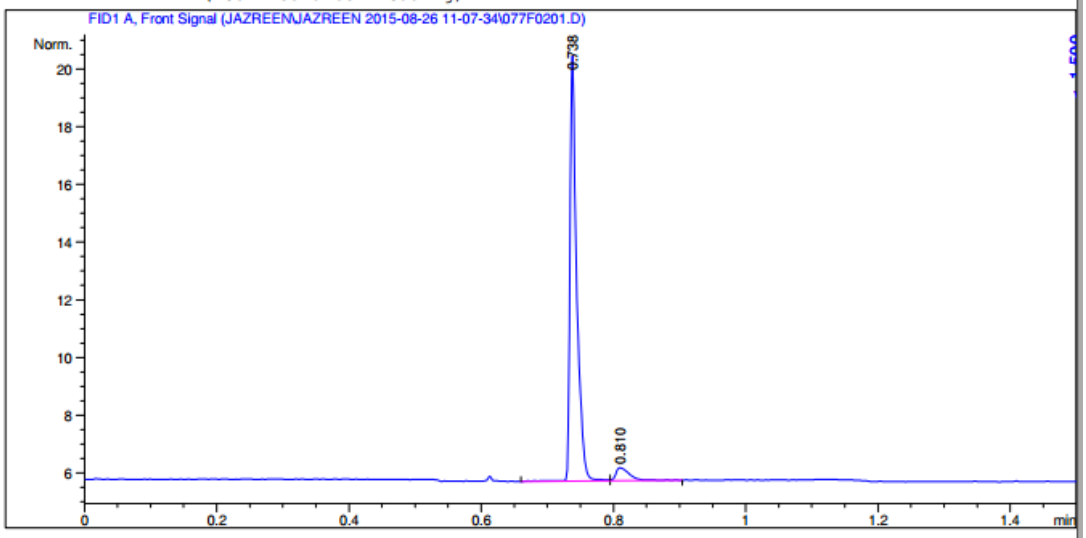

Area Percent Report

Sorted By : Signal
Multiplier: : 1.0000
Dilution: : 1.0000
Use Multiplier & Dilution Factor with ISTDs

Signal 1: FID1 A, Front Signal

Peak #	RetTime [min]	Type	Width [min]	Area [pA*s]	Height [pA]	Area %
1	0.738	BV	0.0103	10.43256	14.74770	93.81689
2	0.810	VB	0.0227	6.87571e-1	4.53269e-1	6.18311

Totals : 11.12014 15.20097

Figure A6.2. Gas chromatogram of controlled potential electrolyzed sample. Using the procedures described in the experimental section (Section 6.5), the methanol peak was detected at ca. 0.810 min as evidence from its increment in intensity following the increase in concentration of the standards, while the other peak which was eluted earlier (observed at ca. 0.738 min) is reasoned to be attributable to the atmospheric air present (refer to Figure A6.3).

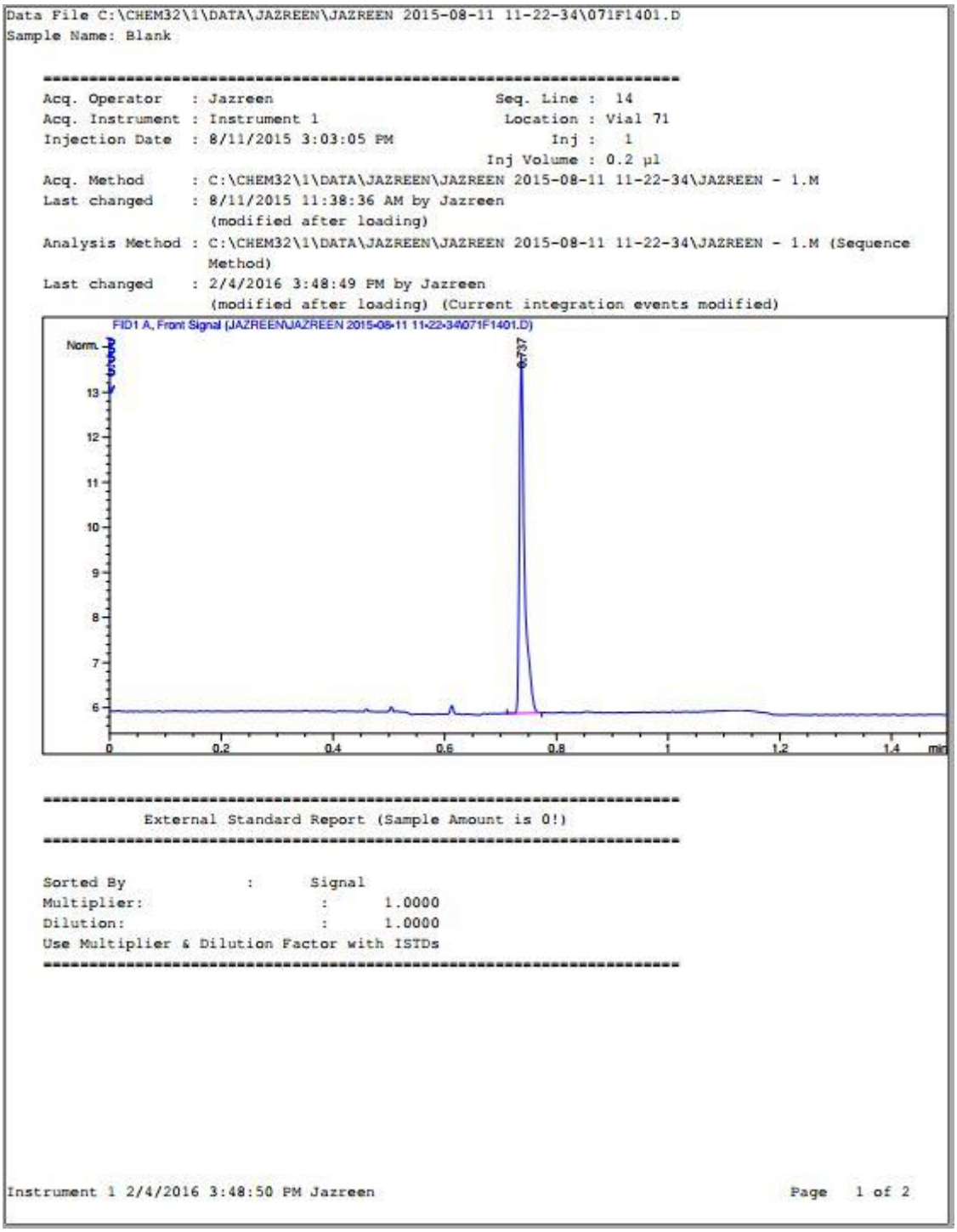

Figure A6.3. Gas chromatogram of blank.

Data File C:\CHEM32\1\DATA\JAZREEN\JAZREEN 2015-08-26 12-00-36\073F0101.D
Sample Name: 5ppm MeOH

Acq. Operator : Jazreen Seq. Line : 1
Acq. Instrument : Instrument 1 Location : Vial 73
Injection Date : 8/26/2015 12:01:57 PM Inj : 1
Inj Volume : 0.2 µl
Acq. Method : C:\CHEM32\1\DATA\JAZREEN\JAZREEN 2015-08-26 12-00-36\JAZREEN - 1.M
Last changed : 8/26/2015 10:57:08 AM by Jazreen
Analysis Method : C:\CHEM32\1\DATA\JAZREEN\JAZREEN 2015-08-26 12-00-36\JAZREEN - 1.M (Sequence Method)
Last changed : 8/26/2015 1:34:04 PM by Jazreen
(modified after loading) (Current integration events modified)

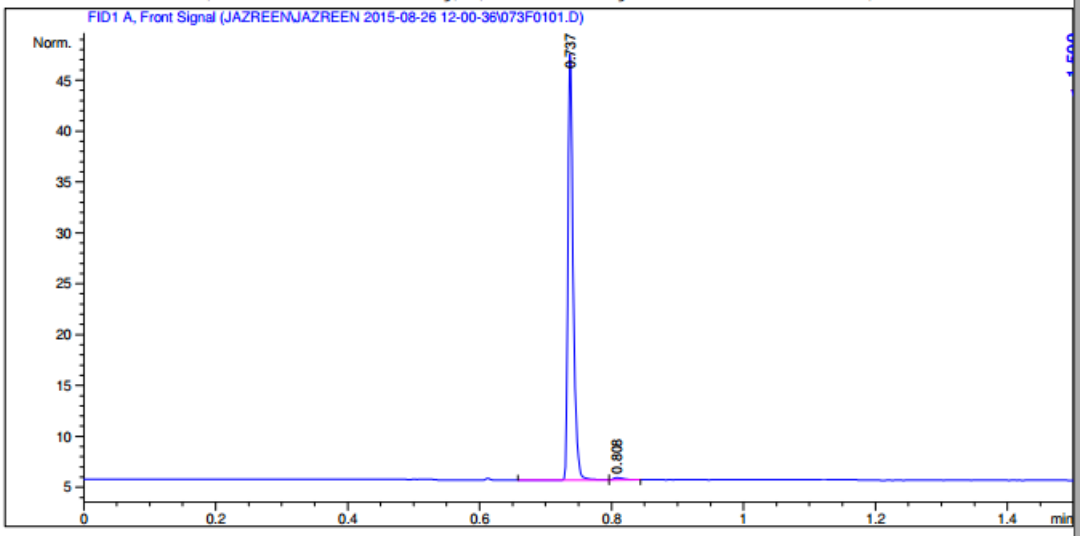

Area Percent Report

Sorted By : Signal
Multiplier: : 1.0000
Dilution: : 1.0000
Use Multiplier & Dilution Factor with ISTDs

Signal 1: FID1 A, Front Signal

Peak #	RetTime [min]	Type	Width [min]	Area [pA*s]	Height [pA]	Area %
1	0.737	BV	8.34e-3	23.21680	42.74749	99.02906
2	0.808	VB	0.0169	2.27632e-1	2.13669e-1	0.97094
Totals :				23.44444	42.96115	

Figure A6.4. Gas chromatogram of 5 ppm of methanol in water (standard).

Data File C:\CHEM32\1\DATA\JAZREEN\JAZREEN 2015-08-26 12-00-36\075F0301.D
Sample Name: 15ppm MeOH

Acq. Operator : Jazreen Seq. Line : 3
Acq. Instrument : Instrument 1 Location : Vial 75
Injection Date : 8/26/2015 12:35:42 PM Inj : 1
Inj Volume : 0.2 µl
Acq. Method : C:\CHEM32\1\DATA\JAZREEN\JAZREEN 2015-08-26 12-00-36\JAZREEN - 1.M
Last changed : 8/26/2015 10:57:08 AM by Jazreen
Analysis Method : C:\CHEM32\1\DATA\JAZREEN\JAZREEN 2015-08-26 12-00-36\JAZREEN - 1.M (Sequence Method)
Last changed : 8/26/2015 1:34:58 PM by Jazreen
(modified after loading)

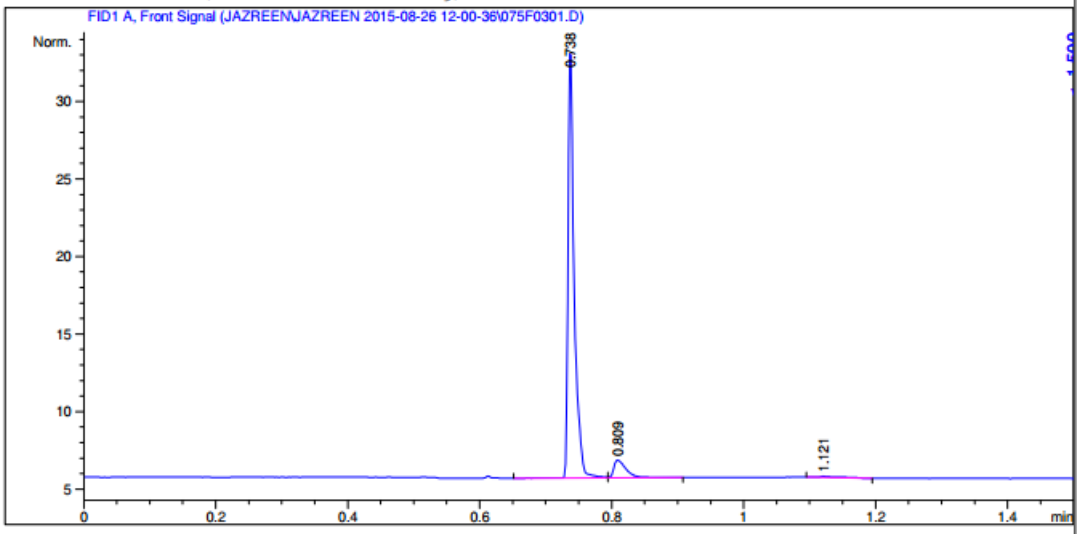

Area Percent Report

Sorted By : Signal
Multiplier: : 1.0000
Dilution: : 1.0000
Use Multiplier & Dilution Factor with ISTDs

Signal 1: FID1 A, Front Signal

Peak #	RetTime [min]	Type	Width [min]	Area [pA*s]	Height [pA]	Area %
1	0.738	BV	9.59e-3	18.00111	27.65717	91.22119
2	0.809	VB	0.0207	1.53236	1.14206	7.76530
3	1.121	BB	0.0289	2.00000e-1	8.52694e-2	1.01351

Figure A6.5. Gas chromatogram of 15 ppm of methanol in water (standard).

Data File C:\CHEM32\1\DATA\JAZREEN\JAZREEN 2015-08-26 11-07-34\076F0101.D
Sample Name: 20ppm MeOH

Acq. Operator : Jazreen Seq. Line : 1
Acq. Instrument : Instrument 1 Location : Vial 76
Injection Date : 8/26/2015 11:08:57 AM Inj : 1
Inj Volume : 0.2 µl
Acq. Method : C:\CHEM32\1\DATA\JAZREEN\JAZREEN 2015-08-26 11-07-34\JAZREEN - 1.M
Last changed : 8/26/2015 10:57:08 AM by Jazreen
Analysis Method : C:\CHEM32\1\DATA\JAZREEN\JAZREEN 2015-08-26 11-07-34\JAZREEN - 1.M (Sequence Method)
Last changed : 8/26/2015 12:47:51 PM by Jazreen
(modified after loading)

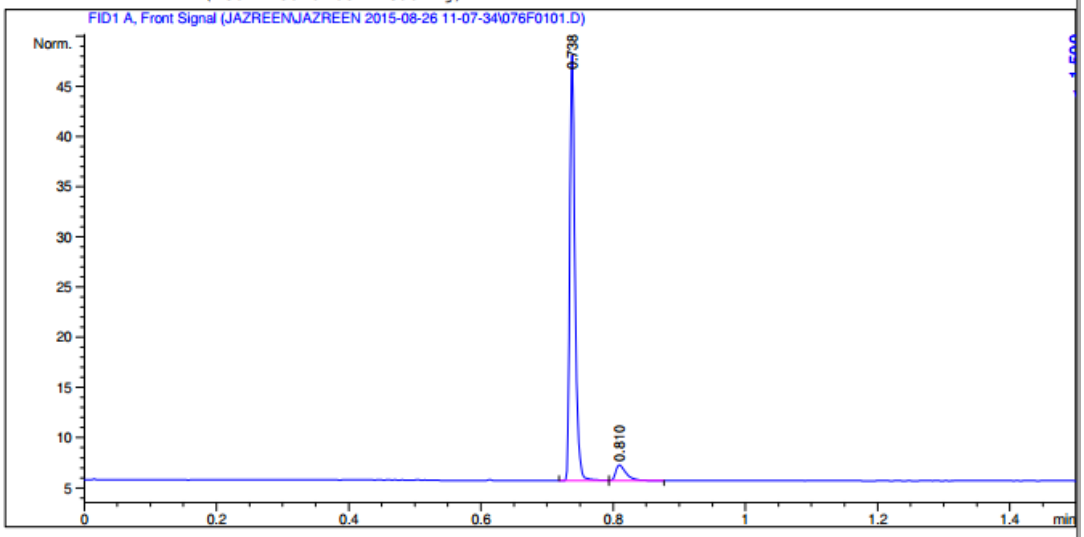

Area Percent Report

Sorted By : Signal
Multiplier: : 1.0000
Dilution: : 1.0000
Use Multiplier & Dilution Factor with ISTDs

Signal 1: FID1 A, Front Signal

Peak #	RetTime [min]	Type	Width [min]	Area [pA*s]	Height [pA]	Area %
1	0.738	BB	8.41e-3	23.35298	42.48772	93.32348
2	0.810	BB	0.0162	1.67071	1.53285	6.67652
Totals :				25.02369	44.02058	

Figure A6.6. Gas chromatogram of 20 ppm of methanol in water (standard).

This page has been intentionally left blank